Synthetic and Bioactivity Studies of Antiplasmodial and Antibacterial Marine Natural Products

A thesis submitted in fulfilment of the requirements for the degree of

Doctor of Philosophy

of

Rhodes University

by

Ryan Mark Young

November 2011

Abstract

This thesis is divided into two parts, assessing marine and synthetic compounds active firstly against *Plasmodium falciparum* (Chapter 3 and 4) and secondly active against methicillin resistant *Staphylococcus aureus* (MRSA, Chapter 5). In Chapter 3 the synthesis of nine new tricyclic podocarpanes (**3.203-3.207** and **3.209-3.212**) from the diterpene (+)-manool is described. Initial SAR study of synthetic podocarpanes concluded that the most active compound was a C-13 phenyl substituted podocarpane (**3.204**, IC_{50} 6.6 μM). By preparing analogues with varying halogenated substituents on the phenyl ring (**3.209-3.212**) the antiplasmodial activity was improved (IC_{50} 1.4 μM), while simultaneously decreasing the haemolysis previously reported for this class of compounds. Inspired by the antiplasmodial activity of Wright and Wattanapiromsakul's tricycle marine isonitriles (**2.16-2.21** and **2.24-2.27**) an unsuccessfully attempt was made to convert tertiary alcohol moieties to isonitrile functionalities in compounds **3.188**, **3.204-3.207** and **3.209-3.212**.

Over a decade ago Wright *et al.* proposed a putative antiplasmodial mechanism of action for marine isonitriles (**2.4**, **2.9**, **2.15**, **2.19** and **2.35**) and isothiocyanate (**2.34**) which involved interference in haem detoxification by *P. falciparum* thus inhibiting the growth of the parasite. In Chapter 4 we describe how we successfully managed to scale down Egan's β-haematin inhibition assay for the analyses of small quantities of marine natural products as potential β-haematin inhibitors. Our modified assay revealed that the most active antiplasmodial marine isonitrile **2.9** (IC_{50} 13 nM) showed total β-haematin inhibition while **2.15** (IC_{50} 81 nM) and **2.19** (IC_{50} 31 nM) showed partial inhibition at three equivalents relative to haem. Using contempary molecular modelling techniques the charge on the isonitrile functionality was more accurately describe and the modified charge data sets was used to explore docking of marine isonitriles to haem using AutoDock.

In Chapter 5 we describe how a lead South African marine bisindole MRSA pyruvate kinase inhibitor (**5.8**) was discovered in collaboration with colleagues at the University of British Columbia (UBC) and how this discovery inspired us to design a synthetic route to the dibrominated bisindole, isobromotopsentin (**5.20**) in an attempt to increase the bioactivity displayed by **5.8**. We devised a fast and high yielding synthetic route using microwave assited organic synthesis. We first tested this synthesis using simple aryl glyoxals (**5.27-5.32**) as precursors to synthesize biphenylimidazoles (**5.21-5.26**), which later allowed us to synthesize the ascidian natural product **5.111**. This method was sucessfully extended to the synthesis of deoxytopsentin (**5.33**) from an N-Boc protected indole methyl ketone (**5.89**). We subsequently were able to effectively remove the carbamate protection

via thermal decomposition by heating the protected bisindole imidazole (**5.90**) in a microwave reactor for 5 min under argon. The synthesis of **5.20** resulted in an inseparable mixture of monoprotected and totally deprotected topsentin products, and due to time constraints we were not able to optimise this synthesis. Nonetheless our synthesis of the marine natural product **5.33** which was faster and higher yielding than previously reported routes could be extended to the synthesis of other topsentin bisindoles (**5.138**-**5.140**). Work towards this goal continues in our laboratory.

Table of Contents

List of Figures

List of Tables

List of Schemes

Abbreviations

$[\alpha]_D$	Specific rotation
1D	One dimensional
2D	Two dimensional
3D	Three dimensional
A	Absorbance
AcOH	Acetic Acid
ADP	Adendosine diphosphate
AMBER	Assisted model building with energy refinement
amu	Atomic mass units
aq.	Aqueous
ATP	Adendosine triphosphate
b.p.	Boiling Point
B3LYP	Becke-Lang-Yee-Parr
BHIA	β-haematin inhibitory activity
Bn	Benzyl
BOA	Born-Oppenheimer approximation
Boc_2O	Di-*tert*-butyl dicarbonate
BOM	Benzyloxymethyl
br.	Broad
c.	Concentration (quoted in g/100mL)
CA	Community associated
calcd	Calculated
CCDC	Cambridge Crystal Database Centre
CDP-ME	4-Diphosphocytidyl-2C-methyl-D-erythritol
CDP-MEP	4-Diphosphocytidyl-2C-methyl-D-erythritol-2-phosphate
CHIPS	Chemotaxis inhibitory proteins of *S. aureus*
cif	Crystal information files
CMK	4-Diphosphocytidyl-2-C-methyl-D-erythritol kinase
CMP	Cytidine monophosphate
CMS	4-diphosphocytidyl-2-C-methyl-D-erythritol synthase
COSY	Correlation spectroscopy
CQ	Chloroquine
CT	Combination therapy
CT	Charge transfer
CTP	Cytidine triphosphate
DCM	Dichloromethane
dd	Double doublet
ddd	Doublet of double doublets
DEPT	Distortionless enhancement by polarisation transfer
DFT	Density functional theory
DHFR	Dihydrofolate reductase
DHODase	Dihydroorotate dehydrogenase
DHPS	Dihydropteroate synthase
DMAP	4-Dimethylaminopyridine

DMAPP	Dimethylallyl pyrophosphate
DMSO	Dimethyl sulphoxide
DMXBA	3-(2,4-Dimethoxybenxylidene)-anabaseine
DNA	Deoxyribonucleic acid
DOXP	1-Deoxy-D-xylulose 5-phosphate
DPPA	Diphenylphosphoryl azide
DXR	DOXP reductase
DXS	DOXP synthase
E.coli	*Escherichia coli*
EBHIA	Egan's β-haematin inhibitory assay
EC_{50}	Half maximal effective concentration
ee	Enantomeric excess
EEF	Exoerythrocytic form
EIMS	Electron impact mass spectrometry
equiv.	Equivalents
ESI	Electron Spray Ionisation
ESP	Electrostatic potentials
Et_2O	Diethyl ether
EtOAc	Ethyl acetate
EtOH	Ethanol
eV	Electron volt
EXSY	Exchangable Spectroscopy
FID	Flame Ionization Detector
FP	Free haem
FT-IR	Fourier Transfer Infrared
FV	Food Vacuole
G	Gibbs free energy
G6PD	Glucose-6-phosphate dehydrogenase
GAF	Gametocyte-activating factor
GC	Gas Chromotography
GSK	GlaxoSmithKline
h	Hour(s)
HA	Hospital associated
HD	Haem Dimer
HDR	HMB-PP reductase
HDS	HMB-PP synthase
HEPES	4-(2-Hydroxyethyl)-1-piperazineethanesulfonic acid
HF	Hocktree-Fock
HIA	Haem inhibition assay
HMBC	Heteronuclear multiple-bond correlation spectroscopy
HMB-PP	(E)-4-Hydroxy-3-methyl-but-2-enyl pyrophosphate
HMD-PP	1-Hydroxy-2-methyl-2-(E)butenyl-4-diphosphate
HPIA	Haem polymerization inhibitory activity
HPLC	High performance liquid chromatography
HREIMS	High resolution electron impact mass spectrometry
HRFABMS	High resolution fast atom bombardment mass spectrometry

HRMS	High resolution mass spectrometry
HRP	Histidine Rich Proteins
HSQC	Heteronuclear single quantum coherence
I	Quantum spin number
IBX	2-Iodoxybenzoic acid
IC_{50}	Half maximal inhibitory concentration
ID	Internal diameter
IPP	Isopentenyl pyrophosphate
IR	Infrared
k_B	Boltzmann Constant (1.38065×10^{-23} $J.K^{-1}$)
LAH	Lithium aluminium hydride
LANL2DZ	Los Alamos National Laboratory 2-double-z
Laser	Light Amplification by Stimulated Emission of Radiation
lit.	Literature
m	Multiplet
MALDI	Matrix-assisted laser desorption/ionization
MAO	Microwave Assisted Organic
MCS	2-C-methyl-D-erythritol 2,4-cyclodiphosphate synthase
MD	Molecular dynamics
Me	Methyl
MeCN	Acetonitrile
MEcPP	2C-methyl-D-erythritol-2,4-cyclodiphosphate
MeOH	Methanol
MEP	Molecular electronic potential
MEP	2-C-methyl-D-erythritol-4-phosphate
min	Minutes
MK	Merz-Singh-Kollman
MM	Molecular mechanics
mmol	Millimoles
MOG	1-Monooleoyl-rac-glycerol
mol	Moles
MOM	Methoxymethyl ether
mp	Melting point
MP2	Møller-Plesset
MRSA	Methicillin Resistant *Staphylococcus aureus*
MS	Mass Spectrometry
MSCRAMMS	Microbial surface components recognising adhesive matrix molecules
MSG	Monostearoylglycerol
MSP	Monopalmitoylglycerol
MWI	Microwave Irradiation
n	Total number of coupling neighbouring nuclei
NAD	Nicotinamide adenine dinucleotide
NADP	Nicotinamide adenine dinucleotide phosphate
NBO	Natural bonding orbital
NCI	National Cancer Institute
NCS	N-chlorosuccinimide

ND	Not determined
NIS	*N*-Iodosuccinimide
NIWA	New Zealand National Institute of Water and Atmospheric Research
NMO	*N*-Methylmorpholine-*N*-oxide
NMR	Nuclear Magnetic Resonance
NOESY	Nuclear Overhauser effect spectroscopy
OAc	Acetyl fuctionality
P.	*Plasmodium*
PABA	*p*-Aminobenzoic acid
PBE	Perdew-Burke-Ernzerhof
PBP	Penicillin binding proteins
PCC	Pyridinium chlorochromate
PDB	Protein Database
PDBQT	Protein Database with Charge and Torsion
PEP	Phosphoenolpyruvate
Pgh1	Glycoprotein homologue 1
Ph	Phenyl functionality
Phi-β	Pyridine hemichrome inhibition of β-haematin
PK	Pyruvate Kinase
PM	Peritrophic matrix
PPh3	Triphenyl phosphine
PP_i	Pyrophosphate
PPIX	Protophorphyrin IX
ppm	Parts per million
PV	Parasitophorous vacuole
PVL	Panton-Valentine leukocidin
q	Quartet
R	Alkyl group
RBC	Red blood cells
rel. int.	Relative intensity
RESP	Restrained Electrostatic Potential
R-factor	Residual Factor
RI	Refractive index
ROV	remotely operated underwater vehicle
rpm	Revolutions per minute
RT	Room temperature
s	Singlet
S. aureus	*Staphylococcus aureus*
s.d.	Standard deviation
SAR	Structural activity relationship
sat.	Saturated
SCUBA	Self-contained underwater breathing apparatus
SEM	Scanning electron microscopy
SEM	2-(Trimethylsilyl)ethoxymethyl
SET	Single electron transfer
sp.	Species

t	Triplet
T	Transmittance
TBS	*Tert*-butyldimethylsilyl
td	Triplet of doublets
tert	Tertiary
TFA	Trifluoro acetic acid
TGA	Thermogravimetric analysis
THF	Tetrahydrofuran
TLC	Thin layer chromatography
TMB	1,3,5-Trimethoxybenzene
TMSCN	Trimethylsilyl cyanide
TMSO	Trimethylsilate
TOF	Time of Flight
TPAP	Tetrapropylammonium perruthenate
t_R	Retention time
Ts	Tosyl
UBC	University of British Columbia
UV	Ultra violet
UV/vis	Ultra violet - visible
v/v	Volume to volume
WHO	World Health Organization
X	Halogen
XRD	X-ray diffraction
YAG	Yttrium aluminium garnet
ε	Energy Level

Acknowledgements

Many thanks to the following people who assisted me in various forms throughout the project:

Professor Mike Davies-Coleman, thank you for the constant support and guidance and always going above and beyond your role as my supervisor. Thank you for being a mentor and a friend.

Thank you to Dr. Kevin Lobb and Matthew Adendorff for you assistance with NMR kinetics and Molecular Modelling. Thank you to Dr Albert van Wyk and Dr Wendy Popplewell for sharing your expertise in synthesis and NMR characterization respectively. Professor Mino Caira, Dr. Edith Atunes, Dr. Ernst Ferg, Dr. Robyn van Zyl, Professor Andersen, Dr. Strangman and Dr. Jessica Goble thank you for assisting me with X-ray crystallography, XRD, TGA and biological assays.

Thank you to Professors Anthony Wright and Brian Robinson for their generous contribution of marine isonitriles and manool respectively.

Thank you to Rhodes University Chemistry Department administrative and technical staff, with particular thanks to Mrs Benita Tarr, Mr Andre Adriaan and Mr Aubrey Sonemann, whose tireless efforts behind the scenes was not unappreciated.

Thank you to the Deutscher Akademischer Austausch Dienst (DAAD) for funding, which without your generous contribution I would have not have been able to complete my studies.

Thank you to all my friends I have made over my pasted eight years here at Rhodes you were my surrogate family. All of you made my time at Rhodes one of the happiest times of my life. I would like to particularly thank Candice Bromley, Emma Smith and Eva Pesce for proof reading chapters of this thesis. Thank you to all my colleagues and friends in S3 and S4, for help with the research and just creating a great work environment.

And finally, to my parents, grandparents and brother; Mike, Jenny, Fred, Margret and Brendan thank you for the support and encouragement throughout my studies. I could not have done it without you.

Chapter 1: Drugs from the sea

1.1. What are natural products?

Natural products or secondary metabolites are chemicals produced by an organism (plant, invertebrate or microbe) for functions seemingly superfluous to the primary metabolism of that organism. These functions may include *inter alia* toxins to reduce predation or growth inhibitors of other organisms competing for the same pool of nutrients or space. The world's oceans cover more than 70% of the world's total surface area and therefore provides vast habitats where organisms may live and diversify. The diverse marine biota inhabiting environments from the deep abyssal plain to the shallow coastal tidal pools provide a unique reservoir of marine natural products. Paradoxically, many marine natural products have been shown to possess potential medicinal properties especially in the treatment of cancer.[1,2] The marine environment hosts approximately 100 000 species of marine invertebrates, a number which is estimated to be far higher due to numerous species undiscovered or undescribed.[3] Many of these invertebrates belong to the Coelenterata, Porifera, Bryozoa, Mollusca and Echinodermata phyla, which include organisms which may be sessile, slow moving or slow growing and lack physical defences such as spines or shells. These soft bodied organisms may therefore contain chemical defences to combat predation by fishes, crustacea *etc.*[3] In a recent model described by Erwin *et al.*[4] an estimated 250,000-600,000 new chemical structures from marine organisms was projected, of which 90-93% have yet to be discovered. Erwin *et al.*[4] further calculated that the successful discovery and testing of these marine compounds would add a US $563 billion-5.69 trillion value to the pharmaceutical industry as anti-cancer drugs. With the ever growing burden of infection and disease there exists an overwhelming need for the discovery of new drugs and the ocean offers a diverse source of new pharmaceuticals for the treatment of many diseases. Currently there are four marine natural products registered by the FDA and one by the EMEA and approximately eleven marine natural products in clinical trials for the treatment of a plethora of afflictions ranging from cancer to schizophrenia.[5]

1.2. Approved and current drugs of marine origin in the drug discovery pipeline

In order for a drug to successfully make it to the consumer market it has to be approved by the Federal Drug Administration (FDA) or the European Agency for the Evaluation of Medical Products (EMEA) for the USA and Europe respectively. These drugs are only approved after successfully passing Phase I, II and III clinical trials. Phase I clinical trials involve the testing of the drug on 20-100

healthy individuals in order to assess the pharmacovigilance, tolerability, pharmacokinetics and pharmacodynamics of a drug. Once the drug has been successfully assessed in Phase I, the drug will be tested in Phase II trials where 100-300 patients are administered the drug/placebo to gauge the effectiveness of the drug on a particular disease or condition and to determine the short-term side effects and risk. Phase III clinical trials are multicentred and require testing on 300-3000 patients as the definitive assessment of safety and effectiveness of the drug in question. Should Phase III be successful the "regulatory submission" containing all the relevant information concerning human and animal testing, manufacturing procedure, formulation details and shelf life is submitted to the relevant regulatory body for final drug approval.[6]

1.2.1. FDA and EMEA approved drugs

Currently there are four marine natural products or marine natural product derived compounds approved by the FDA for the safe use as drugs, namely cytarabine (Cytosar-U®, Depocyt®), vindarabin (Vira-A®), ziconotide (Prialt®) and eribulin mesylate (Halaven®), while the EMEA has recently approved trabectedin (Yondelis®) for use in the treatment of cancer (Figure 1.1).

Cytarabine and vindarabin were the first marine natural products to be approved by the FDA in 1969. Both cytarabine and vindarabin are synthetic compounds inspired by spongothymidine and spongouridine respectively, which were orginally isolated from the Caribbean sponge *Tethya crypta*.[7] Cytarabine acts as an inhibitor of DNA polymerase and hence DNA synthesis and is therefore used in the treatment of acute lymphocytic leukemia, acute mylocytic leukemia and meningeal leukemia.[8,9] Vira-A® inhibits viral DNA polymerase and DNA synthesis in *Herpes*, *Vaccinia* and *Varicella zoster* viruses.[10] Over thirty years later ziconotide was approved by the FDA in 2004 for the treatment of severe pain. Ziconotide binds to N-type calcium channels of nociceptive afferent nerves thus reducing the release of neurotransmitter from the afferent nerve terminal relieving pain.[11,12] Ziconotide is the synthetic equivalent of a naturally occurring 25 amino acid containing peptide ω-conotoxin MVIIA originally isolated from the marine snail *Conus magnus*.[13] Yondelis® received EMEA approval for the treatment of soft tissue sarcoma in 2007 and in 2009 received EMEA approval for the treatment of ovarian carcinoma.[5] Trabectedin was isolated from a tunicate *Ecteinascidia turbinata*, which is found in the Caribbean and Mediterranean sea.[14,15] The problems associated with obtaining sufficient supplies of tabectedin are discussed briefly in Section 1.3.3.2. Tabectedin covalently binds to the minor groove in DNA[16] and interacts with different proteins

involved in the nucleotide excision repair system[17] thus reducing the growth of the cancer. In 2010 the FDA approved eribulin mesylate, a simplified synthetic analogue of the marine natural product halichondrin B, which was originally isolated from a marine sponge *Halichondria okadai*,[18] for the treatment of metastatic breast cancer.[19] Eribulin mesylate has an unique mechanism of action against cancer cells, by inducing an irreversible antimitotic effect leading to apoptosis of the cancer cells.[20]

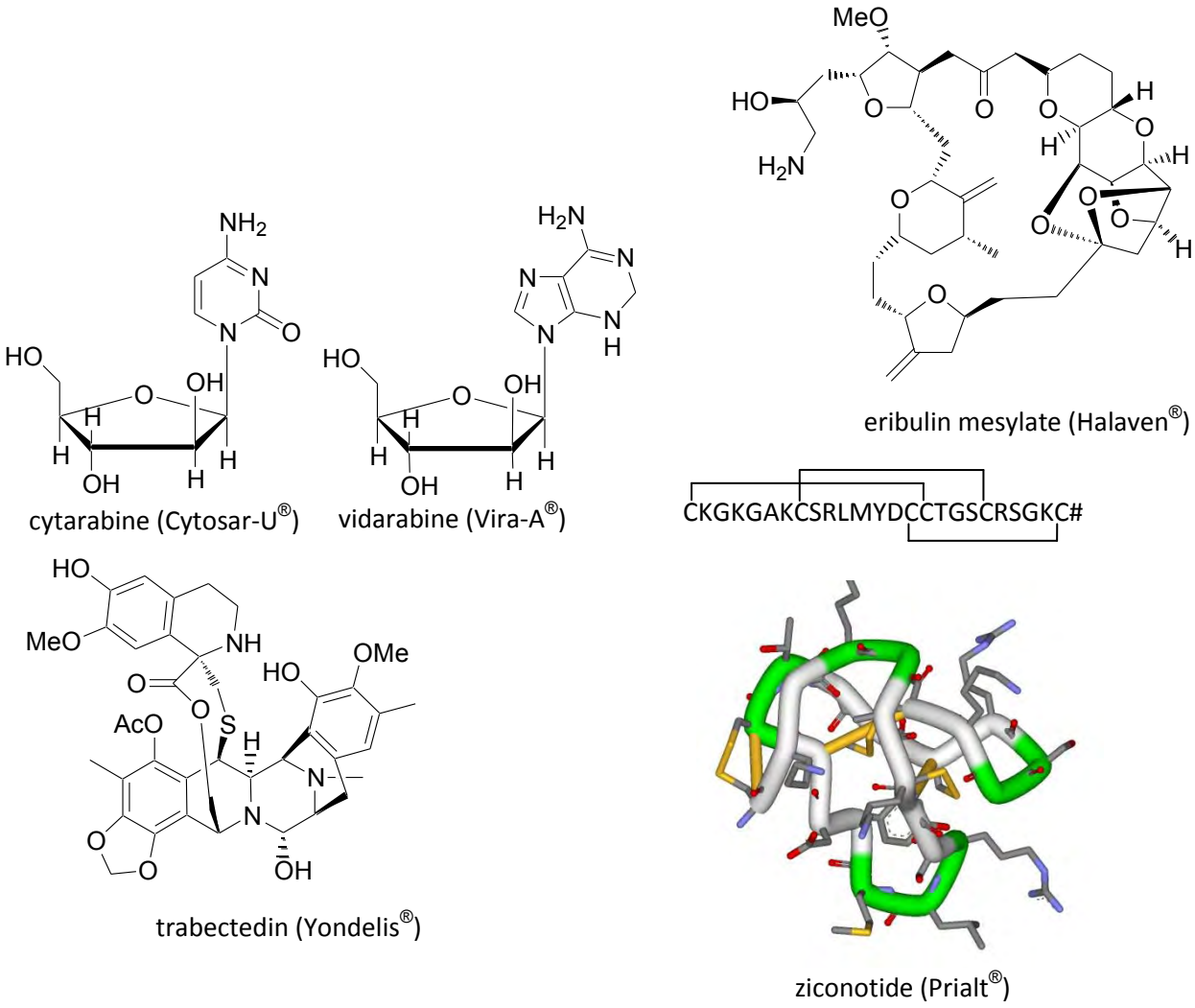

Figure 1.1: Current FDA or EMEA approved drugs of marine origin. The 3D structure of ω-conotoxin MVIIA obtained from the PDB (1TTK) visualized in DSVisualizer[21], peptide backbone tubes coloured by secondary structure and disulfide bonds indicated by large yellow tubes. Amino acid sequence above 3D structure, where # denotes the C terminus.

1.2.2. Phase III clinical trials of marine drug candidate

Currently Yondelis® is completing Phase III trial in the US for soft tissue sarcomas and ovarian cancer and awaiting FDA approval for sale in America. Solidotin is a synthetic derivative inspired by dolastatin 10 which was originally isolated from the sea hare, *Dolabella auricularia*[22,23] and subsequently from a marine cyanobacteria *Symploca sp*. Solidotin is a vascular disrupting agent which results in vasculature failure within tumors, thus resulting in the death of the tumor cells.[24]

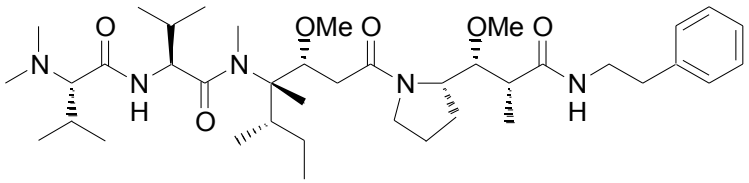

solidotin

Figure 1.2: Solidotin a marine inspired drugs currently in Phase III clinical trials.

1.2.3. Phase II clinical trials of marine drug candidates

Bryostatin 1, isolated from the bryozoan *Bulgula neritina,* has shown an ability to bind protein kinase C[5] and is currently being tested as an anticancer agent.[25] Bryostatin 1 has also recently been approved to begin Phase I clinical trials as an anti-Alzheimer's drug.[25] The full synthetic analogue of the marine *Aspergillus* metabolite halimide,[26] plinabulin inhibits tublin polymerization, leading to vascular disruption within the tumour resulting in the death of the cancer cells.[27] DXMBA is a synthethic analogue of an alkaloid, anabaseine, present in many marine worms (*e.g. Amphiporus lactifloreus*)[28] which selectively stimulates α7 nicotinic acetylcholine receptor.[29] This bioactivity has resulted in DXMBA being tested for the treatment of schizophrenia.[30] The new DNA-binding alkaloid Zalypsis® isolated from the Pacific nudibranch *Joruna funebris*,[31] binds to guanines in DNA resulting in double strand breaks, S-phase arrest and apoptosis in cancer cells.[5] Aplidin® was originally isolated from the Mediterranean tunicate *Aplidium albicans*, however, this compound is now obtained via total synthesis. Aplidin® is a potent inducer of apoptosis in cancer cells and is currently being tested for the treatment of relapsing and refractory multiple myeloma and T cell lymphoma.[32] Tasidotin is a synthetic compound inspired by the marine natural product dolastatin-15. The mechanism of action is thought to be inhibition of tubulin assembly resulting in cancer cell death.[5] Pseudopterosin A is an example of the pseudopterosin class of diterpenes isolated from the marine

octocoral *Pseudopterogorgia elisabethae*.[33-35] Pseudopterosin A has displayed anti-inflammatory and wound healing properties for which it is currently being tested in Phase II clinical trials.[36]

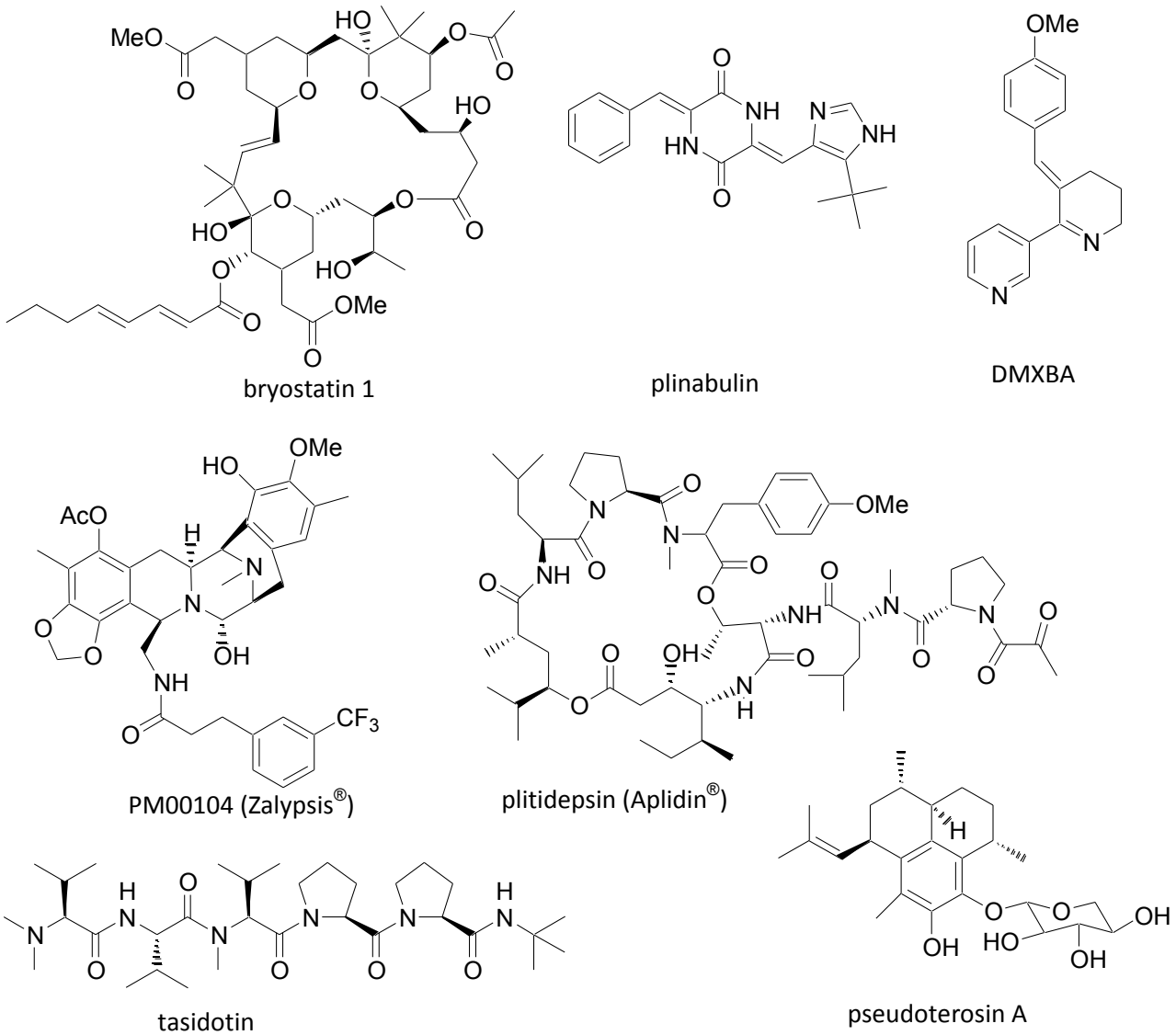

Figure 1.3: Marine inspired drugs currently in Phase II clinical trials.

1.2.4. Phase I clinical trials of marine drug cadidates

The nudibranch, *Elysia rufescens*, metabolite, Irvalec®, has shown potent antitumor activity against a variety of human tumour cell lines. While the exact mechanism of action is unknown, it has been reported that Irvalec® induces cell death via oncolysis as opposed to apoptosis.[5,25] The compound marizomib, isolated from the marine Actinomycete *Salinispora tropica*,[37,38] exhibits potent inhibition

of the proteasome[37] and is currently being tested in the treatment of various cancers.[5] Hemiasterlin which has been isolated from numerous marine sponges (*e.g.* the South African sponge *Hemiasterella minor*)[39] has shown antimiotic activity resulting in cancer cell death via apoptosis.[40] This lead to the development of synthetic analogues *e.g.* E7974 which is currently in Phase I clinical trials for solid malignant tumours.[25,40]

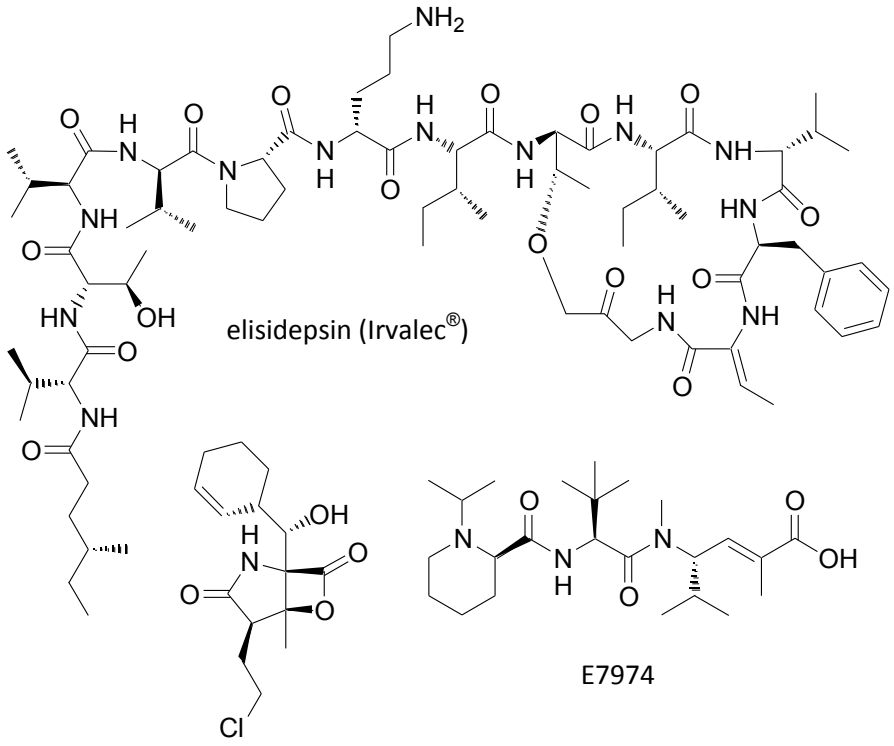

Figure 1.4: Marine inspired drugs currently in Phase I clinical trials.

1.3. Problems associated with marine natural products

1.3.1. The problem of intellectual property rights

A major concern to pharmaceutical companies is ownership of the intellectual property rights for the medical use of natural products. The Rio Convention on Biodiversity[41] highlighted the sovereign rights of countries, from where the natural products originates, ensuring equitable distribution to the host country of the resulting benefits arising from development of the bioactive natural product. With the pharmaceutical industry investing all the financial capital ($ 350 million total average cost

for the development of a drug),[42] the payment of intellectual property rights to a third party unaffected by the enormous financial risk inherent in the drug development process is unappealing.

1.3.2. The problem of dereplication

The general lack of expertise in the field of marine invertebrate taxonomy (with the exception of sponges) often results in the recollection of already studied invertebrates or poses a challenge in the re-isolation of invertebrates of interest.[43] The purification and structural characterization of complex crude mixtures of marine extracts is often difficult and time consuming, which may result in discovery of already known compounds, which cannot be patented.[44] The re-isolation of already known compounds may result in little or no return on investment to the pharmaceutical company and effective dereplication strategies (*e.g.* LCMS) are crucial to minimize wasted effort of time and economic resources.

1.3.3. The problem of supply

The demand for large quantities of test compound (several kilograms are required for the successful completion of preclinical and clinical trials) is often problematic for drug candidates isolated from marine organisms. For example in order to obtain 1 g of Yondelis® from a biological source, one metric tonne (wet weight)[45] of *Ecteinascidia turbinata* is required. The recommended dosage of Yondelis® is 1.5mg/m^2 body surface area every three weeks for the treatment of soft tissue sarcoma. An average male patient would therefore require 2.9 kg of *E. turbinata* every three weeks to provide the required amount of trabectedin. It is estimated that in 2011, 10 980 Americans will be diagnosed with soft-tissue sarcomas resulting in an estimated tri-weekly demand of 31.8 metric tonnes of *E. turbinata* to treat American patients alone.[46] The use of SCUBA in collection of source organism for marine natural products is often expensive and lengthy, while the use of dredging is non-specific and may lead to large patches of the ocean floor becoming uninhabited.[42] The three main methods for the production of marine natural products to solve the supply issue for use as drugs are; aquaculture, fermentation and organic synthesis.

1.3.3.1. Aquaculture

Due to the large quantities of biomass required in order to sustain the supply of the bioactive compound an easily accessible source must be available, *i.e.* the development of aquaculture. The aquaculture of the sponge *Lissodendoryx sp.* (producer of halichondrin B) will be discussed as a case study to illustrate a few of the problems associated with this method of providing a sustainable supply of a marine natural product drug. *Lissodendoryx sp.* is a deep water sponge growing exclusively on the Kaikoura Peninsula, New Zealand. In 1998 a ~5 km^2 'sponge field' was discovered by a remotely operated underwater vehicle (ROV) with a calculated biodensity of 69 ± 21 $g.m^{-2}$ resulting in an estimated biomass of 289 ± 90 tons of *Lissodendoryx*.[47] Should the entire 'field' be harvested, the total yield of halichondrin B would be 62-118 g, enough to sustain 1.2-2.3% of the estimated annual requirement of halichondrin B.[45] Therefore, the New Zealand National Institute of Water and Atmospheric Research (NIWA), in collaboration with University of Canterbury and the National Cancer Institute (NCI) conducted a *Lissodendoryx* aquaculture feasibility study.[47] It was soon discovered that seasonal factors played a huge role in the success of sponge aquaculture with a summertime mortality rate of 95% dropping to 15% in the wintertime.[47] With the increased winter survival rate Munro *et al.* turned their attention to determining whether halichondrin B was being produced under these artificial conditions. They found that the cultured sponges were indeed biosynthesizing halichondrin B, however at only 30-60% of the yield of halichondrin B produced by the wildtype *Lissodendoryx* sponge. This reduced production would of course lead to a greater requirement of cultured biomass resulting in a need for a larger area for aquaculture.[47]

1.3.3.2. Fermentation

A comparison of natural products isolated from sponges, tunicates and other marine invertebrates to those isolated from a microbial origin often have a significant structural similarity, suggesting that the biosynthesis of many marine metabolite may in fact be microbial rather than originating from the marine invertebrate. Filter feeders may incorporate large microbial colonies (endosymbionts) accounting for up to 40% of the sponge's biomass.[45] The discovery of these endosymbiots lead to research being developed in order to isolate and cultivate these putative producers of bioactive metabolites. However, many bacteria and cyanobacteria are highly selective with regards to growth media and conditions, resulting in less than 1% of the microbes present in the marine invertebrate tissue being culturable.[45] The development of novel growth media for sponge-associated bacteria may result in the fermentation of previously un-culturable marine bacteria, affording access to large

quantities of bioactive materials. While bacteria may not produce the complete natural product of interest, microbes may produce a structurally similar compound which could be used a precursor in the semi-synthesis of desired bioactive compound. For example in the case of trabectidin, two thirds of the complex chemical structure is biosynthesised by the culturable bacteria *Pseudomonas fluorescens* in the form of cyanosafricin B.[48] Cuevas *et al.*[49] have described a semi-synthetic pathway to trabectidin using cyanosafricin B as a precursor which has enabled PharmaMar to meet global demands for trabectidin (*ca.* 5 kg *p.a.*).

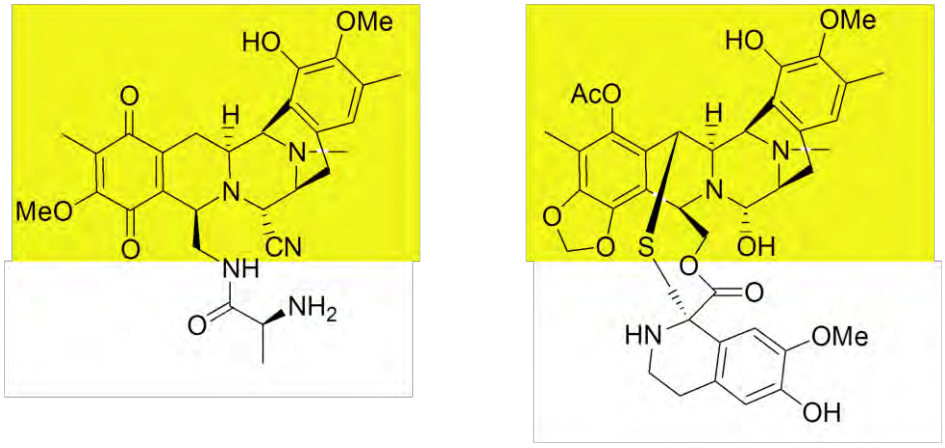

cyanosafriacin B trabectedin (Yondelis®)

Figure 1.5: Structural similarities between cyanosafriacin B and trabectedin.

1.3.3.3. Synthesis

The design of a synthetic route from commercially obtainable reagents is by far the most appealing option in the manufacture of the marine natural products, however many marine natural products are complex; containing numerous sites of oxygenation and an abundance of chiral centres often resulting in intricate and low yielding synthetic pathways.[50] However, should the complexity of marine natural products hinder the development of an economically viable synthetic route, marine natural products are often used as 'lead' drug compounds, where a compromise between synthetic cost and loss of bioactivity is reached.[42] Eribulin mesylate is a good example of how a simpler and synthetically more accessible analogue of a marine natural product (halichondrin B) has proceeded into development.

1.4. Conclusion

Despite the numerous challenges in the development of drugs from Nature, it still remains the most viable cornucopia of potential drugs.[44] The estimated total number of species on this planet is approximately 2-100 million species, with many yet undiscovered.[44] The potential for these numerous species to produce medicinally exploitable compounds is huge.

1.5. Outline of this thesis

In Chapter 2 overviews are presented of firstly, the lifecycle of malaria parasite, *Plasmodium falciparum*, and secondly naturally occurring antiplasmodial marine isonitriles and isothiocyanates. This chapter provides an entre to the syntheses described in Chapter 3 and the *in vitro* haem binding analyses in Chapter 4. Chapter 3's primary focus is on improving the antiplasmodial activity of compounds derived from the naturally occurring botanical diterpene (+)-manool. We proposed that, due to the potent antiplasmodial of marine isonitriles, the conversion of the tertiary alcohol functionalities contained on the tricyclic scaffold of the manool derived compounds to isonitrile moieties would considerably increase their antiplasmodial activity. In Chapter 4 naturally occuring marine isonitriles' ability to inhibit a well established druggable target, *i.e.* the detoxification of haem by the malaria parasite, is explored in an effort to try and shed light on a possible mode of action for these marine compounds. With the technological advances in molecular modelling, we revisit a haem/isonitrile interaction originally proposed a decade ago in an effort to better understand the type of molecular forces involved. Finally, in Chapter 5 we describe an improved synthesis of the natural product dexotopsentin with the use of microwave assisted organic (MAO) synthesis, which is quicker and higher yielding than previously reported syntheses. Our synthesis offers an accessible route to structurally related bisindole alkaloids for the possible development of compounds as molecular probes to explore the inhibition of pyruvate kinase in methicillin resistant *Staphylococcus aureus* (MRSA).

CHAPTER 2: ANTIPLASMODIAL MARINE ISONITRILES

2.1. Malaria

2.1.1. Global distribution of malaria

Although in the past century there have been many successful developments to eradicate the malarial parasite, malaria continues to be widespread. The 2011 WHO fact sheet reports that there were 225 million reported cases of malaria, 781 000 resulting in deaths in 2009.[51] The increase in the spread of malaria has been attributed to several factors including, population movements to malaria infected areas, changes in agricultural practices such as the building of dams and irrigation systems or deforestation, the weakening of public health systems, global climate changes and resistance to antimalarial drugs and insecticides.[52] With the current population growth rates in malaria riddled regions it has been estimated that without effective intervention the cases of malaria will double within the next 20 years.[53]

The global distribution of malaria is centred in the tropics although not confined to this region of the world. Many efforts have attempted to suppress the disease, however these only seem to have been successful in the temperate regions of the globe. This is due to, among other factors, the decreased rate of reproduction of the plasmodial parasite at lower temperature. As the ambient temperature declines, the period for development of the parasite in the mosquito vector increases. If the average temperature drops below 18 ^{o}C the likelihood of transmission becomes less due to the parasite failing to achieve maturation in the lifespan of the mosquito vector. At temperatures lower than 16 ^{o} C the malaria parasite ceases to develop and many species of mosquito postpone biting activity at these low temperatures.[52] The large transmission rate within sub-Saharan Africa has been attributed to the vector, *Anopheles gambiae*, and its high preference towards anthropophily (human biting). Ninety percent of all the fatal cases of malaria occuring in Africa result from *Plasmodium falciparum*.[52] Infection by other plasmodia species may also cause malaria. *Plasmodium malariae* is transmitted throughout the topics and subtropics, although widespread the locations are patchy, *P. vivax* is located throughout the tropics however, this species is uncommon in most of Africa, while *P. ovale* is predominantly found in tropical Africa.[54]

2.1.2. *Plasmodium* biology

2.1.2.1. Differentiation of the parasite within the mosquito

The parasite enters the mosquito when it feeds on an infected host's blood ingesting the *Plasmodium* gametocytes. The gametocytes travel to the posterior midgut lumen, where bloodmeal storage, digestion and absorption occur.[55] Only on the ingestion of the bloodmeal into the mosquito's midgut do the gametocytes differentiate to form gametes.[56] Minutes after ingestion exflagellation takes place whereby each male gametocyte differentiates into eight haploid motile gametes (microgametes). The onset of exflagellation is brought about through a drop in temperature from 37 ^{o}C to 28 ^{o}C, an increase in pH and the addition of the gametocyte-activating factor (GAF), xanthurenic acid.[57] By comparison the female gametocytes undergo very little morphological development, with their shape becoming rounder and enlarged to form female gametes (macrogametes). Fertilization occurs within the midgut when the plasma membranes of the micro and macrogametes fuse, resulting in the microgamete's nucleus travelling into the macrogamete's cytoplasm and passing through the macrogametes endoplasmic reticulum to combine with the macrogamete nucleus to form the diploid zygote.[58-60] The fertilized zygote undergoes transformation into motile ookinetes, little is known about what controls this development. These ookinetes have to transverse two barriers; the peritrophic matrix (PM) and the midgut epithelium. The PM is a chitinous network secreted by the midgut epithelial cells in response to the ingested bloodmeal. In order to cross this barrier the ookinetes secrete a pro-chitinase,[61] which is assumed to cause physical damage to the PM affording access to the midgut epithelium. The invasion of the epithelial cells is initiated by the adhesion of the ookinetes to the mircovillar surface of the epithelial cell membranes.[57] It appears that the ookinetes preferentially invade Ross cells, a specific type of epithelial cell, which has fewer microvilli and has an abundance of vesicular ATPase.[62] After crossing the midgut epithelium, the ookinete encounters an extracellular space between the midgut epithelium and the basal lamina, where it develops into an oocyst. Within each oocyst the parasite undergoes huge asexual amplification known as sporogony. Once the oocyst is fully mature it results in the mass release of thousands of sporozoites into the hemocoel. Once in the hemocoel the sporozoites travel to and invade the salivary gland epithelium. The sporozoites only remain within the cytoplasm of the salivary glands temporarily and soon exit into the secretory cavity where the sporozoites are organised into bundles (Figure 2.1 and 2.2). Once in the secretary cavity of the mosquito's salivary glands each time the mosquito feeds small numbers of sporozoites are injected into the vertebrae host infecting them with the plasmodial parasite.[57]

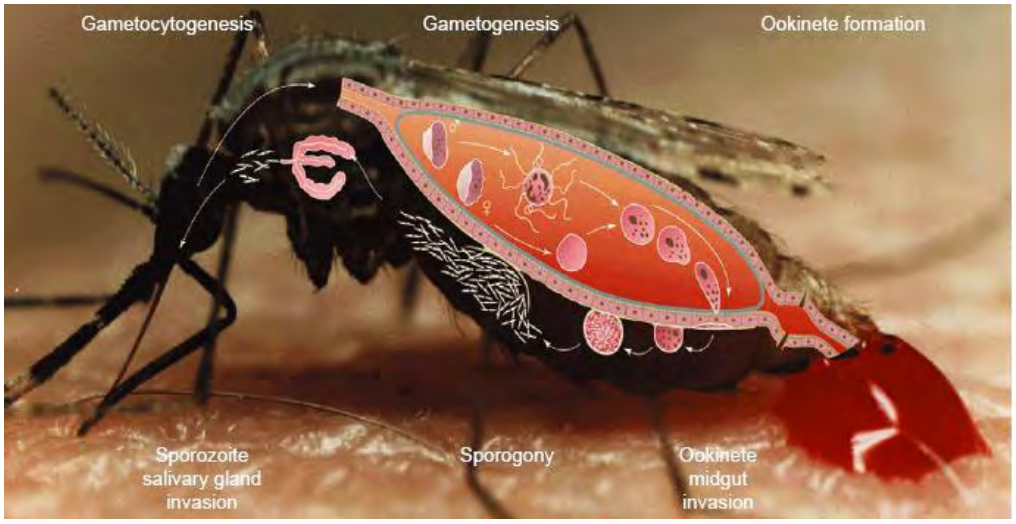

Figure 2.1: The lifecycle of the *P. falciparum* in the mosquito vector.[55]

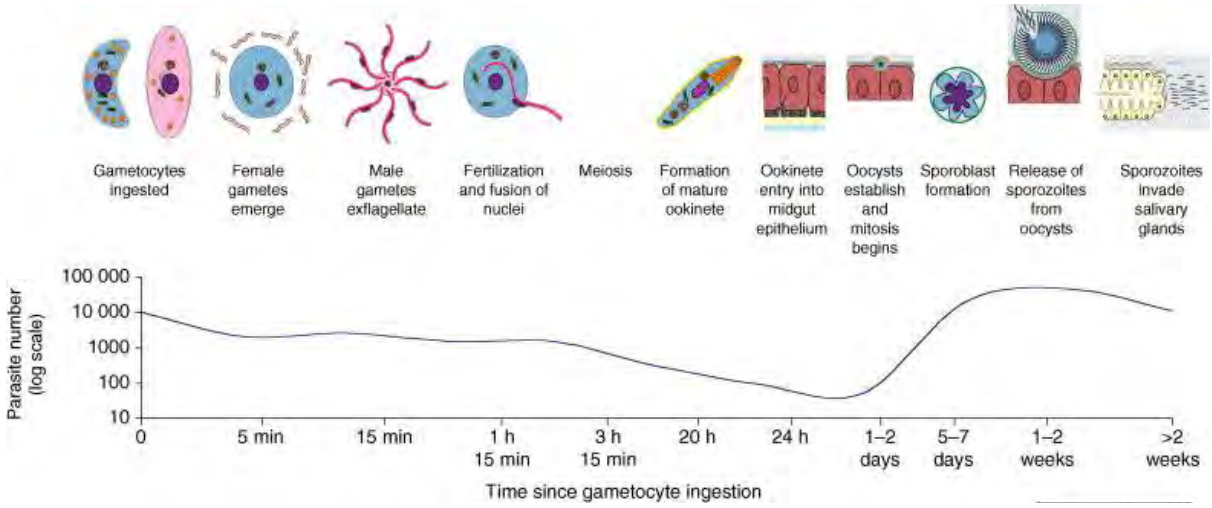

Figure 2.2: The lifecycle of *P. falciparum* within the mosquito vector. The graph illustration parasite population decrease and increase with time in the mosquito.[55]

2.1.2.2. Differentiation of the parasite within the human host

The female *Anopheles* mosquito feeds it does so by either cannulating blood from pools generated by damaged capillaries or directly from larger subcutaneous blood vessels.[63] While feeding the mosquito vector releases a small number of sporozoites into the bloodstream.

Differentiation in the human host occurs in two stages, the hepatic stage (Figure 2.3), and the erythrocytic stage. Within minutes of entering the bloodstream the sporozoites reach the liver cells beginning the hepatic stage.[64] The classic liver lobule consists of a dual blood supply consisting of

the portal venule and hepatic arteriole entering at the portal field, which also includes the bile duct (Figure 2.3A). The blood supplies merge when entering the liver lobule, travel through the sinusoids and exits via the central vein. Found within the sinusoids are Kupffer cells, these cells are macrophages tasked with the removal of foreign substances from the blood (Figure 2.3B).[65] The *Plasmodium* sporozoites enter the liver sinusoid through the portal venule and hepatic arteriole and travel along the endothelia cells until coming into contact with a Kupffer cell (Figure 2.3C).[66] The sporozoites invade and safely navigate the Kupffer cells, by surrounding themselves with a vacuole which does not fuse lysosomes.[65,67] The sporozoites exit the Kupffer cell intact into the space of Disse, where the sporozoites quickly invade hepatocytes. However, the sporozoites do not develop within the first invaded cell but migrate through several hepatocytes (Figure 2.3D). Little is known about the entry into the finial hepatocyte, or even development within the hepatocyte. But what is known is the sporozoite surrounds itself with a parasitophorous vacuole inside which it develops into an exoerythrocytic form (EEF).[68] Development into the EEF involves morphing of the elongated sporozoites into a spherical form (Figure 2.3E).[69] The EEF is the intermediate tissue stage between the mosquito vector and erythrocytic stage.[70] The EEF grows to several sizes larger than that of the host cell and undergoes multiple rounds of nuclear division and differentiate into thousands of merozoites which eventually initiate the erythrocytic stage (Figure 2.3F).[71] The growth and replication of nucleic acid in the liver is far greater than schizogony experience in the blood stage. This is due to the large stores of glycogen found in hepatocytes *i.e.* a large supply of nutrients to fuel schizogony.[65] The merozoites held together by the hosts cytoplasm swell into the sinusoidal lumen and eventually rupture releasing the merozoites (Figure 2.3G).[72]

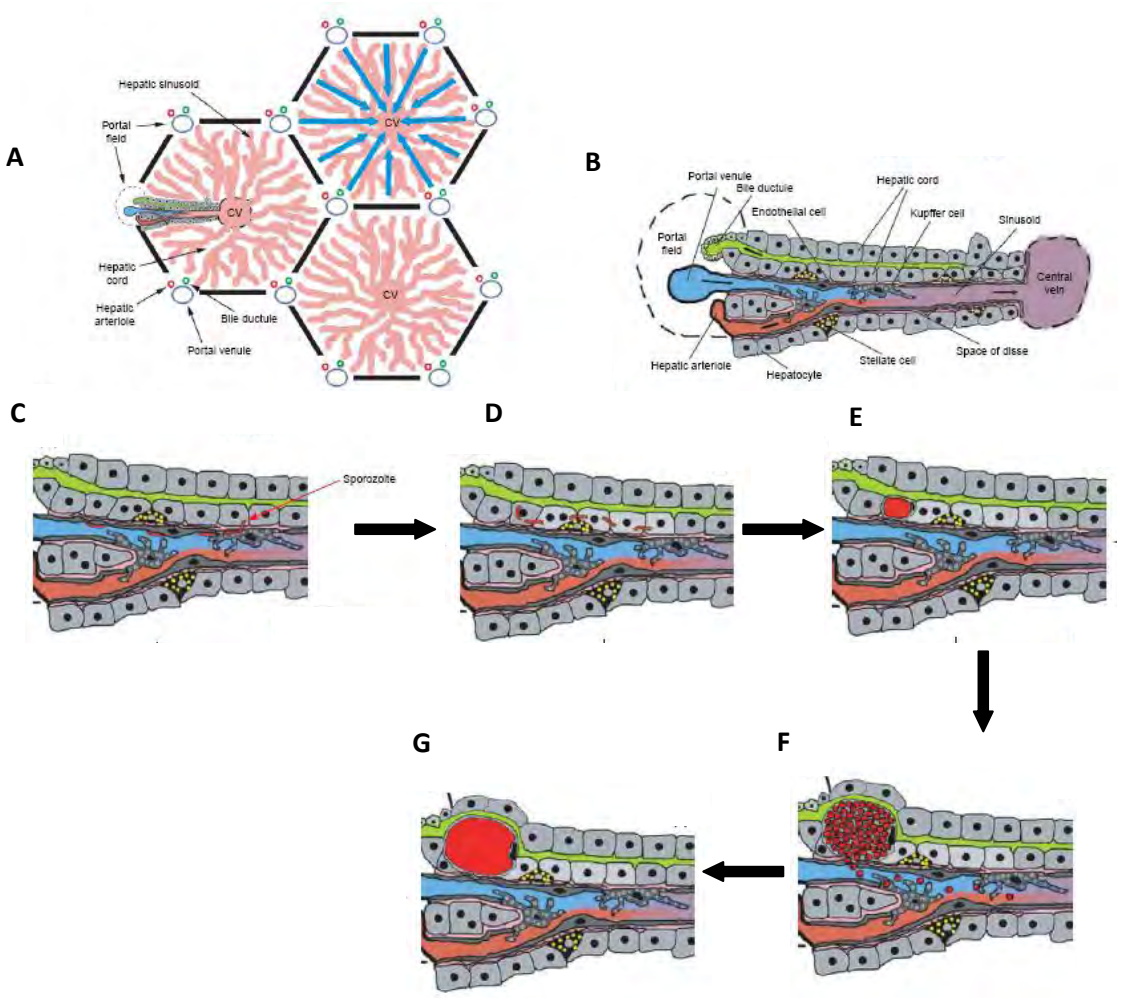

Figure 2.3: A: A healthy liver lobule, the portal venous and arterial supply blood to the liver cells entering the liver lobule at the portal filed. These two blood supplies merge after entering the sinusoid, flow along the hepatic cord and exit via the central venule. B: The hepatic sinusoid is lined with Kupffer cells, which are separated from hepatocytes by the space of Disse. C: A sporozoite (indicated by a red arrow) glides along the hepatic sinusoid until if finds a Kupffer cell, which it evades, passes through and enters a hepatocyte. D: After transmigrating several hepatocytes, the sporozoite will settle in a final hepatocyte and begin to grow. E: The sporozoite begins to grow displacing the hepatocyte's organelles. F: The infected hepatocyte may contain thousands of mature merozoites. G: The hepatocyte finally ruptures releasing the mature merozoites into the sinusoid, to be transport around the body.[65]

Once released into the venule, the merozoites randomly attach themselves to cells surfaces until they finally come into contact with an erythrocyte surface. Once attached to the erythrocyte surface the merozoite reorientates itself to bring its apical prominence into contact with the host cell. The apical prominence is tightly bound to the surface via parasite receptors binding to ligands on the erythrocyte membrane. The proteins required for this binding are secreted or located from or on the apical prominence. The invasion of the cell is initiated by the secretion of a material which creates an invagination (invasion pit) in the host cell. The parasite moves deeper into this cavity until the erythrocyte membrane seals itself off at the posterior of the merozoite. This enclosure is

called the parasitophorous vacuole (PV), whose membrane is made up of both the erythrocyte lipid bilayer and the secretions of the merozoite.[73] Once in the erythrocyte the merozoites loses its invasion organelles and begins to differentiate into a spherical trophozoite (ring stage). The trophozoites increases in size and under goes multiple rounds of schizogonic division eventually causing the erythrocyte to rupture releasing new merozoites into the bloodstream able to invade further erythrocytes.[74] Development of merozoites in the erythrocyte takes approximately 48 hours, resulting in around twenty merozoites per mature parasite.[75] The merozoites only remain in the bloodstream momentarily, roughly 60 seconds, before infecting another erythrocyte to continue the cycle.[76] With the rupture of each erythrocyte the parasite's waste is also released into the blood stream, causing some of the clinical symptom experienced by patients, including fever, chills, headaches, adnominal and back pains, nausea, diarrhoea and occasionally vomiting. During the maturation into trophozoites the erythrocyte loses its biconcave shape and becomes spherical[77-79] and produces adhesive proteins which allow these altered erythrocyte to stick to the lining of blood vessels.[75,80] The purpose of the adherence to the epithelial lining is to protect the parasite from annihilation as free circulating infected erythrocytes are disposed of in the spleen.[81] During the asexual cycle in the erythrocytic stages, a few merozoites develop into male and female gametocytes. These are in turn released into the blood circulation where they are ingested as part of the bloodmeal of the mosquito, continuing the cycle of infection.[82] While the parasite is in the erythrocyte it is greatly dependent upon the digestion of haemoglobin, for the parasite to continue functioning.

2.1.2.3. The digestion of haemoglobin within the erythrocyte by *P. falciparum*

The parasite, which is now contained within the erythrocyte's cytoplasm, creates an invagination at the parasitophorous membrane, engulfing the host cytoplasm (which predominantly consists of haemoglobin) in a pinocytic fashion. This newly formed transport vesicle delivers the haemoglobin to the parasites' food vacuole. The food vacuole is an acidic environment which contains several parasitic proteases, some of which are responsible for the hydrolysis of the haemoglobin into smaller peptide fragments essential for the parasites protein synthesis.[83] The parasite has been shown to digest between 60% - 80% of the total haemoglobin contained within the infected erythrocyte.[84] In the process of the catabolism of haemoglobin, ferrous haem (Fe(II)-protoporphyrin IX) and oxygen is released. Free haem is highly toxic to the cells as it causes inhibition of enzymes, peroxidation of membranes and production of oxidative free radicals, the latter two leading to lysis

of both the erythrocyte and the malaria parasite.[83] The reduced free haem is oxidised to its ferric form (FP-Fe(III)). Due to the high concentration of oxygen and acidity within the food vacuole, oxygen radicals are produced via the Fenton[85] and Haber-Weiss[86] reactions.[87] The oxygen accepts the electrons from the iron, contained in haem, initiating the chain of oxygen radical species metabolism.[87] At the pH 5, as in the digestive vacuole, the superoxide anion is spontaneously converted to H_2O_2 and O_2, leaving the parasite with even a greater problem of disposing of the even more toxic peroxide (Scheme 2.1).

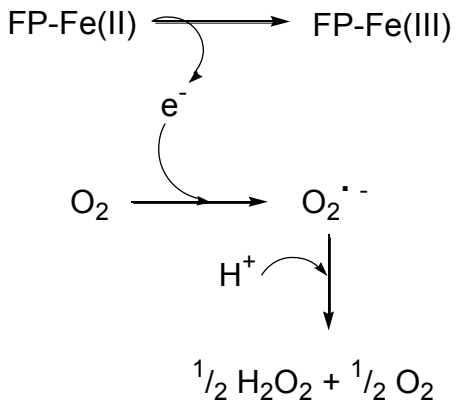

Scheme 2.1: The ferrous iron catalysed formation of hydrogen peroxide.[88]

The parasite does possess an oxidant defence system consisting of superoxide dismutase and glutathione peroxidase,[89,90] however these are thought to be predominately concentrated in the parasite's cytoplasm. A temporary solution exists in which the parasite uses the host's enzymes, which the plasmodia obtains when the parasite engulfs haemoglobin, however these proteins are quickly degraded by enzymes within the food vacuole, leaving the vacuole vulnerable to oxidative damage.[91] Haem can also react with H_2O_2, displaying both catalase-like and peroxidase-like activity. The hydrogen peroxide oxidises the porphyrin ring, to form an active intermediate FP-Fe(IV)* that participates in the catalase-like reaction of H_2O_2 to O_2 and H_2O reducing the porphyrin ring back to FP-Fe(III) (Scheme 2.2). The intermediate FP-Fe(IV)* can also be involved in the peroxidise-like oxidation of glutathione, protein or lipids. Alternatively the oxidation of FP-Fe(III) by H_2O_2 can destroy the porphyrin ring.[88]

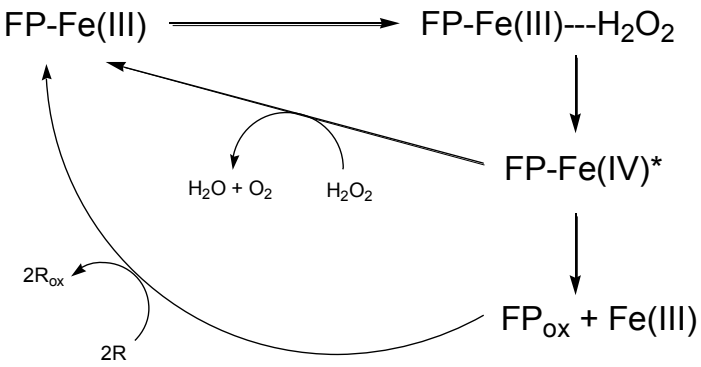

Scheme 2.2: A proposed mechanism for the catalase and peroxidase-like activities of haem.[88]

As previously stated the catabolism of haemoglobin yields toxic monomeric haem. Although FP-Fe(III) is relatively insoluble in the acidic aqueous solution that is contained within the food vacuole, however it can still potentially dissolve in the non-polar lipid membrane.[92] In most higher organisms haem is processed by the enzyme haem oxidase which breaks down the porphyrin ring releasing carbon monoxide, ferric ions and biliverdine.[93] The malaria parasite, however, uses a different method of detoxification, *viz.* forming a haem-polymer, named hemozoin. The advantage of not using haem oxidase is the prevention of potential toxicity problems that may arise from the release of iron and carbon monoxide.[94] It has been found that hemozoin contains a penta-valent iron (III) complex in a high spin state. The central iron atom is coordinated to the four adjacent nitrogen atoms contained in the planar porphyrin ring while the fifth bond results from the oxygen contained in the acid side chain of another haem unit (See Chapter 4).[95,96] In the past two decades there has been much debate on the cause of this polymerization, which will be further discussed in Chapter 4. Regardless of the polymerization mechanism it has been shown that hemozoin is far less active in causing membrane peroxidation.[97] The detoxification of haem will be discussed in greater detail in Chapter 4.

2.1.3. Chemotherapy

The growing severity of malaria infection has elevated this disease to one of the top three commutative diseases. Malaria is on the rise due mainly to a growing resistance of the parasite to antimalarials, resistance of the *Anopheles* mosquito to insecticide as well as the limited resources of many malaria-epidemic countries. It seemed decades ago that malaria might go the same way as smallpox and be completely eradicated however, this is anything but the case.[98] The malaria

parasite is showing resistance to many of the old and newer drugs on the market, this may be due to several factors including; the use of inferior counterfeit drugs,[99,100] poor diagnosis,[101,102] and/or the unique ability of the parasite to develop resistance to these drugs.[103] Another issue, paralleling the crisis of resistance, is the unwillingness of major pharmaceutical companies to develop new antimalarials. The antimalarial market is one of the largest medical markets to date with near to half a billion treatments required each year, however the majority of patients are poor and cannot afford to pay for treatment. Hence there is very little appeal to the pharmaceutical companies to invest major amounts of money on drugs which will see them little or no return on their investment.[104]

For a successful antimalarial, one needs to exploit the metabolic differences between the host and parasite. The continued emergence of resistance to currently available drugs necessitates the urgent need for the development of new drugs, either for existing drug targets or for newly discovered biochemical pathways.[105]

When malaria is referred to in this thesis it refers to malaria caused by the most prominent of the species in the infection of humans, *P. falciparum*, unless stated otherwise. For the purposes of this thesis currently available antimalarial drugs will be divided into two classes, blood schizontocides (Figure 2.4) and nucleic acid inhibitors (Figure 2.5), with the primary focus on blood schizontocides and more specifically the aminoquinolines.

2.1.3.1. Blood schizontocides

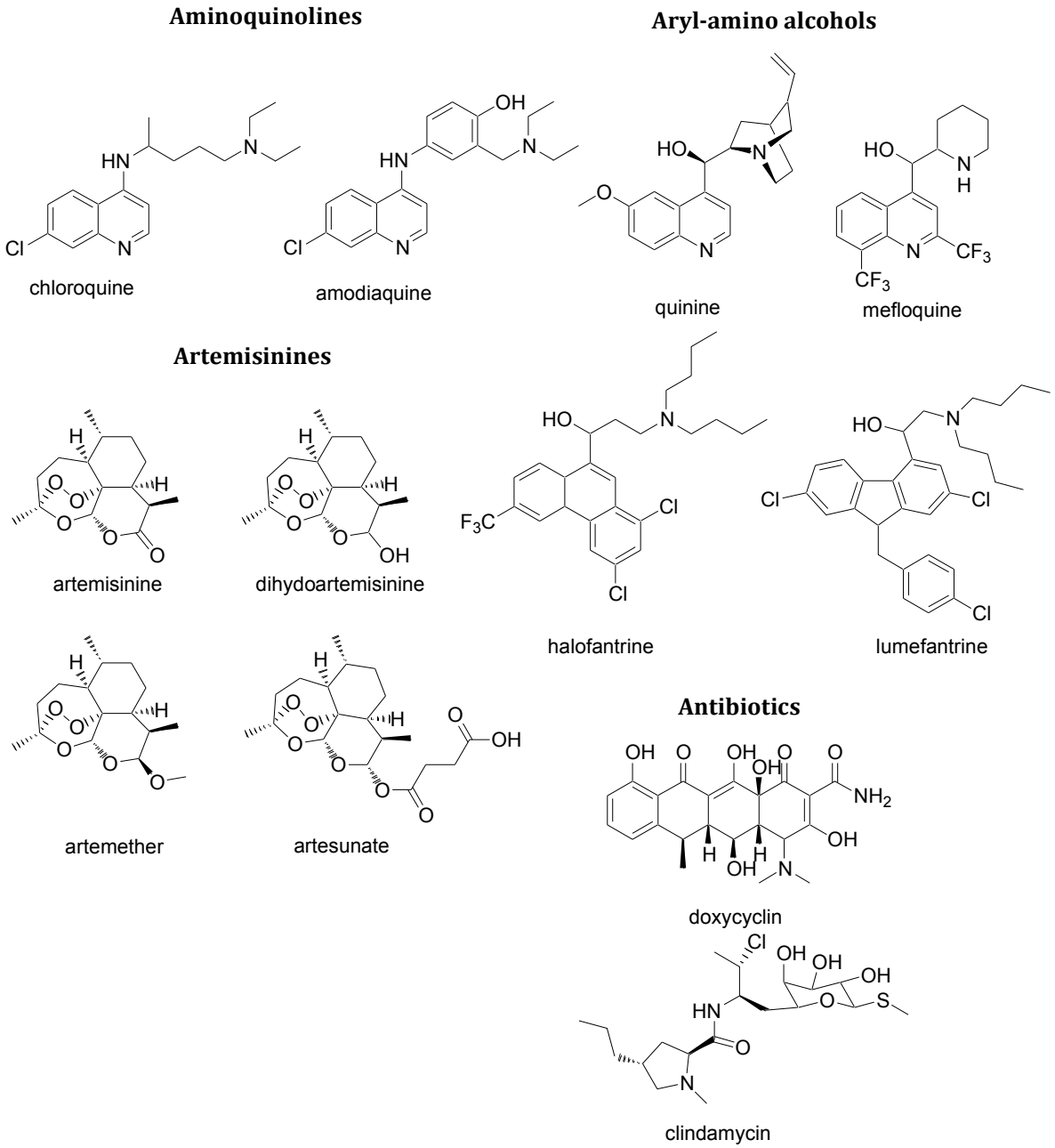

Figure 2.4: Some commonly used antimalarial drugs targeting the blood schizonts.

Quinoline containing drugs are some of the most common drugs in the treatment of malaria. Quinolines are divided into two classes: the aminoquinolines (*e.g.* chloroquine) and the aryl-amino alcohols (*e.g.* quinine) which differ in their physical properties at a neutral pH.

The two major drugs in the aminoquinoline class are chloroquine and amodiaquine (Camoquin®). In the 1940s, while testing for less toxic analogues of quinine, chloroquine was produced.[106] Until the

development of resistance in the 1960s, chloroquine was the most widely used antimalarial,[107] its popularity was due to chloroquine's low cost of production and lack of side effects. Amodiaquine is effective as a treatment by itself, however it is most potent in combination with chloroquine. Amodiaquine is only effective in parasites that have developed a low level of chloroquine resistance.[108] In most western countries amodiaquine is no longer available due to its readiness to undergo biotransformation of its *p*-aminophenol moiety into a toxic quinoneimine, resulting in severe heptotoxicity and agranulocytosis .[108-110] These effects seem to occur over a prolonged exposure to amodiaquine, thus it is still possible to safely use this drug in shortened therapeutic regimes.[111] Chloroquine still remains a major course of treatment for malaria induced by *P. vivax, P. malariae,* and *P. ovale*.[54] Aminoquinolines interfere with the sequestration of haem thus poisoning the parasite on its own metabolic waste and this mechanism will be discussed further in Chapter 4.

The mechanism of action for aryl-amino alcohols is not completely understood, however it does differ from that of aminoquinolines. This class of drugs also seems to interfere with the digestion of haem.[112,113] Quinine is the earliest of all antimalarials, which has been used in one form another for the past 350 years. It was first discovered in South America, where it is found in the bark of the *Cinchona* tree that the local inhabitants used as an antipyretic agent.[114] In the seventieth century it was imported to Europe from Peru to be used as an antimalarial.[115] Quinine is still used today for uncomplicated malaria[116] and is often the only choice for life-threatening cerebral malaria.[117] Quinine has multiple side effects, most of which are not permanent, but some are severe such as its arrhytomogenic potential and the release of insulin which may result in hypoglycaemia.[107] If quinine is used over a prolonged period vasculitus,[118] haemolytic-uraemic syndrome,[119] and thrombocytopaenia[120] may develop. Due to the dependence on raw materials required for the extraction of quinine a need arose for synthetic substitutes which led to the discovery of many new antimalarials. Melfloquine has been used for more than two decades and is regarded as a structurally simplified version of quinine. Melfloquine, when used as a prophylactic, results in neuropsychiatric side effects, such as insomnia, depression and panic attacks. Halofantrine is another quinine analogue but is linked to an increase risk of cardiac arrythmias, as prolonged use inhibits the inward K^+ ion flow.[108] For this reason halofantrine has been withdrawn from several countries.[107] Lumefantrine is less effective against malaria than halofantrine, but lacks the cardiac side effects.[121]

Artemisinine is a natural product which is active against malaria. Artemisinine it is derived from the Chinese herb 'qinghao' (*Artemisa annua*), which was traditionally used in the treatment of fevers.[115]

Many synthetic analogues of artemisinine have been developed which have greatly decreased the cost of this class of antimalarials.[122] Artemether is a more lipophilic molecule than artemisinine and is better absorbed from the gastrointestinal tract, allowing it to be taken orally.[123] Due to the carboxylate fuctionality in artesunate, this drug is a hydrophilic molecule, requiring intravenous administration. This is important in severe malaria case as the patient is often in a state where no other mode of administration is possible.[98] Once in the body all the artemisinines are metabolised to the active dihydroartemisinine. These drugs predominately target the late ring stages, but also act against the small ring stages present in the erythrocytes hours after infection.[124] This class of drugs is highly active in the reduction of the parasites biomass, dropping it 10 000-fold in a single asexual cycle.[125,126] The mode of delivery make artemisinines the most rapid and active drugs in the fight against malaria to date.[107] The pharmacaphore in dihydroartemisinine appears to be the endoperoxide bridge. This has been shown to be broken down by ferrous ions, in the parasites digestive vacoule, resulting in carbon-centred radicals. These radicals in turn alkylate and oxidize proteins and lipids and modify haem[107,127] as well as inhibit a calcium pump (*Pf*ATP6) located on the endoplasmic reticulum.[128] Another proposed method of activation of these drugs is the reductive cleavage of the peroxide bond by iron-sulphur redox centres, which are commonly found in *Plasmodium* enzymes, and that the alkylation of these enzymes may result in the death of the parasite.[129]

Many of the antibiotics show no visible effect on the first erythrocytic intracellular cycle, but rather on the second cycle. The parasites are killed shortly after the second invasion of the erythrocyte. This is known as the 'delayed death phenotype' or 'the delayed kill effect'.[130,131] Antibiotics, therefore, show far longer fever and parasite clearance times when compared to classic antimalarial drugs. Thus antibiotics are used in combination with faster acting drugs in the treatment of acute malaria. The classical antimalarials rapidly reduce the number of parasites while the antibiotic continues to kill any remaining or resistant parasites. Doxycycline is predominately used as a prophylactic but may, in combination with quinine or artesunate, be used in the treatment of uncomplicated or even severe malaria.[132] Doxycycline's major side effects include increased photosensitivity, gastrointestinal disturbances, enamel hypoplasia and depression of bone growth. Due to its effect on developing bones and teeth, doxycycline is unsuitable for children under eight or pregnant women.[107] Clindamycin is used as an alternative to doxycycline in the treatment of malaria, since it is considered safe during pregnancy and for the use in young children.[133] Antibiotics act on the prokaryote-like protein synthesis machinery of the mitochondria and/or apicoplast.[130,134] The antibiotics are thought to inhibit protein synthesis by binding to the 30S ribosomal subunit preventing the 50S and 30S units from bonding.[130]

2.1.3.2. Mechanism of resistance to chloroquine-type antimalarials

For the purposes of this thesis only chloroquine resistance will be discussed in detail while a summary of resistance to the remaining drugs is presented in Table 2.1. Chloroquine resistance is present wherever *P. falciparum* malaria is prevalent. Resistance to chloroquine was first reported in 1957 on the Thai-Cambodian border.[135] However, by 1980 all of South America was affected and by 1989 all *P. falciparum* located in Asia and Oceania were resistant to chloroquine. In East Africa the first case of chloroquine resistance was documented in 1978, and subsequent chloroquine resistance spread to central and southern parts of Africa finally arriving in West Africa by 1989.[136] Due to the high levels of chloroquine resistance many countries in Africa have changed their first-line treatment of malaria to sulfadoxine-pyrimethamine or a combination of chloroquine and sulfadoxine-pyrimethamine (Figure 2.5).[137] The distinguishing difference between chloroquine resistance and chloroquine-sensitive clones is the degree to which chloroquine accumulates in the food vacuole.[138,139] Since drug resistance is related to the decrease in concentration of the drug in the food vacuole there are two possible pathways that are affected by resistance. Firstly the parasite may take up less of the drug into the food vacuole and secondly the drug may be expelled from its food vacuole.[98] If the uptake of chloroquine was totally dependent upon passive diffusion of the drug into the food vacuole (*i.e.* dependent on a pH gradient), a hindrance in the proton pumps should alter the pH of the food vacuole and hence the concentration of chloroquine. However Geary *et al.*[140] showed little difference in the pH, assuming then that the transport of chloroquine into the cell must be an active process. The idea of an expulsion mechanism was supported by Krogstad *et al.*[141] by showing that resistant parasites expel 40-50 times more chloroquine than chloroquine-sensitive parasites from the food vacuole of the parasite. This removal of chloroquine from the food vacuole, is why the primary focus of chloroquine resistance in *P. falciparum* has been on the polymorphism of two genes, the *pfcrt*[142] and the *pfmdr1*,[143] which code for a membrane transporter protein and glycoprotein homologue 1 (Pgh1) respectively. The major mutation of the *pfcrt* gene product in chloroquine-resistant strains is the substitution of Thr^{76} for Lys^{76} and has been found in resistance strains throughout Africa,[142,144-146] Asia[147,148] and South America.[149] The mutation of the Thr^{76} has also been shown to be present in chloroquine-sensitive strains, indicating that other mutations of *pfcrt* are necessary or other genes are involved.[137] Pgh1 has shown several cases of polymorphism associated with chloroquine resistance, the point mutation of Asp^{86} to Tyr^{86} present in resistant strains in Africa,[142,144,150,151] Asia[152] and South America.[153] Other polymorphism exist Phe^{184} in South America,[154] Cys^{1034} in South America,[149] Asp^{1042} in South America,[153] Asia[155] and Africa[151] and Tyr^{1246} in South America[154] and Africa[151] resulting in chloroquine restistant strains of *P.*

falciparum. Amodiaquine has been shown to be effective against low level chloroquine-resistant strains of *P. falciparum*, but show little effect against high level chloroquine-resistant strains.[108]

Table 2.1: A summary of resistance to the current arsenal of antimalarial drugs.

Drug	Introduced	First reported resistance	Location of resistance	Parasite Gene	Mechanism of resistance[156]
Quinine	1632	1910[157]	SE Asia[154]	*pfmdr1*	Reduced influx or increased efflux in the FV
Chloroquine	1945	1957[135]	Worldwide[144,146,152,154,155]	*pfcrt, pfmdr1*	Reduced influx or increased efflux in the FV
Proguanil	1948	1949[158]	S. America[159]	*dhfr*	Mutation at active site
Sulfadoxine-pyrimethamine	1967	1967[160]	Asia[155], Africa,[137] S. America[137]	*dhps*	Mutation at active site
Melfoquine	1977	1985[161]	SE Asia,[152] Africa[162]	*pfmdr1*	Reduced influx or increased efflux in the FV
Artemisinin	1978	2003[163]	Asia[163]	*pfmdr1*	Unknown
Atovaquone	1996	1996[164]	Rare	*pfmdr1*	Mutation at co-enzyme Q

2.1.3.3. Nucleic acid inhibitors

The most widely used nucleic acid inhibitors belong to the folate antagonist class of antimalarials. This class of antimalarial was not obtained from natural products but rather were developed from a comprehensive knowledge of biosynthetic pathways and synthetic organic chemistry (Figure 2.5). Type I antifolates (*e.g.* dapsone) mimic *p*-aminobenzoic acid (PABA) and compete for the active site of dihydropteroate synthase (DHPS). DHPS is responsible for facilitating the conversion of hydroxymethyldihydropterin to dihydropteroate (Scheme 2.3) in the folate pathway. Type II antifolates (*e.g.* pyrimethamine) inhibit dihydrofolate reductase (DHFR) which is responsible for the reduction of H2folate to H4folate (Scheme 2.3). Inhibition of enzymes in the folate pathway results in a decrease in the synthesis of pyrimidine and therefore a reduction in DNA, serine and methionine production. Due to the high level of asexual reproduction erythrocytic stage of the plasmodia lifecycle, antifolate predominately target this stage.[156]

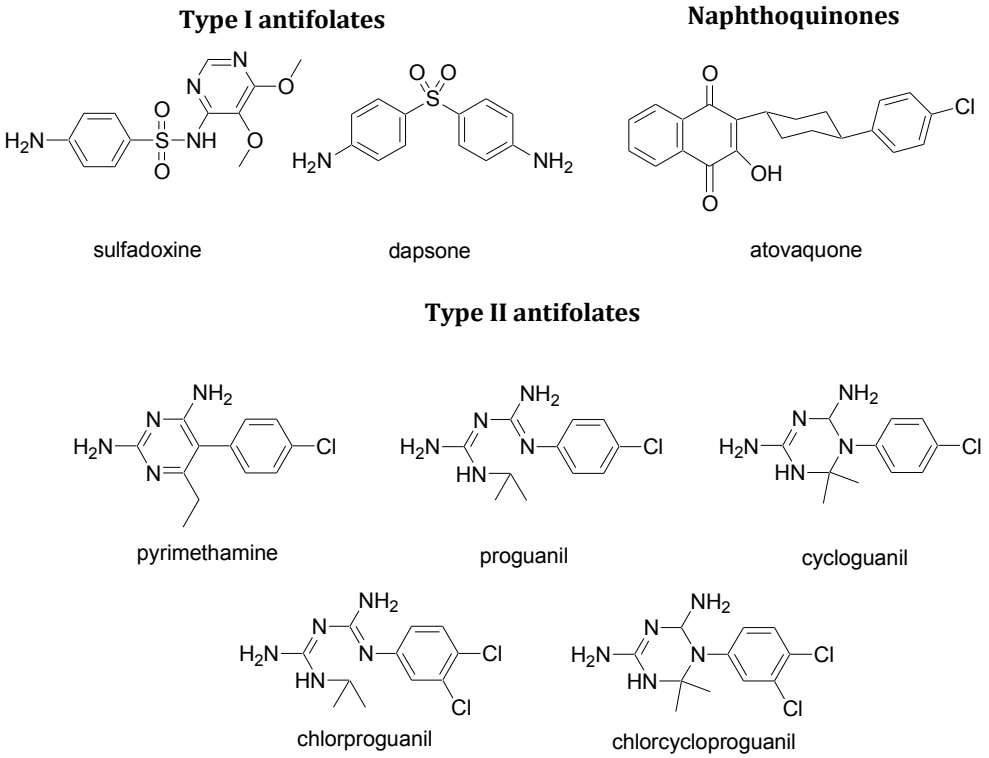

Figure 2.5: Nucleic acid inhibitors used as antimalarials.

This class of drug is often used as a combination; sulfadoxine/pyrimethamine (Fansidar®) and dapsone/chlorproguanil (LapDap®). Fansidar® has now over taken chloroquine as the major first-line antimalarial treatment.[165] While this drug combination is regarded as safe for the treatment of malaria, a prolonged use as a prophylactic has been linked to an increased risk of agranulocytosis and toxic epidermal necrolysis (Steven-Johnson syndrome) resulting in blistering of the skin.[108] This has resulted in many countries discontinuing the use of Fansidar® as a prophylactic.[107] The major appeal of these combinations of drugs lies in their affordability and its slow elimination from the body, meaning only a single dose is often required for treatment.[122] By using these drugs in combination their activity is increased as well as reducing the potential for resistance.[115] The sulfadoxine/pyrimethamine combination has been very successful in the intermittent treatment of malaria during pregnancy.[166]

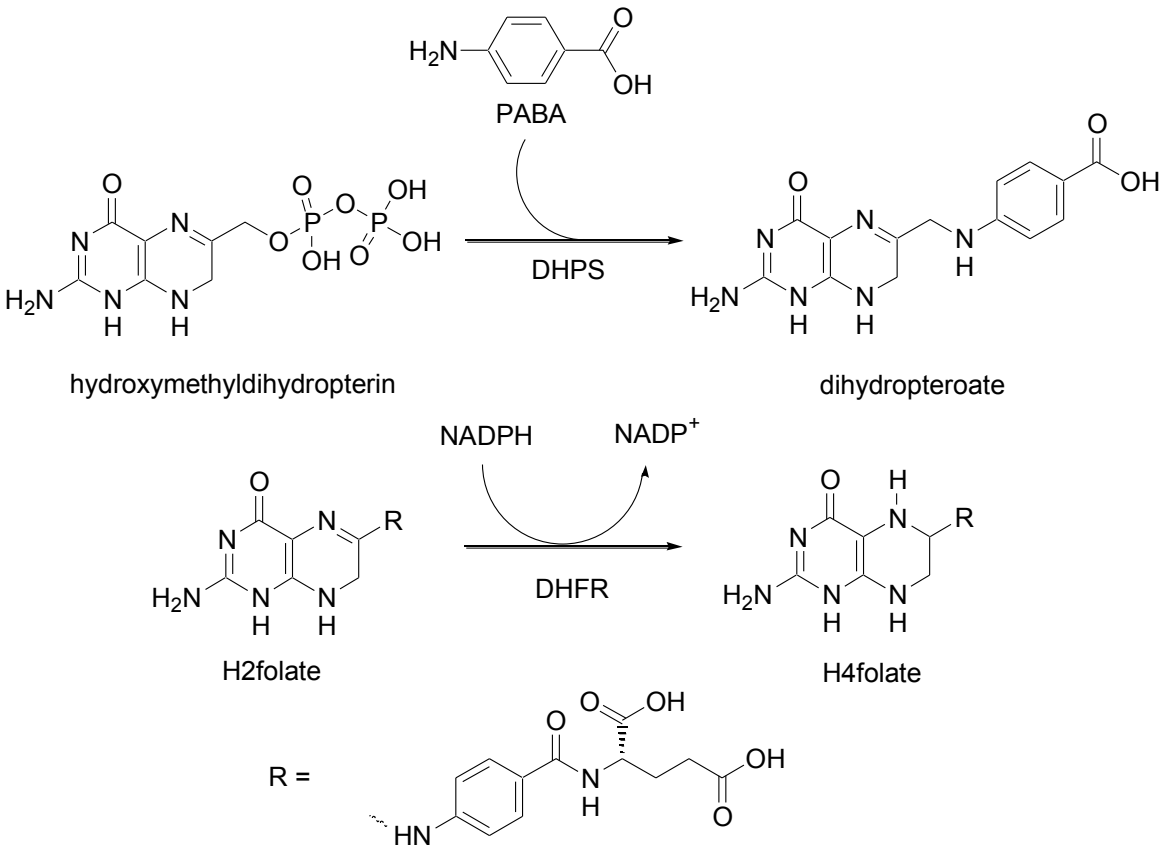

Scheme 2.3: The conversion of hydroxymethyldihydropterin to dihydropteroate facilitated by DHPS (*above*). The conversion of H2folate to H4folate via the NADPH dependent DHFR enzyme (*below*).

The use of the hydroxynaphthoquinone atovaquone (Figure 2.5) as a single agent has resulted in the rapid onset of resistance resulting in serious therapy failure rates,[167] and this resistance has lead to atovaquone being prescribed in combination with proguanil (Malarone®). Malarone® is primarily used as a prophylactic, however due to its high cost it has yet to achieve widespread status in developing countries. The main reason for the high cost is due to the complex synthetic route to atovaquone.[115] Malarone® is also used in the treatment of uncomplicated malaria, where it is effective against early liver stages of the parasite.[107] Malarone® has also thus far shown no severe side-effects.[107] One putative target for atovaquone is the enzyme dihydroorotate dehydrogenase (DHODase),[168,169] which is crucial for electron transport as well as the *de novo* biosynthesis of pyrimidine.[170] Atovaquone has also been shown to bind to the ubiquinone binding site of the cytochrome bc_1 complex, which inhibits the movement of an iron-sulphur cluster, which contains a protein domain essential for electron transport.[107] This disruption of the electron transport chain results in the rapid breakdown of the mitochondrial membrane potential.[107] Atovaquone works in synergy with the non-metabolized proguanil and chlorproguanil. When atovaquone disrupts the mitochondrial membrane potential, an alternative pathway is generated involving ATP hydrolysis.

This pathway involves the exchange of ADP^{3-} and ATP^{4-} by the ATP/ADP transporter. Proguanil inhibits this pathway resulting in a swift reduction in the membrane potential.[171]

2.1.4. New approached to antimalarial drug development

2.1.4.1. Improving therapy of existing drugs [Combination therapy (CT)]

With the development of resistance to nearly all of the existing agents, as shown in Section 2.1, many combinations of current drugs are available. These new dosing regiments may optimise drug activity. There are two major advantages offered by CT, firstly the supplementation of additional antimalarials should increase efficiency or ideally act in synergy with one another. A classic example of this is the proguanil/atovaquone combination; both showed failure rates when used as individual agents, but become a potent antimalarial when combined. The second, and most important, reason for CT is the induced delay of the onset of resistance to the agents used in combination. The use of CT may slow the progression of resistance to any newly developed antimalarials. When designing new drugs for CT, the drugs should both show little or no resistance to the parasite and have similar pharmacokinetics. By having similar pharmacokinetics diminishes the chances of having low concentration of either drug being present in the bloodstream reducing the likelihood of developing resistance. However, it is possible to use of combination of drugs with different pharmacokinetics, by using a potent short-acting drug and a longer-lasting drug although, this has only proven effective if the short-acting drug is potent enough to sufficiently overcome the parasite-burden such that there are limited parasites to develop resistance to the long-lasting drug.[172] A modern CT-drug which was in Phase III trials named LapDap+ (dapson/chlorproguanil/artesunate) showed significant shorter parasite clearance time when compared to the dapson/chlorproguanil combination, however at the time of writing GSK had ceased testing due to patient complications.[107] Nowadays it may be important to consider the use of CT when designing drugs. Developed drugs may show little promise as a single antimalarial agent but may be far more effective if used in a combination therapy.

2.1.4.2. Analogues of existing drugs

The second approach to the development of new antimalarials is the improvement of current antimalarials through their chemical modification. This method requires little or no knowledge of the mechanism of action or biological targets of the parent drug. As previously discussed many drugs on the market were developed in this manner, for example: chloroquine, primaquine and mefloquine are all analogues of quinine or lumefantrine was developed as an alternative to the toxic halofantrine.[173] An even more recent example of this would be the 8-aminoquinoline, tafenoquine, which is currently in the advanced stages of clinical trials. This analogue shows improved activity against the hepatic stages of the parasite over its parent compound primaquine.[174] The addition of the trifluoromethylphenyloxy substituent increases the antiplasmodial activity however, there still exists a risk of haemolysis in G6PD-deficient humans.[107]

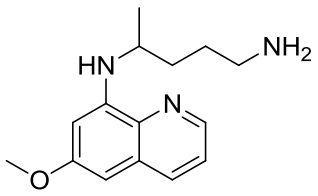

primaquine

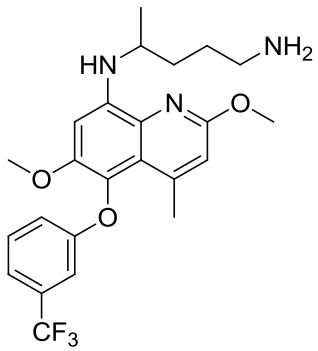

tafenoquine

2.1.4.3. Compounds active against other diseases

The third approach involves the discovery of novel antimalarials amongst drugs designed for treatment of other diseases. This approach has both advantages and disadvantages. As previously stated malaria is a disease of poverty, and funding for the development of new antimalarial is usually a major concern, however by looking at an assortment of already developed drugs all the major costs of safety test for human consumptions are complete and therefore, the cost of developing these drugs as antimalarials may be minimal. Drugs developed for diseases in wealthier nations, such as cancer, often are too expensive to develop into antimalarials, but may become less expensive as patents expire.[172] A good example of this type of approach is the development of

tetracyclines, such as doxycycline, which were developed for their antibacterial properties and were only later discovered to show activity against the malaria parasite. [172]

2.1.4.4. Drug resistance reversers

With antimalarial drug resistance on the rise, many potent inexpensive drugs are rendered obsolete. A number of compounds however, have been shown to have the ability to reverse the resistance of *P. falciparum* to chloroquine. For example the antidepressant, desipramine,[175] the anthypertensive verapamil[176] or the antihistamine chlorpheniramine[177] have all shown an increase in sensitivity to chloroquine in the plasmodial parasite when supplemented with chloroquine. A major downfall to resistance reversers is the unacceptable concentrations required to be effective. With the design of new resistance reversers,[178,179] chloroquine may see a resurrection and once again be used as the primary treatment for malaria.

2.1.4.5. Malaria vaccines

During the writing of this thesis GlaxoSmithKline (GSK) was in the process of conducting the Phase III clinical trial of their malaria vaccine, RTS,S. After the success of the Phase II clinical trial,[180-185] GSK began conducting drug trials on 15,460 infants and young children in 11 sites across seven African countries. RTS,S triggers an immune response to help prevent *P. falciparum* from infecting, maturing and multiplying in the liver, while simultaneously preventing the parasite from re-entering the bloodstream and re-infecting erythrocytes. RTS,S fuses a circumsporozoite protein, a surface protein which assists *P. falciparum* in invading human liver cells with GSK's hepatitis B vaccine, resulting in an immune response.[186] The initial results of the Phase III clinical trial for 6 000 children aged 5 to 17 months were released in November 2011. The children received three doses of the RTS,S vaccine or a non-malaria comparator vaccine over a twelve month period. The initial results show a 56% and 47% decrease in risk of the children experiencing clinical and severe malaria respectively.[187] The results of the Phase III clinical trials for infants (6 to 12 weeks old) will be available in the fourth quarter of 2012 while the results from the long term study of the RTS,S vaccine will be released in the fourth quarter of 2014. The WHO has indicated that the RTS,S vaccine may become available for national immunisation programs in early 2015.[188] The possible success of this vaccine may change the direction of antimalarial prophylactic research completely.

2.1.4.6. Natural products

The final approach to development of antimalarial chemotherapy is natural products. Natural products are responsible for two of the most widely used antimalarials to date, quinine and artemisinin. In regions afflicted by malaria there often exists a traditional knowledge of medicinal plants and organisms, which may prove to be an invaluable resource in the development of new antimalarials. The use of marine natural products in drug discovery is covered in Chapter 1.

2.2. Antiplasmodial marine isocyanate, isothiocyanate and isonitrile terpenoids

Terpenoids are common secondary metabolites found in marine organisms such as sponges and nudibranchs many of which show antiplasmodial activity.[189] For the purposes of this review and in the context of research described later in this thesis, only isonitriles and isothiocyanates marine secondary metabolites which exhibit antiplasmodial activity will be discussed here (Table 2.2). The first reported isolation of a marine isonitrile-containing metabolite occurred in 1973 when axisonitrile-1 (**2.1**) was isolated from the sponge *Axinella cannabina*,[190] shortly afterwards other isonitrile and isothiocyanate-containing sesquiterpenoids (**2.2, 2.3** and **2.5**) as well as axisonitrile-3 (**2.4**) where isolated from the same source.[191,192] Nearly two decade later **2.4** and **2.5** was once again isolated, this time from the North Eastern Australian sponge *Acanthella klethra* (Figure 2.6, *Left*) along with the isothiocyanates **2.6-2.8**.

Figure 2.6: Underwater photographs of *Acanthella* sp. sponge (*left*) and *Phyllidia sp.* nudibranch (*right*).[193]

Angerhofer *et al*.[194] first described the antiplasmodial activity of compound **2.4-2.8**, with the most active compound being **2.4** which exhibited antiplasmodial activity of 71 nM.[194] With the conversion of the isonitrile to the isothiocyanate the antiplasmodial activity was shown to be reduced by 500 fold.[194] This discovery indicated that activity of the compound was dependent upon the presence of isonitrile functional group. The discovery of antimalarial potential in marine isonitriles sparked in-depth research into sponges of the Axinellidae and Halicondridae families. A series of isonitrile, isothiocyanate and isocyanate diterpenes consisting of isocycloamphilectane (**2.9-2.13**), cycloamphilectane (**2.14** and **2.15**), amphilectane (**2.16-2.21**) and isoamphilectane (**2.22**) backbones and **2.23** were isolated from the halichondrid sponge *Cymbastela hooperi*.[195] Generally all these molecules showed good antimalarial activity. Of the isocycloamphilectanes, compound **2.12** showed the most potent antiplasmodial activity of (7 nM).[196] When comparing this compound with the amphilectanes and isocycloamphilectanes there was a general decrease in antiplasmodial activity with the exception of **2.19** which showed antiplasmodial activity (31 nM).[196] In more recent years Wattanapiromsakul *et al*.[197] isolated four tricyclic diterpene isonitriles (**2.24-2.27**) from the *Ciocalapata* sp. sponge collected off the coast of Kho-Tao, Thailand, which showed antiplasmodial activity. A recent study of a Puerto Rican sponge *Hymeniacidon* sp. has yielded monamphilectine A (**2.28**), a new β-lactam containing isonitrile which shows promising antiplasmodial activity.[198] A series of kilihinane diterpenoids (**2.29-2.33**) were discovered from the Okinawan sponge *Acanthella sp.* These kilihinane diterpenoids are known for their anthelmintic, antibacterial and antifouling abilities, in addition they showed potent antiplasmodial capabilities.[199] The most active in the series was kalihinol A **2.29** which exhibited a very significant antiplasmodial activity (1 nM). The bicyclic isothiocyanate (**2.34**) was isolated from a *Halichondria* sp. sponge collected off the Hawaiian island Oahu.[200] While compound **2.35** has not been tested for its antiplasmodial activity it is worth noting as it will be discussed further in Chapter 4. 3-Isocyanotheonellin (**2.35**) was isolated from the Sri Lankan *Phyllidia* sp. nudibranch[201] (Figure 2.6, *Right*) and displayed moderate antiplasmodial activity.[202] The reported antiplasmodial activity of marine isonitriles, isocyanates and isothiocyanates are presented in Table 2.2.

Table 2.2: Antiplasmodial activity of marine isonitriles **2.4-2.35**

Compound	IC_{50} [μM]	Compound	IC_{50} [μM]	Compound	IC_{50} [μM]
2.4	0.61[a] / 0.071[b]	**2.15**	0.25[a] / 0.081[b]	**2.26**	0.44[c]
2.5	46.89[a] / 11.8[b]	**2.16**	1.02[a] / 0.45[b]	**2.27**	0.98[c]
2.6	8.51[a] / 2.32[b]	**2.17**	1.75[a] / 0.81[b]	**2.28**	0.04[b]
2.7	15.20[a] / 2.09[b]	**2.18**	1.32[a] / 0.31[b]	**2.29**	0.001[d]
2.8	38.0 [a,b]	**2.19**	0.047[a] / 0.031[b]	**2.30**	1.8[d,e]
2.9	0.015[a] / 0.013[b]	**2.20**	0.20[a] / 0.086[b]	**2.31**	2.6[d,e]
2.10	0.13[a] / 0.08[b]	**2.21**	2.31[a] / 1.23[b]	**2.32**	0.01[d,e]
2.11	0.22[a] / 0.16[b]	**2.22**	0.30[a] / 0.10[b]	**2.33**	0.08[d,e]
2.12	0.009[a] / 0.007[b]	**2.23**	30.19[a,b]	**2.34**	5.7
2.13	0.21[a] / 0.066[b]	**2.24**	0.09[c]	**2.35**	ND
2.14	0.29[a] / 0.08[b]	**2.25**	1.07[c]	Chloroquine	0.29

[a] Tested against the Serra Leone chloroquine-sensitive *P. falciparum* clone D6
[b] Tested against the Indochinese chloroquine-resistant *P. falciparum* clone W2
[c] Tested against the Loatian chloroquine-resistant *P. falciparum* clone K1
[d] Tested against the Gambian chloroquine-resistant *P. falciparum* clone FCR-03
[e] Values quoted as EC_{50}

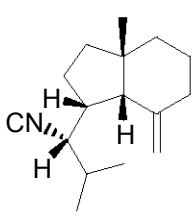

2.1

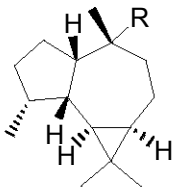

R
2.2 NC
2.3 NCS

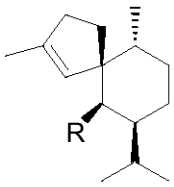

R
2.4 NC
2.5 NCS

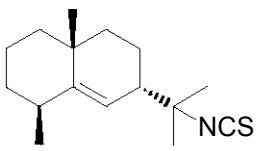

2.6

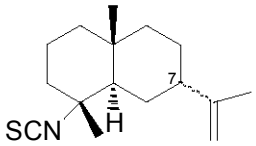

R
2.7 C-7 (*S*)
2.8 C-7 (*R*)

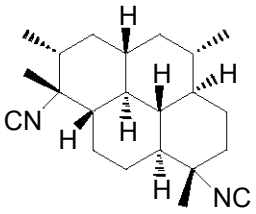

2.9

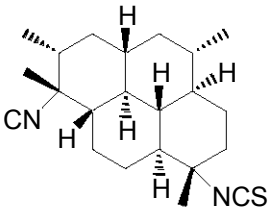

2.10

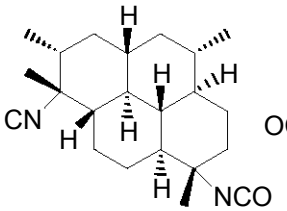

2.11

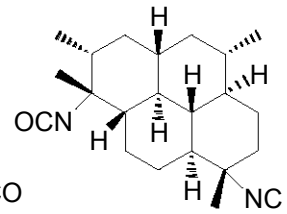

2.12

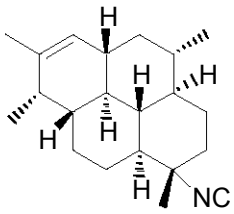

2.13

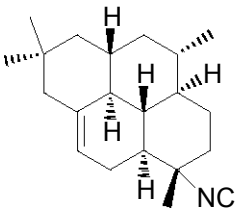

2.14

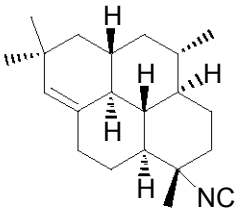

2.15

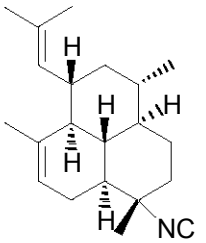

2.16

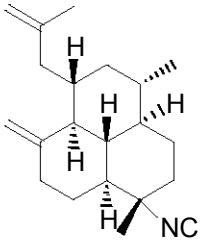

2.17

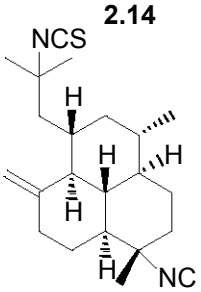

2.18

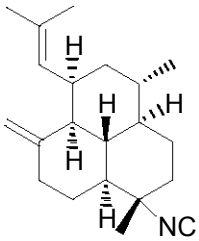

2.19

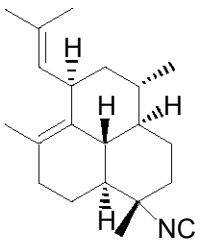

2.20

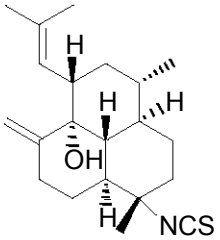

2.21

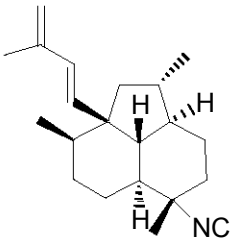

2.22

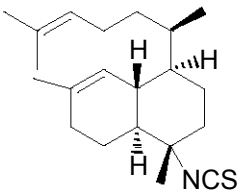

2.23

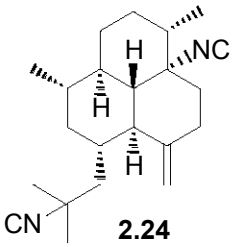

2.24

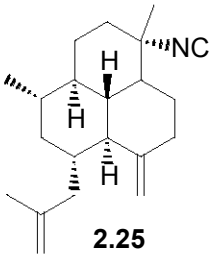

2.25

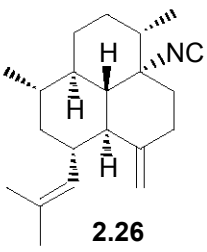

2.26

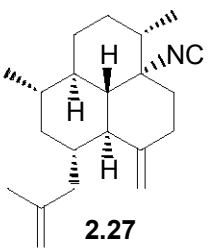

2.27

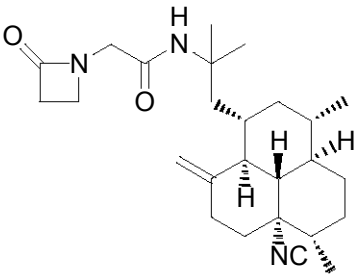

2.28

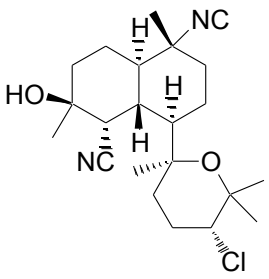

2.29

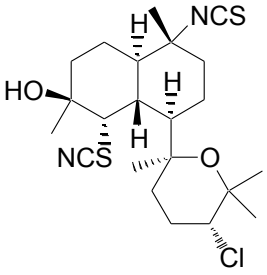

2.30

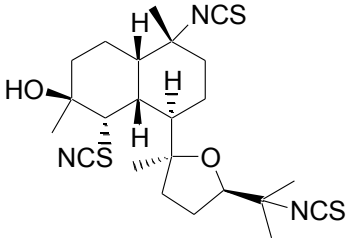

2.31

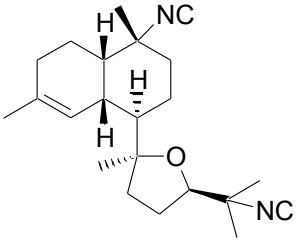

2.32

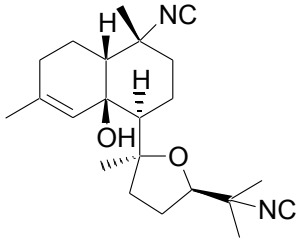

2.33

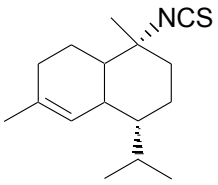

2.34

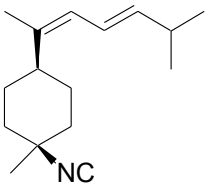

2.35

2.3. Putative mechanism of marine isonitrile antiplasmodial activity

Based on a series of spectroscopic experiments (*e.g.* UV/vis and mass spectroscopy), Wright *et al.*[196] concluded that marine isonitriles (**2.4** and **2.9-2.23**) have the ability to form ligand-haem complexes. They continued to elaborate on the binding motif of the isonitrile-haem by creating a generated 3D pseudoreceptor envelope based on the proposed pharmacophore calculated on the marine isonitrile/isothiocyanate haem interaction through force field molecular dynamics. An averaged receptor surface was generated by surrounding the inhibitor models with envelope-defining virtual particles possessing physiochemical descriptors, such as hydrophobicity, partial charge, electrostatic potential and hydrogen-bonding affinity. The outcome of this pseudoreceptor suggested the electrostatic interaction between the axial isonitrile/isothiocyanate at C-7 or C-20 and the iron atom within the porphyrin of haem (Figure 2.7, *Left*). Wright *et al.*[196] therefore, proposed that the antiplasmodial activity of **2.4** and **2.9-2.23** was a result of the parasites inability to successfully sequester haem into hemozoin. A toxic build-up of haem results in the irreversible damage to parasite proteins and membranes resulting in the death of the plasmodia. The major criticism of the use of a pseudoreceptor model is the assumption that these compounds inhibit one target and the

compounds corresponding IC_{50} value is directly related to the compounds ability to better bind to the pseudoreceptor. When in fact the pseudoreceptor may describe, for example a transport protein responsible for the accumulation of the compound at the active site and therefore the IC_{50} value may be related to a higher availability of the compound at the active site as opposed to a higher affinity for the active site.[203]

Ten years later Wright and co-workers[204] revisited the biological effect of marine isonitriles by evaluating **2.4**, **2.9**, **2.15**, **2.19** and **2.20** for anti-algal, anti-tubercular, anti-bacterial anti-photosynthetic and anti-fouling activities. The initial success shown by these compounds to inhibit the growth of the freshwater algae *Chlorella fusca* led them to the hypothesis that the mode of action may lie in the interference with the photosynthetic process within symbiotic organism that reside in the algae and would account for a decrease in algal growth. Therefore, these isonitriles where further analysed for their ability to inhibit photosynthesis, which **2.9**, **2.19** and **2.20** showed a decrease in photosynthesis of 37, 45 and 69% respectively at a test concentration of 0.2 $mg.mL^{-1}$. Wright and co-workers postulated that the antiplasmodial and anti-photosynthetic activity may be related through the inhibition of haem-containing proteins such as cytochromes b and f both of which are involved in the carbon fixation cycle of photosynthesis and promulgation of malaria. They therefore docked **2.4**, **2.9**, **2.15**, **2.19** and **2.20** into deoxy-human haemoglobin and plant cytochrome CYP74A as representations of haem-containing proteins. They observed that **2.4**, **2.9**, **2.15**, **2.19** and **2.20** had an affinity for a cavity directly adjacent to haem, which was contained in both proteins. They consequently named this cavity the “heme trench”. The binding motif of **2.4**, **2.9**, **2.15**, **2.19** and **2.20** showed the hydrophobic scaffold occupies the heme trench while the isonitrile moiety interacts with one of the carboxylic acid side chains of haem (Figure 2.7, *Right*). While this new description of the antiplasmodial activity in the inhibition of haem-containing proteins is feasible the original hypothesis of the inhibition of hemozoin is far more attractive as a drug target and motivated us to revisit isonitriles binding to haem in Chapter 4.

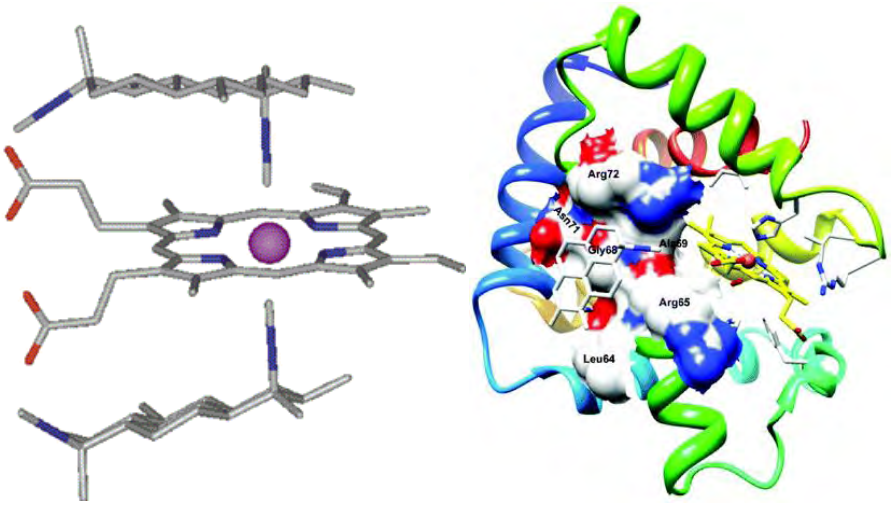

Figure 2.7: The proposed docking conformation of **2.9** and free haem (*left*).[196] The docked conformation of **2.9** and deoxy-human haemoglobin (PDB code 2DN2). Compound **2.9** is represented as sticks and coloured by atom; the haem molecule is represented as sticks coloured yellow and by heteroatom type. The "heme trench" is represented as partial solid surface and coloured by hydrophobicity (*Right*).[204]

CHAPTER 3: ANTIPLASMODIAL DITERPENES

3.1. Background

3.1.1. A review of naturally occurring antiplasmodial diterpene natural products

The diterpene class of compounds contains a plethora of structures and functionalities and they have been isolated from a multitude of marine and terrestrial sources. In this section we will review the chemical literature published in the past decade, focusing on diterpene compounds which displayed antiplasmodial activity (Table 3.1 and Table 3.2).

3.1.1.1. Isolation of antiplasmodial diterpenes from a terrestrial source

In the past decade numerous diterpenes and triterpenes have been isolated from natural sources, many of which have shown antiplasmodial activity. Numerous furanocassane and furanonorcassane diterpenes (**3.1-3.50**)[205,206] extracted from the seed kernels of *Caesalpinia crista*, have shown antiplasmodial activity against *P. falciparum*, with IC_{50} values ranging from 0.1->10 μM.[205] *Caesalpinia crista* is a plant found in the tropical and subtropical regions of Southeast Asia and is widely used by the local population for its medicinal properties.[206] All furanocassane-type diterpenes showed antiplasmodial activity with the most potent of the series, norcaesalpinin E (**3.4**), displayed an IC_{50} value of 90 nM *cf.* chloroquine (290 nM).[205] Other furan-containing diterpenes have shown antiplasmodial activity such as gromphosten and gromphosten A (**3.51** and **3.52**) isolated from *Gomphostemma niveum*[207] and hautriwaic acid lactone and viscidone (**3.53** and **3.54**) isolated from *Baccharis dracunculifolia*.[208]

A triad of diterpene lactones (**3.55-3.57**), isolated from *Parinari capensis,* showed promising antiplasmodial activity (IC_{50} of 1.6, 2.0 and 5.0 μM) against chloroquine-resistant strains of *P. falciparum*.[209] The South American shrub *Azorella compacta* afforded the mulinane-type diterpenoid (**3.58-3.62**) with antiplasmodial activity against *P. berghei in vivo*.[210] Two new diterpenoids (**3.63** and **3.64**) containing a similar scaffold to the mulinane-type diterpenes were isolated from the leaves of the Southern African plant *Croton steenkampianus*[211] and an additional four rearranged mulinane diterpenes (**3.65**-**3.68**) were obtained from the roots of the Thai plant *Jatropha integerrima*.[212]

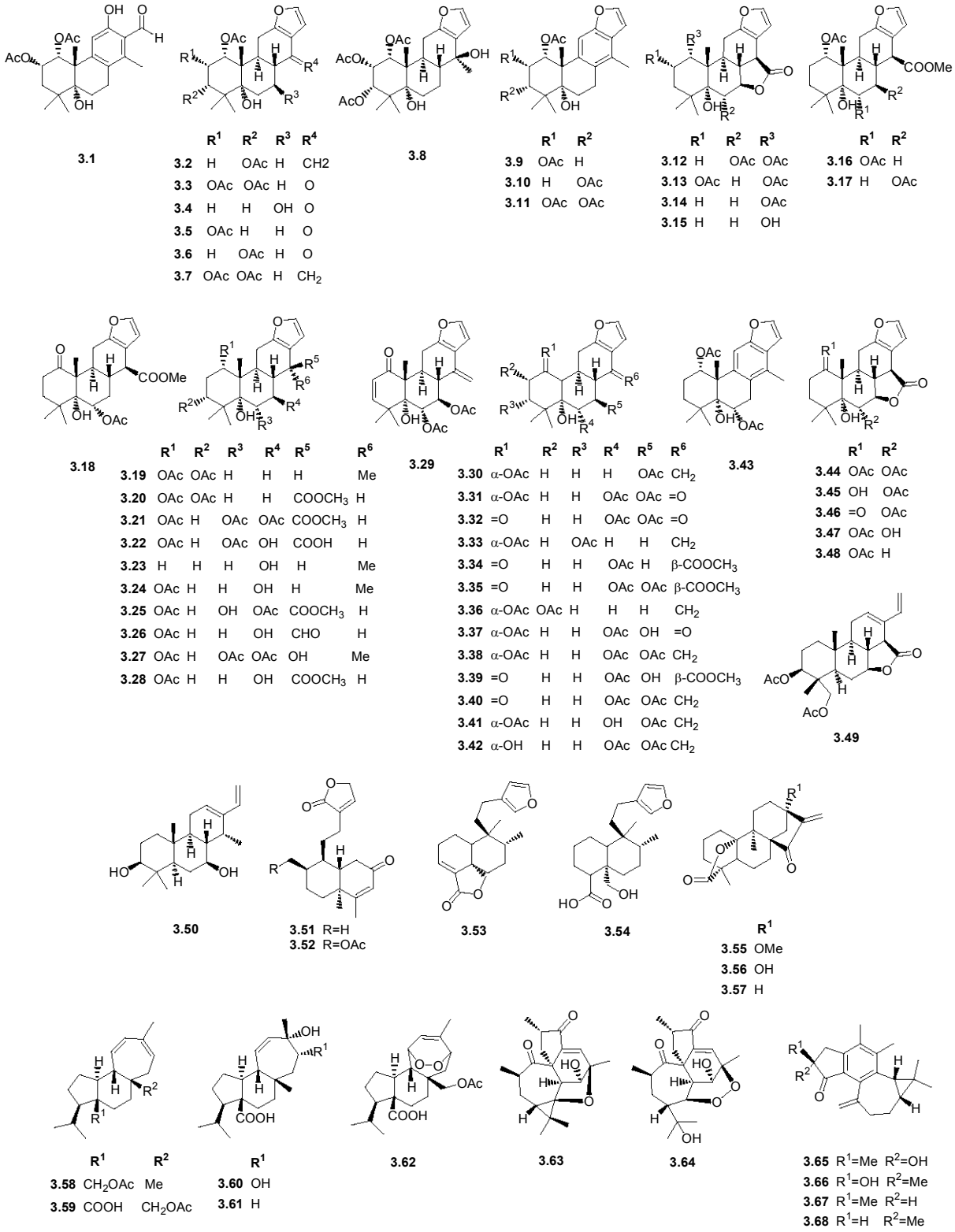

Figure 3.1: Antiplasmodial terrestrial plant diterpenes: furanocassane and furanonorcassane diterpenes (**3.1-3.50**), gromphosten and gromphosten A (**3.51** and **3.52**), diterpene lactones (**3.55-3.57**) and mulinane-type diterpenoid (**3.58-3.68**).

Clerodane diterpenoids (**3.69-3.75**) were isolated from the tree bark of *Laetia procera* with significant antiplasmodial activities against *P. falciparum* with IC_{50} in the low (0.5 µM) range.[213] A totarane (**3.76**) and an abietane (**3.77**) diterpene were isolated from the Southern African plant *Harpagophytum procumbens* (Devil's Claw) both of which showed antiplasmodial activity.[214] The extraction of the leaves of *Hyptis suaveolens* led to the isolation of an abietane-type diterpanoid endoperoxide (**3.78**) (IC_{50} of 0.3 µM).[215] Diterepene **3.78** was later re-isolated from aerial parts of *Anisochilus harmandii* along with the new diterepene (**3.79**) and the quinone-containing diterpenes (**3.80** and **3.81**).[216] A study of five *Plectranthus* species provided seven known abietane-type diterpenes (**3.82-3.88**) all showing antiplasmodial activity.[217] Six new pimarane-type diterpenes (**3.89-3.94**) were isolated from the Thai medicinal plant *Kaempferia marginata* with only compound **3.90** and **3.92** showing an IC_{50} antiplasmodial activity of 28.9 and 10.5 µM respectively.[218] The Butanese medical planted *Aconitum orochryseum* afforded atisinium chloride (**3.95**),[219] while *Scoparia dulcis* afforded scopadulcic acid A (**3.96**)[220] both with antiplasmodial activity.

The anti-plasmodial activity of the plant derived diterpenes (**3.1-3.96**) is presented in Table 3.1. Of interest is the variety of *P. falciparum* clones used in the various screening assays. Interestingly, only 14 of the 96 compounds presented in Table 3.1 have been screened against more than one *P. falciparum* clone. The variation in antiplasmodial activity of individual compounds *e.g.* **3.63** and **3.74** against different clones is noteworthy.

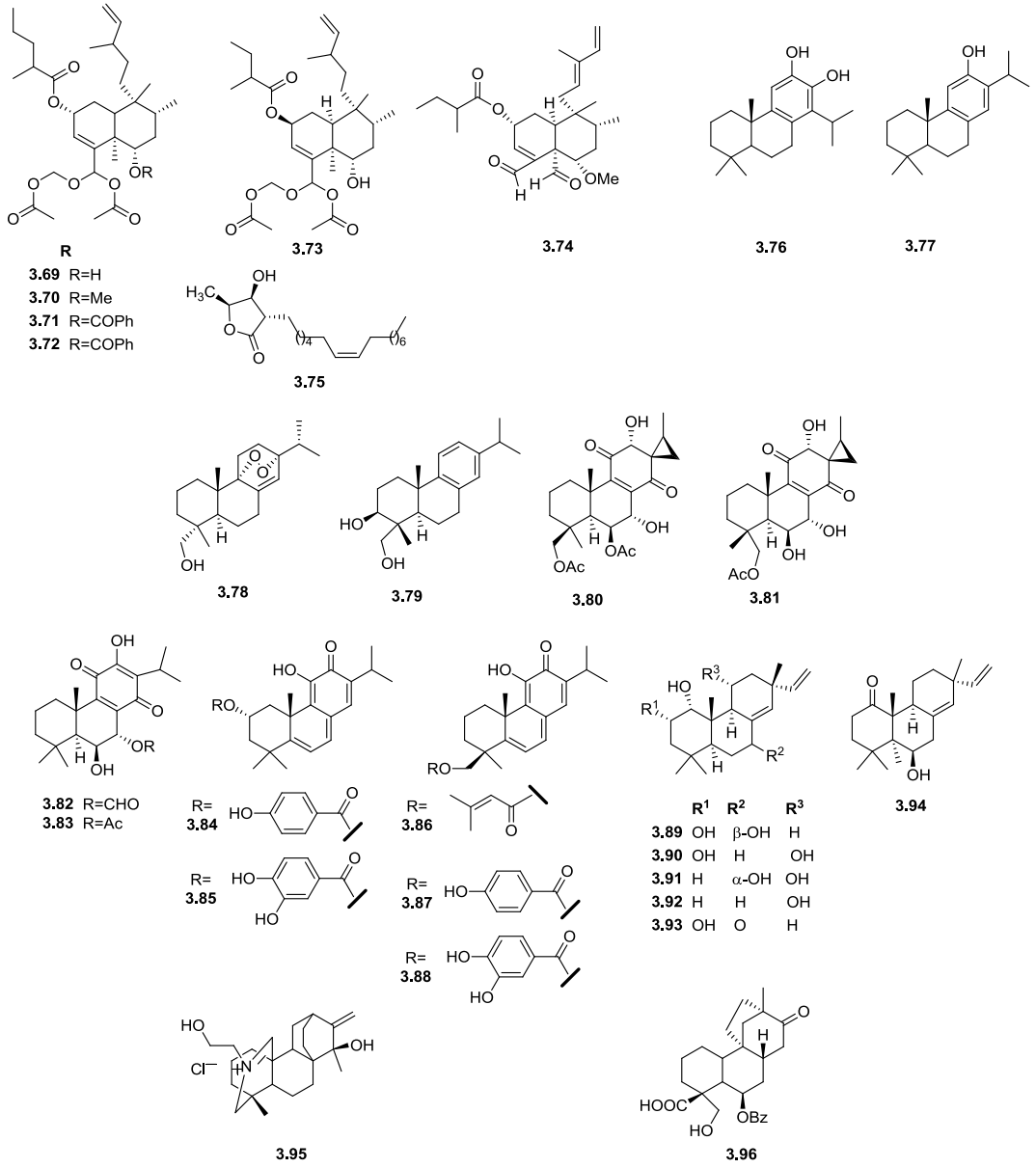

Figure 3.2*:* Antiplasmodial terrestrial plant diterpenes: clerodane diterpenoids (**3.69**-**3.75**), totarane diterepene (**3.76**), abietane diterpene (**3.77**), abietane-type diterpanoid endoperoxide (**3.78**), quinone containing diterpenes (**3.80** and **3.81**), abietane-type diterpenes (**3.82**-**3.88**), pimarane-type diterpenes (**3.89**-**3.94**), atisinium chloride (**3.95**) and scopadulcic acid A (**3.96**).

Table 3.1: Antiplasmodial activity of terrestrial diterpenes **3.1-3.96**

Compound	IC_{50} [µM]	Compound	IC_{50} [µM]	Compound	IC_{50} [µM]	Compound	IC_{50} [µM]
3.1	5.0[a]	**3.25**	>10[a]	**3.49**	3.6[a]	**3.78**	0.31
3.2	0.8[a]	**3.26**	0.1[a]	**3.50**	0.7[a]	**3.79**	15.6[a]
3.3	2.0[a]	**3.27**	>10[a]	**3.51**	126.4[b]	**3.80**	6.5[a]
3.4	0.09[a]	**3.28**	0.6[a]	**3.52**	9.9[b]	**3.81**	17.7[a]
3.5	0.8[a]	**3.29**	>10[a]	**3.53**	2.5[c]/7.0[d]	**3.82**	4.6[a]
3.6	0.3[a]	**3.30**	1.9[a]	**3.54**	9.0[c]/7.8[d]	**3.83**	29.2[a]
3.7	0.2[a]	**3.31**	3.1[a]	**3.55**	1.6[a]	**3.84**	5.3[a]
3.8	ND	**3.32**	1.0[a]	**3.56**	2.0[a]	**3.85**	3.1[a]
3.9	0.098[a]	**3.33**	0.8[a]	**3.57**	5.0[a]	**3.86**	6.0[a]
3.10	4.0[a]	**3.34**	0.7[a]	**3.63**	91[c]/28.5[e]	**3.87**	14.7[a]
3.11	6.5[a]	**3.35**	1.0[a]	**3.64**	72.2[c,e]/25[d]/43.4[f]	**3.88**	4.7[a]
3.12	0.8[a]	**3.36**	1.7[a]	**3.65**	13.2[g]	**3.89**	-[g]
3.13	ND	**3.37**	0.1[a]	**3.66**	-[g]	**3.90**	28.9[g]
3.14	0.8[a]	**3.38**	3.4[a]	**3.67**	18.4[g]	**3.91**	-[g]
3.15	>10[a]	**3.39**	0.2[a]	**3.68**	-[g]	**3.92**	10.5[g]
3.16	6.5[a]	**3.40**	2.9[a]	**3.69**	0.6[h]/0.5[i]	**3.93**	-[g]
3.17	0.6[a]	**3.41**	>10[a]	**6.70**	0.6[h] /0.7[i]	**3.94**	-[g]
3.18	0.7[a]	**3.42**	>10[a]	**3.71**	4.4[h]/6.1[i]	**3.95**	3.6[g]
3.19	3.5[a]	**3.43**	>10[a]	**3.72**	4.7[h] / 5.4[i]	**3.96**	27.0[c]/19.0[d]
3.20	4.1[a]	**3.44**	0.8[a]	**3.73**	0.6[h] / 0.6[i]		
3.21	2.5[a]	**3.45**	>10[a]	**3.74**	6.0[h] / 3.8[i]		
3.22	7.0[a]	**3.46**	>10[a]	**3.75**	57.6[h] / 2.8[i]		
3.23	2.1[a]	**3.47**	>10[a]	**3.76**	2.5[f]/ 2.7[g]		
3.24	0.4[a]	**3.48**	0.8[a]	**3.77**	3.3[f]/ 2.2[g]		

[a] Tested against the Gambian chloroquine-resistant *P. falciparum* clone FCR-03
[b] Tested against the chloroquine-sensitive clone *P. falciparum* MRC-02
[c] Tested against the Serra Leone chloroquine-sensitive *P. falciparum* clone D6
[d] Tested against the Indochinese chloroquine-resistant *P. falciparum* clone W2
[e] Tested against the Loatian chloroquine-resistant *P. falciparum* clone Dd2
[f] Tested against the Papua New Guinean chloroquine-sensitive *P. falciparum* clone D10
[g] Tested against the Loatian chloroquine-resistant *P. falciparum* clone K1
[h] Tested against the Tanzanian chloroquine-sensitive *P. falciparum* clone F-32
[i] Tested against the Columbian chloroquine-resistant *P. falciparum* clone FcB1
- Not active
ND Not determined

3.1.1.2. Isolation of antiplasmodial diterpenes from a marine source

Terpenoids are a common secondary metabolite found in marine organisms such as sponges, soft corals, gorgonians and nudibranchs many of which show antiplasmodial activity.[189,221] Marine antiplasmodial diterpenes bearing isonitrile, isocyanate and isothiocyanate functionalities have been presented in Chapter two. Three purine-substituted diterpenes (**3.97**-**3.99**) were isolated from a marine sponge (*Agelas* sp.) collected from the Solomon Islands, all of which displayed activity against *P. falciparum* with IC_{50} values of 6.6, 8.3 and 18.0 µM respectively.[222] Previous studies of the genus *Agelas* have afforded structurally similar compounds (**3.100** and **3.101**).[223,224] More recently ten novel eunicellin-type diterpenes (**3.102**-**3.113**) were isolated from *Briareum polyanthes*. It was found that compounds containing an alkene at C-7 and compounds containing –OR functional group (R = H, OH or Ac) at C-6 (**3.103**-**3.107**) displayed the highest antiplasmodial activity of this class of diterepenes with IC_{50} values of 39, 22, 21, 18 and 32 µM respectively.[225]

Studies of the *Pseudopterogorgia* species of gorgonian afforded the novel bielschowskysin (**3.114**)[226] as well as six new diterpenoids, caucanolides A-F (**3.115-3.120**),[227] from *Pseudopterogorgia kallos* and *Pseudopterogorgia bipinnata.* The West Indian sea whip *Pseudopterogorgia elisabethae* afforded a previously undescribed aberrarane diterpene scaffold with the isolation of aberrarone (**3.121**).[228] This same Rodriguez research group previously isolated the tetra cyclic colombiasin A (**3.122**) from the same organism, *Pseudopterogorgia elisabethae*.[229] In 2010 Rodriguez and co-workers, isolated ten new (**3.123-3.132**)[230] and eight known diterpenes (**3.133-3.140**)[231] containing a dolabellane skeleton from the Colombian gorgonian octocoral of the *Eunicea* genus. The most active compound against *P. falciparum in vitro* proved to be **3.131** with an IC_{50} of 9.4 µM while the remaining dolabellane diterpenes exhibited activity up to *ca.* 60 µM.[230] The specific antiplasmodial activities of **3.123-3.130** and **3.132-3.140** were not reported and thus omitted from Table 3.2.

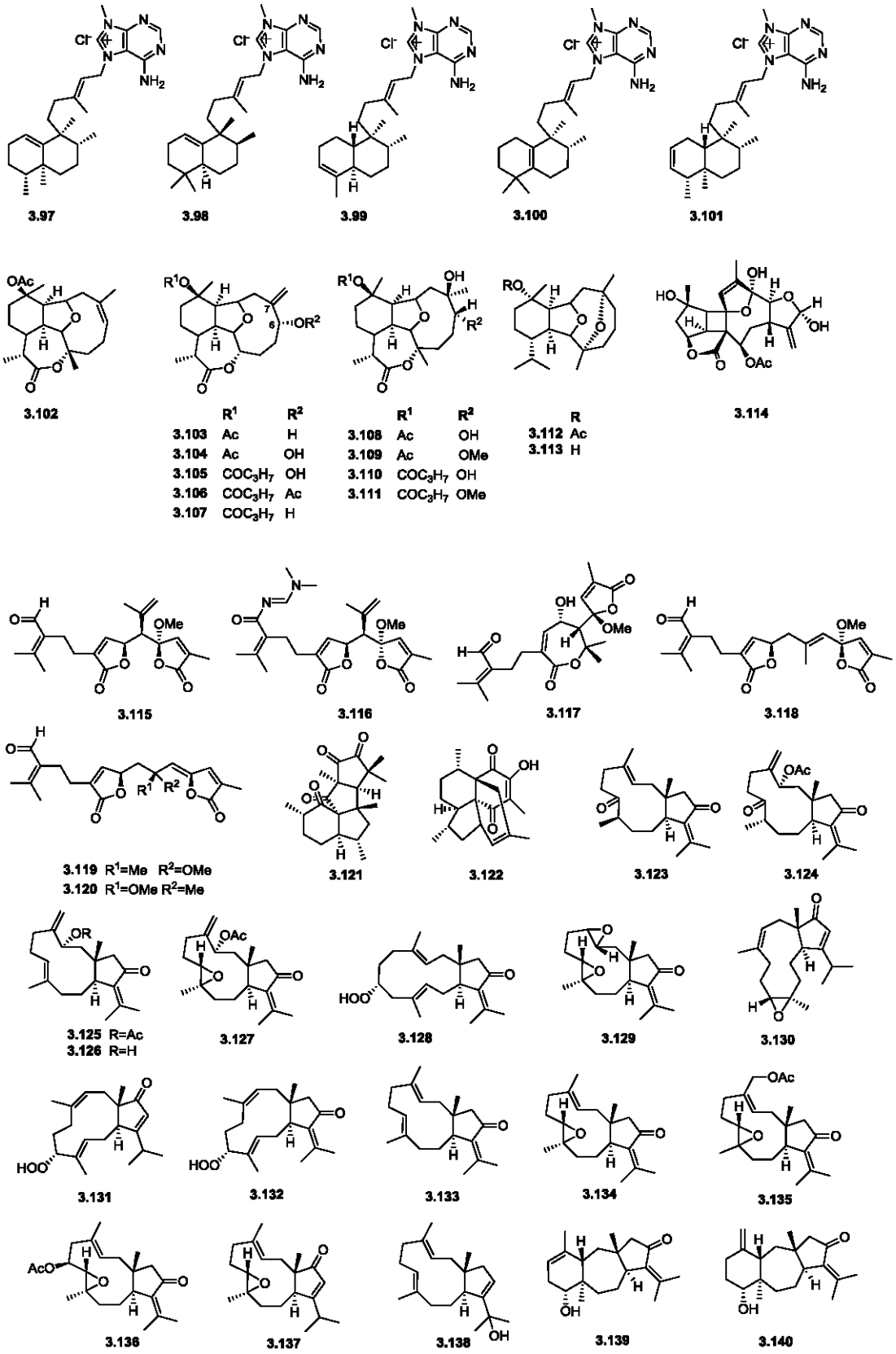

Figure 3.3: Antiplasmodial marine diterpenes: purine-substituted diterpenes (**3.97**-**3.101**), eunicellin-type diterpenes (**3.102**-**3.113**), bielschowskysin (**3.114**), caucanolides A-F (**3.115**-**3.120**), aberrarone (**3.121**), colombiasin A (**3.122**) and dolabellane type diterpenes (**3.123**-**3.140**).

A series of brominated diterpene-benzoate macrolides (**3.141-3.158**)[232] as well as callophycolide A (**3.159**)[233] were isolated from the Fijian red alga *Callophycus serratus* some of which exhibited antiplasmodial activity (<1 μM).[232] The antiplasmodial activity of **3.97-3.122**, **3.131** and **3.141-3.159** are summarized in Table 3.2. There are no examples of the same marine natural product being screened against multiple *P. falciparum* clones. This trend may reflect the paucity of marine natural products generally isolated from marine organisms.

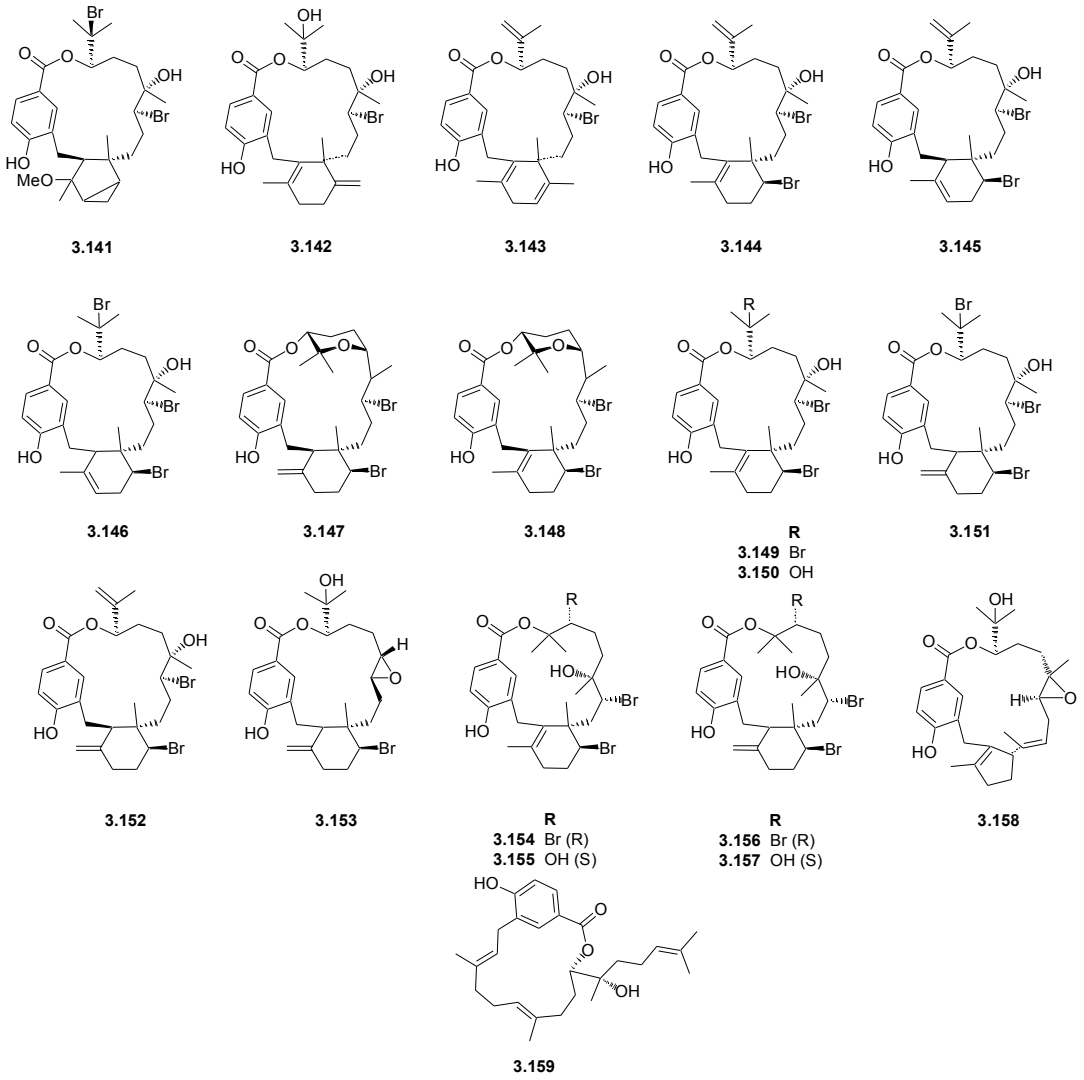

Figure 3.4: Antiplasmodial marine diterpenes: brominated diterpene-benzoate macrolides (**3.141-3.158**) and callophycolide A (**3.159**)

Table 3.2: Antiplasmodial activity of marine diterpenes **3.97-3.122, 3.131** and **3.141-3.159**.

Compound	IC_{50} [μM]	Compound	IC_{50} [μM]	Compound	IC_{50} [μM]	Compound	IC_{50} [μM]
3.97	8.3[a]	**3.109**	ND	**3.121**	30.3[c]	**3.150**	4.8[d]
3.98	ND	**3.110**	52.8[b]	**3.122**	31.8[c]	**3.151**	56.0[d]
3.99	ND	**3.111**	29.9[b]	**3.131**	9.4[c]	**3.152**	0.3[d]
3.100	6.6[a]	**3.112**	43.9[b]	**3.141**	2.7[d]	**3.153**	0.8[d]
3.101	18.0[a]	**3.113**	49.7[b]	**3.142**	44.0[d]	**3.154**	18.0[d]
3.102	>132.9[b]	**3.114**	23.0[b]	**3.143**	9.8[d]	**3.155**	14.0[d]
3.103	39.7[b]	**3.115**	45.0[c]	**3.144**	0.5[d]	**3.156**	0.9[d]
3.104	22.8[b]	**3.116**	>100[c]	**3.145**	1.4[d]	**3.157**	2.5[d]
3.105	21.3[b]	**3.117**	>100[c]	**3.146**	1.4[d]	**3.158**	>100[d]
3.106	17.8[b]	**3.118**	40.0[c]	**3.147**	2.9[d]	**3.159**	5.2[d]
3.107	32.0[b]	**3.119**	>100[c]	**3.148**	1.4[d]		
3.108	51.6[b]	**3.120**	>100[c]	**3.149**	0.9[d]		

[a] Tested against the Columbian chloroquine-resistant *P. falciparum* clone FcB1
[b] Tested against the Tanzanian chloroquine-sensitive *P. falciparum* clone F-32
[c] Tested against the Indochinese chloroquine-resistant *P. falciparum* clone W2
[d] Tested against the African chloroquine-sensitive *P. falciparum* clone 3D7
ND Not determined

3.1.2. Diterpenes ability to alter erythrocyte morphology

The red blood cell membrane consists of a lipid bilayer supported by an underlying protein network. The membrane is responsible for the shape and elasticity of the erythrocyte cells.[234] Under normal conditions the erythrocytes exist as discocytes (disc-shaped). Erythrocytes are highly deformable cells, in which shape changes may be induced by a range of compounds, including many semi-polar natural products. These shape changes may result in either stomatocytic (cup-shaped) or echinocytic (speculated) forms of red blood cells.[235] In the past, a number of compounds which have shown antiplasmodial activity have had the ability to induce echinocytic or stomatocytic change to the red blood cells membrane and in some cases cause lysis of the erythrocyte.[236] Sheetz and Singer[237] have postulated that such compounds incorporate into the erythrocytic membrane causing the change to these cells' membrane. In general, alterations to the erythrocyte morphology appear to be induced by amphiphillic and lipophillic compounds which can be incorporated into the lipid bilayer. Sheetz and Singer explained this change in the red blood cell membrane in their bilayer couple hypothesis,[237,238] which postulates that the formation of stomatocytes or echinocytes is due to the expansion of one of the two monolayers. Echinocytogenic amphiphiles are thought to be

trapped in the outer monolayer thus expanding it relative to the inner monolayer. Conversely stomatocytes are induced through incorporation of the amphiphile into the inner monolayer causing expansion of this layer relative to that the outer layer.

Once the malaria parasite has entered the erythrocyte, the successful development of the parasite is dependent upon the integrity of the membrane of the red blood cell remaining intact. It is therefore thought that the antiplasmodial activity of many naturally occurring compounds lies in their ability to alter the shape of the red blood cells thus hindering the growth of the parasite.[239] Plasmodia species are dependent upon the functioning of the erythrocyte membrane and are able to alter its permeability in order to obtain nutrients. Any modifications to the erythrocyte membrane would seriously hinder the parasites growth.[239] Therefore, compounds that alter erythrocyte membrane integrity are responsible for an indirect toxic effect on the malaria parasite and cannot be regarded as inducing genuine antiplasmodial toxicity.[236] The desirability of a malarial prophylactic that induces possibly irreversible change in erythrocyte membrane morphology is questionable.

Many natural products (and their synthetic analogues which have shown promising antiplasmodial activity), have also altered the ethrocyte's membrane shape *e.g.* the series of triterpenoids (**3.160-3.168**),[235,240,241] abietane-type diterpene (**3.169**),[242] norditerpenoids (**3.170-3.175**),[236] labdanes and isopimaranes (**3.176-3.186**).[236] A summary of the eyrthrocyte shape transformation, induced by antiplasmodial natural compounds **3.160-3.185** in erythrocyte is presented in Table 3.3.

At equilibrium anionic amphilphiles tend to be echinocytogenic while cationic amphiphiles tend to be stomatocytogenic.[237,238,243] This observation was confirmed when a series of synthetic long chain anionic, cationic and zwitterion amphiphiles (structures not shown here) were tested for erythrocyte deformation.[240] All the triterpenoid compounds (**3.160-3.168**) tested for their ability to change cell membrane morphology showed concentration dependent changes in the shape of the erythrocytes. The triterpenoids **3.160**, **3.163** and **3.165** induced formation of echinocytes and the triterpenoid compounds **3.161**, **3.162**, **3.164**, **3.166**, **3.167** and **3.168** transformed the healthy erythrocytes into stomatocytes. The former group of compounds initially formed exovesicles on the erythrocyte membrane, due to the compounds incorporation into the outer layer of the red blood cell leading to the formation of echinocytes. These compounds all have a functional group at C-18 with the ability to act as a hydrogen bond donor (COOH, $CONH_2$, CH_2OH), with the amide **3.160** being the most active echinocytogenic compound. The stomatogenic compounds **3.161**, **3.162** and **3.164** also contain functional groups at C-18 (CH_3, CHO, and $COOCH_3$) which are not hydrogen bond donors. This result suggests that hydrogen bonding in pentacyclic triterpenes is important in facilitating their incorporation into the red blood cells' membrane.[235] It is interesting to note that compounds **3.166**,

3.167 and **3.168** induced cell lysis at high concentration.[241] The abietane-type diterpene dehydroabietinol **3.169** was incorporated into the inner monolayer of the erythrocytes thus causing the formation of stomatocytes at concentrations close to the IC_{50} values for the inhibition of *P. falciparum*.[242] The norditerpenoids **3.171**, **3.172** and **3.175** showed stomatogenic effects on the erythrocytes and eventually lead to the lysis of the red blood cell at a concentration range of 100-200 $\mu g.mL^{-1}$. Compound **3.173** induced a modest increase in echinocytes while interestingly compounds **3.170** and **3.174** demonstrated no change to the erythrocytes shape (Figure 3.6).[244] The three isopimaranes (**3.183-3.185**) caused the formation of echinocytes. Compound **3.183** showed the lowest IC_{50} value but showed significant echinogenic behaviour at very low concentrations, whereas the remaining two isopimaranes only started inducing the echinocytic formation at higher concentrations. Compound **3.183** differs from compounds **3.184** and **3.185** in that it contains only a single oxygen functional group and thus has the most significant amphiphillic character. Compound **3.185** contains a polar group situated on one end of the molecule and showed echinocytosis at low concentrations and induced cell lysis at higher concentrations. Less pronounced membrane effects were seen in solutions containing compounds **3.178**, **3.180** and **3.181**, all of which contain two hydroxyl groups located at opposite ends of the molecule. The methyl ester **3.176** was a more potent stomatogenic compound than its corresponding carboxylic acid **3.177**. Haemolysis occurred at a concentration of 100 $\mu g.mL^{-1}$ for compounds **3.176**-**3.179**, **3.182** and **3.185**.[236]

A structural comparison of erythrocyte altering antiplasmodial diterpenes (Figure 3.5), shows that many of the compounds contain functionalities that may act as hydrogen bond donors as well as containing terminal or unhindered alkenes. This would suggest that alteration of the red blood cell membrane may result from the presence of these functionalities in combination with other factors which have yet to be established.

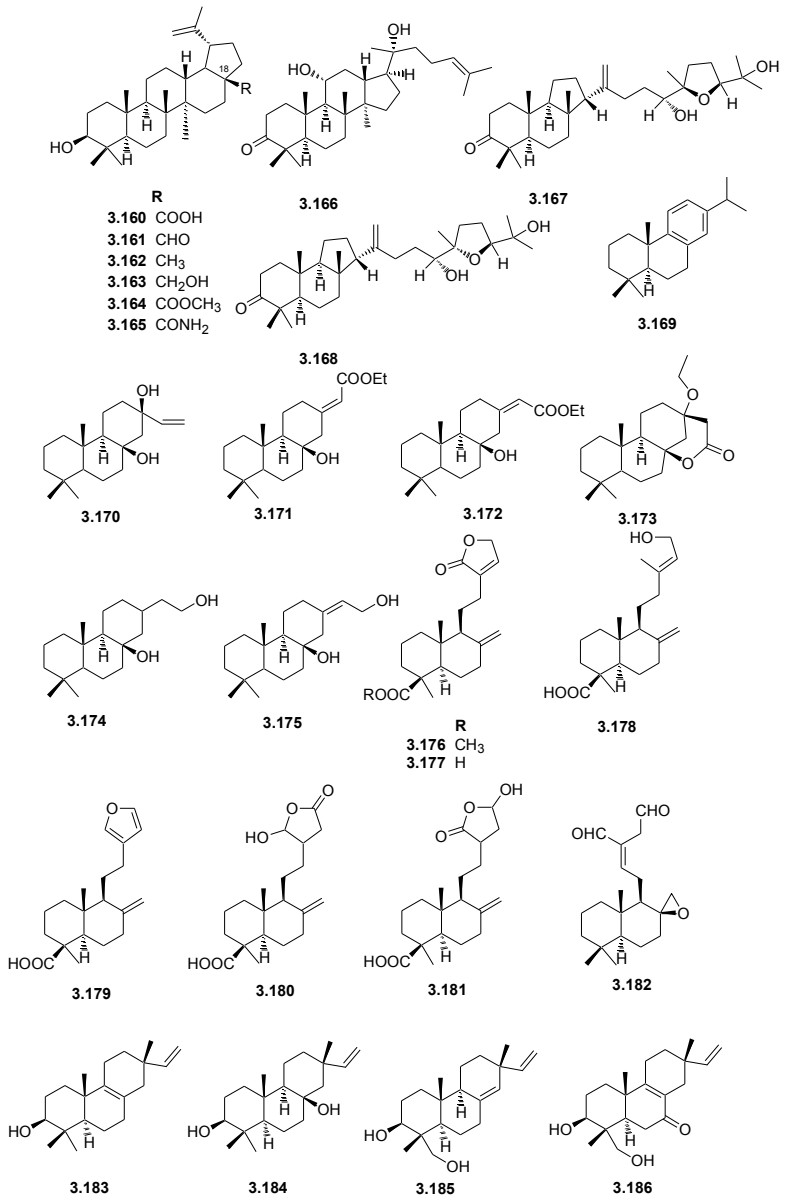

Figure 3.5*:* Antiplasmodial diterpene (**3.169**-**3.186**) and triterpenoids (**3.160**-**3.168**) natural products responsible for the erythrocyte morphology changes summarized in Table 3.3.

Table 3.3: The shape transformation induced by antiplasmodial natural compounds **3.160-3.185** in erythrocytes.

	Compound								
	3.160[235]	**3.161**[235]	**3.162**[240]	**3.163**[235]	**3.164**[235]	**3.165**[235]	**3.166**[241]	**3.167**[241]	**3.168**[241]
Source	*Zataria*	*Zizyphus*	*Rinorea*	Synthetic	Synthetic	Synthetic	*Caloncoba*	*Caloncoba*	*Caloncoba*
IC_{50} [µM]	13.9[a]	14.0[a]	27.7[a]	<27[a]	7.0[a]	14.1[a]	<30[a]	<30[a]	<30[a]
Conc. [µg.mL^{-1}]									
200	-	-	SS	E1, D	-	-	S1, S2, SS*	S1, S2, SS*	S1, S2, SS*
100	-	-	SS	-	-	-	S1, S2, SS*	S1, S2, SS*	S1, S2, SS*
50	E2	S2, SS	SS	E2	-	E3	S1, S2, SS*	S1, S2, SS*	S1, S2, SS*
25	-	-	SS	E2	S2	-	S1, S2, SS*	S1, S2, SS*	S1, S2, SS*
12.5	E2	S2, SS	S1, **SS**	-	-	E3	S1	S2	S3
6.25	E1	S1	D, S2	E1, D	S1	E1	**D**, S1, S2	**D**, S1, S3	**D**, S1, S4
3.13	D, E1	S1	**D**, S1	D	D, S1	E1	-	-	-

	Compound								
	3.169[244]	**3.170**[244]	**3.171**[244]	**3.172**[244]	**3.173**[244]	**3.174**[244]	**3.175**[244]	**3.176**[236]	**3.177**[236]
Source	*Salvia*	Synthetic	Synthetic	Synthetic	Synthetic	Synthetic	Synthetic	*Playcladus*	*Playcladus*
IC_{50} [µM]	25.6[a]/27.4[b]	36.6[a]	17.0[a]	11.7[a]	58.6[a]	45.2[a]	36.2[a]	53.4[a]	163.9[a]
Conc. [µg.mL^{-1}]									
200	*	-	*	*	-	-	*	-	-
100	*	D	S2	S3	E1	D	S3	SS*	S2*
50	*	D	-	-	D	D	-	S2, S3	D, E1
25	S2	D	-	-	D	D	-	D, S2	D
12.5	S1, S2	D	-	-	D	D	-	D	D
6.25	S1, S2	D	-	-	D	D	-	-	-
3.13	D, S1	D	-	-	D	D	-	-	-

	Compound							
	3.178[236]	**3.179**[236]	**3.180**[236]	**3.181**[236]	**3.182**[236]	**3.183**[236]	**3.184**[236]	**3.185**[236]
Source	*Playcladus*	*Playcladus*	*Playcladus*	*Playcladus*	*Playcladus*	*Playcladus*	*Playcladus*	*Playcladus*
IC_{50} [µM]	104.5[a]	130.2[a]	84.1[a]	145.2[a]	76.3[a]	24.6[a]	80.9[a]	93.3[a]
Conc. [µg.mL^{-1}]								
200	-	-	-	-	-	-	-	-
100	S2*	S2*	D, E1	D, E1	SS*	E3	E1	SE2*
50	D, E1	D, S1	D, E1	D	SS	E3	D	SE1, E2
25	D	D	D	D	D	E2	D	E3
12.5	D	D	D	D	D	E1	D	E1
6.25	-	-	-	-	-	-	-	-
3.13	-	-	-	-	-	-	-	-

Dominating erythrocyte shapes in bold; D, discocyte; E1, E2, E3, echinocyte types 1, 2 and 3; SE1, SE2, spheroechinocyte type 1 and 2; S1, S2, S3, stomatocyte types 1, 2 and 3; SS1, SS2, spherostomatocyte type 1 and 2; (*) designates haemolysis, (-) indicates not determined at that concentration.

[a] Tested against the African chloroquine-sensitive *P. falciparum* clone 3D7

[b] Tested against the Loatian chloroquine-resistant *P. falciparum* clone Dd2

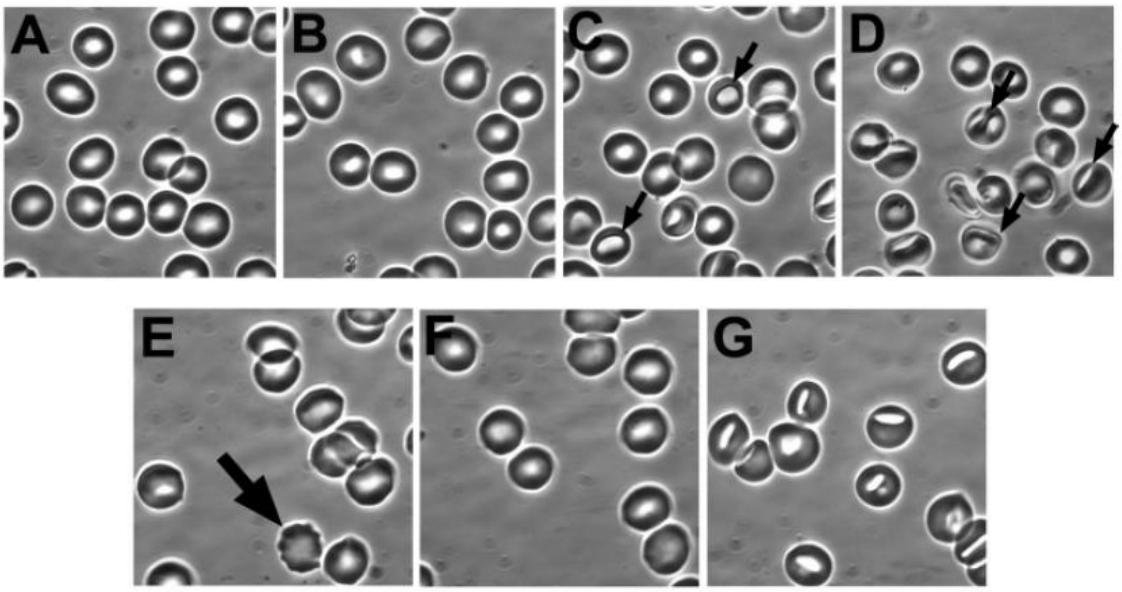

Figure 3.6: A: Erythrocytes incubated with media alone, B: 100 µg.mL^{-1} of compound **3.170**, C: **3.171**, D: **3.172**, E: **3.173**, F: **3.174**, G: and **3.175**. Small arrows represent stomatocytes type 2. Large arrow denotes echinocytes type 1. Reproduced with permission from van Wyk *et al.*[244]

3.2. Research aims

As discussed in Chapter 2 and Section 3.1, both diterpene isonitriles and diterpene alcohols have shown antiplasmodial activity. In this Chapter, we discuss the synthesis of a series of tricyclic podocarpane type diterpenes for the possible development of new antiplasmodial compounds (Figure 3.7). In the past our laboratory has successfully synthesized podocarpanes, through a series of transformations of the naturally occurring diterpene (+)-manool (**3.187**). Since these types of antiplasmodial compounds have been synthesized before, *e.g.* **3.170**,[244] we thought a structural activity relationship (SAR) study involving the addition of a variety of functionalities at the chiral centre C-13, would afford some insight into how the antiplasmodial activity may be increased while simultaneously reducing the haemolytic activity also observed in this series of compounds. Due to the potency of the tricyclic marine isonitriles against the plasmodium parasite, we also hypothesized that the conversion of the tertiary alcohols to isonitriles moiety would possibly significantly increase the antiplasmodial activity of these synthetic compounds.

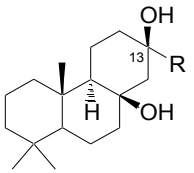

Figure 3.7: General podocarpane scaffold for proposed synthetic diterepenes.

3.3. Synthesis of antiplasmodial podocarpanes

3.3.1. Synthesis of the tricyclic ketone (3.188)

The pyridium chlorochromate (PCC) oxidation of (*13R*)-manool[245] (**3.187**) involves the migration of the Δ^{14} olefin to Δ^{13} with concurrent oxidation of the transposed alcohol functionality to yield the aldehydes (*E*)-labda-8(17)dien-15-al (**3.189**) and (*Z*)-labda-8(17)dien-15-al (**3.190**). We proposed that this transformation proceeds through a mechanism in which **3.187** forms a π complex with PCC (**3.191**) that can rearrange to form the chromate ester (**3.192**). The chromate ester undergoes ionization to form the ion pair (**3.193**), which is facilitated through steric crowding in the chromate ester. Sundararaman and Herz showed that this mechanism is favoured with the addition of bulky ligands on the chromium atom.[246]

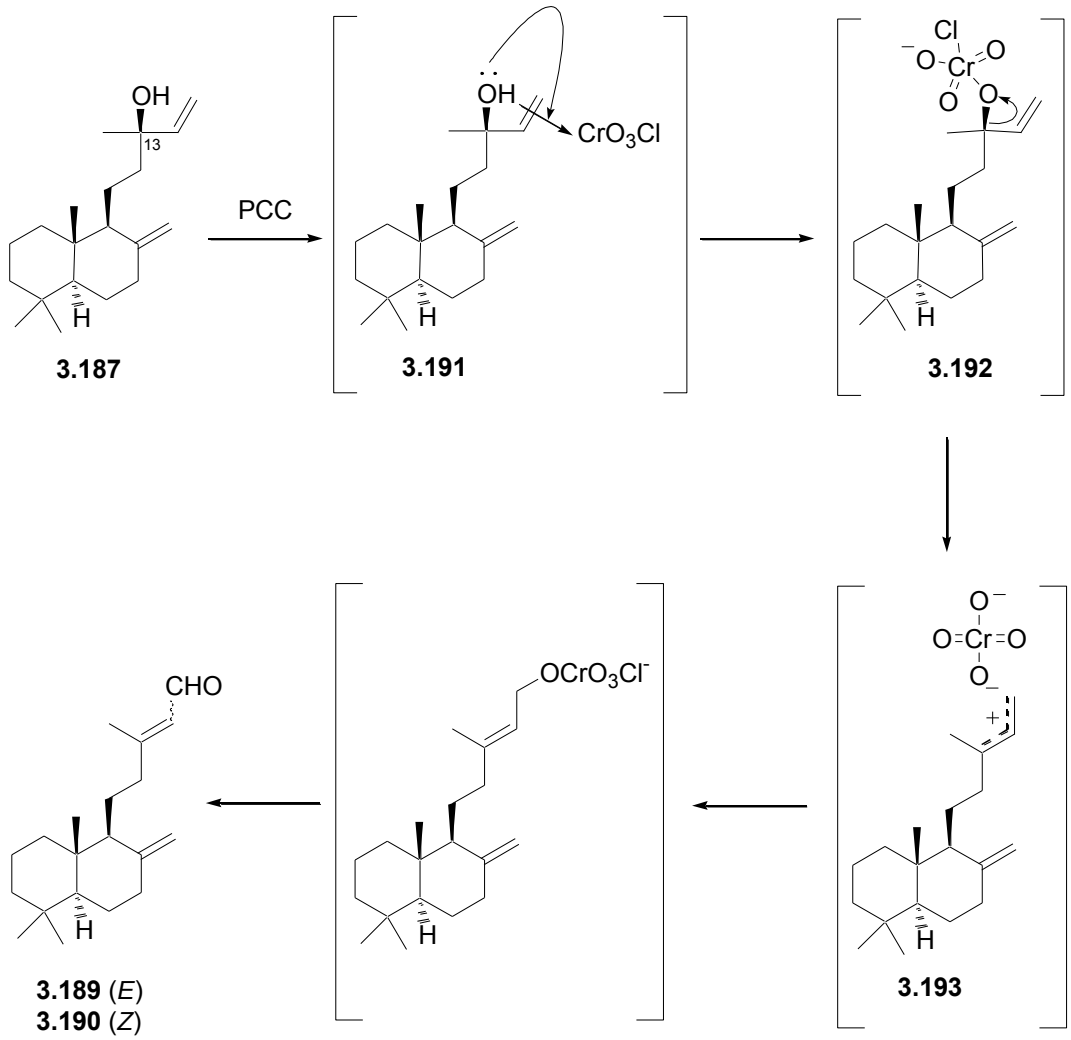

Scheme 3.1: Proposed mechanism for the oxidation rearrangement **3.187** facilitated by PCC.

The ^{1}H NMR spectrum of the PCC oxidation product immediately revealed the presence of two pairs of deshielded doublets (δ_H 9.97 and δ_H 9.82) which correspond to the aldehyde protons of the *E* and *Z* isomers (**3.189** and **3.190)** (ratio 2:1). The mixture of aldehydes was purified by silica flash chromatography to afford a combined isolated yield of 88%. The ^{1}H and ^{13}C NMR data of the mixture of aldehydes were consistent with those published in literature.[246,247] The aldehydes **3.189** and **3.190** were found to be unstable and thus ozonolysis was performed immediately.[248]

Following the oxidation rearrangement (Scheme 3.1), reductive ozonolysis of the Δ^{8} and Δ^{13} olefins was performed to afford the diketone **3.194** (Scheme 3.2). A constant stream of ozone was bubbled through a cooled dichloromethane solution of a mixture of the *E* and *Z* isomeric aldehydes **3.189** and **3.190**. Ozone was continuously administered until the solution had turned a pale blue colour indicating ozone saturation. The ozone was purged by bubbling nitrogen through the solution and the ozonide (**3.195**) intermediate was reduced by the addition of triphenylphosphine. Once the completion of the reaction had been confirmed by TLC, hydrogen peroxide was added in order to precipitate excess triphenylphosphine as triphenylphosphine oxide (**3.196**) which could be removed via filtration through a silica plug. The mechanism of ozonolysis of **3.189** and **3.190** is illustrated in Scheme 3.2.

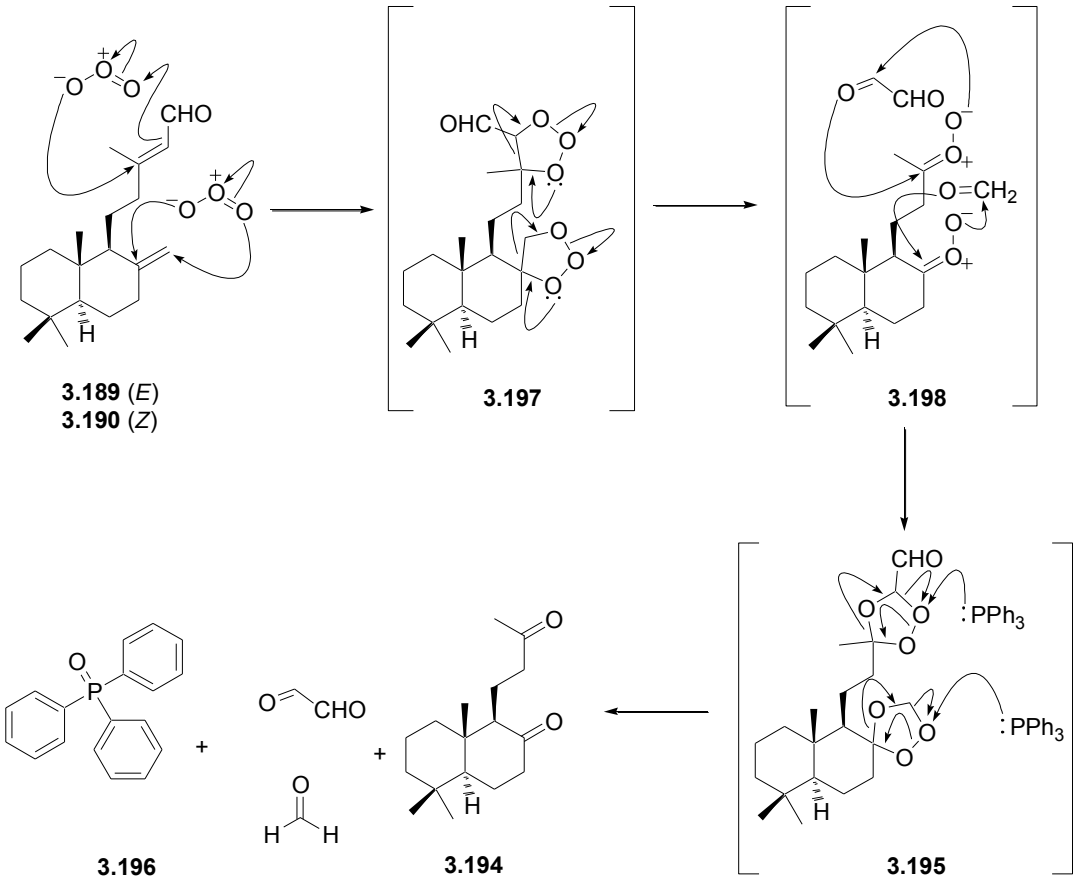

Scheme 3.2: Mechanism of ozonolysis of **3.189** and **3.190** to afford the diketone **3.194**.[249]

Ozonlysis is a 1,3-dipolar cycloaddition, involving the cleavage of π bonds in an oxidative fashion resulting in two new carbonyls per alkene. Ozone is a symmetrical bent molecule consisting of a positively charged central oxygen with two negatively charged terminal oxygen atoms.[249] The 1,3-dipole cycloaddition yields (**3.197**) which immediately decomposes by reverse 1,3-dipole cycloaddition, resulting in a simple aldehyde and an unstable carbonyl oxide (**3.198**). The carbonyl oxide now adds to the aldehyde by attacking its carbonyl carbon through an oxyanion nucleophillic attack, for a third cycloaddition step to afford the ozonide (**3.195**). The ozonide is the first stable product of this reaction, but is removed with the addition of triphenylphosphine to yield a ketone functionality (**3.194**) and triphenylphosphine oxide (**3.196**).

The crude yellow oil was purified further by flash silica chromatography (50% EtOAc, 50% hexane) to afford **3.194** in 76% yield. The diketone **3.194** could be easily distinguished from the aldehyde precursors with the appearance of a methyl singlet in the ^{1}H NMR spectrum (δ_H 2.07) and the disappearance of the deshielded doublets (δ_H 9.97 and δ_H 9.82). The ^{13}C NMR spectrum further supported the successful synthesis of **3.194** with the appearance of two singlets downfield (δ_C 212.3 and δ_C 209.2) corresponding to the formation of two new carbonyl carbons.

With the addition of the base sodium hydride to an anhydrous solution of the diketone **3.194** in tetrahydrofuran an intramolecular aldol condensation was initiated (Scheme 3.3). The hydride ion removes a proton from the terminal methyl group adjacent to the carbonyl carbon resulting in a carbanion. The carbonyl at C-8 can now undergo nucleophilic attack by the carbanion resulting in cyclization as shown in Scheme 3.3. After 4 hours the reaction was quenched with a saturated solution of ammonium chloride, as it was found that the addition of acid resulted in dehydration of the tertiary alcohol at C-8. Normal phase HPLC (10% EtOAc 90% hexane) proved to be very time consuming when trying to purify **3.188** as this compound was the final product to elute off the column (t_R = 40 min). As a result other methods of purification were pursued. Many solvents and combinations of solvents were tried in order to purify this product through recrystalization. Eventually it was found that a hot 20% dichloromethane 80% hexane solvent system, cooled slowly on ice, resulted in an 80% isolated yield of pure white needle-like crystals of **3.188**.

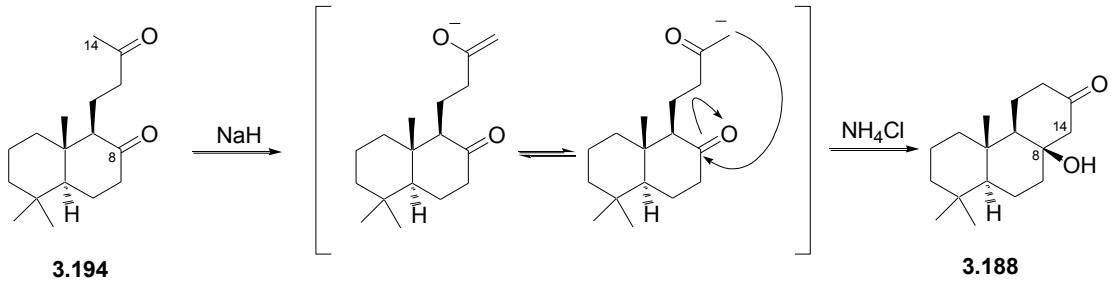

3.194 **3.188**

Scheme 3.3: Hydride induced intramolecular aldol condensation of **3.194**

The cyclization of **3.194** was deemed successful as the deshielded peak (δ_C 212.3) corresponding to the carbonyl carbon on C-8 of the ketone in **3.194** disappeared from the ^{13}C NMR spectrum of the product while a new carbon signal (δ_C 75.5) corresponding to an oxy-quaternary carbon was detected in the ^{13}C NMR spectrum. This observation was confirmed by ^{1}H NMR and DEPT135 NMR experiments revealing the loss of a methyl resonance (δ_H 2.07 and δ_C 14.5) and the addition of a methylene signal (δ_H 2.53, 2.23 and δ_C 57.3) in the ^{1}H and DEPT135 spectra of **3.188** respectively. Interestingly, we discovered that the optimal time for this reaction was 4 hrs as an increased exposure of compound **3.188** to basic conditions resulted in the dehydration of the C-8 alcohol.

3.3.2. Grignard addition to 3.188

As previous work had highlighted the antiplasmodial activity of podocarpane **3.170**,[244] the ketone on C-13 of **3.188** afforded us an opportunity to conduct a SAR study, through the convenient addition of a series of different functionalities to C-13 via standard Grignard methodology. Grignard reagents are organometallic compounds with the general formula RMgX, and are one of the most versatile group of reagents for the alkylation of ketones and aldehydes. The magnesium-carbon bond is polarised resulting in an alkyl nucleophile, which is highly unstable and thus moisture and air sensitive. Therefore all Grignard reactions are required to be conducted under inert and anhydrous conditions. Unfortunately, the Grignard reaction's desired product is often isolated with side products such as reduction products (from β-hydride transfer from the alkyl group),[250] aldol products (from the enolization of the ketone as a result of the strong basicity of the Grignard reagent),[250] as well as side products involving conjugate addition, condensation and pinacol coupling.[251] In some cases these abnormal adducts are the major products in the reaction prevailing over the formation of the desired tertiary or secondary alcohol.[250]

The mechanism by which Grignard alkylation of the ketone (**3.199**) proceeds is one of two pathways either through a polarised intermediate (**3.200**) or via a single electron transfer (SET) and the formation of radical species (**3.201** and **3.202**, Scheme 3.4). The preferred pathway is dependent upon the reduction potential of the ketone, the oxidation potential of the Grignard rearrangement, the nature of the solvent system and the nature of the halogen.[252]

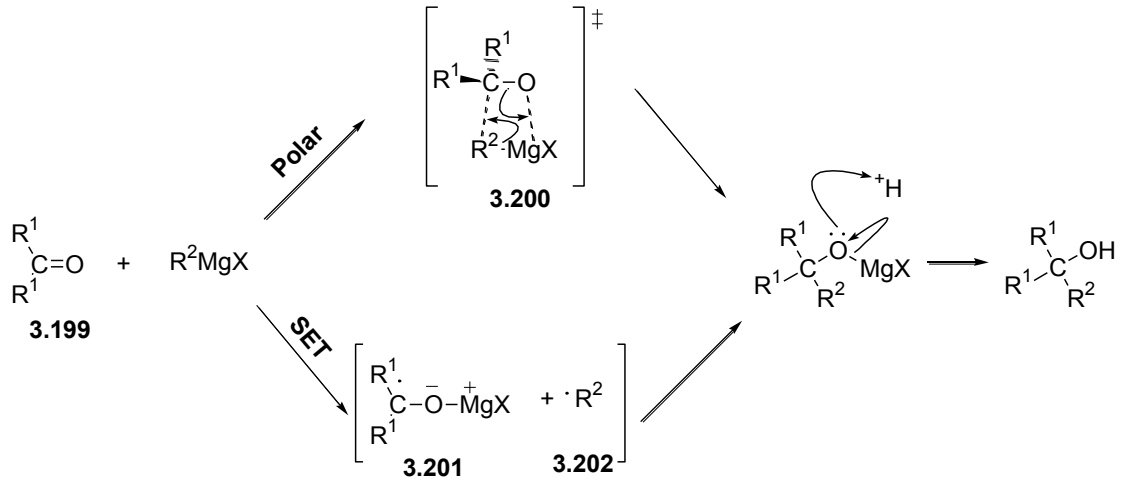

Scheme 3.4: The two proposed mechanistic pathways of Grignard synthesis.[252]

Fortunately, the addition of equal or greater equimolar amounts of anhydrous cerium chloride enhances the carbonylophilicity of Grignard reagents while suppressing the formation of the undesirable side products. Cerium is a member of the rare earth metals which possess f-orbitals with exploitable electronic and sterochemical properties, making cerium useful as a reagent or catalyst for organic synthesis.[253] Cerium chloride possesses great oxophilicity and has shown promise in its ability to activate carbonyl functionalities via coordination.[254] This activation may be the driving force in the promotion of carbonyl nucleophilic addition reaction by $CeCl_3$. It is also interesting to note that the Gignard reagents basicity is lower on mixing with cerium chloride.[251] Although the use of $CeCl_3$ for organometallic alkylation is widely used the mechanism is poorly understood.[255] A putative mechanism has been described by Hatano *et al.*[250] detailing the ability of $CeCl_3$ to act as a Lewis acid activating the carbonyl compound or the additives ability to increase the nucleophilicity of the alkylating agent via metal complexations of transmetalations. In the past $CeCl_3$ has been used as an additive to suppress undesired side products and synthesize key intermediates of highly hindered natural products.[256] For this reason $CeCl_3$ was used in the synthesis of the podocarpane derivatives (**3.203-3.207**, Scheme 3.5).

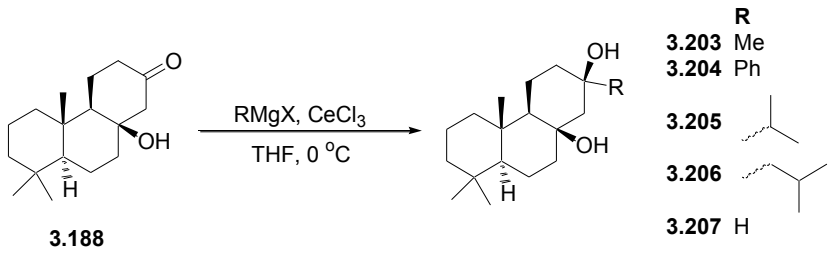

3.188

Scheme 3.5: The Grignard addition of **3.188**. (X = Br, Cl)

All the alkylation reactions of C-13 of **3.188** were carried out in the absence of $CeCl_3$ resulting in none or in very poor yield of the desired tertiary alcohol (Table 3.4). The addition of $CeCl_3$ to the reaction mixture via the procedure laid out by Imamoto *et al.*[257] resulted in the formation of the desired product and an increase in yield, most notably in **3.203** with an increase in yield from 17 to 57%. Reduced amounts of $CeCl_3$ (< 1.5 equiv.) resulted in poor yields and 1.5 equivalents (relative to **3.188**) was established as the most suitable equivalency and used in all our Grignard reactions. The use of THF or a THF/ether solvent system produced the highest yield while a pure ether system resulted in a poorer yield.[251] All reactions were therefore carried out in an anhydrous THF solvent system.

Table 3.4*:* Yields of Grignard addition products **3.203-3.207** in the presence and absence of $CeCl_3$

Compound	Yield [%] Absence of $CeCl_3$	$CeCl_3$
3.203	17	57
3.204	19	34
3.205	0	20
3.206	2	27
3.207	ND	19

All reactions were carried out under standard conditions outlined in Chapter 6.

The success of the alkylation with the use of Grignard reagents was easily determined from the ^{13}C NMR spectra, in which the loss of the signal at δ_C 210.7 in **3.188** and the appearance of a signal around δ_C 67 indicate the reduction of the ketone carbonyl to a tertiary alcohol carbon (C-13 in **3.203-3.207**, Figure 3.8). In addition two broad signals (δ_H 2.5-4.0) in ^1H NMR spectra (Figure 3.9) corresponding to the hydrogen on the hydroxyl functionality confirming the successful addition of the carbon nucleophile to C-13. The Grignard reaction involving the addition of an *iso*-butyl nucleophile to **3.188** resulted in formation of the reduction side product **3.207**. *Tert*-butyl magnesium bromide is a strong reducing agent[258] and perhaps *iso*-butyl magnesium bromide behaves in a similar way accounting for the formation of **3.207**.

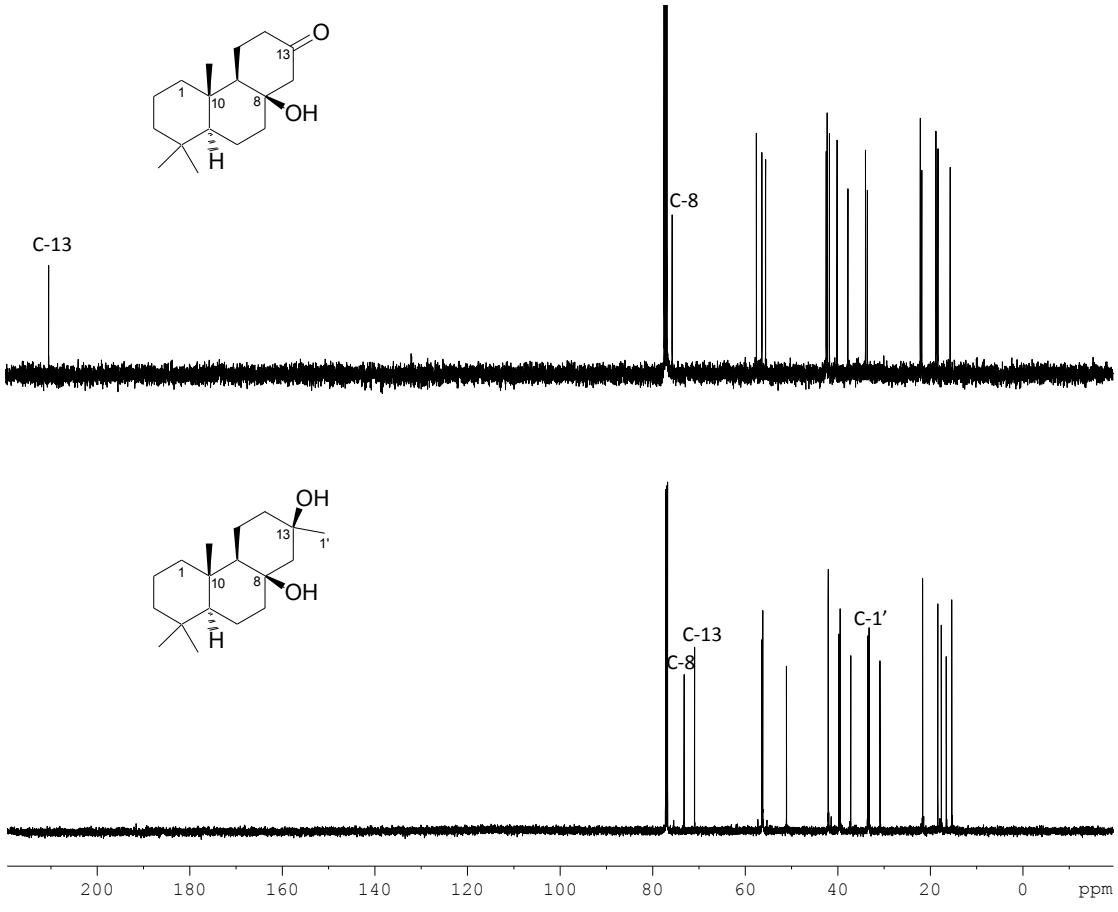

Figure 3.8: The ^{13}C NMR ($CDCl_3$, 150 Hz) spectra obtained for compounds **3.188** (*top*, Shown inset) and **3.203** (*bottom,* Shown inset).

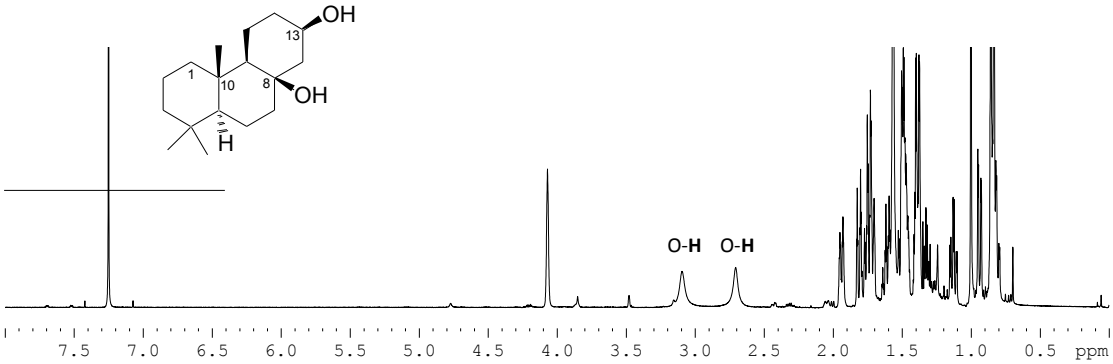

Figure 3.9: The ^{1}H NMR ($CDCl_3$, 600 MHz) spectra of **3.207** (shown inset). The proton signal attached to the oxygen of the hydroxyl functionality at positions 8 and 13 is indicated.

3.3.3. Determination of the absolute configuration of 3.203-3.207

While the absolute configuration of the diterpene ring of (+)-manool has been previously reported,[244] the Grignard alkylation created a new chiral centre at C-13. We therefore wanted to determine the absolute configuration of this carbon and thus submitted two podocarpanes (**3.204** and **3.207**) for X-ray crystal structure analysis. The orthorhombic crystal of **3.204** contained the space group $P2_12_12_1$ and the asymmetric unit comprised a single molecule. Given that the absolute configurations at C-5, C-8, C-9 and C-10 were known: C-5: (*S*), C-8: (*R*), C-9: (*R*), C-10: (*S*) and C-13: (*R*). The X-ray crystal structure established an (*R*) configuration at C-13.

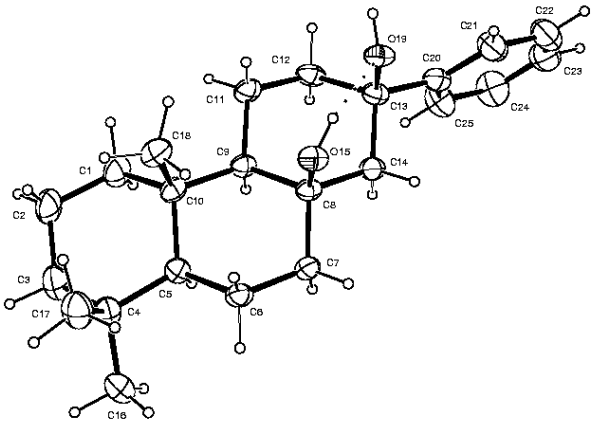

Figure 3.10: An ORTEP diagram of the perspective view of a molecule of **3.204** from the crystal structure. Thermal ellipsoids for the non hydrogen atoms are shown at the 50% probability level. Only the intramolecular O-H···O hydrogen bond is shown.

Interestingly, hydrogen bonding patterns were evident from the X-ray crystal structure of **3.204**, where there is an intramolecular O-H•••O hydrogen bond linking the two hydroxyl groups across the ring. The H atom attached to the acceptor oxygen atom then forms an intermolecular hydrogen bond with a neighbouring molecule. This hydrogen bonding leads to infinite chains of screw-related molecules running parallel to the crystal α-axis.[259]

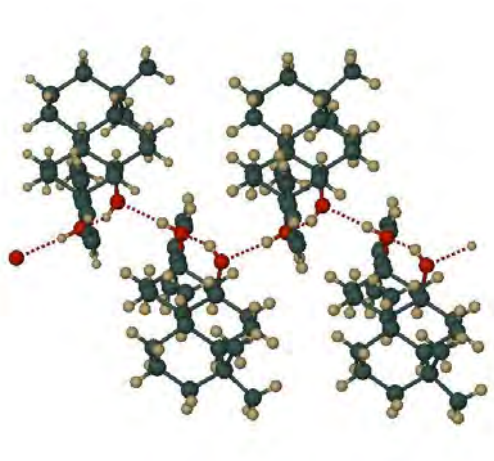

Figure 3.11: Hydrogen bonding in the crystal of **3.204**. Alternating intra- and intermolecular O-H···O hydrogen bonds form infinite spirals running parallel to the crystal a-axis.

We were also interested in the absolute configuration at C-8 and C-13 in the side product **3.207**. The formation of the hydroxyl at C-13 allows for the carbon-oxygen bond to form in either an axial or an equatorial position *i.e.* the alkylating nucleophile may attack the sp^2 hybridized carbonyl from either the *si* of the *re* face. We initially assumed that an equatorial orientation of the hydroxyl moiety would be favoured. On purification of **3.207** with HPLC only a single peak was identified with refractive index (RI) detection. To ensure that the steroisomers did not have identical retention times, and that a pure sample of **3.207** had been obtained, **3.188** was reduced using LAH to yield a 2:1 mixture of the two epimers **3.207** and **3.208**. Comparison of the ^{1}H NMR spectra of the mixture of **3.207** and **3.208** with that of **3.207** obtained from the Grignard reaction showed that only one isomer was produced in the reaction involving *iso*butylmagnesium (Figure 3.12).

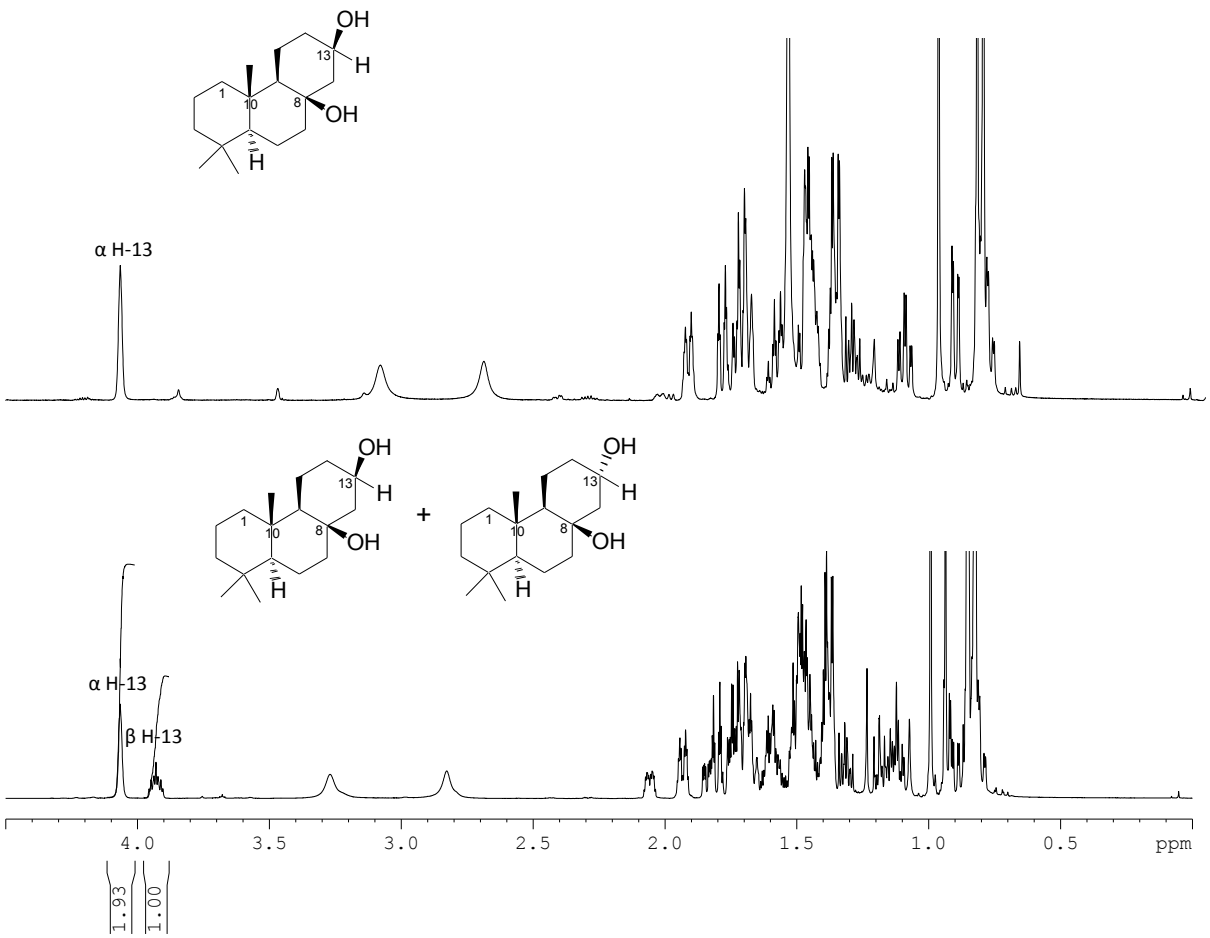

Figure 3.12: The ^{1}H NMR ($CDCl_3$, 600 MHz) spectra of **3.207** obtained from the Grignard reaction (*top,* shown inset) and the reaction mixture of **3.207** and **3.208** (*bottom*, shown inset) after reduction of **3.188** with LAH.

The absolute configuration of **3.207** was established by X-ray crystallography. The crystals of **3.207** were monoclinic, containing the space group C2 (which was transformed to the alternative setting I2 for technical reasons)[259] and it contained two molecules in the asymmetric unit with common configurations at the chiral centres. A quantitative comparison of these molecules yielded a root mean square fit of 0.077Å, indicating that they are virtually superimposable. Again it was assumed that the absolute configurations at C-5, C-8, C-9 and C-10 had been correctly assigned from other data and the molecules comprising the respective asymmetric units in the crystal were therefore chosen to be consistent with those assignments. The configurations at the chiral centres of **3.207** from the crystal structure are: C-5: (*S*), C-8: (*R*), C-9: (*R*), C-10: (*S*) and C-13: (*R*).

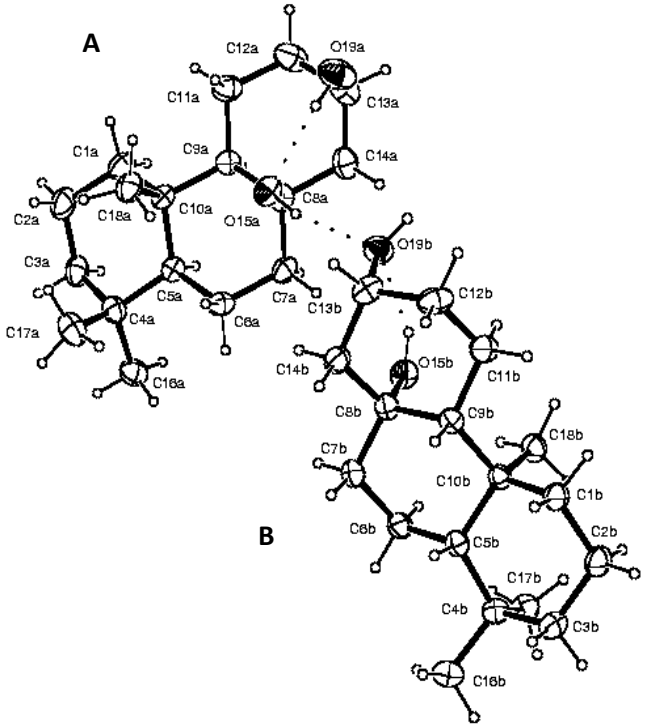

Figure 3.13: ORTEP diagram for **3.207** showing the two independent molecules A and B in the asymmetric unit as well as the unique hydrogen bonds associated with this unit.

Interesting hydrogen bonding patterns were also evident in the crystal structure of **3.207**. There is an intramolecular O-H···O hydrogen bond linking the two hydroxyl groups of each molecule (Figure 3.13). The H atom attached to the acceptor oxygen atom then forms an intermolecular hydrogen bond with a neighbouring molecule. In the crystals of **3.207**, molecules A and B are linked to one another and to a pair of molecules A', B' related to the former by a twofold rotation axis, which results in the formation of a closed, tetrameric motif (Figure 3.14).[259]

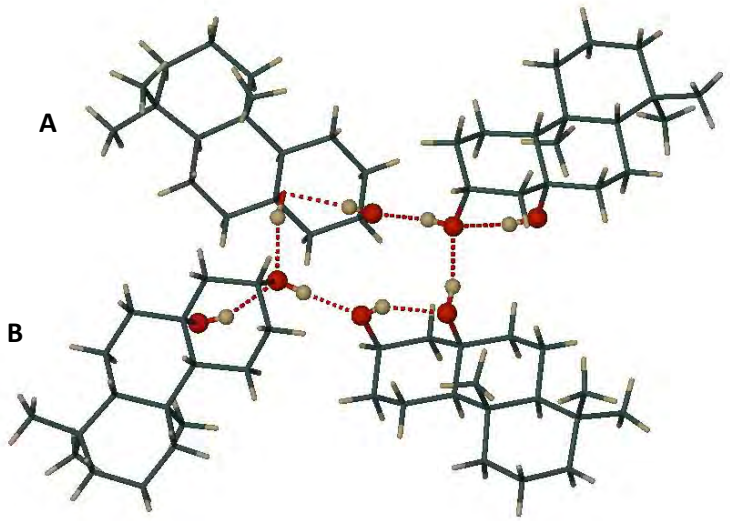

Figure 3.14: Tetrameric motif in the crystal of **3.207** formed by alternating intra- and intermolecular H-bonding and involving molecules A and B and their counterparts (the latter related to A and B by a twofold rotation axis running approximately normal to the page). Note the formation of a ring of homodromic hydrogen bonds involving six of the hydroxyl groups.

3.3.3.1. Spectroscopic characterization of the podocarpanes 3.204-3.207

The orientations of the hydrogens around the ring were assigned after careful analysis of the proton-proton coupling constants. A representative example of the way in which we assigned the NMR data in these compounds will be discussed here. In the ^{1}H NMR spectrum of **3.207** a doublet of triplets can clearly be seen at 1.81 ppm (Figure 3.15).

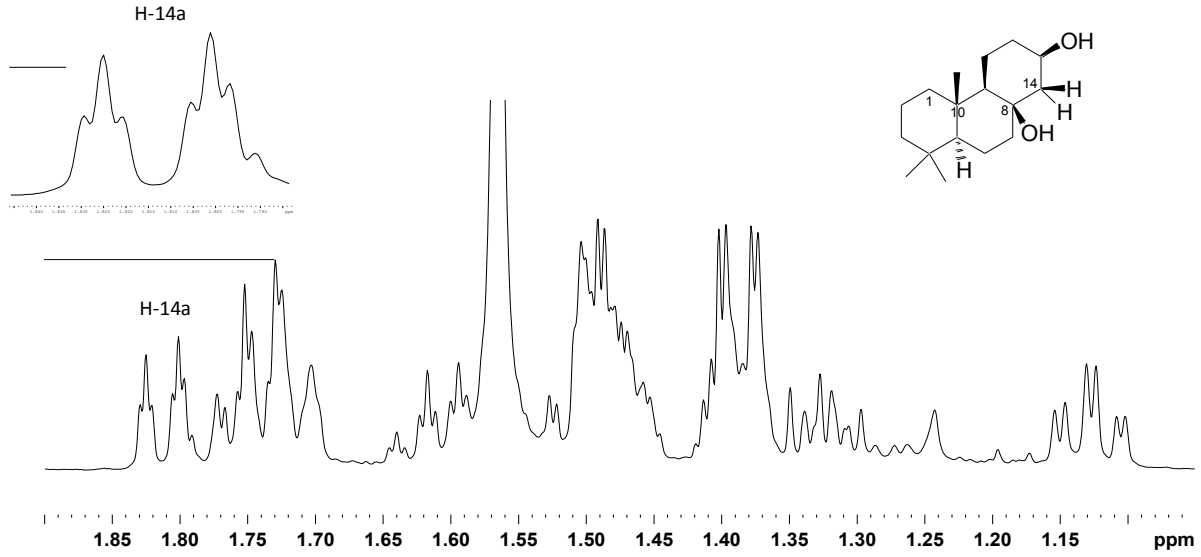

Figure 3.15: The ^{1}H NMR ($CDCl_3$, 600 MHz) spectrum of **3.207**. A doublet of triplet can be seen, corresponding to H-14a.

This chemical shift corresponds to one of the protons on C-14. The large coupling constant corresponds to the coupling of one of the protons on C-14 to its geminal partner ($J \approx 14$ Hz). Since the only other adjacent proton is on C-13 the expected splitting pattern of H-14 is a doublet of doublets with a smaller coupling constant of approximately 5-6 Hz due to the approximate 45° angle between the protons. However, the HSQC spectrum of **3.207** indicates two different proton signals on C-14, a multiplet (δ_H 1.39) and a doublet of triplets (δ_H 1.81). Inspection of the COSY spectrum of **3.207** (Figure 3.16) shows the signal at 1.81 ppm coupling to a proton on C-12 (δ_H 1.94), this was unusual as coupling between spins separated by four or more bonds is rare. However, in cyclic or sterically constrained environments, ^4J coupling or 'W-coupling' is often observed. It is called 'W-coupling' because the four bonds between the two coupling protons are all coplanar and form the shape of a W (Figure 3.16). The coupling constant of this type of ^4J coupling rarely exceeds 2-3 Hz.[260] 'W-coupling' would account for the splitting pattern observed (Figure 3.17). Since the hydroxyl on C-13 is β-axial the two adjacent hydrogens on C-12 are β-equatorial and α-axial, therefore in order for 'W-coupling' to occur the β-equatorial H-12 must couple with a hydrogen aligned in the same plane. We therefore concluded that the signal at 1.81 ppm corresponded to the β-equatorial hydrogen on C-14. This was supported by the lack of coupling, seen in the COSY spectrum, between the two α-axial hydrogens on C-12 and C-14. The ^{1}H NMR chemical shifts of remaining hydrogen atoms were assigned with similar rigour except where there was extensive signal overlap in the methylene envelope.

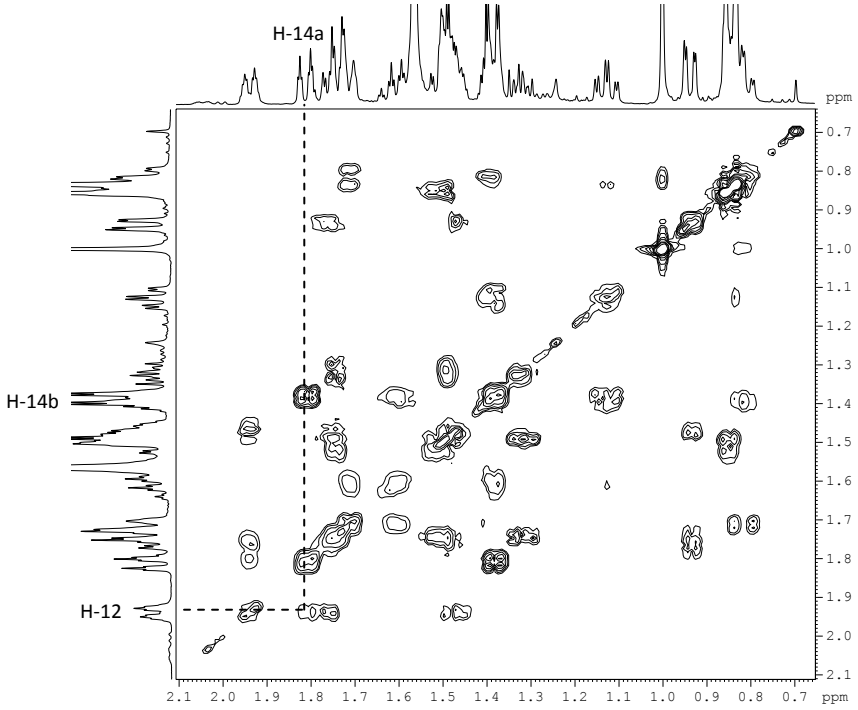

Figure 3.16: COSY spectrum ($CDCl_3$, 600 MHz; relaxation time [d1] = 1.00 sec; F1 and F2 = δ_H 0.65 – 2.10) obtained for **3.207**. The broken line indicates the COSY correlation between H-12 and H-14a.

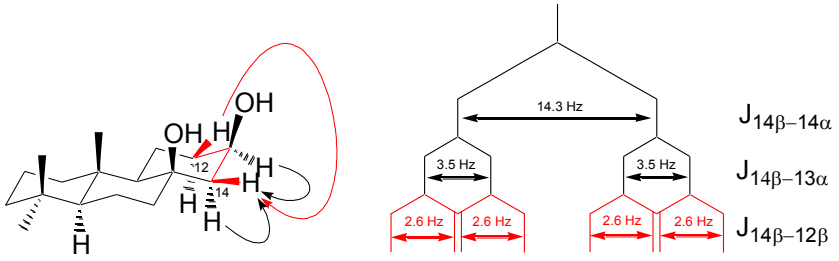

Figure 3.17: A graphical representation of the 'W-coupling' experienced by compound **3.207**. The red outline of the structure of **3.207** (*left*) show the protons involved in the W-coupling. The image on the right is a schematic diagram explaining the splitting pattern experienced by H-14β.

3.3.4. Structural activity relationship study of the podocarpanes

The compound with the strongest antiplasmodial activity in the first series of podocarpanes synthesised was the phenyl ring containing compound **3.204** (IC_{50} 6.6 µM) and **3.204** also did not appear to alter the shape of the erythrocyte. Due to the many examples of antimalarial drugs containing halogens (e.g. chloroquine and halofantrine) we proposed that by halogenating the phenyl ring of **3.204** we may improve the antiplasmodial activity. While several methods exist[261-263] for the halogenation of a phenyl ring the 4/3-chlorophenyl magnesium bromide, 4-chloro-2-methylphenyl magnesium bromide and 4-fluorophenyl magnesium bromide Grignard reagents were all commercially available, enabling us to synthesize **3.209-3.212** by Gringard methodology (Scheme 3.6). Using the $CeCl_3$ mediated Grignard addition method we had optimized earlier we were able to synthesize **3.209**-**3.212** in 32-64% yield.

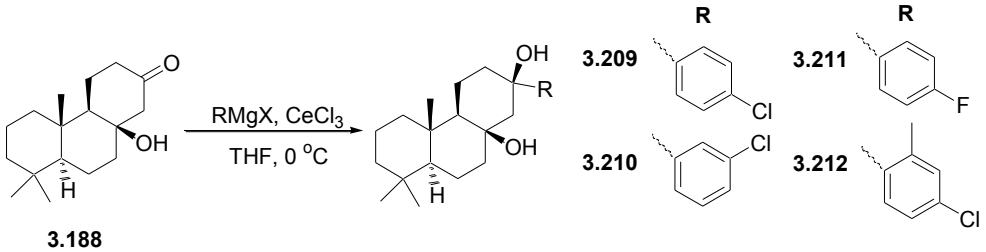

Scheme 3.6: The synthesis of halogenated phenyl containing podocarpanes **3.209-3.212** via a Grignard addition.

Interestingly, the ^{1}H and ^{13}C NMR spectra of compound **3.211** (Figure 3.18) clearly shows the fluorine atom in the *para* position of the phenyl ring coupled to the surrounding carbons and protons. The magnitude of the $J_{F,C}$ and $J_{F,H}$ coupling constants decrease over two, three and four bonds as

expected (Figure 3.18)[264] and proved useful in assigning the aromatic ^{1}H and ^{13}C chemical shifts in **3.211**. The assignment of the ^{1}H and ^{13}C NMR data for **3.209**-**3.212** were made from careful analysis of both the 1D and 2D NMR spectra and are reported in Chapter 6. The antiplasmodial activity and conclusions made about structural activity relationships are presented in Section 3.5.

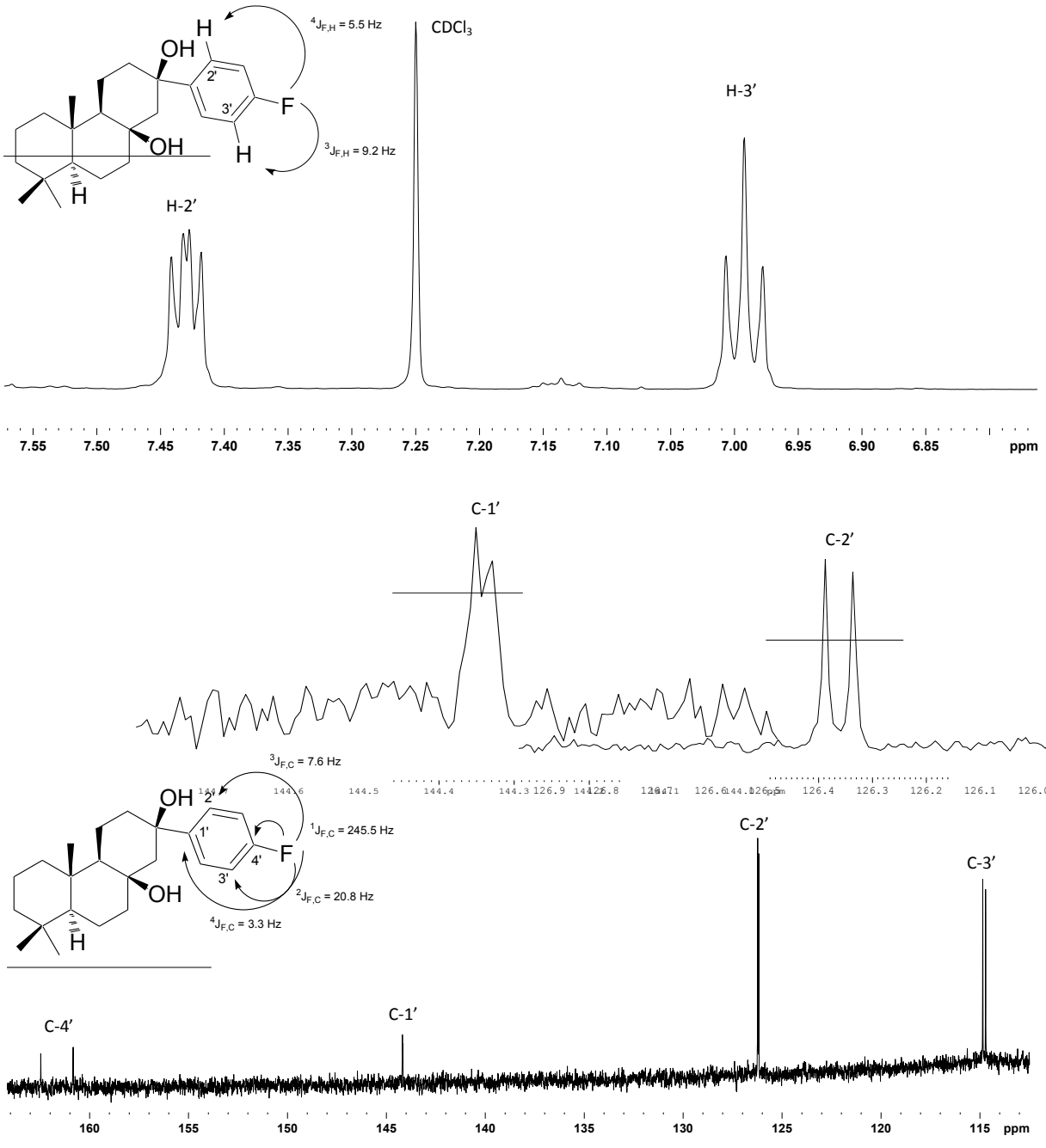

Figure 3.18: ^{1}H ($CDCl_3$, 600 MHz) and ^{13}C ($CDCl_3$, 600 MHz) spectra obtained for **3.211**. The inset describes the fluoride splitting experiences by the protons and carbons respectively.

3.4. Attempted synthesis of podocarpane isonitriles

The nanomolar antiplasmodial activity of Wright and Wattanapiromsakul's tricyclic marine isonitriles (**2.16-2.21** and **2.24-2.27**) inspired us to attempt to convert the tertiary alcohols on C-8 and C-13 of **3.188**, **3.204-3.207** and **3.209-3.212** to isonitrile functionalities, thus hopefully increasing the potency of the podocarpanes' antiplasmodial activity.

3.4.1. Isonitrile synthesis in a model compound

Kintano *et al.*[265] originally describe a method for the conversion of tertiary alcohols to isonitriles facilitated by zinc halides. This method also required trimethyisilyl cyanide (TMSCN), which will produce the highly toxic hydrogen cyanide on contact with water, thus the use of hygroscopic zinc halides would be problematic. Kintano *et al.*[266,267] later improved their method by substituting zinc halides with silver salts, the most notable being anhydrous silver perchlorate ($AgClO_4$), thus increasing safety while apparently simultaneously reducing reaction times in converting alcohols to isonitriles in near quantative yield. We hoped to extend Kintano's capricious method to the synthesis of isonitrile containing podocarpanes and set about first testing this method on a simpler compound *i.e.* **3.213**.

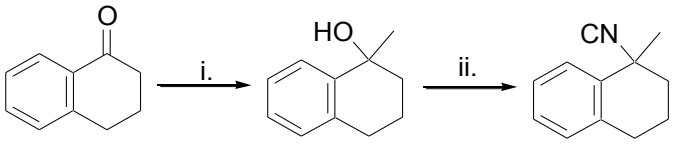

3.214 **3.213** **3.215**

Scheme 3.7: The synthetic scheme for the synthesis of the model isonitrile compound **3.215**. *Reagents and conditions:* i) MeLi, THF, -78 ˚C, 76%; ii) TMSCN, $AgClO_4$, DCM, 68%

The commercially available α-tetralone (**3.214**) was reduced using methyl lithium to afford a racemic mixture the tertiary alcohols (**3.213**). The protocol outlined by Kintano[267] dictates the addition of the TMSCN to a DCM solution of the tertiary alcohol, followed by the addition of the silver salt. However, we had no way of adding the insoluble silver salt without perturbing the sealed system, thus possibly exposing ourselves to highly toxic hydrogen cyanide gas. Therefore, we added the silver salt to the reaction mixture prior the addition of TMSCN, resulting in no detection of the isocyanide. We subsequently modified a three-necked round bottom flask to allow the addition of the silver salt to the alcohol-TMSCN mixture without disrupting the closed system. TMSCN followed

by anhydrous $AgClO_4$, using our modified apparatus, was carefully added to a solution of **3.213** in anhydrous dichloromethane to yield the isonitrile **3.215** in 68% yield after normal phase HPLC (22.5% EtOAc 87.5% hexane) purification (Scheme 3.7). After two hours, the reaction was quenched with saturated $NaHCO_3$ solution and allowed to stir and vent in a sealed fumehood for 10 minutes to remove any unreacted TMSCN. The highest safety precautions were taken when carrying out this reaction, a cyanide antidote kit was always close at hand. In addition immediately after the reaction was completed all experimental apparatus was soaked in solution of saturated $NaHCO_3$ followed by subsequent addition of $HClO_4$ to convert all cyanide to harmless cyanates for safe disposal. The ^{13}C NMR spectrum of **3.215** clearly showed the removal of the hydroxyl moiety on C-9, however, the appearance of a new signal corresponding to the carbon of the isonitrile was not apparent (δ_C 150-170 ppm, Figure 3.19) and the ^{13}C NMR data required further interrogation.

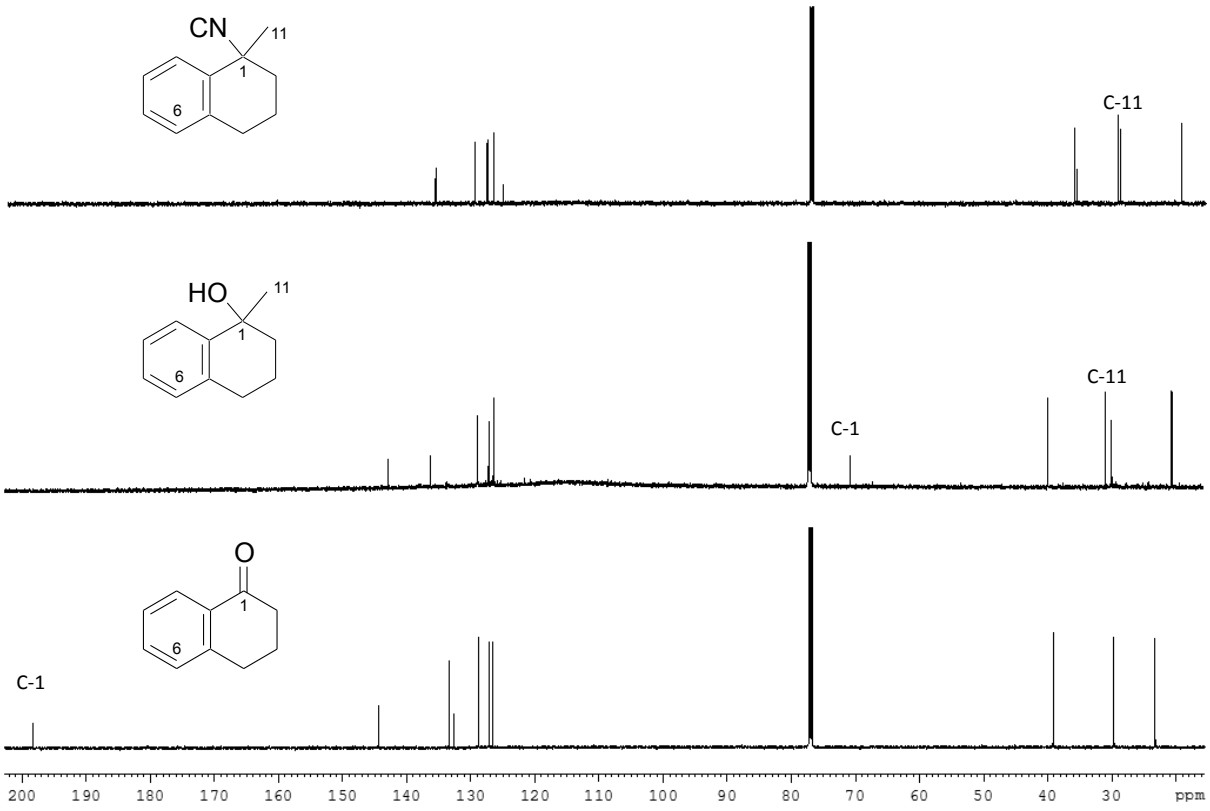

Figure 3.19: ^{13}C ($CDCl_3$, 150 MHz) spectra obtained for **3.215** (*top*), **3.216**, (*middle*) and **3.214** *(bottom*). The structures are shown inset.

3.4.1.1. Optimization of the ^{13}C NMR acquisition parameters to detect the isonitrile functionality

The ^{13}C NMR spectrum of the comerically available *tert*-butyl isocyanate **3.216** (Figure 3.20) revealed a ^{13}C-^{14}N triplet at δ_C 152.4.

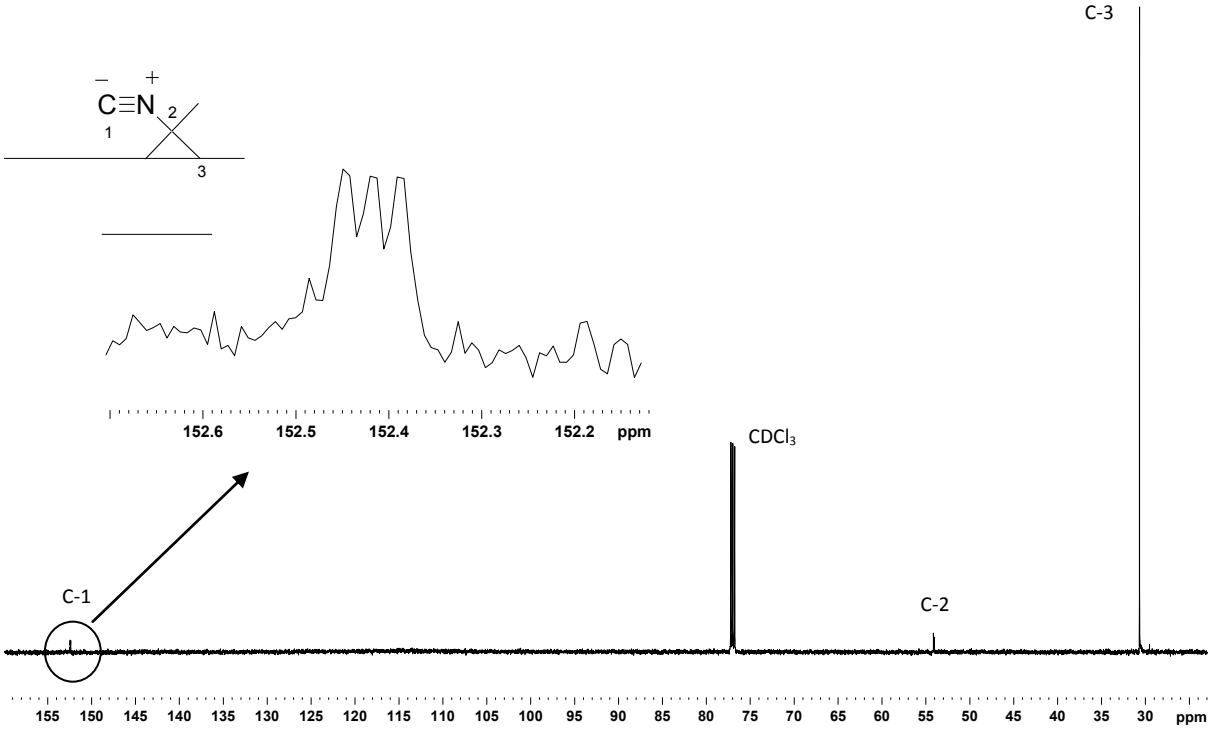

Figure 3.20: The ^{13}C NMR ($CDCl_3$, 150 MHz) of *tert*-butyl isocyanide (**3.216**, shown inset), with an enlarged view of the isonitrile signal. [d1] = 5.00 sec

The carbon is split into a triplet due to the coupling of the $^{13}C - ^{14}N$, since ^{14}N has a quantum spin number (I) of 1 which results in a 2*n*I + 1 splitting pattern, where n = total number of coupling neighbouring nuclei. There was no triplet signal ($^1J_{N,C}$ = 4.5 Hz) observed in this region for compound **3.215**, possibly due to the long relaxation time of the isonitrile carbon. The relaxation time of a saturated $CDCl_3$/ *tert*-butyl isocyanide (**3.216**) solution was used to investigate the relaxation time of this carbon. An increase of the d_1 delay time from one to five seconds and a prolonged acquisition time resulted in an increase in the signal to noise ratio. These data aquistion parameters were used to acquire a ^{13}C NMR spectrum of **3.215** in $CDCl_3$ resulting in a triplet signal appearing at δ_C 167.9 (Figure 3.21) indicating the presence of an isonitrile carbon. The presence of an isonitrile functionality was also supported by IR data in which a peak at 2190 cm^{-1}, corresponding to the N≡C stretching frequency was observed.[268]

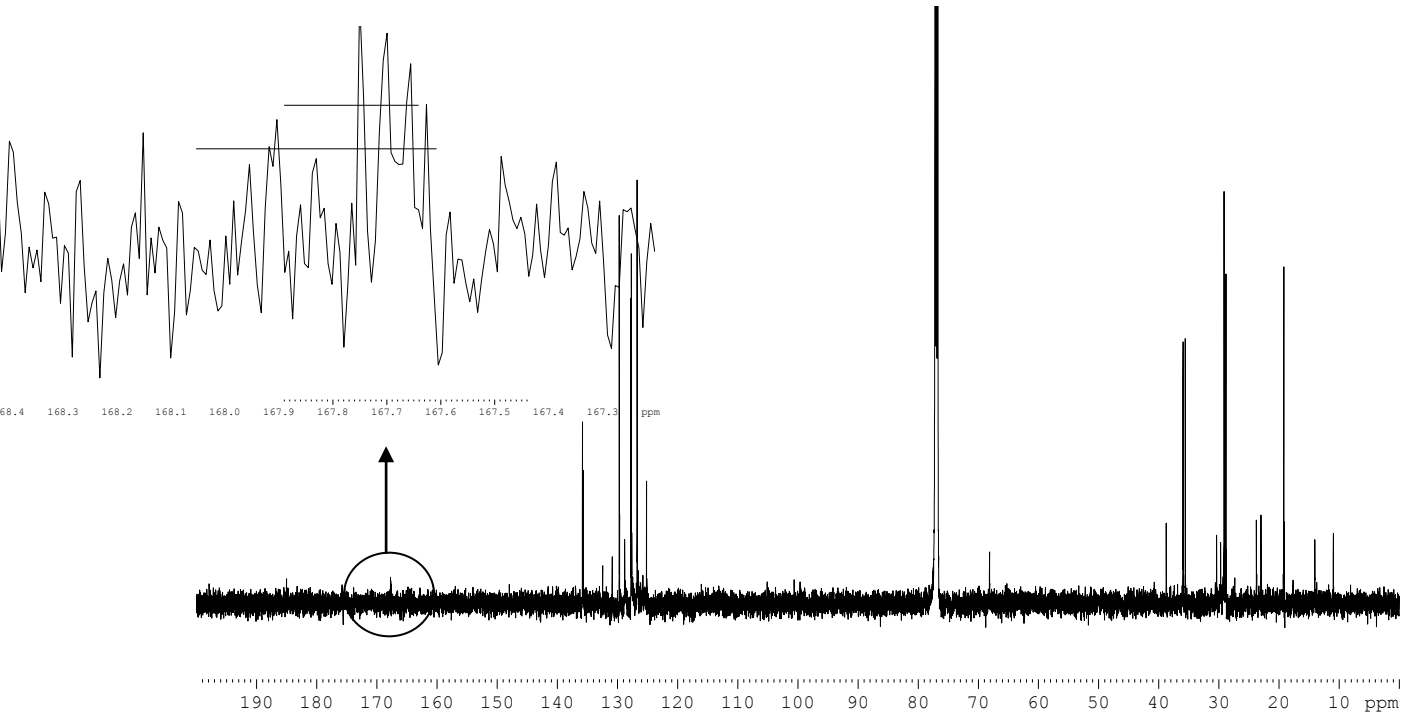

Figure 3. 21: The ^{13}C NMR ($CDCl_3$, 150 MHz) of **3.215**, (shown inset), with an enlarged view of the isonitrile signal. [d1] = 5.00 sec. Number of scans = 20480 (Total time 34 hrs)

3.4.2. Attempted conversion of 3.188, 3.204-3.207 and 3.209-3.212 to isonitriles.

With the successful conversion of **3.213** to **3.215**, we attempted to convert the tertiary alcohols of **3.188**, **3.204-3.207** and **3.209-3.212** into isonitriles (Scheme 3.8). We attempted to synthesize the isonitriles using two different silver salts ($AgClO_4$ and $AgBF_4$), however on inspection of the ^{13}C NMR spectrum of the reaction product of **3.188**, no triplet was observed in the δ_C 150-170 ppm region although the C-OH signals at 75.5 (q, C-8) ppm and 57.3 (CH, C-14) ppm had disappeared while two new signals at 125.8 (CH, C-8) ppm and 165.9 (C, C-14) ppm had appeared in the downfield region, suggesting the dehydration of **3.188** to afford **3.217** (Figure 3.22). We explained this dehydration after carefully considering permutations around the proposed mechanism of isonitrile formation presented in Scheme 3.9. This mechanism is based on an S_N1 nucleophilic substitution reaction via a carbocation intermediate (**3.218**). The cyanide anion (**3.219**) usually favours alkylation at the cyanide carbon forming the nitrile as opposed to the isonitrile. However, should the cyanide ion be 'complexed' with a heavy-metal counter-ion such as silver (**3.220**), alkylation preferentially occurs via the nitrogen atom. The use of the aprotic solvent DCM, which does not have the ability to form

hydrogen bonds that hinder nucleophilic attack via the nitrogen atom allows for the formation of the isonitrile.

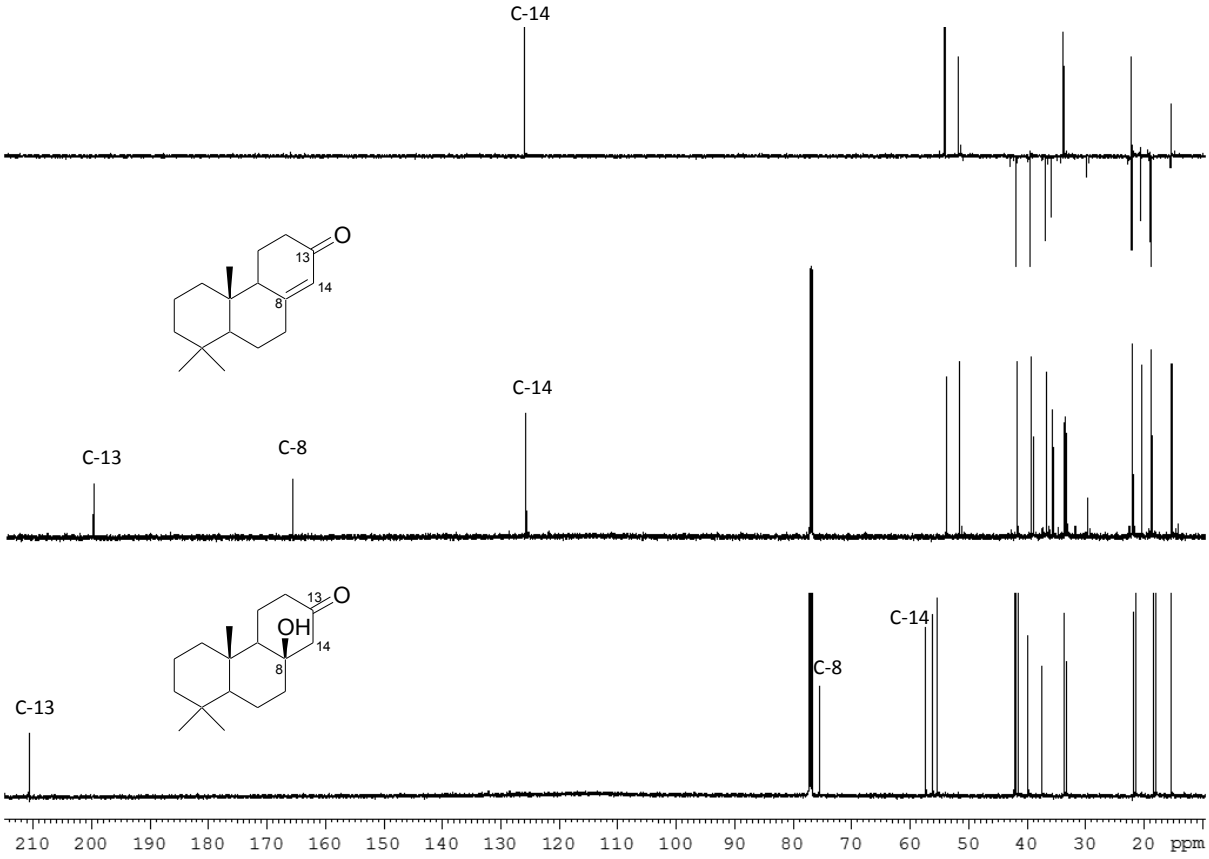

Figure 3.22: ^{13}C NMR spectra ($CDCl_3$, 150 MHz) spectra of **3.188** (*bottom*) and **3.217** (*middle*) and DEPT135 ($CDCl_3$, 150 MHz) spectrum of **3.217** (*top*). Structures shown as insets.

The proposed mechanism (Scheme 3.9) starts with the TMSCN (**3.221**) removing the tertiary alcohol moiety (**3.222**) by forming the trimethyl silate (**3.223**), simultaneously releasing the cyanate anion into the solution. This initial step may account for why the reaction failed when the silver salt was added prior to the addition of TMSCN. The carbocation (**3.218**) formed with the loss of the trimethylsilyl leaving group **3.223** and is a bulky highly hindered carbocation. Steric hindrance may therefore account for the failure of the cyanate anion to attack the carbocation **3.224**. Quenching of the carbocation through the loss of a proton (Scheme 3.10) to yield the α,β-unsaturated ketone (**3.217**) appears to be preferable. A similar result was obtained for all podocarpanes (**3.204 - 3.207**).

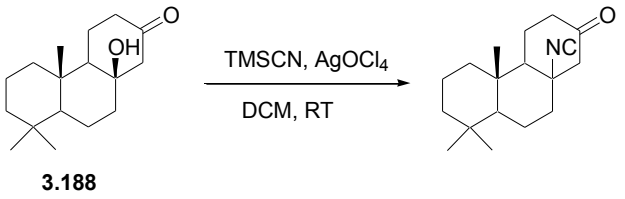

3.188

Scheme 3.8: The synthesis of a isonitrile from tertiary alcohol **3.188** using silver perchlorate and TMSCN.

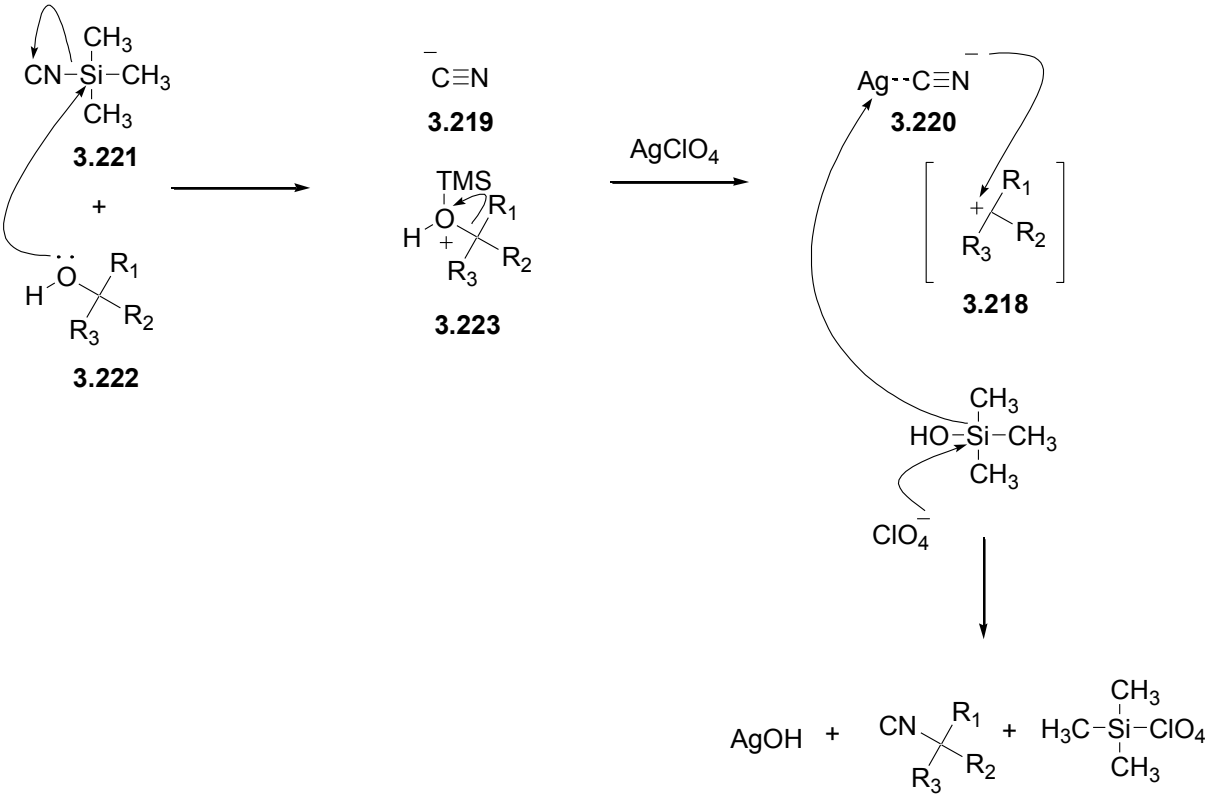

Scheme 3.9: The proposed mechanism of the formation of an isonitrile from a tertiary alcohol **3.222** facilitated by TMSCN and $AgOCl_4$

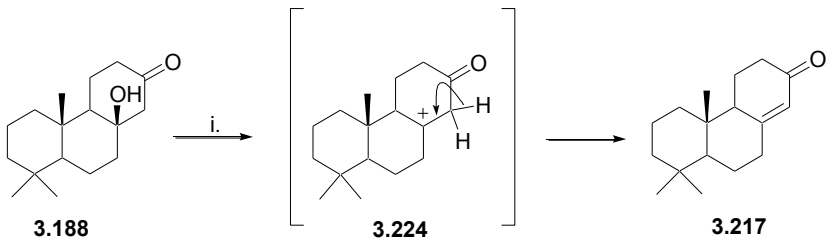

3.188 **3.224** **3.217**

Scheme 3.10: Proposed mechanism for the formation of **3.217**. *Reagents and conditions:* i) TMSCN, $AgOCl_4$, DCM, RT

3.5. Antiplasmodial and haemolytic activity of 3.188, 3.204-3.207, 3.209-3.212 and 3.213-3.215

Although, podocarpanes **3.188**, **3.204-3.207** and **3.209-3.212** all displayed, moderate antiplasmodial activity, none showed antiplasmodial activity within the range of the currently available drugs used for the treatment of malaria (Table 3.5). The most active of the cohort of compounds screened were the podocarpanes containing an aromatic phenyl ring at C-13 *i.e.* **3.204, 3.209-3.212** and the ketol **3.188**. The antiplasmodial activity for all the halogenated compounds **3.209-3.212** was improved when compared to the activity of **3.204**. The antiplasmodial results (Section 3.5) show three structural activity relationships. Firstly the substitution of the chlorinated C-4 aromatic ring (**3.209**) and not C-3 (**3.210**) enhances antiplasmodial activity. Secondly the fluorinated compound (**3.211**) has a moderately lower IC_{50} value than that of its chlorinated counterpart (**3.209**) and finally a disubstituted phenyl ring (**3.212**) shows relatively better antiplasmodial activity compared to all the halogenated compounds. These results would suggest that the position of the substituent as well as the electronegativity plays a role in these compounds' bioactivity. Since the phenyl containing podocarpanes are the most active, this may suggest the activity of these compounds resides in their ability to fit into and possibly π-stack into a hydrophobic pocket in the active or effector site of an unidentified enzymatic target.

All the podocarpane derivatives were tested for their ability to alter erythrocyte membrane shape. No formation of echinocytes or stomatocytes was observed. This suggests that none of these compounds were incorporated into the red blood cells lipid bilayer. At a drug concentration of 100 µM, only a very small percentage of erythrocytes underwent lysis (Table 3.5). It would appear that the removal of the alkene functionality attached to C-13 present in **3.170-3.172**, **3.175** and **3.183-3.186** eradicates the compounds ability to change erythrocyte morphology.

The synthetic isonitrile (**3.215**) caused total haemolysis of the erythrocytes at both 50 and 100 µM concentrations (Table 3.5). The precursors **3.213** and **3.214** were tested for haemolytic activity in order to gauge the role the isonitrile moiety plays in the disruption of the erythrocytes membrane. α-Tetralone **3.214** and the tertiary alcohol **3.213**, both showed 0.2 % lysis at 50 µM and 0.2 and 0.3% lysis at 100 µM respectively. We can thus conclude that the isonitrile functionality in **3.215** plays a direct role in haemolysis.

Table 3.5: The antiplasmodial and haemolytic activity of compounds **3.188**, **3.204-3.207**, **3.209-3.212** and **3.215**.

Compound	Antiplasmodial activity (μM)			Haemolytic activity at 100μM			Haemolytic activity at 50μM		
	IC_{50}	s.d.	n	% Haemolysis	s.d.	n	% Haemolysis	s.d.	n
3.188	7.2	1.2	5	0.6	0.3	5	0.7	0.2	5
3.203	29.1	1.2	4	1.0	0.4	3	0.5	0.1	3
3.204	6.6	0.3	4	0.6	0.3	5	0.7	0.2	4
3.205	22.3	1.6	4	0.5	0.3	4	0.4	0.2	6
3.206	26.1	0.8	4	0.8	0.4	5	0.5	0.2	3
3.207	21.3	2.9	4	0.6	0.3	3	0.6	0.3	3
3.209	4.1	0.5	4	0.1	0.1	3	0.001	0.001	3
3.210	8.2	1.7	3	0.5	0.2	3	0.06	0.02	3
3.211	3.5	0.4	4	0.2	0.1	3	0.02	0.02	3
3.212	1.4	0.2	3	0.4	0.2	3	0.03	0.003	3
3.215	3.1	0.6	4	105.2	2.1	3	103.8	3.4	3
Chloroquine	0.07	0.01	3	0.2	0.1	5	0.06	0.04	4
Quinine	0.1	0.01	5	0.5	0.3	6	0.6	0.1	5
Primaquine	0.6	0.04	5	0.6	0.3	6	0.3	0.2	5
Pyrimethamine	0.1	0.02	4	0.4	0.2	6	0.4	0.3	5
Cycloproguanil	11.3	1.9	7	0.07	0.05	5	0.2	0.2	4

3.6. 1-Deoxy-D-xylulose-5-phosphate (DOXP) reductase (DXR) inhibition

Once **3.209-3.212** were synthesized, these compounds were submitted to a *P. falciparum* and *E. coli* DXR inhibition assays.[269]

3.6.1. Background

Isoprenoids constitute the largest single class of natural products with over 35 000 compounds being described to date.[270] This class represents a large collection of bioactive compounds, comprising

many primary and secondary metabolites. Many isoprenoids carry out biological functions essential to the functioning and development of living organisms. Despite the plethora of biological functions, they all stem from two C_5 precursors, isopentenyl diphosphate (**3.225**, IPP) and its isomer dimethylally diphosphate (**3.226**, DMAPP). The non-mevalonate pathway consists of seven enzymatically controlled steps (Scheme 3.11) resulting in the precursors **3.225** and **3.226**.[271] The initial step consists of the condensation of pyruvate (**3.227**) and glyceraldehyde-3-phosphate (**3.228**) forming DOXP (**3.229**), mediated by DOXP synthase (DXS).[272] The DOXP is converted to 2-C-methyl-D-erythritol-4-phosphate (**3.230**, MEP) by an intramolecular rearrangement and reduction in a single step catalysed by DXR.[273] This mechanism of conversion of **3.229** to **3.230** is not clearly understood, two proposed hypothesises are discussed below in Section 3.6.2. The conversion of MEP to 4-diphosphocytidyl-2C-methyl-D-erythritol (**3.231**, CDP-ME) is CTP dependent and catalyzed by CMS.[274] 4-Diphosphocytidyl-2C-methyl-D-erythritol-2-phosphate (**3.232**, CDP-MEP) is formed by the phosphorylation of **3.231** at the 2-hydroxyl position, and is mediated by 4-Diphosphocytidyl-2-C-methyl-D-erythritol kinase (CMK).[275] The two phosphates on either end of **3.232** are joined by the enzyme MCS, resulting in the formation of 2C-methyl-D-erythritol-2,4-cyclodiphosphate (**3.233**, MEcPP) and the removal of cytidine monophosphate (CMP).[276] The formation of 1-hydroxy-2-methyl-2-(E)butenyl-4-diphosphate (**3.234**, HMD-PP) requires the cleavage of two carbon oxygen bonds and this is thought to be facilitated via a $2e^-$ transfer from the iron-sulphur cluster of HMDPP synthase.[277] In the final step HMDPP is converted to a mixture of DMAPP and IPA (usually 5:1 or 3:1) catalyzed by the NAD(P)H dependent HMBPP reductase.[278]

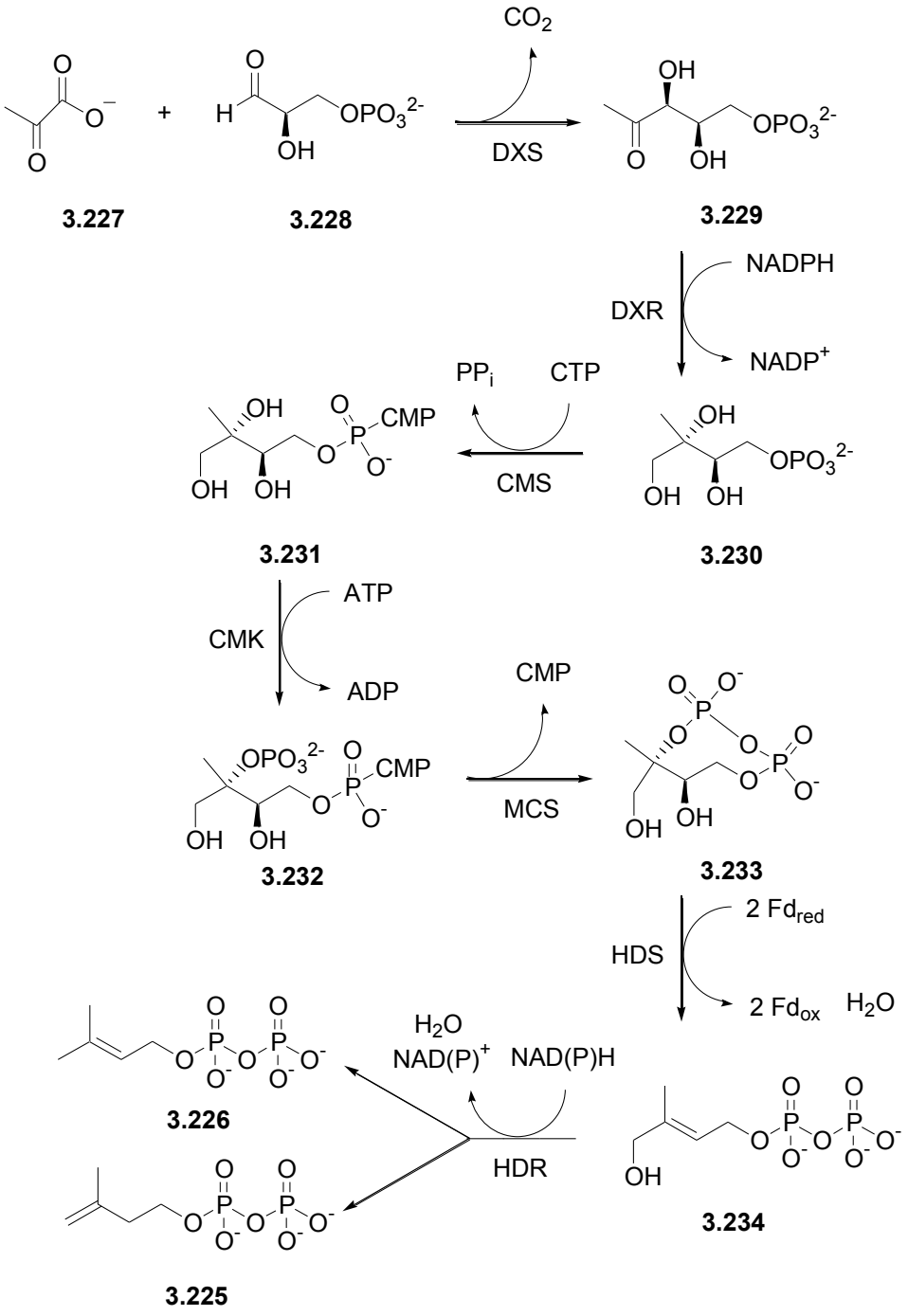

Scheme 3.11: The non-mevalonate pathway in *P. falciparum*.[277] Abbreviations: DXS, DOXP synthase; DXR, DOXP reductase; CMS, 4-diphosphocytidyl-2-C-methyl-D-erythritol synthase; CTP, cytidine triphosphate; CMP, cytidine monophosphate; MCS, 2-C-methyl-D-erythritol 2,4-cyclodiphosphate synthase; HDS, (E)-4-hydroxy-3-methyl-but-2-enyl pyrophosphate synthase; HDR, (E)-4-hydroxy-3-methyl-but-2-enyl pyrophosphate reductase

3.6.2. DOXP reductase (DXR)

DOXP reductase (DXR) is the second enzyme in the non-mevalonate cascade, and exists as a homodimer of a molecular weight of 42-45 kDa. The optimum pH range is 7-8 for the function of this enzyme with a maximum temperature range of 50-60 °C.[279] DXR requires the assistance of a divalent metal ion for catalysis, usually Mg^{2+}, Mn^{2+} or Co^{2+}. The addition of other divalent metal (Ca^{2+}, Ni^{2+} or Zn^{2+}) *in vitro* resulted in a reduction or loss of activity.[273,280] Due to the abundance of Mg^{2+} *in vivo* it has been suggested that Mg^{2+} is the relevant cation used for the transformation of DOXP to MEP (Scheme 3.12).[280] Each *Pf*DXR subunit contains a single NADPH molecule and a divalent metal ion (Figure 3.23). These subunits each contain two large domains, a linker region and a small C-terminal domain. The one large domain is responsible for NADPH binding while the other is responsible for metal and substrate binding and thus catalysis.[281]

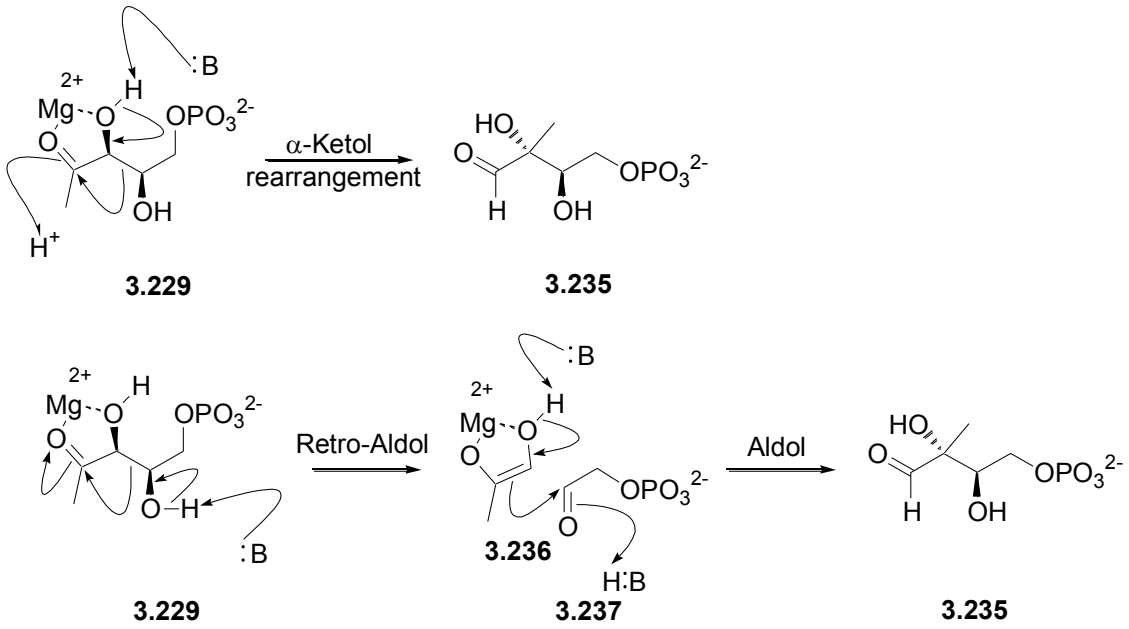

Scheme 3.12: Proposed mechanisms of the rearrangement of DOXP (**3.229**) to form the intermediate 2-C-methyl-D-erythrose-4-phosphate (**3.235**). *Above:* α-ketol rearrangement; *below*: sequential retro-aldol/aldol reactions. Reproduced from Proteau.[279]

2-C-methyl-D-erythrose-4-phosphate (**3.235**) was proposed as an intermediate for the conversion of **3.229** to **3.230**.[282] The two proposed mechanisms involve either a α-ketol rearrangement or a sequential retro-aldol/aldol synthesis (Scheme 3.12). The α-ketol rearrangement requires the divalent metal directed deprotonation of the hydroxyl on C-3 of DOXP (**3.229**), assumedly via a basic residue on DXR, initiating the migration of the phosphate bearing C_2 subunit to afford **3.235**. The

second mechanism requires the basic deprotonation of the alcohol on C-4, followed by the cleavage of the bond between C-3 and C-4 to afford the enolate, hydroxyacetone (**3.236**) and glycoaldehyde phosphate (**3.237**). Recombination of the two moieties via an aldolization, forms a carbon-carbon bond between C-2 and C-4 of **3.229**, resulting in **3.235**.[283]

Figure 3.23: The ribbon representation of the crystal structure of the homodimer of *P. falciparum* DXR (PDB 3AUA) and co-factors.[281] The α-helices coloured in red, the β-sheets in blue. The co-factor NADPH in the active site is displayed in stick representation and Mg^{2+} displayed in yellow in CPK representation.

The formation of MEP is under strict stereochemical control.[279] The stereospecific delivery of a hydride from NADPH occurs from the pro*S* hydride,[280] which attacks the aldehyde intermediate **3.235** at the *re* face.[284] This results in the formation of 2-C-methyl-D-erythritol-4-phosphate **3.230**.

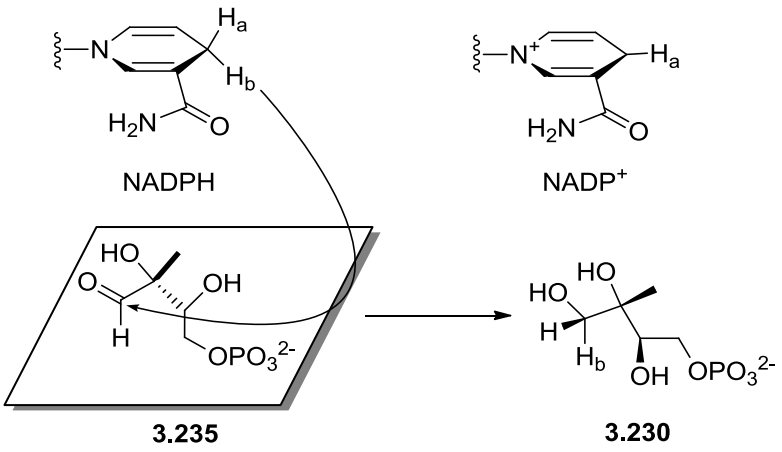

Scheme 3.13: The stereochemical formation of **3.230** in DXR. The pro*S* hydride of NADPH attacks the aldehyde of **3.235** at the *re* face. Reproduced from Proteau.[279]

3.6.3. Current DXR inhibitors

The natural antibiotic fosmidomycin (**3.238**) was isolated from *Streptomyces lavendulae*[285] and identified as a DXR inhibitor.[286] Another related natural product FR900098 (**3.239**) was also shown to be a potent inhibitor of DXR.[287] The bound crystal structures of these compounds indicate a similar binding fashion to that of DOXP.[281,288] Over the years several analogues of **3.238** and **3.239** have been synthesized.[289,290] A few examples of these and their relevant IC_{50} values against *E. coli* DXR are presented in Figure 3.24.

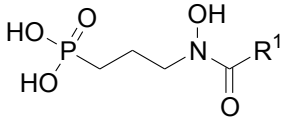

3.238 R^1=H 0.034 µM
3.239 R^1=Me 0.032 µM

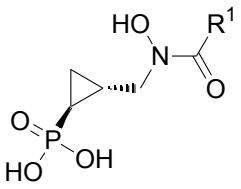

R^1=H 0.313 µM
R^1=Me 0.050 µM

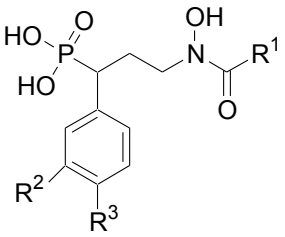

R^1=H	R^2=OMe	R^3=H	0.156 µM
R^1=H	R^2=Cl	R^3=Cl	0.059 µM
R^1=Me	R^2=H	R^3=H	0.311 µM
R^1=Me	R^2=Me	R^3=H	0.396 µM
R^1=Me	R^2=OMe	R^3=H	0.459 µM
R^1=Me	R^2=Cl	R^3=H	0.099 µM
R^1=Me	R^2=Cl	R^3=Cl	0.119 µM

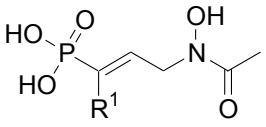

R^1=Ph >30 µM
R^1=(3-NO_2)Ph >30 µM
R^1=(4-NO_2)Ph 34 µM
R^1=2-thienyl 42 µM
R^1=3-thienyl >30 µM

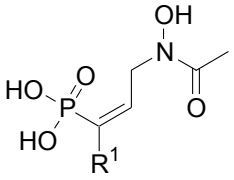

R^1=Ph 5.4 µM
R^1=(4-CN)Ph 5.5 µM
R^1=(3,4-Cl_2)Ph 16 µM

Figure 3.24: The structures of fosmidomycin (**3.238**), FR900098 (**3.239**) and analogues, with IC_{50} values of *E .coli* DXR.[289,290]

Another approach to DXR inhibition focuses on the inhibition of NADPH binding site. While all the compounds tested showed DXR inhibition (Figure 3.25),[291] however the danger of using NADPH analogues is that they may bind and inhibit other unrelated biosynthetic pathways.

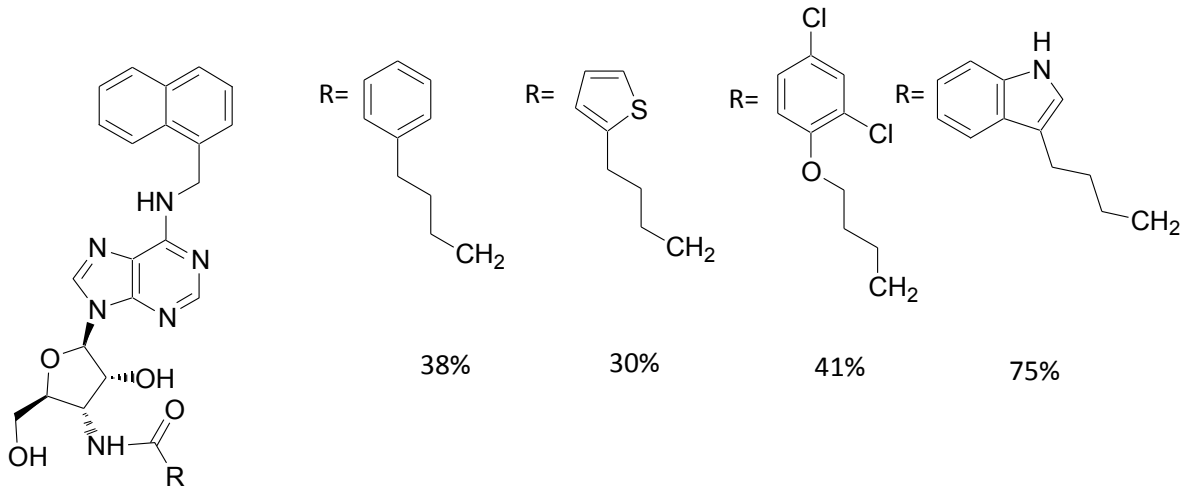

Figure 3.25: Structures of adenosine type DXR inhibitors and there % inhibition value. All inhibition studies were tested at a concentration of 30 µM.[291]

3.6.4. Results of DXR inhibition studies

The compounds **3.209-3.212** were tested for their ability to inhibit both *Pf*DXR and *Ec*DXR derived from *P. falciparum* and *E. coli* repectively. The enzymatic activity was monitored via the reduction of NADPH, which is essential for the function of the reaction. From Figure 3.26 it is clear that compounds **3.209-3.211** jointly show a trend in which there is a reduction in activity in *Pf*DXR and *Ec*DXR of >40% and >60% respectively. Interestingly, our most active antiplasmodial podocarpane, **3.212**, showed very little inhibition of DXR.

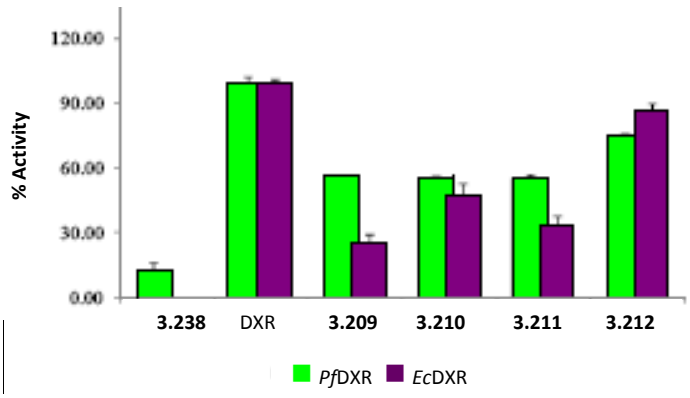

Figure 3.26: Relative percentage *Pf*DXR inhibition (shown in green) and *Ec*DXR inhibition (shown in purple) for compounds **3.238, 3.209-3.212**. All compounds tested at 250 µM.[269]

3.7. Conclusion

We successfully managed to synthesis compounds **3.203-3.207** and **3.209**-**3.212** using $CeCl_3$ mediated Grignard alkylation. By introducing a halogen atom to the phenyl ring of the podocarpanes we generally improved the antiplasmodial activity by 3-5 times. None of our synthesized diterpenes (**3.203-3.207** and **3.209**-**3.212**) exhibited any erythrocyte shape change. We attempted to improve the activity through the conversion of the tertiary alcohols of **3.203-3.207** and **3.209**-**3.212** to isonitriles, however this reaction resulted in the dehydration products (e.g. **3.217**).

We subsequently tested the most active compounds **3.209**-**3.212** for the ability to inhibit DXR thus attempting to identify the podocarpanes antiplasmodial mode of action. To best of our knowledge this is the first recorded use of diterpene inspired molecules in the inhibition of DXR. We were unable to determine whether these compounds bind to the DOXP receptor or the NADPH receptor. Gelb[292] has provided evidence to suggest that micromolar anti-plasmodial activity may be indicative of multi-target binding in *Plasmodium* and it is probable that **3.203-3.207** and **3.209**-**3.212** act at more than one, as yet unidentified, target in *P. falciparum*. The ability of **3.203-3.207** and **3.209**-**3.212** to inhibit the sequestration of haem will be evaluated in Chapter 4.

CHAPTER 4: *IN VITRO* AND *IN SILICO* STUDIES OF β-HAEMATIN INHIBITION

4.1. Background

4.1.1. Quinolines and the inhibition of haem detoxicification in *P. falciparum*

Chloroquine has been the primary treatment for malaria over the past seven decades. Its mode of action has been studied in great detail and the consensus of the mode of action of chloroquine is the inhibition of the polymerization of haem thus poisoning the parasite as described in Chapter 2. As such chloroquine is often used as a positive control in assays designed to evaluate potential inhibitors of haem polymerisation.

Several variants of haem will be discussed in this Chapter and to avoid confusion it is important to clearly present their structures upfront (Figure 4.1). The term haem applies to free haem or protophorphyrin IX [Fe(III)PPIX] in which there is no ligand bound to the iron atom at the centre of the porphyrin ring. Two commercial haem compounds are available *viz.* haematin [H_2O-Fe(III)PPIX] or [HO-Fe(III)PPIX] (pH-dependent) and haemin [Cl-Fe(III)PPIX] in which water and chloro ligands are bound to the central iron atom of haem respectively. *Plasmodium falciparum* is able to facilitate the dimerization of haem to form a haem dimer and then undergo further polymerization, often also referred to as sequestration, to form a crystalline substance known as hemozoin. β-Haematin is a synthetic analogue of hemozoin that has been shown by three different research groups to be identical in all respects to hemozoin.[96,293-295]

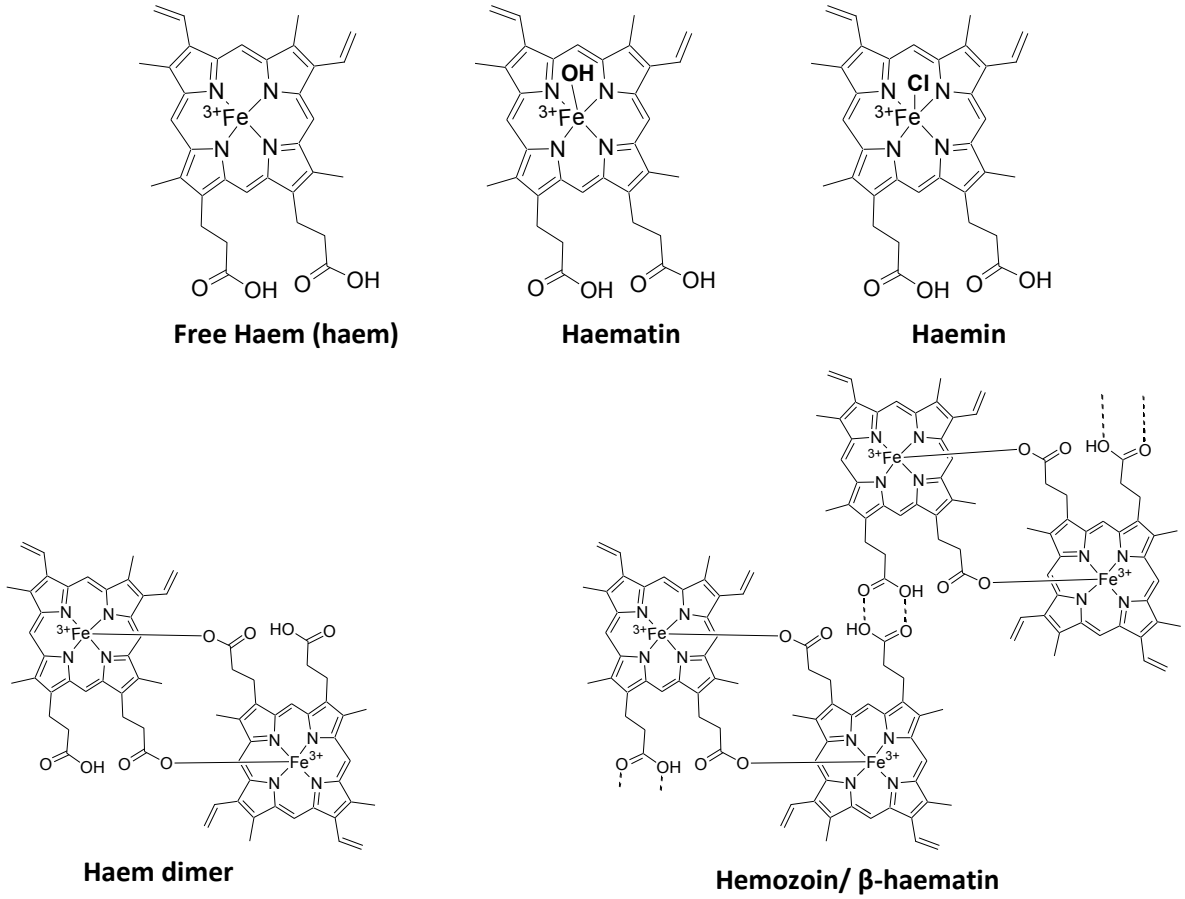

Figure 4.1: The five relevant forms of haem: Free hame, Haematin [HO-Fe(III)PPIX], haemin[Cl-Fe(III)PPIX] the haem dimer and hemozoin/ β-haematin

Chloroquine interacts with free haem through vertical π-stacking with the aromatic quinoline ring orientating itself above the haem porphyrin ring (Figure 4.2).[296] In the haem dimer the amine side chain of chloroquine orientates itself at 45^{o} to the planes of the porphyrin rings and occupies the space immediately adjacent to the haem dimer (Figure 4.2). The combination of this orientation of the amine side chain coupled with the π-stacking of the quinoline ring across the monomeric and dimeric porphyrin faces prevents hemozoin crystal growth both vertically and laterally.

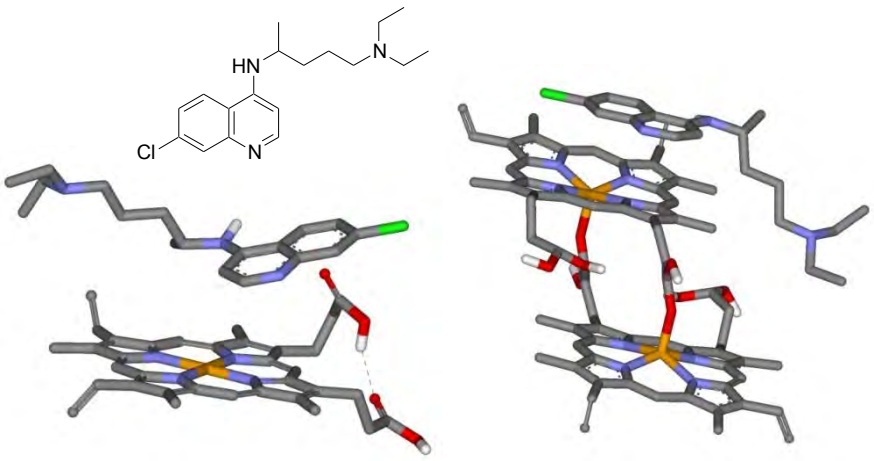

Figure 4.2*:* A graphical display of chloroquine (shown inset) binding to free haem (*left*) and the haem dimer (*right*). Oxygen atoms, red; carbon atoms, grey; nitrogen atoms, blue; chlorine atoms, green; hydrogen atoms, white and iron atoms, orange. Chloroquine was optimized using the B3YLP correcting functional and 6-31G(d) basis set. Docking simulation calculated in AutoDock[297] and results visualized in DSVisualizer.[21]

There are two primary theories for the mode of action of quinoline antimalarial drugs: complexation with haem dimer thus minimizing access to crystal cell units (Figure 4.2)[94,298] and inhibition of hemozoin formation through attachment of the drug to the growing crystal (Figure 4.3).[299-301] Both theories involve the non-covalent binding of quinolines to the haem, haem dimer or the developing hemozoin crystal. Buller *et al.*[296] propose a quinoline binding site at the end face of the fastest growing crystal face (the [001] crystal face)[302] of β-haematin (the synthetic equivalent of hemozoin). The [001] face contains the exposed carboxylic acids of haem as well as aromatic surfaces which encourage further propagation of the β-haematin crystal. In their model the quinoline ring fits snugly within the cleft of the corrugated surface (Figure 4.2). The loosely bound quinoline results in no further crystallization of haem onto the crystal face. The addition of chlorine to the quinoline ring *e.g.* in chloroquine, helps anchor the inhibitor within the crevice of hemozoin.[302]

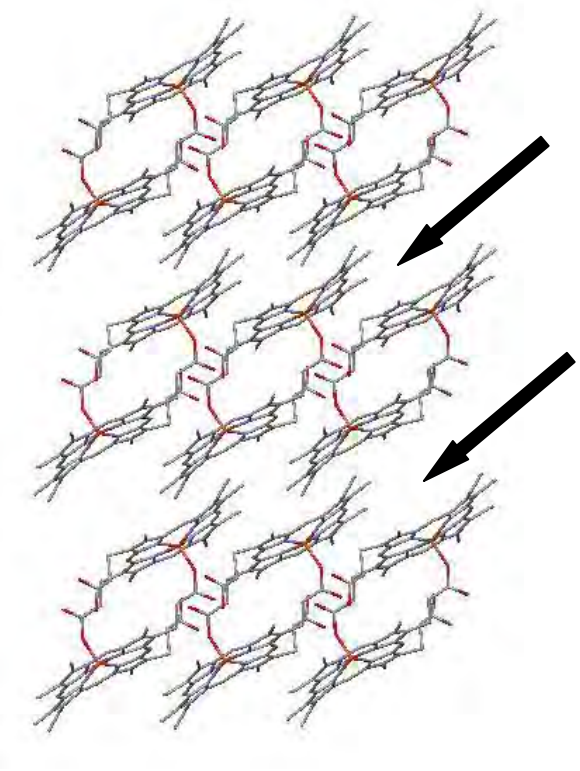

Figure 4.3*:* β-Haematin viewed along the a-axis, bold arrows indicate the exposed corrugated face, [296,302] with crevices where chloroquine is proposed to fit snugly (bold arrows). The cif file (CCDC 162267)[303] was visualized in Mercury 2.4.5.[304] Note how the β-haematin crystal lattice is comprised of haem dimers.

4.1.2. A review of assays to determine inhibition of haem polymerization

The earliest description of an assay designed to detect inhibitors of haem polymerization was presented by Slater and Cerami in a letter to *Nature* in 1992.[305] In their assay red blood cell-derived trophozoite extracts were centrifuged, affording a pellet capable of facilitating the formation of hemozoin from free haem. Radiolabelled ^{14}C haem was added to the pellet and incubated for 12 hrs and subsequent purification of the product mixture yielded ^{14}C containing hemozoin. The addition of chloroquine to the trophozoite pellet and ^{14}C-labelled haem mixture resulted in no radiation being emitted from the purified hemozoin in other words this hemozoin had formed prior to incubation with ^{14}C-labelled haem and no ^{14}C-labelled hemozoin formed from the addition of ^{14}C-labelled haem. Dorn *et al.* extended the study of trophozoite extracts and hemozoin formation by concluding that haem sequestration into hemozoin is protein independent. Their argument is based on the observation that hemozoin is still synthesized after heating the trophozoite extract (Note: heating denatures most proteins). From this observation they suggested that the polymerization of haem is a chemical process.[306] Sullivan *et al.* subsequently further explored the interaction of chloroquine

with haem and hemozoin. They incubated a mixture of haem and purified hemozoin in sub inhibitory concentrations of ^{3}H-labelled chloroquine overnight at 37 °C. After incubation they discovered tritium in both free haem and hemozoin and concluded that chloroquine binds initially to haem and is then incorporated into the hemozoin crystal. Sullivan *et al.*, also proposed that chloroquine essentially "end caps" the nascent crystal of hemozoin thereby preventing elongation of the crystal lattice.[299] They went on to demonstrate that the addition of histidine-rich proteins (HRPs), which are found in the parasites food vacuole, appear to initiate hemozoin formation.[307] Dorn and co-workers[308] later elaborated and improved on their original assay with the addition of acetonitrile trophozoite extracts. They suggested, as lipids dominated the acetonitrile extract, that the sequestration of haem into hemozoin may be lipid catalyzed. While these methods have the potential to identify haem polymerization inhibitors, the use of radiolabelled compounds is expensive, reliant on access to specialized equipment and facilities and necessitates the final disposal of radioactive waste. Slater and Cerami also showed that there was a decline in activity of the trophozoite pellet over time,[305] thus fresh trophozoites need to be continuously available in order to conduct this assay. A limitation of Sullivan's method is clearly the availability of suitably radiolabelled inhibitors. Despite the challenges of a radiolabelled based assay a high throughput screen was reported using ^{14}C-labelled haematin.[309]

Basilico and co-workers[310] exploited the solubility differences between haematin [H_2O-Fe(III)PPIX] and β-haematin in creating a method to determine the **h**aem **p**olymerization **i**nhibitory **a**ctivity (HPIA) of potential antimalarial drugs. An acidic solution of haematin (final pH of 2.7) was incubated for 24 hours at 37 °C, to ensure complete polymerization. The solid matter was collected via centrifugation and resuspended in DMSO to remove any soluble unreacted haematin before being centrifuged once again. The pelleted portion, containing pure β-haematin, was finally analyzed via FTIR. The lack of precipitated material after incubation with a suspected inhibitor indicated inhibition of β-haematin. The advantage of the HPIA assay is that it is inexpensive and suitable for high throughput screening of both water soluble and water-insoluble compounds (solvents used to solubilise test compounds do not interfere with the assay). The disadvantage of this assay is that it is time consuming, requiring a 24 hour incubation period and two centrifugation steps. The assay was found to be flawed when it was later discovered that, several salts including chlorides and phosphates gave a false positive result. This is of concern because many aminoquinoline drugs are formulated as salts, *e.g.* chloroquine phosphate and primaquine diphosphate. The limitations of HBIA led to the development of the **β**-**h**aematin **i**nhibitory **a**ctivity (BHIA) assay.[311] By replacing haematin [H_2O-Fe(III)PPIX] with haemin [Cl-Fe(III)PPIX] as the porphyrin source and replacing the NaOH solution with DMSO to dissolve the porphyrin, adding of the test solution followed by

acidification, no salt induced false positive results were observed.[311] Baelman *et al.* used a slightly modified BHIA assay, in an attempt to identify bioactive natural products from Bolivia, by reducing the number of centrifuge steps and monitoring β-haematin formation with UV/vis spectroscopy as opposed to FTIR.[312] Unfortunately, the use of FTIR as a detection method for β-haematin requires the β-haematin samples to be solvent and water free which necessitates a lengthy drying period in addition to the 12-48 hour incubation period.

Egan and co workers developed two methods for determining a compound's ability to interfere with the formation of hemozoin, namely the **P**yridine **h**emichrome **i**nhibition of **β**-haematin (Phi-β)[313] and β-haematin inhibition assays (which we have abbreviated to EBHIA – **E**gan's **β**-**h**aematin **i**nhibitory **a**ssay).[314] In both methods the β-haematin crystals are grown in an acetate buffer (pH 5.00) in the presence of potential inhibitors, thus providing a means to assay the inhibitors ability to hinder the biocrystallization of haem under similar pH conditions to those found in the plasmodial food vacuole. We used both Phi-β and EBHIA to study the inhibition of haem polymerization, in the presence of both naturally occurring (**2.4**, **2.9**, **2.15**, **2.19**, **2.34** and **2.35**) and synthetic (**3.215**) compounds, because of the accessibility of these methods with regards to availability of reagents, analytical techniques, cost and incubation times. While others have reported alternative methods for determining the presence of β-haematin, including fluorometry[315] and HPLC,[316] spectroscopy still remains the most convenient and widely used analytical technique.

The discovery that β-haematin (the synthetic equivalent of hemozoin) may be synthesized in a laboratory has initiated a debate as to whether the polymerization *in vivo* is a spontaneous chemical or biological facilitated process, as many of these *in vitro* methods are conducted in supraphysiological conditions, such as high temperature (60 °C) in the EBHIA and Phi-β or lengthy incubation times (18-24 hrs) in both the HPIA and the BHIA assays. However, the consensus view is that the sequestration of haem into hemozoin *in vivo* occurs by a multifarious mechanism, where lipids may play a major role in mediating the polymerization of haem to hemozoin.[83,317] A summary of known mechanisms of haem polymerisation and valid criticisms of each mechanism is presented in Table 4.1.

Haem polymerization still attracts the interest of a number of research groups and Stiebler *et al*.[317] recently proposed the following mechanism for the polymerisation of haem to hemozoin within the food vacuole of *Plasmodium* (Figure 4.4): Firstly protein (*e.g.* α-glucosidase) initiates the nucleation of haemozoin via the formulation of the intial seeds of haemozoin. Secondly, the haemozoin crystal elongates at the lipid-water interface mediated by membrane lipids. Thirdly, the nascent hemozoin

crystal is released from the lipid membrane where it may continue to slowly elongate via autocatalysis.

Table 4.1: A summary of the mechanisms proposed for the sequestration of haem into hemozoin by the *Plasmodium* parasite.

Mechanism	Proof for mechanism theories	Criticisms
Spontaneous	- Synthesis of β-haematin occurs despite the removal of all biological components.[310,311,313,314]	- Rates of β-haematin formation do not mirror those observed for hemozoin formation in the parasite.[83]
Lipids	- The addition of lipids into *in vitro* β-haematin inhibition assays minimises the discrepancy between experimental and physiological conditions.[301,318,319]	- The calculated stoichiometric ratio of lipids required to sequester the amount of haem contained with the parasite is inconsistent with the actual quantities of lipids contained with the FV.[83]
Autocatalytic	- The addition of hemozoin or β-haematin, increases the formation of hemozoin.[306]	- The formation of the original hemozoin nucleation site is unknown.
Proteins:		
HRP II and III	- The rate of β-haematin synthesis *in vitro is* accelerated in the presence of HRP.[299]	- Removal of the genes which code for HRP II and III in *P. falciparum* still result in the formation of hemozoin.[87] - HRP genes are not found in other species of *Plasmodium* however, hemozoin is produced in all of them.[320]
Heme-detoxicfication protein (HDP)	- HDP actively converts haem to β-haematin *in vitro*.[321] - HDP is localized in the FV of the parasite.[321]	- Heating of the trophozoite extracts still results in the formation of hemozoin.[306]
α-Glucosidase	- Removal of the α-glucosidase or pharmacological inhibition of this enzyme reduces the formation of hemozoin.[322]	- Only discovered in *Rhodnius prolixus* (a haemoglobin /haemolyph feeding insect), which also sequesters haem into hemozoin.[322]

Abbreviations: FV – Food Vacuole
HRP – Histidine Rich Proteins

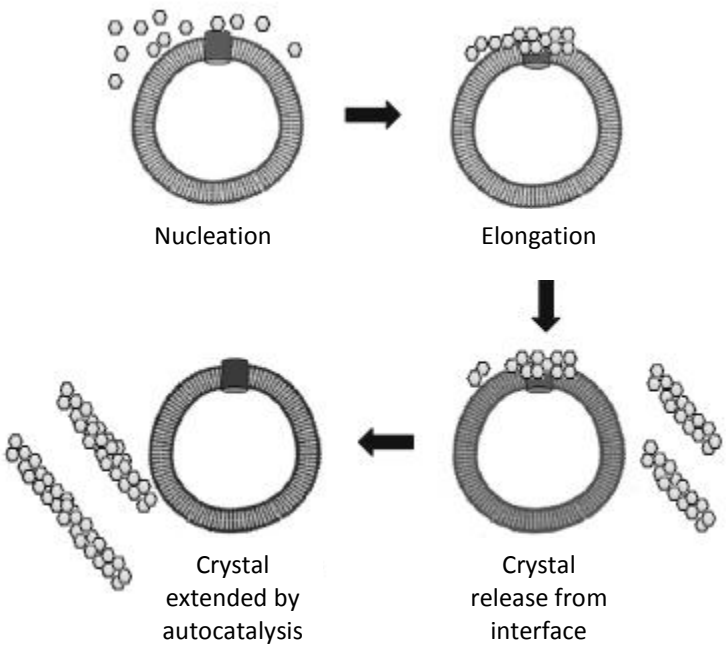

Figure 4.4: The proposed mechanism of haem polymerization in the *Plasmodium* parasite.[317]

In more recent years the reports of new β-haematin inhibition assays have decreased in the literature although several modifications to existing methods have been recorded, most notably the introduction of lipids as initiators of haem sequestration into β-haematin. The addition of lipids (such as MOG, polysorbate 20, lectin, MSG or MPG) to the assay has many advantages. Lipids appear to stabilize haem stock solutions,[318] and reduce incubation time[319] and temperatures,[318,319] the latter being of particular importance should the potential inhibitor be thermally unstable. The incorporation of lipids into β-haematin inhibition assays, and subsequent reduction in the incubation temperatures and duration of the assay has the advantage of making the assay a closer match to physiological conditions. While our study was in progress the use of lipids in β-haematin inhibition assays was not well-established and to the best of our knowledge has still not become standard practise.

4.1.3. Egan's β-haematin inhibition assay (EBHIA) and Phi-β assay

Egan reported that without scrupulous experimental accuracy the variables of the EBHIA assay may alter the outcome, (*e.g.* pH, temperature, acetate concentration and stirring rate).[301] The EBHIA method is discussed in Chapter 6, however the reaction condition we used will be discussed here. Whilst testing marine natural products we were limited by the quantity of material and therefore, all natural products were tested at three equivalents relative to haem. Synthetic material, however,

was abundant and we tested these compounds at ten equivalents (the highest practical concentration is 20 equivalents).[173] Unfortunately, due to limitation of the quantities of the marine isonitrile inhibitors in hand, we had to scale down Egan's method to one fifth of the reported quantities (reported mass of required haemin was 75 mg).[301] Due to the capricious nature of this assay, we deemed it necessary to therefore scale down all reaction apparatus accordingly and all subsequent reactions were conducted in a 20 mL cylindrical glass vial (20mm in diameter and 64 mm in height). The rate of stirring can alter the results and thus all reactions were stirred at consistent rate by a stirrer bar (2mm in diameter and 5mm in length). The 100 mL of 12.8 M stock acetate buffer was made up to a final pH of 5.00 ± 0.005 and incubated at 60 °C. The acetate buffer was supersaturated at ambient temperatures and it was critical to the success of the assay that the NaOAc remained dissolved. When transferring the warmed acetate buffer to the reaction vessels a new pipette tip was used every time. NaOAc microcrystals contaminating the pipette tips resulted in rapid crystallization of NaOAc out of the buffer solution thus altering the pH and acetate concentration of the buffered solution. It must be noted that all potential inhibitors were added in methanol after neutralization of 0.1M NaOH with 1 M HCl in strict accordance with the method reported in literature.[313] The assay reaction mixture was sealed to avoid evaporation and heated in a water bath at 60 ± 0.5 °C surrounded by aluminium foil to remove any interference by light.

4.1.3.1. UV/vis spectroscopy (Phi-β assay)

This Phi-β assay is based on pyridine's ability to form a monomeric low spin complex with only unreacted haematin and not with β-haematin. The presence of this complex can be measured by UV/vis spectroscopy. In an aqueous medium haematin exhibits a broad and relatively weak Soret band (389 nm), which is typical of the aggregated state of porphyrins, possibly from dimerization.[323] Aqueous solutions of haematin also exhibit a very weak Q-band (450-700 nm) and a prominent charge-transfer (CT) band (625 nm)[313] in the UV/vis spectrum. With the addition of pyridine, the Soret band of haematin experiences a red-shift of 15 nm as well as an increase in intensity and sharpening with a maximum peak emerging at 405 nm. In the longer wavelength region, the Q-band becomes more prominent at 527 nm indicating the formation of low spin Fe(III)-protoporphyrin IX-pyridine complex. These changes are indicative of the displacement of the axial water from the central Fe(III) atom of haematin with two pyridine ligands coordinating in its place (Figure 4.5).[324] Under aqueous neutral conditions the axial ligand in haem is thought to be H_2O rather than ^{-}OH. Water is a weak field ligand and will readily be replaced by the strong-field ligand pyridine.[313]

β-Haematin consists of dimers in which one of the acid side-chains of one porphyrin is coordinated to the Fe(III) centre of the other porphyrin in the dimer (see Section 4.1.3.2).[325] However, it was shown by Hempelmann *et al.*[326] that at high concentrations of imidazole (similar coordination properties to that of pyridine) and subsequent strongly basic conditions, β-haematin may be broken down to form a haem-imidazole complex. It is thus essential that this interaction of pyridine and haematin takes place in a medium buffered to a pH of 7.5. In strongly basic conditions pyridine also promotes the formation of the μ-oxo dimer of Fe(III)-protoporphyrin IX instead of coordinating itself to Fe(III) of haematin.[327] These changes in the UV/vis spectra of haematin in the presence of pyridine are the basis for a potentially good assay for the following three reasons. Firstly the sharpening and increase in intensity of the Soret band increases the sensitivity of the assay. Secondly, the red shift experienced in the UV/Vis spectra on the addition of pyridine will allow a higher degree of accuracy as there is no overlap of the spectra of free haematin and pyridine coordinated haem. And finally, pyridine is thought to remove any other molecules that may have coordinated to the iron(III) centre.[313]

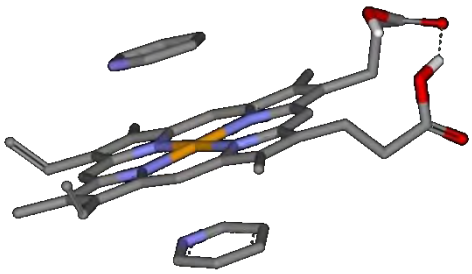

Figure 4.5: The image of two pyridine molecules chelating to the iron core of haem.

From the intense Soret band in the UV/vis spectra (Figure 4.6, purple) below, it can be seen how chloroquine inhibits the formation of β-haematin *i.e.* pyridine has a high concentration of free haem to coordinate to. The control spectrum in the Phi-β assay is acquired in the absence of any chloroquine type compounds, *i.e.* a negative control. However, a small peak at 405 nm is still observed indicating that not all haematin was polymerized to β-haematin. Interestingly, on the addition of pyridine to the chloroquine containing solution of haematin the resultant solution turned an orange-pink colour reflecting the red-shift. This colour change was almost instantaneous indicating that the complexation of pyridine to haematin is a very rapid reaction.

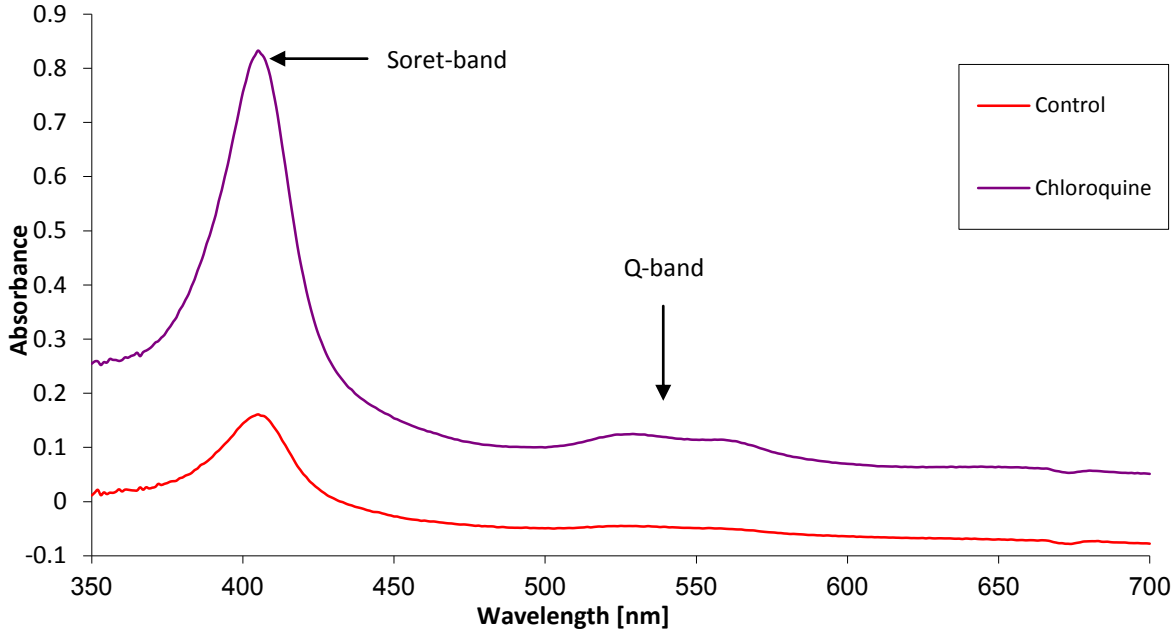

Figure 4.6: The UV/vis spectra (350-700 nm) of Phi-β assay solutions containing chloroquine (purple) and no inhibitor (red). The Soret and Q-bands are indicated.

This methodology has been validated in that there is a good correlation with results obtained in the BHIA and the HPIA assays.[313] The advantages of the Phi-β method is that it is fast, cheap and requires easy detection methods, even visual confirmation would tentatively suffice. The appeal of this assay for the identification of potential natural product β-haematin inhibitors, is the sensitivity of the assay (only 0.17 µmol of material is required) and that it is suitable for use in the field. Disadvantages of this assay are firstly that poorly water soluble compounds appear to prevent solubilisation of haematin producing a false negative result. However, poorly water soluble compounds may never reach bioactive concentrations *in vivo*, and thus may not be considered as viable antimalarial drugs in the long term. Secondly, the use of strongly coloured samples may interfere with the absorbance spectra recorded in this assay and a change in the Soret band absorbance does not necessarily always provide definitive proof of β-haematin inhibition. Other scenarios may also be envisioned, such as haematin degradation in the presence of the test compound, and slow crystallization of the test compound-haematin complex resulting in a product that does not readily react with pyridine. Alternatively, the drug may replace pyridine or preferentially bind to free haem, but still allow polymerization to occur. For these reasons, the results from the Phi-β assay cannot be accepted unilaterally and further validation of the inhibition

of β-haematin formation must be provided by other complementary analytical techniques *e.g.* FTIR, XRD and SEM.

4.1.3.2. FTIR spectroscopy

The coordination of the carboxylate group to the iron (III) centre in hemozoin is readily identifiable using FTIR *viz* two peaks (*ca.* 1663 and 1210 cm^{-1}) in the IR spectrum of hemozoin corresponding to the respective C=O (blue in Figure 4.7) and C-O (red in Figure 4.7) stretching frequencies of the carboxylate group bound to iron.[328] These two peaks are absent in the IR spectra of haematin and only present when the dimer is formed, in which water/hydroxyl bound to the iron in haematin is displaced by the carboxylate bonds. The haem dimer subsequently congregates through hydrogen bonding to form hemozoin crystals (Figure 4.1).

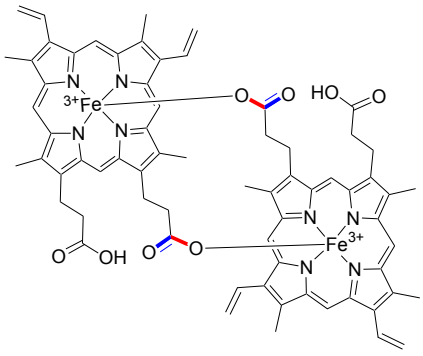

Figure 4.7: The chemical structure of the haem dimer, the red bond indicates the C-O bond responsible for the IR peak at 1210 cm^{-1} while the blue bond is indicative of the C=O responsible for the IR peak at 1663 cm^{-1} in FTIR spectra.

A comparison of the FTIR spectra of the precipitate chloroquine-added sample obtained from EBHIA assay and a precipitate obtained without chloroquine (negative control) are presented in Figure 4.8. The two strong peaks at 1210 and 1663 cm^{-1} in the spectrum of the negative control indicates the successful sequestration of haem to β-haematin. The absences of these two distinct stretching frequencies in the purple FTIR spectrum (Figure 4.8) show the lack of the formation of the Fe-O bond *i.e.* the haem dimer, indicating inhibition.

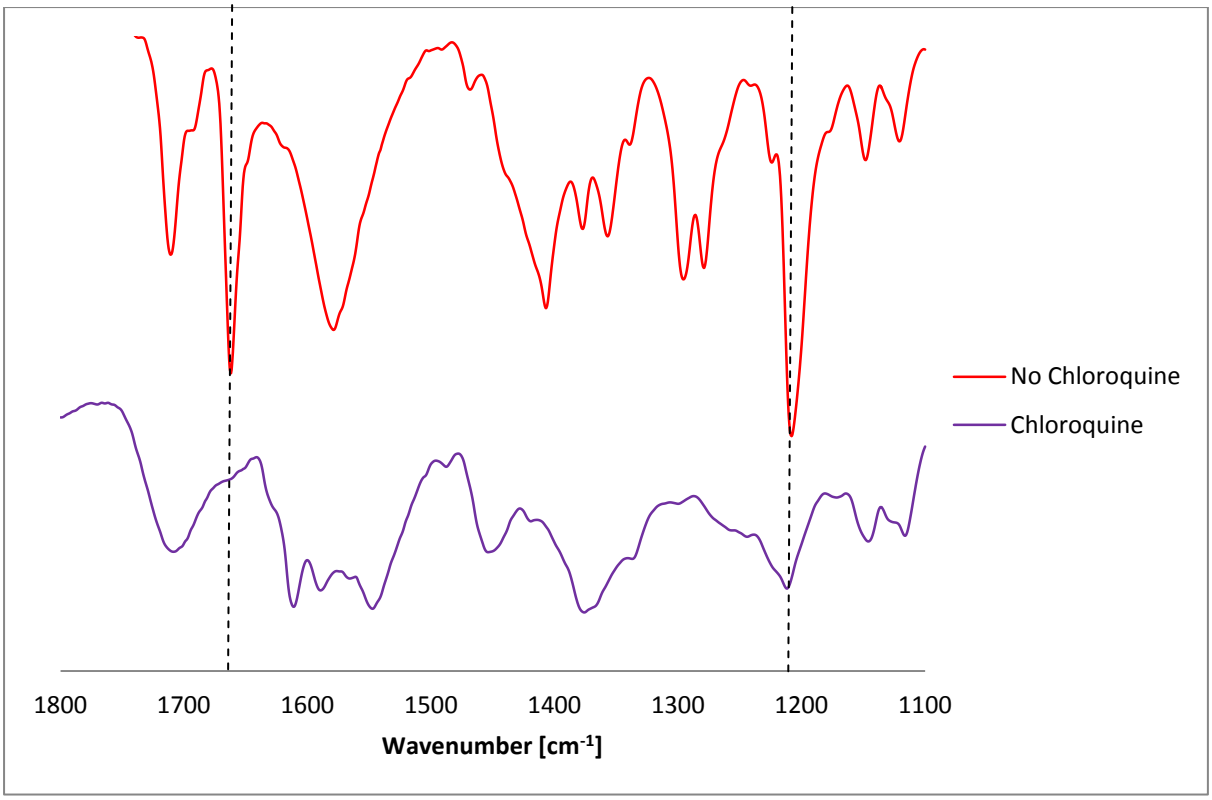

Figure 4.8: The FTIR spectra (1100-1800 cm^{-1}) of the precipitates obtained in EBHIA, containing chloroquine (purple) and no chloroquine (red). The IR peaks of interest (1663 and 1210 cm^{-1}) are indicated by a dotted line.

The advantages of FTIR are that it is fast and requires minimum amounts of material. Due to the intensity and location of the monitored IR peaks the sample does not need to be pure and a mixture of haematin and β-haematin would still yield useful results, which has been proved from previous reports where this technique has been used successfully.[305,306,314,329] The disadvantages of this methodology predominately stem from the use of compounds containing carboxylic acid moieties, which may bind to the central iron atom and produce a false negative result. The other limitation of this analytic technique for monitoring β-haematin polymerization inhibition is that it will only be representative of the inhibition of free haem rather than further polymerization of the haem dimer, where iron-carboxylic acid bond may have already been established. Results arising from this analytical technique, therefore, also require further validation with supplementary techniques *e.g.* X-ray powder diffraction and SEM.

4.1.3.3. X-ray powder diffraction

As can be seen from the X-ray diffraction pattern, the diffraction angles of our synthesized β-haematin corresponded to those in the X-ray powder diffraction pattern reported by Pagola *et*

al.[303] for pure β-haematin (Figure 4.9) indicating a similar powder diffraction pattern. The peaks for our synthesized β-haematin are much broader and can be attributed to the source of the X-rays. Pagola *et al.* used a synchrotron which is greatly superior to a conventional source of X-rays such as the one used in our experiments. Secondly the β-haematin crystals formed in an acetate solution are of a smaller size and are of poorer crystallinity thus broadening the peaks.[313] What must be noted is that the intensity of the peaks is related to structure and orientation, not concentration. Also what is unique to all crystalline compounds is the position of the Bragg reflections, *i.e.* the 2θ values corresponding to each peak.[330] Although the peaks may be broader the general diffraction patterns are essentially the same which provides a crystalline compound with a definitive X-ray powder diffraction fingerprint.

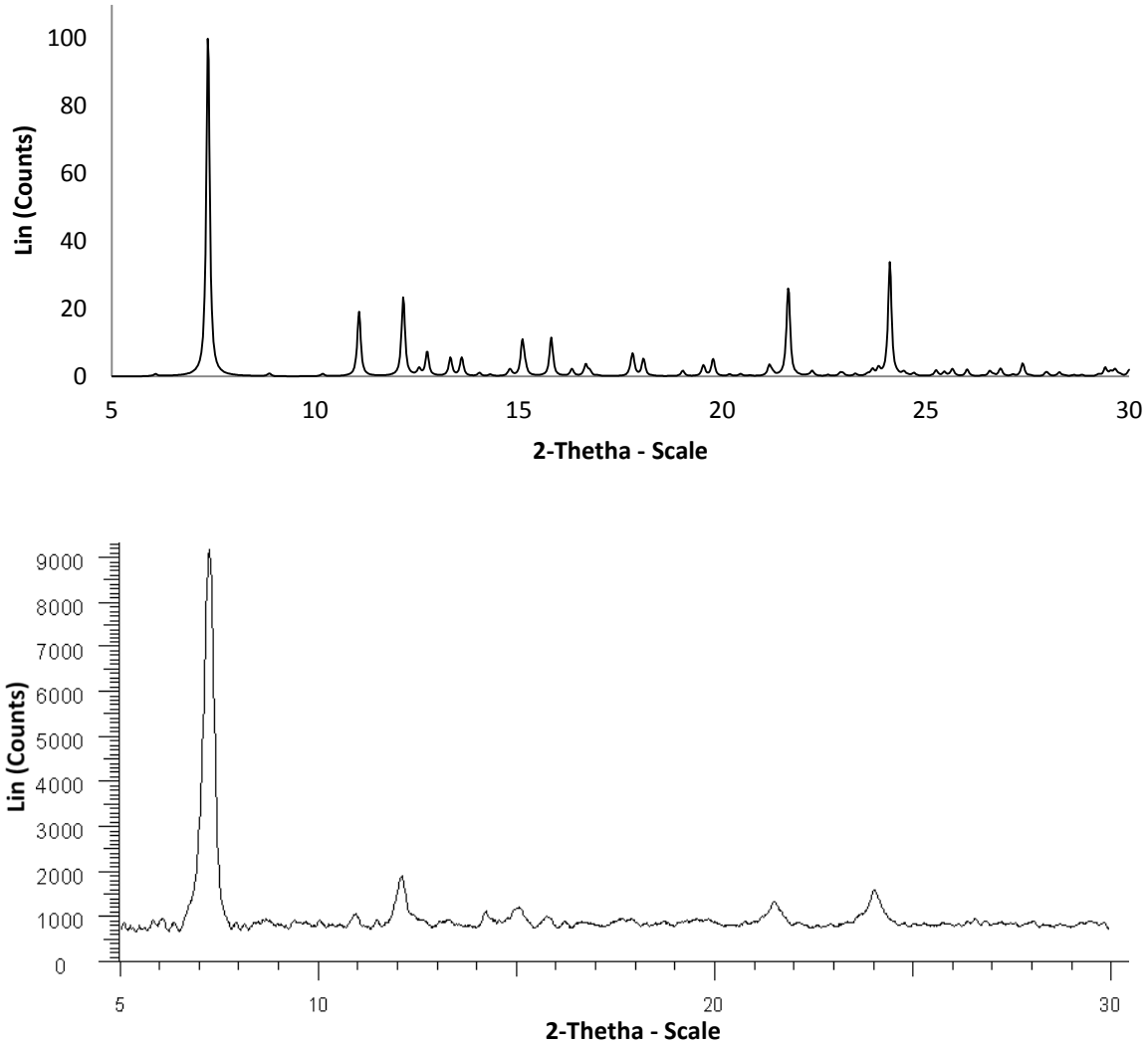

Figure 4.9: The X-ray powder diffraction pattern (2θ: 5°-30°) of β-haematin obtained with synchrotron radiation using X-rays of wavelength 1.16192Å (*above*).[303] Reproduced from the cif file (162267)[303] in Mercury.[304] The X-ray powder diffraction pattern (2θ: 5°-30°) we obtain from EBHIA in the absence of an inhibitor (*below*). X-ray powder diffraction patterns were recorded on a Bruker D8, Discover equipped with a proportional counter, using Cu-Kα radiation (λ = 1.5405 Å, nickel filter).

In X-ray powder diffraction it is important to note that amorphous solids do not have crystalline surfaces with which to reflect X-rays and therefore no diffraction pattern is detected. Amorphous haematin is a product of the EBHIA assay when polymerization is inhibited whereas β-haematin, the product when there is polymerization, is crystalline. This difference in the solid states of these two compounds can be exploited to determine if haem polymerization inhibition has occurred. The X-ray powder diffraction patterns of Figure 4.10 shows chloroquine's ability to inhibit hemozoin formation.

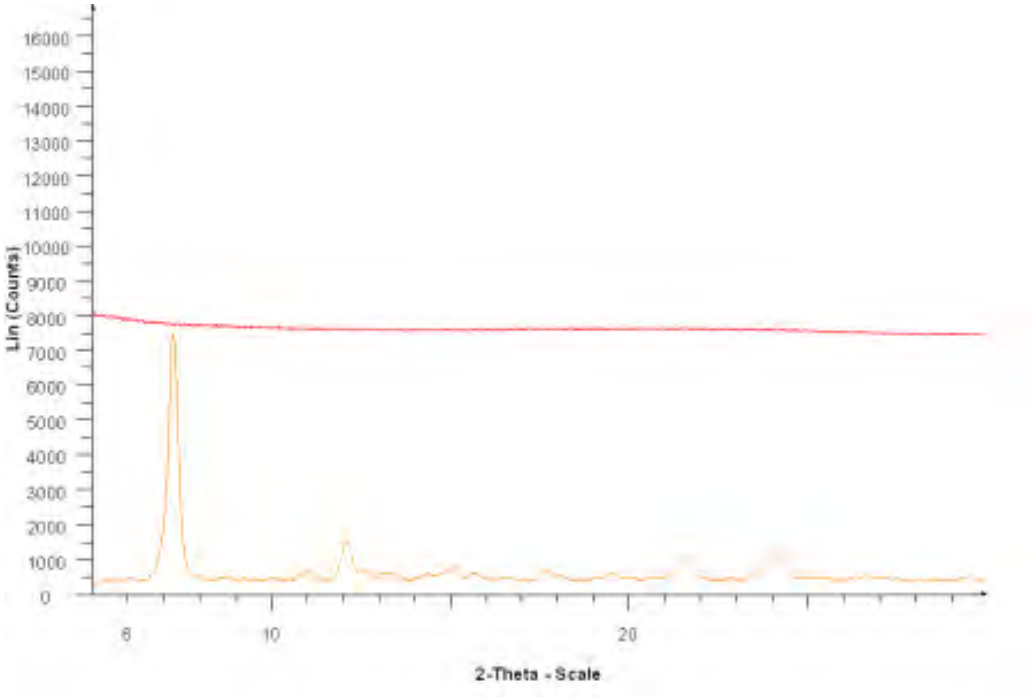

Figure 4.10: The X-ray powder diffraction patterns (2θ: 5°-30°) of the precipitates of the EBHIA containing; chloroquine (red) and control (orange). X-ray powder diffraction patterns were recorded on a Bruker D8, Discover equipped with a proportional counter, using Cu-Kα radiation (λ = 1.5405 Å, nickel filter).

Due to the micro-crystalline nature of synthetic β-haematin produced in the EBHIA, a relatively large amount of sample is required in order to obtain enough precipitate to afford X-ray powder diffraction peaks of sufficient intensity. The minimum with which we managed to achieve reasonable X-ray powder diffraction patterns was 5 mg of β-haematin/haematin containing precipitate. It must be noted that the same amount of EBHIA precipitate was used for each X-ray powder diffraction analysis and therefore the lack of peaks in the diffraction pattern was a true indication of an inhibitor's ability to hinder haem sequestration as opposed to a limitation in the sensitivity of the detector in the X-ray diffractometer. The EBHIA requires the addition of a minimum of three equivalents, relative to haem, of potential inhibitor which requires significant

amounts of test compounds. Although, this technique is not quantifiable it is the most conclusive for determining if β-haematin has formed.

4.1.3.4. Scanning electron microscopy (SEM)

Figures 4.11A-C are SEM micrographs, with increasing magnification, showing the external morphology of commercially available haematin. In these images large angular amorphous structures can be seen. On increased magnification the surfaces of haematin appear smooth and unobstructed (Figure 4.11C). Large smooth amorphous particles can again be seen in Figure 4.11 D and G, which is to be expected as these scanning electron micrographs were obtained from haematin collected at the beginning of the EBHIA. On allowing the EBHIA to proceed in the absence of a polymerization inhibitor *e.g.* chloroquine for 15 min the external appearance of haematin is altered with the addition of small but distinguishable lath-like[331] microcystals of β-haematin (150-350 nm in length)[301] on the surface of haematin (Figure 4.11 E and H). After the 30 minute interval (not shown) there is a significant increase in the β-haematin with the majority of the orginal haematin covered with microcrystals of β-haematin. After 60 minutes the total surface appears covered with β-haematin with no evidence of the original amorphous haematin (Figure 4.11 F and I). Egan has shown that *de novo* β-haematin microcrystals formed in an acetate solution are smaller and less ordered than naturally formed hemozoin, β-haematin formed through seeding by pre-existing β-haematin or crystals grown in a non-aqueous medium.[332-334] The SEM micrographs of the precipitate obtain after the addition of chloroquine (Figure 4.11J and K) shows large smooth amorphous particles of haematin comparable to 4.11A-C. SEM provides impressive visualization of the formation of β-haematin from haematin in the absence of inhibitor *e.g.* chloroquine.

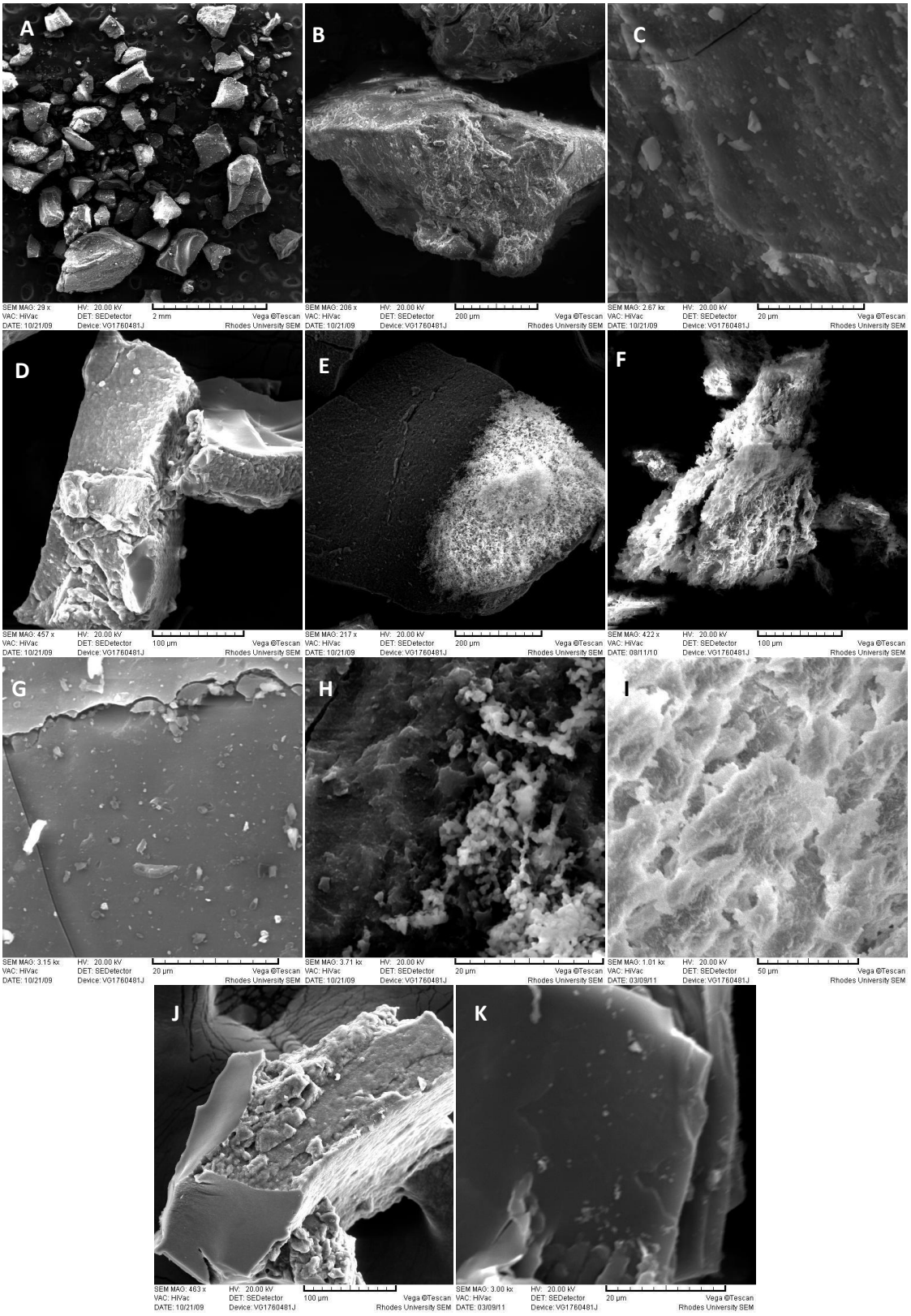

Figure 4.11: The SEM micrographs of A-C: Commercial haematin at 29, 206 and 2600x magnification respectively; D: The growth of β-haematin at t = 0 min; E: t = 15 min; F: t = 60 min; G-I: surface images at t = 0, 15 and 60 min; respectively. J and K: SEM micrographs of the precipitates from the EBHIA containing chloroquine at 463x and 3000x magnification respectively.
All images taken using a Tescan Vega scanning electron microscope at 20 kV and a working distance of 20mm. Scale at the bottom of the image.

4.2. Research aims

As discussed in Chapter 2 several mono, di, tri and tetracyclic marine isonitriles and isothiocyanates have exhibited potent antiplasmodial activity. In this Chapter, the ability of a representative group of this class of marine compounds as well as the synthetic isonitrile (**3.215**) to inhibit the polymerization of haem will be evaluated. The interference of haem detoxicification remains a viable drug target as sequestration of haem to hemozoin is a chemically fixed process, *i.e.* not subject to mutation.[335] In this Chapter, the antiplasmodial mode of action of **2.4**, **2.9**, **2.15**, **2.19**, **2.34**, **2.35** and **3.215** will be evaluated to determine whether this antiplasmodial activity is based in **2.4**, **2.9**, **2.15**, **2.19**, **2.34** and **2.35**'s ability to inhibit the detoxicification of haem. The ability to disrupt haem polymerization was determined with Egan's β-haematin inhibition assay (EBHIA), and β-haematin formation was monitored by XRD, SEM, UV/vis and FTIR spectroscopy.[323] A putative computer generated model of marine isonitriles ability to bind to haem was reported a decade ago.[196] However, with the availability of more advanced computational methods we chose to revisit this haem-isonitrile interaction, focusing particularly on the charges associated with the isonitriles functionality. We hoped to discover a haem/haem dimer binding motif in the hope that future β-hematin inhibitors could be identified from the way these inhibitors dock to haem receptors in modelling studies.

4.3. *In vitro* evaluation of haem polymerization inhibition by marine and synthetic isonitriles and isothiocyanate (2.4, 2.9, 2.15, 2.19, 2.34, 2.35 and 3.215)

The marine isonitriles (**2.4**, **2.9**, **2.15**, **2.19** and **2.35**) and the isothiocynate (**2.34**) were kindly provided by Professor Wright, College of Pharmacy, University of Hawaii at Hilo, Hawaii, USA, so that we could explore their ability to inhibit haem polymerization *in vitro*. The results of our investigation using the practical procedure outlined in Chapter 6 are presented here.

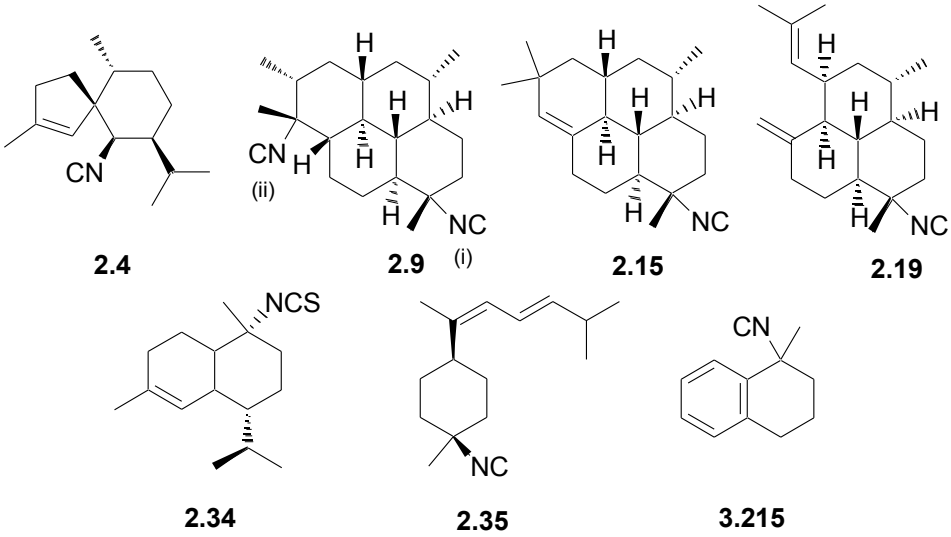

2.4 **2.9** **2.15** **2.19**

2.34 **2.35** **3.215**

4.3.1. UV/vis spectroscopy (Phi-β assay)

Only the synthetic isonitrile **3.215** was tested for β-haematin inhibition using the Phi-β assay.[313] Given the small quantity of (**2.4**, **2.9**, **2.15**, **2.19**, **2.34** and **2.35**) in hand and since Wright *et al.*[196] had already proposed mode of action of **2.4**, **2.9**, **2.15**, **2.19**, **2.34** and **2.35,** may be the interference with haem polymerization, it was not deemed necessary to screen these compounds in the Phi-β assay. The Soret-band evident in the pyridine containing solution of **3.215**, indicated the presence of free haem and that possibly some inhibition of β-haematin formation had occurred (Figure 4.12). While the peak intensity for the solution containing **3.215** (10 equiv.) was not as intense as the one obtained for chloroquine, the continued assessment of **3.215** as a β-haematin inhibitor was merited.

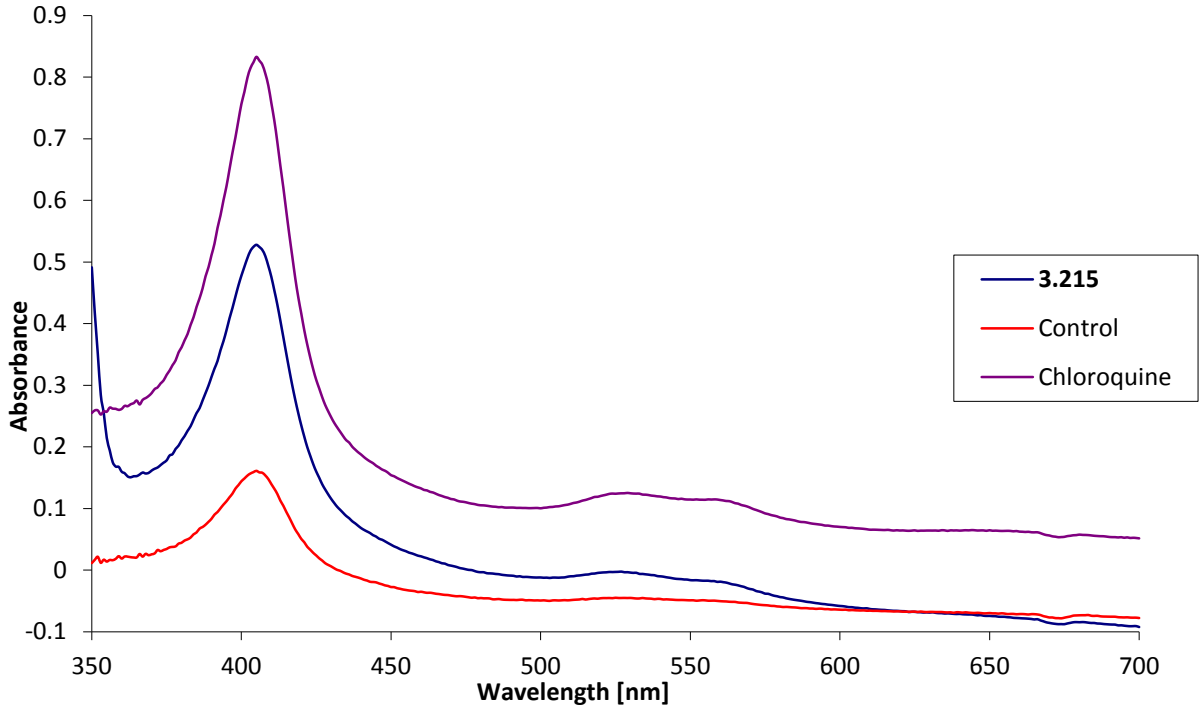

Figure 4.12: The UV/vis spectra (350-700 nm) of Phi-β assay solutions containing chloroquine (purple), 3.215 (blue) and no inhibitor (red).

4.3.2. FTIR spectroscopy

Egan and co-workers[301] developed an FTIR method for approximately quantifying the amount β-haematin formed in EBHIA assay. By measuring the change in absorbance ($-\log[\%T]$) of the peak at 1210 cm^{-1} relative to the shoulder peak at 1229 cm^{-1} the intensity of which remains constant (Figure 4.13, *Left*) for various molar ratios of haematin mixed with β-haematin they were able to show that a liner relationship exists (Figure 4.13, *Right*). The difference in these two absorbances (ΔA) could be easily determined and thus a percentage value calculated for the β-haematin present in each precipitate resulting from the EBHIA assay carried out with chloroquine, no inhibitor (control) and isonitriles **2.4**, **2.9**, **2.15**, **2.19**, **2.34**, **2.35** and **3.215** (Table 4.2).

The precipitates (1.0 ±0.2 mg) resulting from each of the EBHIA assays performed with **2.4**, **2.9**, **2.15**, **2.19**, **2.34**, **2.35**, **3.215** and chloroquine were analyzed using FTIR and the presence of the two IR peaks (1210 and 1663 cm^{-1}) monitored. All marine metabolites **2.4**, **2.9**, **2.15**, **2.19**, **2.34** and **2.35** were added at three equivalents, while **3.215** was added at ten equivalents relative to haem. Interestingly, the compounds which exhibited good (*i.e.* < 50% calculated formation of β-haematin) inhibition of β-haematin formation were **2.9**, **2.15** and **2.19**. These compounds all contained a tri- or

tetracyclic scaffold with isonitrile functionalities attached. Compound **2.9** showed total inhibition of haem polymerisation at 3 equivalents, whereas compounds **2.15** and **2.19** all showed good potential to inhibit β-haematin formation at the same equivalency and may show greater inhibition at higher concentrations. Interestingly, compound **2.9** also exhibited the greatest antiplasmodial activity (4 nM), although **2.19** and **2.15** are not as active, with IC_{50} values of 47 and 84 nM they managed to limit the amount of β-haematin formed in the assay (14 and 26% respectively). The results, obtained for **3.215** appear to correlate to those obtained in the Phi-β assay, *i.e.* only partial inhibition of haem polymerization.

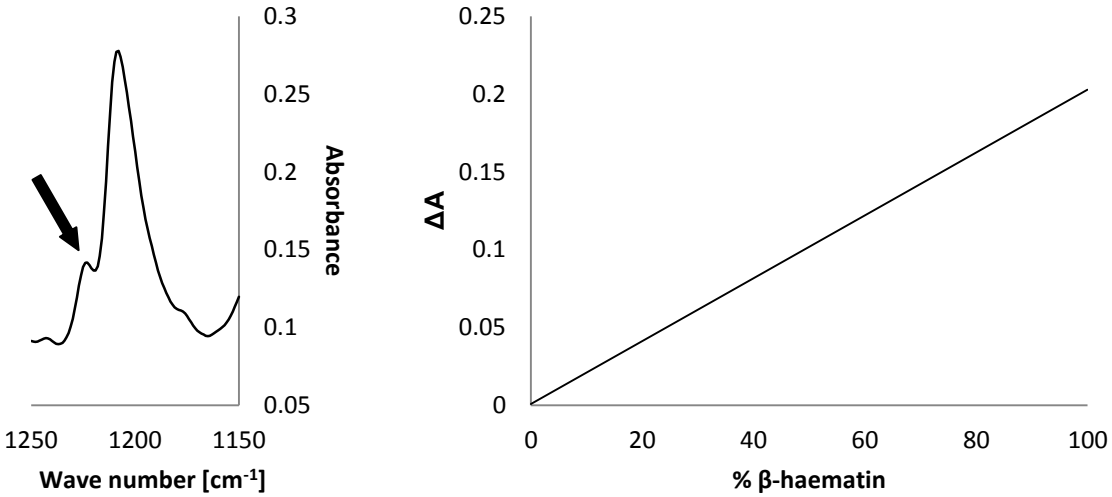

Figure 4.13: A section of the IR absorbance spectrum (1150-1250 cm^{-1}) of the precipitate obtained in the EBHIA assay (*left*). The arrow indicates the shoulder peak at 1229 cm^{-1}. A reproduced plot of ΔA vs. percentage of β-haematin (*right*).[301]

Table 4.2: A comparison of the conversion of haemin to β-haematin in the presence of **2.4**, **2.9**, **2.15**, **2.19**, **2.34**, **2.35** and **3.215**. All conversions calculated from the change in the FTIR absorbance spectra of the precipitates obtained from EBHIA assay. (ND = not determined)

Compound	% β-haematin contained in the precipitate.	Antiplasmodial Activity
Control	97	-
Chloroquine	4	70 nM
Commercial Haematin	2	-
2.4	76	71 nM
2.9	0	4 nM
2.15	26	84 nM
2.19	14	47 nM
2.34	71	5.7 µM
2.35	62	ND
3.215	52	3.1 µM

4.3.3. X-ray powder diffraction

The X-ray powder diffraction patterns (Figure 4.14) shows the ability of **2.9** to completely inhibit β-haematin formation as no reflections were detected. X-ray powder diffraction peaks were present in all other compounds tested (**2.4**, **2.15**, **2.19**, **2.34**, **2.35** and **3.215**), indicating the presence of β-haematin. These data supported the results obtained from the other analytical techniques discussed above.

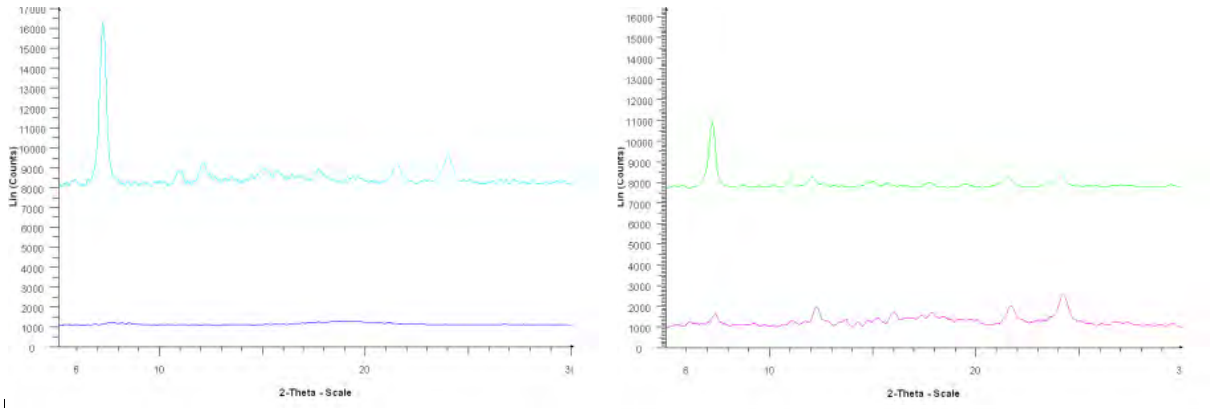

Figure 4.14: The representative X-ray powder diffraction patterns (2θ: 5°-30°) of the precipitates of the EBHIA incubated in the presence of: **2.35** (light blue), **2.9** (dark blue), **3.215** (green) and **2.15** (pink). X-ray powder diffraction patterns were recorded on a Bruker D8, Discover equipped with a proportional counter, using Cu-Kα radiation (λ = 1.5405 Å, nickel filter).

4.3.4. Scanning electron microscopy

The scanning electron micrographs (Figure 4.15A and 4.15B) were obtained from the precipitate formed during the addition of chloroquine and a control experiment *i.e.* when no inhibitor was added in the EBHIA assay and β-haematin was free to form, respectively. Figure 4.15A shows large smooth amorphous particles of haematin, comparable to Figure 4.11A-C, whereas Figure 4.15B illustrates the presence of β-haematin as layers of fine microcrystals. Figures 4.15C-F are representative SEM images of the precipitates from the EBHIA assays when **2.9, 2.15**, **2.34**, and **2.35**, respectively had been added. Figure 4.14C shows complete inhibition of haem polymerization (Figure 4.15E) partial inhibition (Figure 4.14F) and no inhibition (Figure 4.15C and D). The SEM micrographs support the results obtained from both FTIR and XRD analyses of the EBHIA assay precipitates.

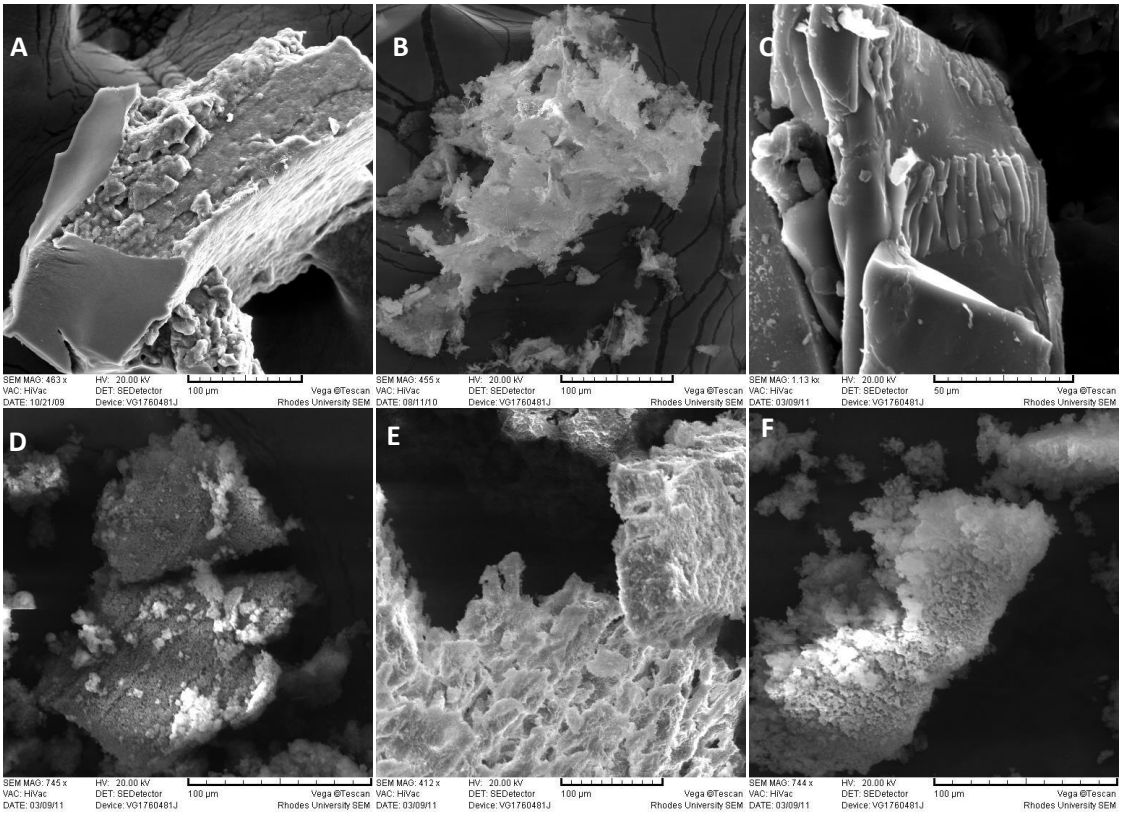

Figure 4.15: The representative SEM micrographs of the precipitates from the EBHIA carried out with; A: chloroquine, B: no β-haematin polymerisation inhibitor, C: **2.9**, D: **2.15**, E: **2.34** or F: **2.35**, at various magnifications. Images taken using a Tescan Vega scanning electron microscope at 20 kV and a working distance of 20mm. Scale given at the bottom of the image.

4.4. *In silico* studies of marine and synthetic isonitrile/haem and isonitrile/haem dimer interaction

4.4.1. Background into molecular modelling and optimization of docking studies

In the case of modelling very large molecular systems two modelling approaches are used, molecular mechanics (MM) and molecular dynamics (MD). Both of these use Newtonian motion equations to monitor the trajectory of a system's components. The major difference between these two methods is that MD caries out energy evolutions at a finite temperature while MM does not. The accuracy of the energy calculations performed by these two computational methodologies is determined by the way in which the inter atomic forces are defined. In this study the inter atomic forces were first determined by means of a force field approach, allowing for both the equilibrium thermodynamic and dynamic properties of the system to be calculated.

The force field models are limited because they often fail to take electronic polarization effects into account and can only manage chemical reactivity through specialized techniques *e.g.* an empirical valence bond approach.[336,337] For this reason *ab initio* methods are becoming the preferred method for exploring chemical reactivity. The ability of this method to simulate bonding breaking and formation affords invaluable information. Basic *ab initio* calculations are based on the assumption that there exist a finite number of nuclei and electrons for a given system, and that the Born-Oppenheimer approximation (BOA) may therefore be applied to the system. The BOA treats the nuclei as stationary due to their lack of momentum relative to the electrons; thus allowing for the Schrödinger equation to be solved for only the electron wavefunctions.[338] The total energy of the system is expressed as the sum of the electron and nuclear energies, where the nuclear term is given an approximate value.[336,339]

A modern method incorporating *ab initio* calculations is the Kohn-Sham formulation of density functional theory (DFT).[340] This has become the preferred method amongst molecular modellers and as such was used here for the optimization calculation for all receptors (haem and haem dimer) and ligands (**2.4**, **2.9**, **2.15**, **2.19**, **2.34**, **2.35** and **3.215**) in this study. In DFT the atomic forces acting on a system are expressed as a functional of the electronic density where the electron density is described as a series of single electron orbitals.[336,338] These approximations treat the electrons' motion as independent of one another, and suggests a greater interaction between electrons than would normally be experienced in a true multi-electron system. This leads to an over estimation of

the inter-electron repulsion term, resulting in an inflated total energy. To correct this an electron correlation term is introduced, the most popular being Møller-Plesset (MP2), Becke-Lang-Yee-Parr (B3LYP) and Perdew-Burke-Ernzerhof (PBE) gradient correcting functionals. The MP2 is a pure Hocktree-Fock method, whilst the PBE is a pure DFT and the B3LYP is a hybrid of the two.[341-344] Thus for all minimization calculations the B3LYP correcting functional was used here. Currently the preferred DFT formulation is 6-31G(d) basis set which describes the core electronic states by means of six Gaussian functions and then describes the valence states with two vector sets containing three and one vectors respectively.

4.4.2. Electronic configuration of haem

Haem can exist in four different electronic states: singlet, triplet, quintet and septet.[345] In order to ascertain which state to use in our studies, the haem model was minimized in the singlet, triplet and quintet states and the one possessing the lowest energy was used for subsequent analyses. We chose not to minimise the septet as this electronic state has been shown to be much higher in energy than the other three states.[345] The free haem model was therefore successfully minimized in both the singlet and triplet electronic states with electronic energies of -8.13507×10^{6} kJ.mol^{-1} and -8.13524×10^{6} kJ.mol^{-1} respectively. Hence, the triplet state is 0.0017×10^{6} kJ.mol^{-1} lower in energy than the singlet. The quintet state repeatedly failed to achieve electronic self-consistency and it was thus deemed necessary to use a pseudopotential to describe the iron atom's core electrons and then use the standard DFT method to account for the valence electrons. The LANL2DZ[346] double zeta pseudopotential was used and the minimized quintet structure was found to have an electronic energy of -5.14×10^{6} kJ.mol^{-1}, which correlates to an energy 3.00×10^{6} kJ.mol^{-1} kJ higher than the triplet model. From this optimization study we decided that the triplet haem model would be used for all subsequent modelling of haem-ligand interactions.

4.4.3. Charge state of the isonitrile functionality

One of the most arduous tasks facing molecular modellers is the quantification of charge on each atom in a given system. Simply put, the nucleus may be treated as a point charge, whereas the electrons are treated as a distribution of charge. This distribution is more concentrated around the

individual nuclei or where two atoms are in a close proximity to one another *i.e.* are bonded.[338] Thus atomic charge is unique to the environment in which it is situated.

The use of empirical charges in docking calculations is limited due to their inability to accurately describe the charge of uncommon functional groups, such as isonitriles *i.e.* $R\text{-}N^{+}\equiv C^{-}$. These charges are defined from structural libraries or an empirical methods' databases e.g. AutoDock's modified AMBER forcefield.[297] AutoDock uses methods such as Gasteiger-Marsilli[347] algorithms to describe the charges on ligands, often inaccurately as we have found in unusual moieties *e.g.* isonitriles. Due to accessibility and ability to afford reliable simulations in a plethora of binding situations, AutoDock has become the most cited docking methodology.[348] While the use of Gasteiger-Marsilli charge calculation is sufficient for a large system such as proteins where high accuracy is often not affordable. In the case of haem-ligand interactions we needed a definitive charge calculation in order to determine if the interaction between the negative carbon of the isonitrile and the iron core is electrostatic as originally proposed by Wright *et al*.[196] We therefore looked at three other charge theories in order to obtain an accurate docking study. Charges pertaining to the isonitrile functionalities are provided in Table 4.3, using different atomic charge theories including Mulliken,[349] Merz-Singh-Kollman (MK)[350] and Natural Bonding Orbitals (NBO).[351]

Gasteiger and Marsilli pioneered the concept of equalization of electronegativity. Their algorithm is based on the concept of highly electronegative atoms drawing electrons away from less electronegative ones. This was appealing to us as it was founded on empirical data, performed rapid calculations and may be transferred over a range of different molecules. Unfortunately, this theory's major fault is dealing with formal charge were it often fails.[352] Mulliken Population Analysis is a charge partition scheme where the electrons are equally distributed over the basis set (the functions linearly combined, which make up a set of molecular orbitals).[338] Fitting the charges to electrostatic potentials (ESP), such as MK charge theory, relies on the computation of the *ab initio* quantum mechanic at sampling points around the molecule. This may become complicated if the molecule is large and may result in hours of computer time. ESP charges are also dependent upon the conformation of the molecule, due to changes in the electron environment also altering charges and changes in the conformation which will alter the distribution of sampling points. ESP tends to assign different charges to chemically equivalent moieties, *e.g.* the protons of a methyl functionality.[352] However, this has been addressed by the Restrained Electrostatic Potential (RESP) method,[302,353] which divides the sum of the charge across chemically equivalent atoms. In NBO charge calculation the nearest Lewis structure to the desired molecule is determined. This calculation generates orbitals which are localized electron pair orbitals for bonding pairs and lone

pairs *i.e.* NBOs. The hybridization of the atoms and the weight of each atom in each localized electron pair bond is calculated in this idealized Lewis structure. [354]

Table 4.3: The Gasteiger-Marsilli, Mulliken, Merz-Singh-Kollman and NBO charges calculated for the nitrogen and carbon atoms in the isonitrile functionality of the marine isonitriles **2.4**, **2.9**, **2.15**, **2.19**, and **2.35**.

Compound	Gasteiger-Marsilli		Mulliken		Merz-Singh-Kollman		NBO	
	N	C	N	C	N	C	N	C
2.4	-0.434	0.188	-0.188	-0.094	0.718	-0.565	-0.544	0.269
2.9 (i)	-0.430	0.188	-0.192	-0.110	0.574	-0.520	-0.549	0.275
2.9 (ii)	-0.430	0.188	-0.189	-0.096	0.737	-0.566	-0.555	0.274
2.15	-0.430	0.188	-0.192	-0.113	0.522	-0.512	-0.548	0.272
2.19	-0.430	0.188	-0.191	-0.112	0.540	-0.512	-0.548	0.273
2.35	-0.430	0.188	-0.200	-0.102	0.533	-0.516	-0.551	0.274

It is clear from the Table 4.3, that the charges for the Gasteiger-Marsilli algorithm do not adequately describe the isonitrile functionality. The terminal carbon has not been allocated enough electron density and appears as a positively charged atom. Conversely, the nitrogen of the isonitrile appears far more negative than expected. This is again true with NBO theory resulting in an isonitrile containing a negative nitrogen and a positive carbon. Mulliken charge theory reduces the positive and negative charge on the carbon and nitrogen respectively, leaving the MK theory in our opinion affording the most accurate description of charge distribution in the isonitrile functionality.

Charges are essential to accurately solve the electrostatic term (ΔG_{elec}) in the AutoDock energy equation (Equation 4.1).

$$\Delta \mathbf{G\ Total} = \Delta \mathbf{G_{vdW}} \sum_{\mathbf{i,j}} \left(\frac{A_{ij}}{r_{ij}^{12}} \frac{B_{ij}}{r_{ij}^{6}} \right) + \Delta \mathbf{G_{hbond}} \sum_{\mathbf{i,j}} \mathbf{E(t)} \left(\frac{\mathbf{C_{ij}}}{\mathbf{r_{ij}^{12}}} \frac{\mathbf{D_{ij}}}{\mathbf{r_{ij}^{10}}} \mathbf{E_{hbond}} \right) + \Delta \mathbf{G_{elec}} \sum_{\mathbf{i,j}} \left(\frac{\mathbf{q_i q_j}}{\boldsymbol{\varepsilon}(\mathbf{r_{ij}}) \mathbf{r_{ij}}} \right) + \Delta \mathbf{G} \quad \text{Equation 4.1}$$

The charges on all the atoms were consequently changed from the Gasteiger-Marsilli to the MK charges in our docking studies. The charge corrected isonitriles **2.4**, **2.9**, **2.15**, **2.19**, **2.34**, **2.35** and **3.215** were subsequently docked against free haem and the haem dimer to determine what role the electrostatic charge has in their binding to haem and the haem dimer. Despite our initial concerns about the influence which incorrect charges (especially on the isonitrile moiety) may have on either

the haem or the haem dimer docking studies, there appeared to be no apparent difference in the docking models obtained when each of the four modified per atom charges for all the atoms were changed in the respective input files from Gasteiger-Marsilli to Mulliken, MK or NBO charges respectively. From the docking models below in Figure 4.16 it is clear that the interaction between the marine isonitriles and the iron centres in free haem and the haem dimer are not electrostatic but rather reflect ring stacking which occurs between the terpene scaffold and the porphyrin ring with the isonitrile functionalities directed away from the haem ring.

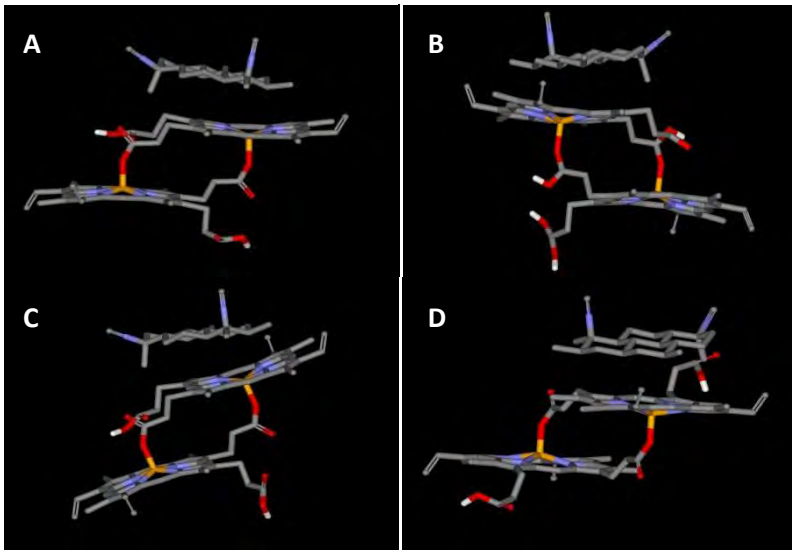

Figure 4.16: Docking images of **2.9** and haem dimer with different atomic charges A: Gasteiger-Marsilli; B: Mulliken; C: Merz-Singh-Kollman and D: NBO charges. All ligands docked in AutoDock[297] and visualized in DSVisualizer.[21]

4.4.4. Docking of marine and synthetic isonitriles to haem and haem dimer

Despite there being no apparent difference related to the charge set used to produce the final AutoDock model, we opted to use MK charges throughout our study because this charge theory most accurately represents the isonitrile functionality. A representative selection of the docking of compounds **2.4**, **2.9**, **2.15**, **2.19**, **2.34**, **2.35** and **3.215** to haem and haem dimer is shown in Figure 4.17. All the compounds docked align their carbon scaffold along the porphyrin rings of both the haem and haem dimer receptors. In all cases the functional groups (*i.e.* isonitriles and isothiocyanates) are directed away from the iron centre of haem and the haem dimer. None of the ligands orientated themselves in such a way that a feasible distance existed between the anionic

functionalities and the iron core for the formation of a formal bond as originally proposed by Wright *et al*.[196]

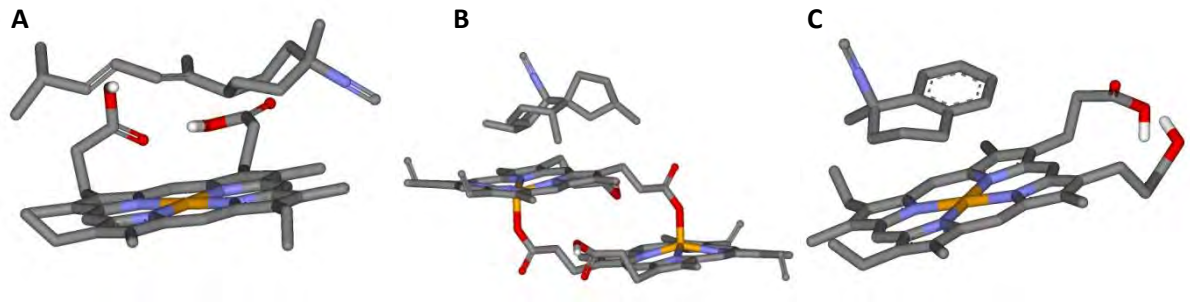

Figure 4.17: A: **2.35** Docked against haem; B: **2.4** docked against haem dimer; C: **3.215** docked against free haem. All ligands docked in AutoDock[297] and visualized in DSVisualizer.[21] All ligands charges changed using MK charge theory.

4.4.5. Attempted validation of the AutoDock approach

4.4.5.1. Comparison with the halofantrine haem complex

In order to validate our AutoDock docking model, the crystal structure of a known haem binder halofantrine[355] (**4.1**) was compared to that of the proposed docking conformation of **4.1** to triplet haem. The structural conformation of **4.1** was optimized and the MK charges of halofantrine calculated using Gaussian03 at the B3LYP density function and the 6-13G basis set. The S-halfantrine enantiomer was used in our docking studies as it was found to be the more active enantiomer against *P. falciparum*.[356] The optimized structure of **4.1** was imported into AutoDock where the PDBQT (Protein Database with Charge and Torsion) file was generated. This PDBQT file, containing all the Gasteiger-Marsilli per atom charges for halofantrine, were changed to those per atom charges calculated using MK theory contained in the DFT log file. The charge corrected halofantrine was subsequently docked against free haem (Figure 4.18, *Right*).

The X-ray crystal structure was obtained from CSD (CSD 659633) of a crystal structure described by de Villiers *et al.* of halofantrine bound through the C-1' oxygen atom to the iron atom in haem.[355] The bond length of the iron-oxygen bond calculated from the crystal structure was described as 1.838 Å (Figure 4.18, *Left*). The image of **4.1** obtained from AutoDock indicates a distance of 2.105 Å between the oxygen of the alcohol on C-1' in halofantrine and the iron core of haem, which suggests that a formal bond between the OH in **4.1** may be possible as observed in the crystal structure. It

must be noted that the X-ray crystal structure is a solid state structure whereas the docking studies are performed *in vacuo*.

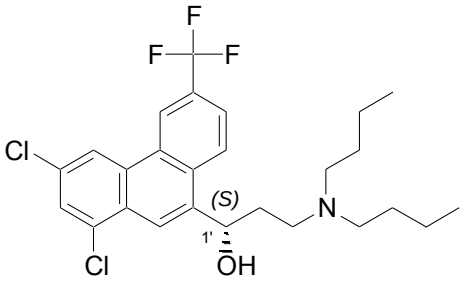

4.1

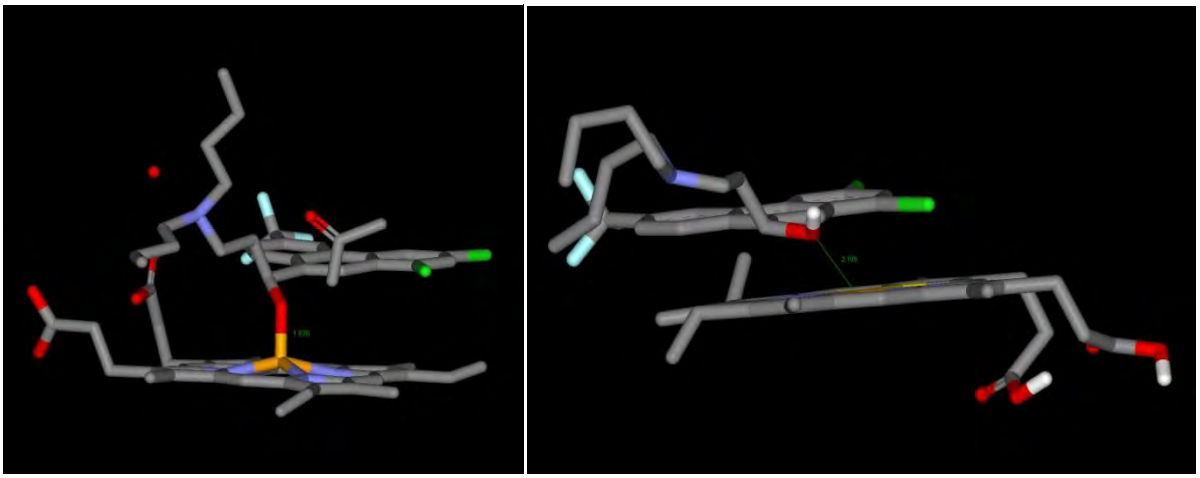

Figure 4.18: The crystal structure of halofantrine (**4.1**) bound to haem (CSD 659633)[355] visualized in DS Visualizer[304] (*left*). The image of **4.1** docked to haem using AutoDock,[297] also visualized in DS Visualizer[304] (*right*).

4.4.5.2. MALDI-TOF mass analysis of a haem-isonitrile complex

The precipitate obtained in the EBHIA (see Section 4.3) after the addition of **2.9**, was subjected to MALDI TOF mass analysis (Figure 4.19). The soft ionization provided by the laser should result in Fe-isonitrile bond remaining intact, should it exist. From the mass spectrum (Figure 4.19), there is no mass corresponding to *m/z* 941.008 (the mass of a haem-**2.9** complex) or *m/z* 1555.752 (the mass of a haem dimer-**2.9** complex, not shown in Figure 4.19), thus suggesting no isonitrile-haem complexes had formed. These data reinforced the idea that the interaction between marine isonitriles and free haem or the haem dimer is not an ionic one but suggests the ring stacking implied by the AutoDock studies.

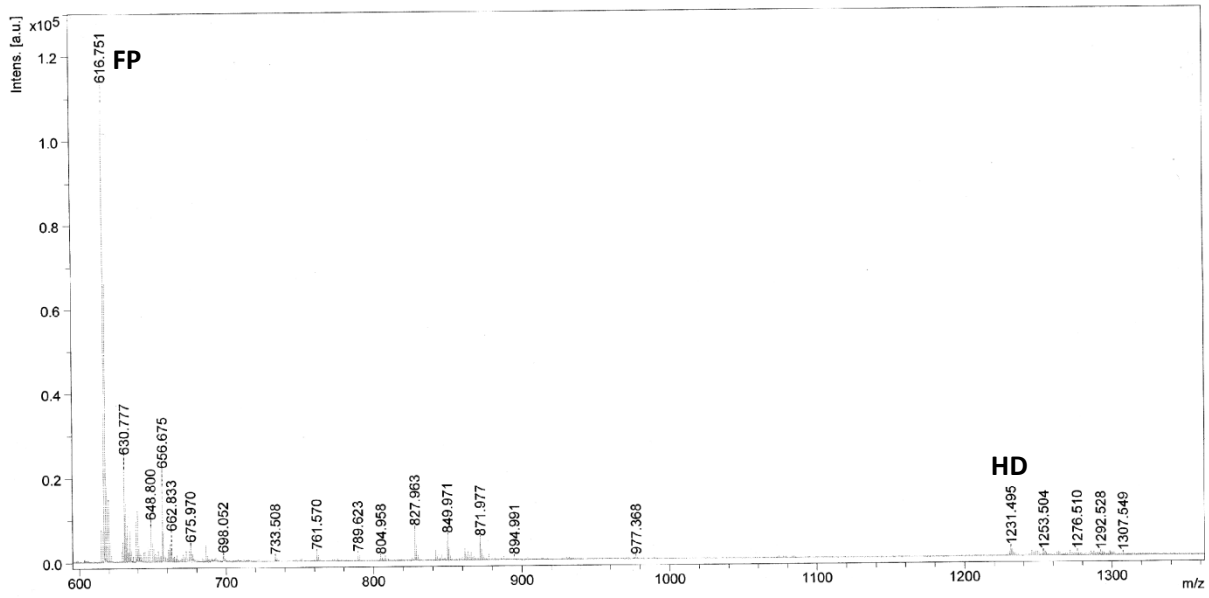

Figure 4.19: The deconvoluted MALDI-TOF mass spectra of the precipitate obtained in the β-haematin inhibition assay containing **2.9**. FP represents free haem while HD represent the haem dimer. The matrix used was α-cyano-4-hydroxycinnamic acid as the MALDI matrix, using a 354 nm Nd:YAG laser. The masses of the free haem (*m/z* = 616.751) and the haem dimer (*m/z* = 1231.495) are indicated.

4.5. *In silico* and *in vitro* studies of podocarpane-haem interaction

4.5.1. Docking of podocarpanes to haem and haem dimer

Now that a representative ligand-haem docking model had been established for known and newly discovered β-haematin inhibitors, it was hoped that this model may be extended to other ligands in order to identify potential inhibitors of haem polymerization *in silico*. We therefore docked our previously synthesized podocarpanes (**3.203-3.212**) against the haem and haem dimer, using the AutoDock method, to gauge their theoretical ability to inhibit the sequestering of haem in the malaria parasite (Figure 4.20). All the docking models of **3.203-3.212** show a similar docking conformation to those obtained for **2.4**, **2.9**, **2.15**, **2.19**, **2.34**, **2.35** and **3.215**, with the diterpene ring scaffold stacking above the porphyrin ring of haem. Interestingly, the most active phenyl containing compounds **3.204** and **3.209-3.212**, aligned themselves with the phenyl ring more centred above the iron core. A notable difference found in the docking of podocarpanes to haem and the haem dimer when compared to the docking studies of the marine and synthetic isonitriles was the ability of the hydroxyl functionalities of **3.203-3.212** to form hydrogen bonds with the flexible carboxylic acid side chains of the receptor.

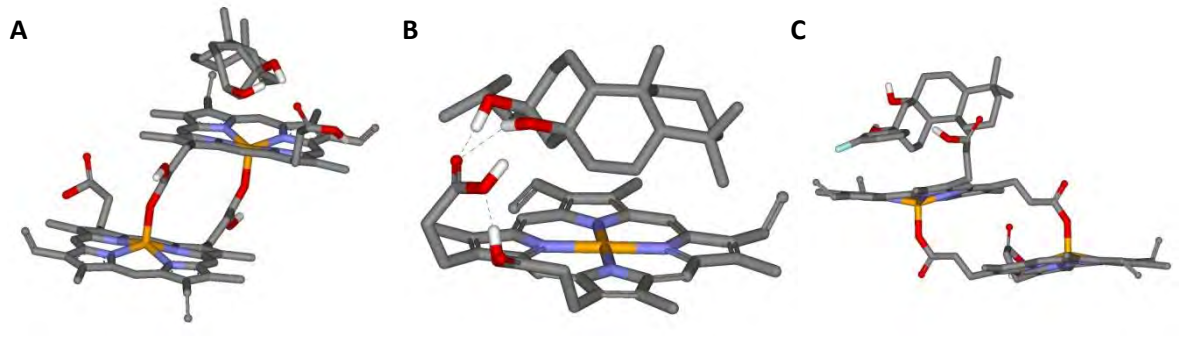

Figure 4.20: A: **3.207** Docked against the haem dimer; B: **3.206** docked against free haem and C: **3.211** docked against the haem dimer. All ligands docked in AutoDock[297] and visualized in DSVisualizer. All ligands charges changed using MK charge theory. Broken green lines indicative of hydrogen bonding.

.

4.5.2. *In vitro* evaluation of haem polymerization inhibition by podocarpanes 3.203-3.207 and 3.209-3.212

Since the docking studies of podocarpanes and haem suggested a docking model similar to that obtained for the marine isonitriles, we once again used Egan's β-haematin inhibition assay to determine the podocarpanes' (all tested at 10 equiv. relative to haem because of the large quantities of synthetic compounds in hand) ability to inhibit haem polymerization. While none showed any promise as potential β-haematin inhibitor, **3.212** (the most active antiplasmodial podocarpane) will be used here as a representative compound to support this conclusion. The Phi-β assay indicated very little inhibition, with only a weak Sorret-band appearing at 405 nm (Figure 4.21A). The preliminary UV/vis data was corroborated by an the FTIR analysis of precipitate of EBHIA containing **3.212**, which indicated a 89% conversion of haemin to β-haematin. The SEM micrograph showed the presence of microcrystals in all the precipitates of EBHIA containing **3.203-3.207** and **3.209-3.212** (e.g. Figure 4.21B). Finally the lack of β-haematin inhibition exhibited by **3.203-3.207** and **3.209-3.212** was confirmed by the identification of β-haematin peaks in the X-ray powder diffraction pattern of all precipitates isolated from EBHIA which contained podocarpanes.

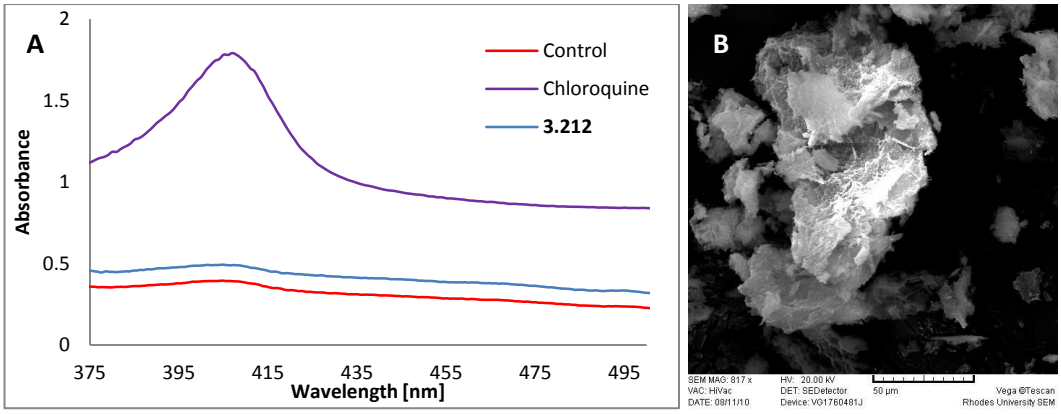

Figure 4.21: UV/vis spectra (375-500 nm) of Phi-β assay solutions containing chloroquine (purple), **3.212** (blue) and no inhibitor (red) (*Left*). The SEM micrographs of the precipitates from the EBHIA contain **3.212** (*Right*). Images taken using a Tescan Vega scanning electron microscope at 20 kV and a working distance of 20mm. Scale given at the bottom of the image.

4.6. Conclusion

We have unequivocally shown the ability of **2.9** to completely inhibit haem polymerization at 3 equivalents relative to haem, which suggests that the primary antiplasmodial mode of action of **2.9** may be the inhibition of the formation of hemozoin within the parasite as originally proposed by Wright *et al*.[196] Compounds **2.19** and **2.15** also exhibited promise in their ability to inhibit β-haematin formation and may show greater inhibition of β-haematin sequestration at higher concentrations.

We have addressed the limitations of certain charge theories in describing unusual functionalities and have used this newly acquired knowledge to determine a more accurate docking study for marine isonitriles with free haem and the haem dimer. These docking studies have shown that the interaction between the isonitriles and haem porphyrin is possibly a result of ring-stacking rather than ionic interaction between the Fe(III) core and the carbon of the isonitrile as previously proposed by Wright *et al*.[196] The β-haematin inhibition assays would suggest that a tri- or tetracyclic ring scaffold increases the ability of a compound to inhibit haem polymerization. While we have shown that the isonitrile functionality is not relevant for ionic bonding to the iron of haem, the isonitrile group may still play a significant role in antiplasmodial activity, which can clearly be seen in the decrease in antiplasmodial activity (from the nanomolar to the millimolar range) with the addition of an isothiocyanate moiety *i.e.* **2.34**. The exact function of the isonitrile moiety in determining the parent compound's bioactivity is unknown but it may be essential for facilitating entry into the cell across membranes or through ion channels. The molecular models of marine

isonitriles docked with haem dimers suggest that the isonitrile moieties are directed outwards, thus possibly repelling other haem or haem dimer units from adding to the growing crystal lattice of β-haematin. The lack of the inhibition of β-haematin shown by the tricyclic podocarpanes, suggests that a tricyclic scaffold alone may not be enough to inhibit haem polymerization.

A summary of the *in vitro* antiplasmodial activities of all compounds **2.4**, **2.9**, **2.15**, **2.19**, **2.34**, **2.35, 3.188**, **3.203-3.207**, **3.209-3.212** and **3.215** may be seen in Table 4.4.

Table 4.4: A summary of the results obtained from the EBHIA and DXR inhibition assay.

Compound	HA[a]	UV/ vis[b]	FTIR[c]	XRD[d]	SEM[e]	*Pf*DXR[f]	Conclusion
2.4	×	ND	×	×	×	ND	Not a β-haematin inhibitor
2.9	×	ND	✓	✓	✓	ND	β-haematin inhibitor
2.15	×	ND	✓	×	✓	ND	β-haematin inhibitor
2.19	×	ND	✓	×	✓	ND	β-haematin inhibitor
2.34	×	ND	×	×	×	ND	Not a β-haematin inhibitor
2.35	×	ND	×	×	×	ND	Not a β-haematin inhibitor
3.188	×	×	×	×	×	ND	Not a β-haematin inhibitor
3.203	×	✓	✓	×	×	ND	Some β-haematin inhibition, but not sufficient at 10 equiv.
3.204	×	✓	×	×	×	ND	Not a β-haematin inhibitor
3.205	×	×	×	×	×	ND	Not a β-haematin inhibitor
3.206	×	×	×	×	×	ND	Not a β-haematin inhibitor
3.207	×	×	×	×	×	ND	Not a β-haematin inhibitor
3.209	×	✓	×	×	×	✓	Possible mode of action, PfDXR inhibition
3.210	×	✓	×	×	×	✓	Possible mode of action, PfDXR inhibition
3.211	×	×	×	×	×	✓	Possible mode of action, PfDXR inhibition
3.212	×	×	×	×	×	×	Neither a β-haematin nor PfDXR inhibitor
3.215	✓	✓	×	×	×	ND	Causes haemolysis ∴not a good drug candidate

[a] HA (Haemolytic Activity): A positive results was determined by haemolytic activity being > 60% at 50 µL
[b] A positive results was determined by a difference in absorbance from the baseline to the crest at 405 nm > 0.4
[c] A positive results was determined by conversion of haematin to β-haematin < 50%
[d] A positive results was determined by no detection of peaks corresponding to β-haematin
[e] A positive results was determined by a visual inspection concluding that the majority of the precipitate was not microcrystals
[f] A positive results was determined by < 40% conversion of NADPH to $NADP^+$ at 250 µM

CHAPTER 5: MARINE BISINDOLE ALKALOIDS

5.1. Background

The original discovery of the penicillin class of antibiotics, (*e.g.* **5.1** and **5.2**) revolutionised the war on bacterial infection.[357] Penicillin targets the bacterial cell wall, which is important for maintaining the shape of the bacterial cell and providing protection against osmotic lysis. Penicillin covalently binds and inhibits penicillin binding proteins (PBPs). These bacterial proteins (PBP 1-4) are essential for construction, maintenance and regulation of the cell wall and its functions.[358-360] However, the discovery of penicillin over 80 years ago appeared to initially lull the medical fraternity into a false sense of security, possibly slowing the further development of antibiotics. For example, in a 1966 issue of Time magazine an article appeared stating "...experts agree that by year 2000, viral, and bacterial diseases will have been eliminated."[361] Ironically, by 1941 strains of *Staphylococcus aureus* had already appeared that could degrade penicillin by means of the enzyme β-lactase (Scheme 5.1). Today in excess of 95% of all strains of *S. aureus* worldwide are resistant to penicillin. While the development of the semi-synthetic antibiotic methicillin (**5.3**) initially filled the void left by penicillin resistance up until the 1980s, the emergence of methicillin resistant *S. aureus* (MRSA) ultimately negated the efficacy of this drug.[362] The addition of a bulky substituent to the basic penicillin scaffold, *e.g.* 2,6 dimethylphenyl in methicillin, resulted in the bacterial β-lactase being unable to facilitate methicillin's conversion to the inactive penicilloic acid (**5.4**).[363] However, the *mecA* gene encodes for a 76 kDa protein called PBP2a, which exhibits a low affinity for methicillin and therefore enables MRSA bacteria processing this protein to resume cell wall maintenance in the presence of methicillin.[364]

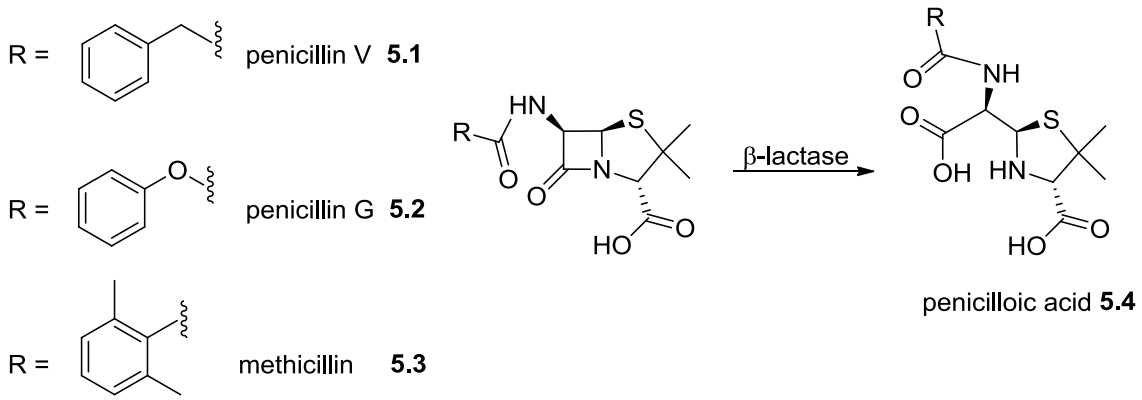

Scheme 5.1: The enzyme facilitated breakdown of penicillin compounds to penicilloic acids.

Resistance to antibiotics may occur in several ways. Firstly, the antibiotic may be pumped out of the bacterial cell via over expressed membrane proteins,[365] which are increasingly able to recognise a wider spectrum of antibiotics. Secondly by metabolising and/or altering an antibiotic through specially mutated enzymes[366] such as methicillin-hydrolyzing β-lactase and thirdly downregulating, modifying or deleting proteins targeted by antibiotics.[367] The latter is the major form of resistance to penicillin antibiotics.

Methicillin resistant *S. aureus* (MRSA) is responsible for severe post-operation infection in hospitals around the world, *i.e.* hospital associated (HA-MRSA), and has led to entire hospital wings being closed.[368] In one study it was reported that the percentage of MRSA related hospital deaths was as high as 39% and several years ago the associated costs of the prolonged treatment of MRSA infected patients in the USA alone was a staggering $ 14.5 billion (Figure 5.1).[369] Asymptomatic hosts act as a reservoir for the human to human spread of *S. aureus*. For example the predominate mode of infection is skin-to-skin contact of a colonised source or contact with colonised fomites (any inanimate object on which bacteria may grow).[370] To initiate infection *S. aureus* forms colonies on host tissue via a series of surface proteins, referred to as MSCRAMM (microbial surface components recognising adhesive matrix molecules),[371] with each MSCRAMM is unique to each strain of *S. aureus*. Once adhered to the surface tissue the colony of *S. aureus* begins to produce a biofilm in order to evade the host immune response and keep out antibiotics, thus ensuring successful initial colonization and infection.[372] While infections can be prevented via physical barriers, *i.e.* epithelial and endothelial tissue; in burn and post-operation patients this first line physical barrier is severely compromised often leading to successful invasion of *S. aureus*. *S. aureus* has several mechanisms, which it uses to evade the host's immune system and facilitate infection. Firstly, *S. aureus* may also secrete a special type of MSCRAMM, known as the fibronectin-binding protein, which creates a fibronectin bridge between bacterial and endothelial/epithelial β1 intergrins resulting in absorption of *S. aureus* into the host's tissue. The refuge afforded by fibronectin bridges provides protection against phagocytic cells such as neutrophils, monocytes and macrophages.[373-375] Secondly, *S. aureus* may secrete Protein A, a protein which binds to the universal Fc region of host's immunoglobins and thus inhibits opsonisation and phagocytosis.[376] Thirdly, *S. aureus* may secrete a substance called CHIPS (chemotaxis inhibitory proteins of *S. aureus*), which hinders the recruitment of neutrophils. Fourthly, the secretion of leukocidins by *S. aureus* can result in disruption of leukocytes membranes, thus severely impairing their function.[377] Finally, *S. aureus* may secrete a series of enzymes including lactamases, proteases, lipases, nucleases, hyaluronate lyase, phospholipase C and metalloproteinases, which aid in further infection and tissue damage.[378] The successful infection of the host's skin by *S. aureus* results in a number of unpleasant afflictions including: skin abscess,

cellulitis, bullous impetigo, folliculitis, furunculosis and necrotizing fasciitis.[379] Exfoliating toxins produced by the bacterium can also result in erythema, skin exfoliation and Ritter's Disease.[380] Should *S. aureus* penetrate the skin-barrier, via the mechanism discussed *vide supra*, endocarditis, septic arthritis (the purulent invasion of the joints), osteomyelitis, sepsis and toxic shock syndrome induced by the superantigens secreted by *S. aureus*, may result.[381,382]

In the last two decades the infection of MRSA has no longer been confined to hospital environments. Non-hospital contained MRSA infections were first described in the town of Kimberly in Western Australia in the 1990s and have subsequently spread worldwide.[383,384] What is of particular concern, are individuals infected by community associated MRSA (CA-MRSA), whom have had no contact with a health-care setting prior to infection. The appearance of CA-MRSA suggests a new *S. aureus* virulence.[385] Genetic analysis of CA-MRSA clones have shown that these carry SCC*mec* allotypes IV and V and also the *lukSF-PV* genes, which encode for the leukotoxin, Panton-Valentine leukocidin (PVL).[385,386] This toxin has been hypothesized to play a role in the pathogenesis of CA-MRSA, due to 90 percent of all CA-MRSA cases presenting severe skin and soft tissue infections.[385,387] Fortunately while the newest CA-MRSA clones, are resistant to β-lactam antibiotics, they are still susceptible to other non-penicillin based antibiotics, such as tetracyclines and quinolones.[388] Conversely, HA-MRSA clones are multidrug resistant, thus increasing the urgency for the discovery and development of new MRSA bioactive compounds and the ongoing identification of novel MRSA specific targets.

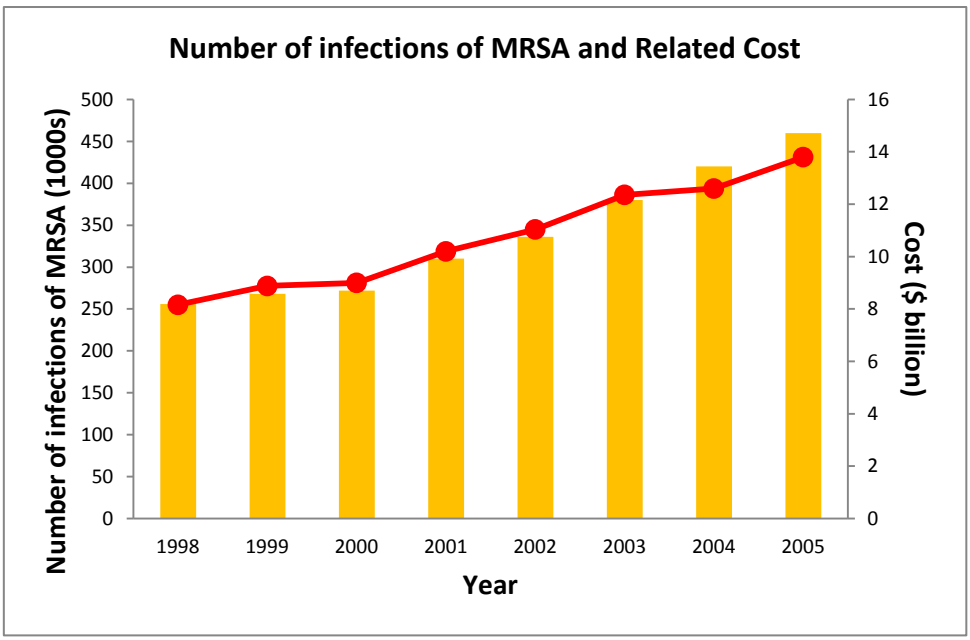

Figure 5.1: Increase of MRSA infections (bar) and related cost (line) in the United States from 1998-2005[369]

Professor Raymond Andersen and co-workers at the University of British Columbia (UBC) recently identified the inhibition of pyruvate kinase (PK) in MRSA as a viable drug target given the significant structural differences between *S. aureus* PK and mammalian PKs.[389-391] Pyruvate kinase plays a key role in regulating carbohydrate metabolism and catalyzes the final step in glycolysis, where it irreversibly transfers the phosphoryl moiety from phosphoenolpyruvate (PEP) to ADP forming ATP and pyruvate, which then feeds into a number of other biosynthetic pathways.[392] The bacterial PK enzyme is highly conserved and exists as homo-tetramers of identical subunits, each monomer consisting of three or four domains (designated N-terminal and A-C domains). The active site of this protein lies at the interface between the A and B domains while the allosteric effector site lies in the C domain (Figure 5.2).[393]

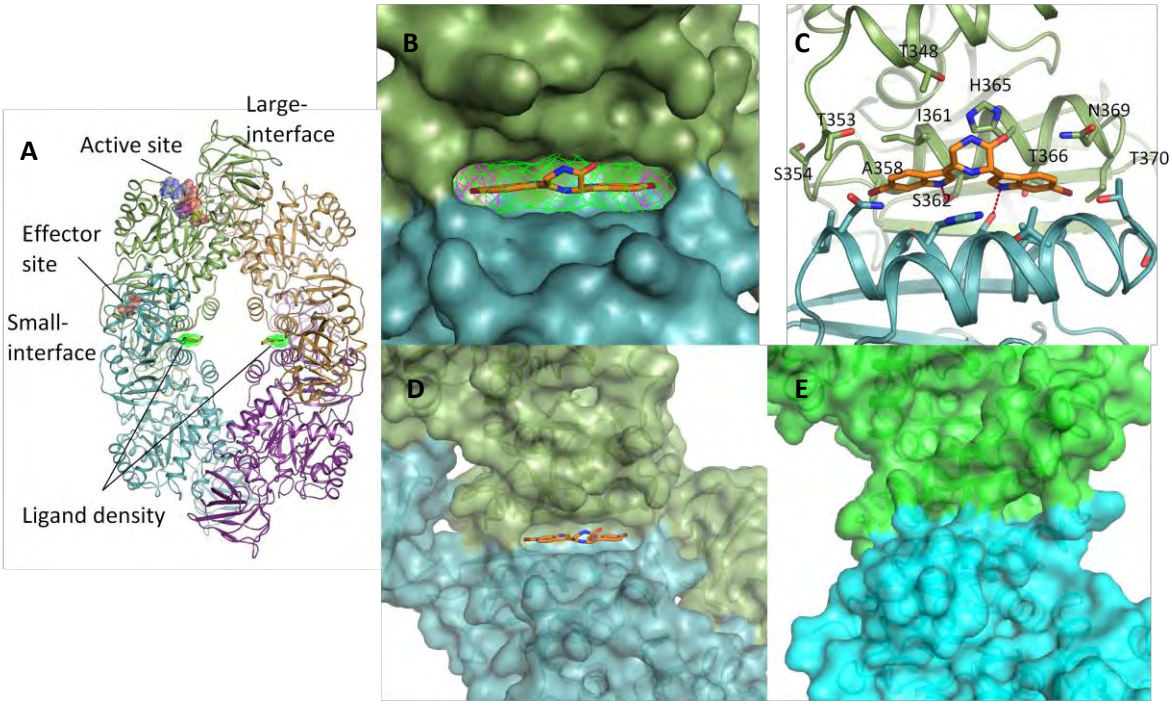

Figure 5.2: A: The binding of **5.7** to the small interface of the bacterial PK.
B: An enlargement of **5.7** binding to the receptor site.
C: The anti-parallel interaction of helix 357-370 with **5.7**.
D and E: The binding pocket of human PK consists of much tighter dimeric packing around the 'small' interface, which drastically alters the nature of the pocket, and also the closer interaction of a helix 340-350 above the interface, thereby limiting access to the pocket. Reproduced from Andersen and co-workers.[393]

A total of 968 crude extracts of marine benthic invertebrates, collected from Papua New Guinea, Indonesia, Dominica, Brazil, British Columbia, South Africa and Norway were screened in a programme designed to find potential inhibitors of MRSA PK. Despite the comprehensive nature of this screening programme, only one extract from the South African sponge (Figure 5.3) *Topsentia*

pachastrelloides (Topsent, 1892) collected off the Aliwal Shoals in Kwa-Zulu Natal, showed promising activity. Bioactivity-guided fractionation of this extract resulted in the isolation of a series of bisindole alkaloids, spongotine A (**5.5**), bromotopsentin (**5.6**), *cis*-3,4-dihydrohamacanthin (**5.7**) and bromodeoxytopsentin (**5.8**).[393]

Figure 5.3: Surface photograph of SAF94-035 (*Topsentia pachastrelloides)* taken immediately after collection.

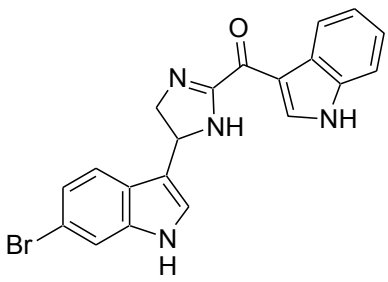

5.5

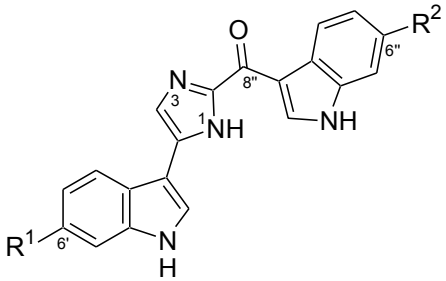

5.6 R^1 = Br; R^2 = OH
5.8 R^1 = Br; R^2 = H

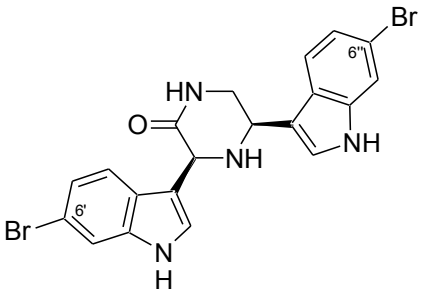

5.7

Two of these marine bisindoles alkaloids (**5.7** and **5.8**) showed a 166-600 fold preference for the *S. aureus* PK over human PKs (Figure 5.4). In the X-ray crystal structure of *cis*-3,4-dihydrohamacanthin (**5.7**) complexed with PK, the bisindole is bound to a remote site on the protein (Figure 5.2). Andersen and co-workers hypothesized that this remote binding may prevent the enzyme from folding correctly, thus retarding the phosphoryl transfer of the active site.[393] The two most active compounds **5.7** and **5.8** exhibited an activity against MRSA of 6 and 60 nM respectively.[393]

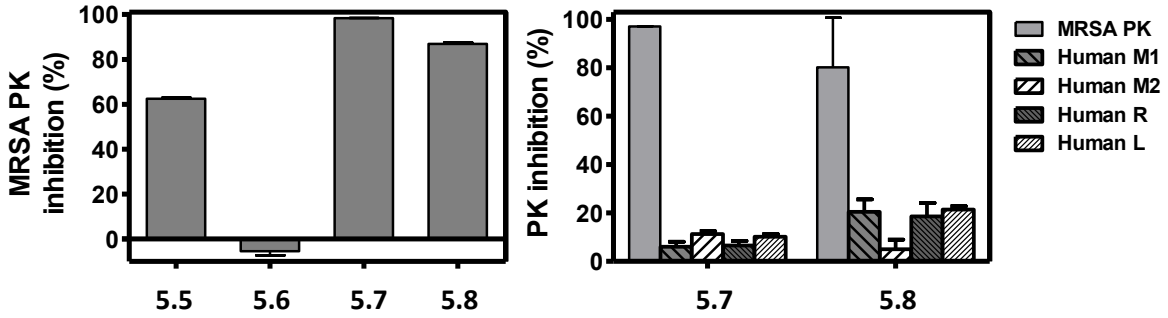

Figure 5.4: MRSA inhibition assay results of compound 5.5-5.8 (*Left*). Selective inhibition of compounds **5.7** and **5.8** between bacterial and human PK's (*Right*)

Strangman *et al.*[394] at UBC synthesized **5.7** and compared the antibacterial activity of several synthetic precursors (**5.9**-**5.12**) and structural analogues (**5.13**-**5.19**) of this compound (Table 5.1).

Table 5.1: A comparison of **5.7**, **5.9-5.19** ability to inhibit MRSA pyruvate kinase[394]

Compound	MRSA PK inhibition*
5.7	98%
5.9	35%
5.10	22%
5.11	4%
5.12	35%
5.13	43%
5.14	No Activity
5.15	38%
5.16	23%
5.17	No Activity
5.18	86%
5.19	24%

* All inhibition levels reported at 10 µM

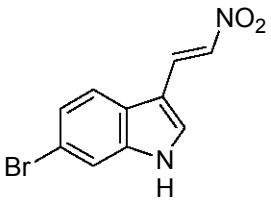

5.9

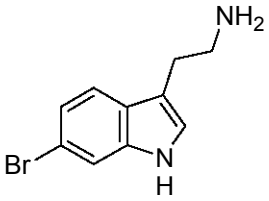

5.10

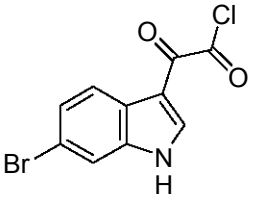

5.11

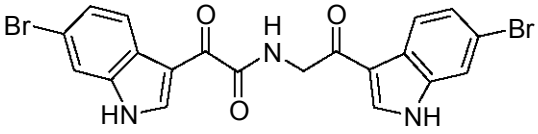

5.12

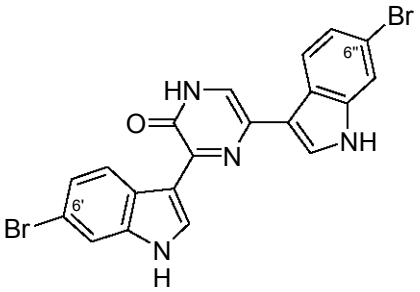

5.13

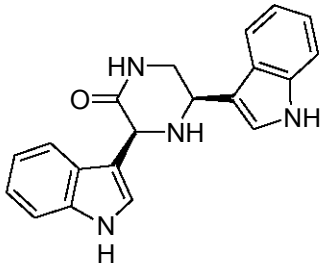

5.14

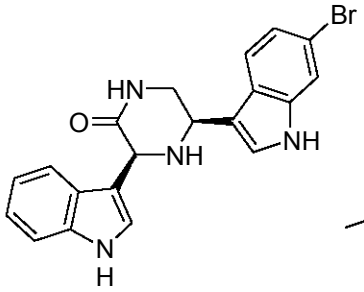

5.15

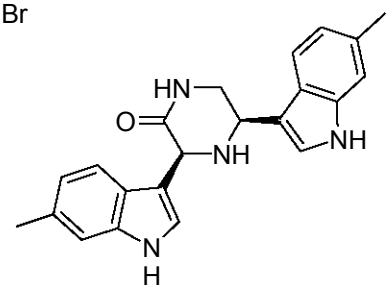

5.16

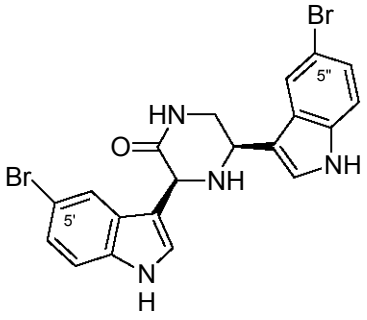

5.17

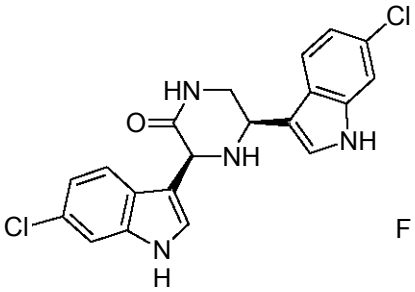

5.18

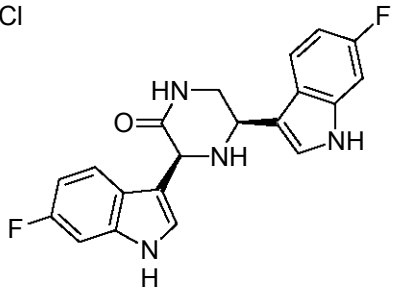

5.19

Strangman *et al.*[394] were able to draw four major conclusions from the results present in Table 5.1. Firstly, the full structure of **5.7** is required for inhibition activity of MRSA PK, since none of the intermediates (**5.9**-**5.13**) showed promising activity including the pyrazine containing **5.13**. Secondly, the removal of the bromine substituent greatly decreases the bioactivity. The complete removal of the bromines (**5.14**) shows no activity while, the mono-substituent decreases the activity of **5.7** by approximately half. The 6',6''-dimethyl substituted analogue (**5.16**) was tested as the methyl moiety fills similar chemical space to that of bromine, however this compound failed to achieve equal bioactivity. Thirdly, the position of the bromine on the indole ring is important for bioactivity. Substituting bromine atoms on the 5' and 5'' positions on the ring (**5.17**), afforded no inhibition. Finally, as the electronegativity of the 6-substituent (**5.18** and **5.19**) decreases the bioactivity increases.

Stangman *et al.*, supported by their SAR study and by the X-ray structure (Figure 5.2) highlighted the importance of the two bromine atoms at C-6' and C-6'' in the binding of MRSA PK. A halogen bond occurs when a halogen is shared between a donor (**5.7**) and an acceptor (*e.g.* an amino acid contained in the active site).[395] In halogen bonding both the donor and especially the acceptor tends to be electronegative or electron-withdrawing, resulting in unusually short atomic distances *i.e.* less than the sum of van de Waal's radii of the atoms involved.[395] In the past many biologically significant examples of halogen-bonded complexes have been described,[396-398] demonstrating the potential for using such interaction in drug design. Surprisingly the mono-brominated **5.8** was significantly active against MRSA PK and it occurred to us that preparing the dibromobisindole imidazole (**5.20**, isobromotopsentin) and analogues of **5.20** might result in a more active compound. The research presented in this Chapter records our attempts to find a new and more efficient method for preparing **5.20** and related analogues for future SAR studies.

5.2. Research aims.

Our approach to the SAR studies of **5.20** was to firstly prepare a series of simple diphenylimidazole (**5.21**-**5.26**) analogues of **5.20**. Although these are all known compounds[399] we envisaged that microwave assisted selenium dioxide (SeO_2) oxidation might prove to be a more efficient method of preparing the prerequisite synthetic phenyl glyoxal precursors (**5.27**-**5.32**) required for the synthesis of these compounds. Once the microwave assisted organic (MAO) synthetic methodology had been established on simple model compounds we planned to extend this method for the preparation of indole glyoxals which surprisingly, have not previously been used to synthesize bisindole imidazoles. Initial preparation of deoxytopsentin (**5.33**) was to be followed by the attempted synthesis of bis-

5-bromoindole imidazole (**5.34**) and our target molecule isobromotopsentin (**5.20**). Our goal throughout this work was to find a simple, fast and high yielding route to bioactive imidazole alkaloids.

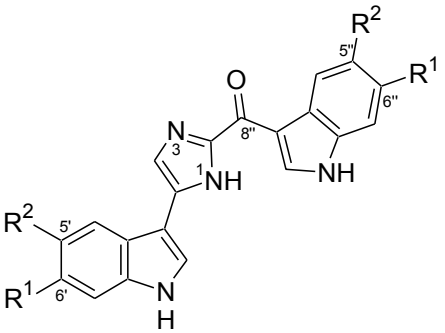

5.20 R^1 = Br R^2 = H
5.33 R^1 = H R^2 = H
5.34 R^1 = H R^2 = Br

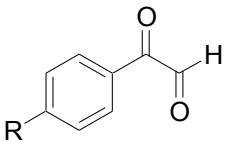

5.27 R = H
5.28 R = OMe
5.29 R = NO_2
5.30 R = Cl
5.31 R = Br
5.32 R = F

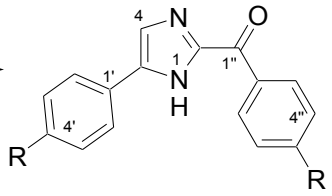

5.21 R = H
5.22 R = OMe
5.23 R = NO_2
5.24 R = Cl
5.25 R = Br
5.26 R = F

5.3. Naturally occurring topsentin alkaloids from marine sponges.

In order to contextualize the synthetic work presented in this Chapter an intial overview of the naturally occurring marine sponge secondary metabolites from the topsentin class of alkaloids is presented here. We summarized some aspects of Yang's comprehensive 2004 review[400] of these compounds and elaborated on further progress made in the discovery and synthesis of bisindole topsentin type alkaloids up until June, 2011.

5.3.1. Structure and isolation.

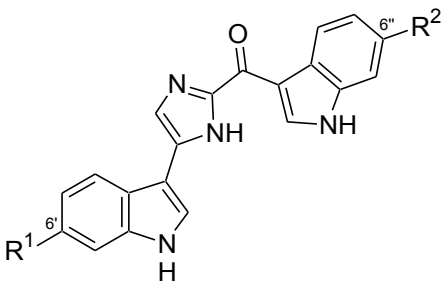

5.6 R^1 = Br; R^2 = OH bromotopsentin
5.8 R^1 = Br; R^2 = H bromodeoxytopsentin
5.20 R^1 = Br; R^2 = Br isobromotopsentin
5.33 R^1= H; R^2 = H deoxytopsentin
5.35 R^1 = OH; R^2 = Br isotopsentin
5.36 R^1 = H; R^2 = OH topsentin
5.37 R^1 = OH; R^2 =OH hydroxytopsentin
5.38 R^1 = H; R^2 = Br isobromodeoxytopsentin

Topsentin alkaloids contain a 2-acylimidazole moiety inserted between two indole rings, mostly brominated or hydroxylated at the C-6' and C-6'' positions. This class of bisindole alkaloids was first

isolated from sponges in 1987 and the geographic location and taxonomy of sponges producing topsentin like compounds is summarized in Table 5.2.

Since Yang and co-workers'[400] comprehensive review seven known and one new (**5.20**) topsentin-like alkaloid have been isolated from marine sponges. In 2005, Bao *et al.*[401] isolated the bisindole alkaloids **5.6**, **5.8**, **5.20**, **5.33**, **5.35-5.38** from a sponge *Spongosorites sp.* collected off the coast of Jeju Island, Korea. Again off the coast of Jeju island, compounds **5.8**, **5.33** and **5.38** were isolated this time from the sponge *Discodermia calyx*.[402] More recently in 2010, our laboratory isolated compounds **5.6** and **5.8** from the South African sponge *Topsentia pachastrelloides*.[393] Bao *et al.*[403] later isolated a series of tryptophan modified monoindoles (**5.39-5.45**) from the sponge *Spongosorites sp.* These compounds are believed to be putative precursors in the biogenesis of the topsentin and hamacanthins classes of marine alkaloids where the imidazole ring is formed through the nucleophillic attack by the amino group of one monoindole precursor (either **5.42** or **5.43**) on the adjacent carbonyl group of another monoindole (**5.42** or **5.43**)(Scheme 5.2). The mechanism for the removal of the ketone functionality of the imidazolone ring (**5.46**) is unknown and is assumed to be facilitated by an, as yet, unidentified enzyme, resulting in the topsentin scaffold.

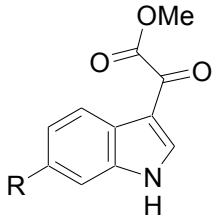

5.39 R = Br
5.40 R = H
5.41 R = OH

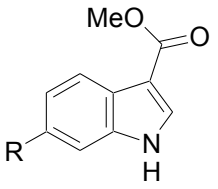

5.44 R = H
5.45 R = OH

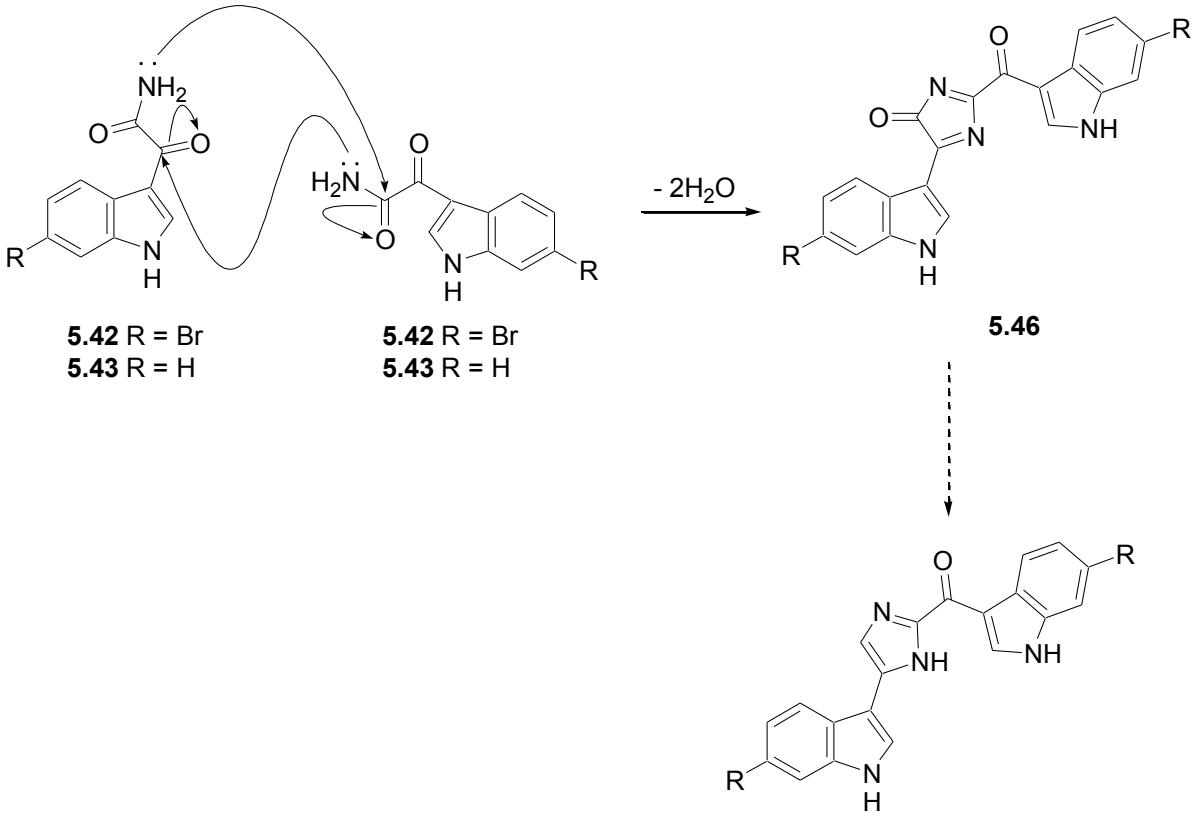

5.42 R = Br
5.43 R = H

5.42 R = Br
5.43 R = H

Scheme 5.2: The proposed biogenesis of the topsentin scaffold reproduced from Boa *et al*.[403]

Table 5.2: Geographical location and taxonomy of sponges producing the topsentin class of alkaloids 1987-2011

Year	Organism	Location	Compounds
1987[404]	*Topsentia genitrix*	Banyuls, France	**5.6**; **5.33**; **5.36**
1988[405]	*Spongosorites*	Chub Cay and Goulding's Cay, Bahamas	**5.6**; **5.8**, **5.35-5.37**
1989[406]	*Hexadella sp.*	Jervis Inlet, British Columbia	**5.33**
1991[407]	*Spongosorites ruetzleri*	Bahamas	**5.6**; **5.36**
1995[408]	*Spongosorites sp.*	Southern Australia	**5.6**; **5.8**; **5.33**; **5.36**
1999[409]	*Spongosorites genitrix*	Jaeju* Island, Korea	**5.6**; **5.8**; **5.3**; **5.38**
2000[410]	*Rhaphisia lacazei*	Ustica, Italy	**5.6**; **5.8**; **5.33**; **5.36**
2005[401]	*Spongosorites sp.*	Jeju Island, Korea	**5.6**; **5.8**; **5.20**; **5.33**; **5.35-5.38**
2007[402]	*Discodermia calyx*	Jeju Island, Korea	**5.8**; **5.33**; **5.38**
2010[393]	*Topsentia pachastrelloides*	Umkomaas, South Africa	**5.6; 5.8**

*Note: The spelling of the name Jeju Island is not consistent in the literature.

5.3.2. Past syntheses of topsentins

In 1987, Braekman and co-workers[411] published the first total synthesis of deoxytopsentin (**5.33**). Their synthetic procedure (Scheme 5.3) involved the conversion of indole acyl bromide (**5.47**), to the quaternary dimethyl hydrazine ion (**5.48**). The hydrazine ion product was refluxed in alcohol to afford the indoylglyoxaldimine (**5.49**) and dimethylamine. Dehydrative condensation of the intermediate **5.49** afforded the natural product **5.33**. While this approach appears relatively simple, the multiple steps are low yielding (8.2%).

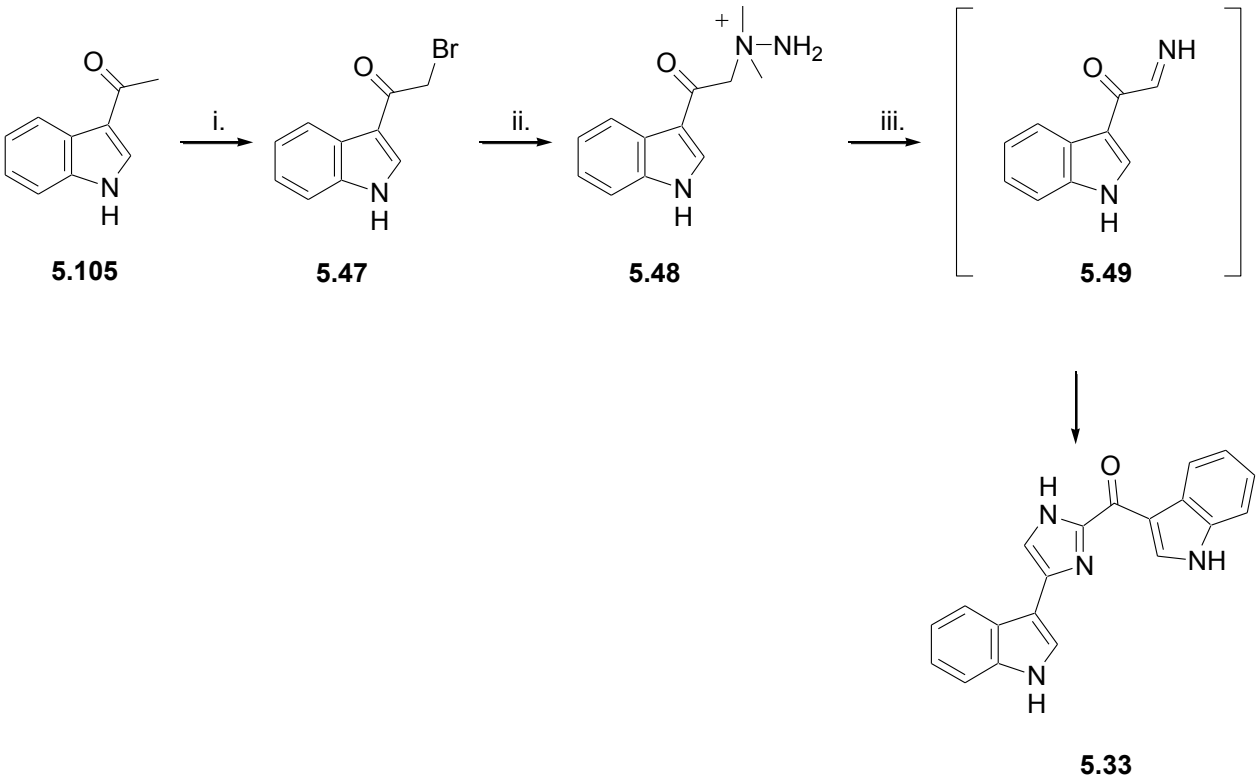

5.105 **5.47** **5.48** **5.49**

5.33

Scheme 5.3: Braekman and co-workers' synthesis of deoxytopsentin (**5.33**). [411] *Reagents and conditions:* i) $CuBr_2$, $CHCl_3$/EtOAc, 37%; ii) 1,1-dimethylhydrazine, EtOH, -15 °C, 82%; iii) *n*-propanol, reflux, 27%

Horne and co-workers[412] (Scheme 5.4) synthesized deoxytopsentin (**5.33**), firstly through the conversion of the 3-indole-α-oxoacetyl chloride (**5.50**) to indole acylcyanide (**5.51**). Subsequent hydrogenation of the acyl cyanide in the presence of a Pd/C catalyst afforded oxotryptamine (**5.52**). Oxidative dimerization of **5.52** in NH_4OH afforded the marine natural product **5.33**, in a total yield of 36.2%.

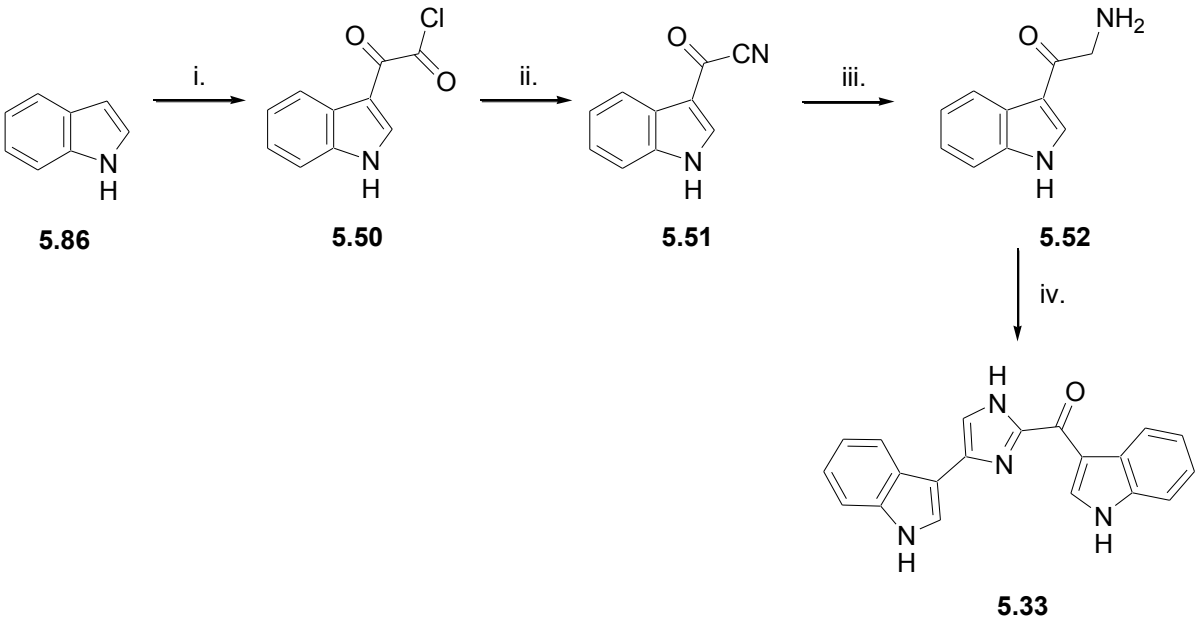

Scheme 5.4: Horne and co-workers' synthesis of deoxytopsentin (**5.33**).[412] *Reagents and conditions:* i) $(COCl)_2$, ether; ii) CuCN; iii) H_2, Pd/C, AcOH, 90%; iv) NH_4OH, 100 °C, 80%

Arcab and co-workers[413] applied a completely different approach to the synthesis of **5.6**, **5.33**, **5.36** and **5.38** (Scheme 5.5), in which they coupled sulphonamide protected indole-3-carboxaldehydes (**5.53-5.55**) with either a 2-(trimethylsilyl)ethoxymethyl (SEM) or a benzyloxymethyl (BOM) protected 2-lithioimidazole (**5.56** and **5.57** respectively), to yield the corresponding alcohols (**5.58-5.61**). Alcohols **5.58-5.61** were subsequently oxidized with MnO_2 to yield keto iodides (**5.62-5.65**). Compounds **5.64-5.67** were coupled with variably substituted indole-stannanes (**5.66** and **5.67**) to afford the variably protected bisindoles products (**5.86-5.71**). Final cleavage of the N-S sulphonamide bond was achieved by saponification under standard conditions. The hydroxyl protecting groups; methoxymethyl ether (OMOM) and SEM or benzyl (OBn) and BOM were simultaneously removed either by acidification or hydrogenolysis respectively to afford the natural products **5.6**, **5.38**, **5.36** and **5.33**. Yields for this synthesis range from 27-60%. Despite the difficulty of working with lithium and tin compounds in synthesis this synthetic approach is target orientated and minimizes the production of side products. Arcab and co-workers subsequently also synthesized isotopsentin (**5.35**) using this synthetic method.[414]

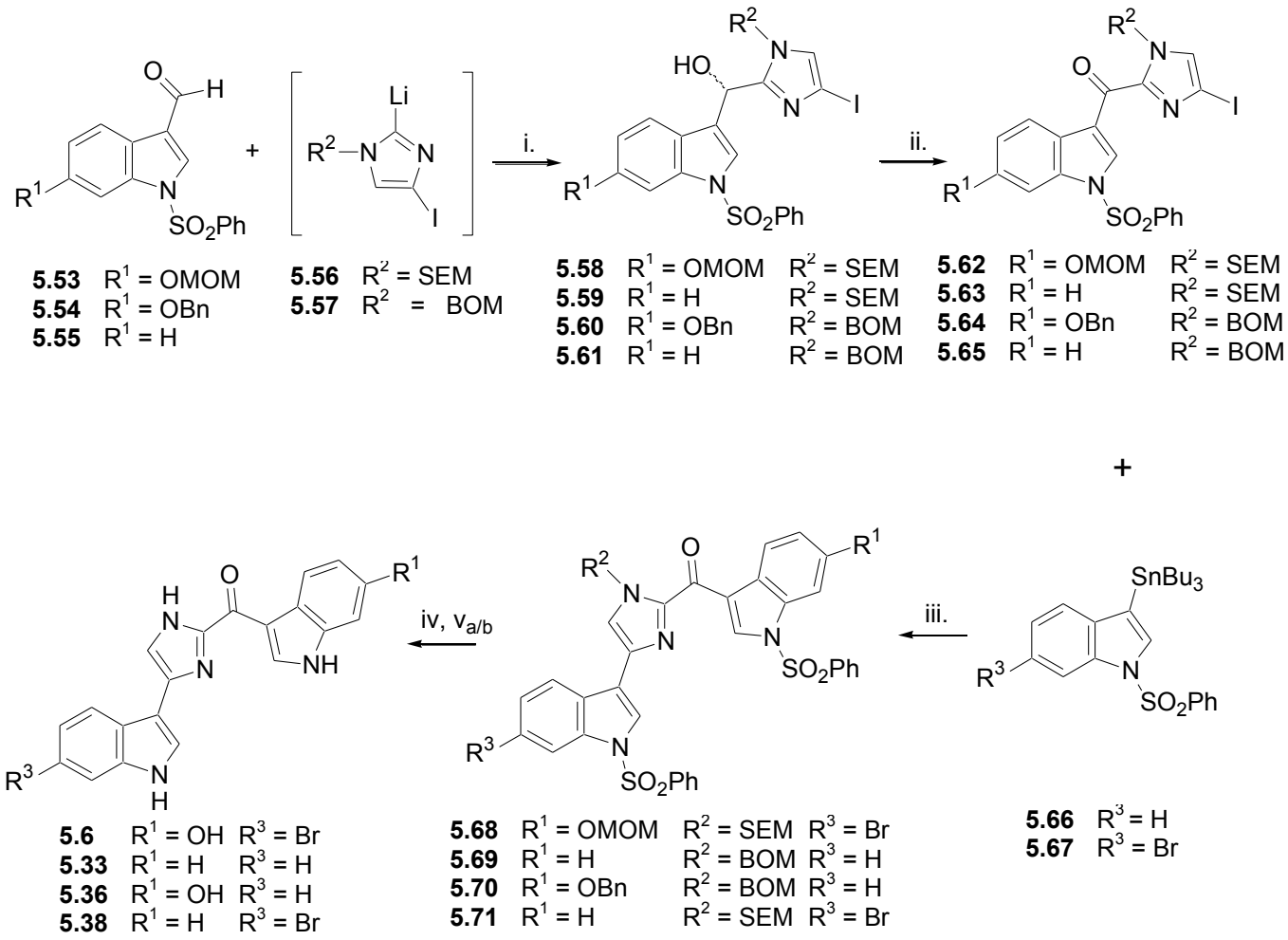

Scheme 5.5: Arcab and co-workers' synthesis of **5.6**, **5.33**, **5.36** and **5.38**.[413] *Reagents and conditions:* i) THF, -78 °C, 63-84%; ii) MnO_2, CH_2Cl_2, RT, 5 hrs, 95%; iii) $PdCl_2(PPh)_2$, CuI, DMF, 120 °C, 2 hrs, 76-81%; iv) 10% KOH, EtOH-THF, reflux, 2 hrs, 86-97%; v_a) 5M HCl, EtOH, reflux, 3 hrs, 68% (R^2 = SEM) or v_b) EtOH, HCO_2NH_4, 10% Pd/C, reflux, 4 hrs, 88-96% (R^2 = BOM)

Kawasaki *et al.*[415] synthesized topsentin (**5.36**) through coupling *tert*-butyldimethylsilyl (TBS) protected indole-3-boronic acid (**5.72**) and a SEM protected 4,5-iodoimidazole **5.73** (Scheme 5.6). Protected O-methoxytopsentin (**5.74**) was subsequently synthesized through the reaction of the indole imidazole (**5.75**) and the tertiary amine (**5.76**). Subsequent deprotection of the N- and O-methoxy moieties with 20% HCl and boron tribromide respectively afforded in **5.36** in a 36.3% overall yield.

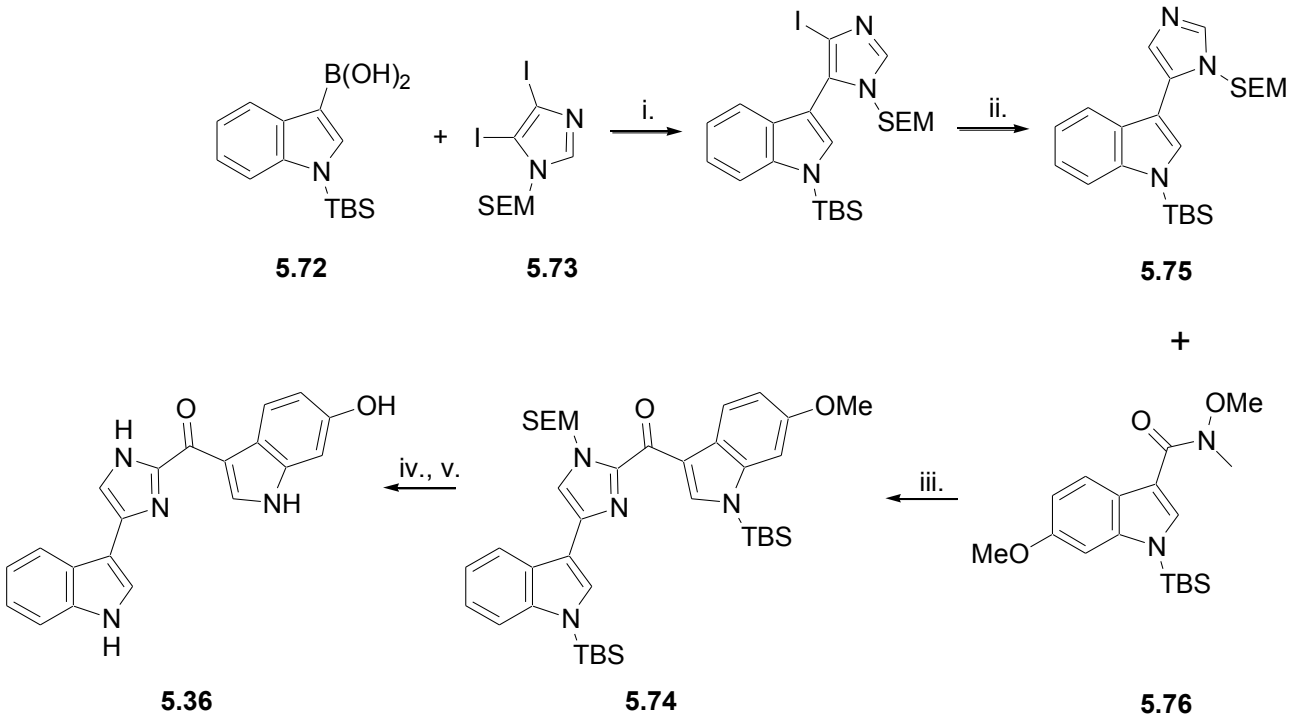

Scheme 5.6: Kawasaki *et al.*'s synthesis of topsentin (**5.5**).[416] *Reagents and conditions:* i) $Pd(Ph_3)_4$, $NaCO_3$, 75%; ii) EtMgBr, H_2O, 84%; iii) *n*-BuLi, 73%; iv) 20% HCl, 66%; v) BBr_3, 69%

In a more recent synthesis, Denis and co-workers[417] used α-ketothioimidate salts (**5.77** and **5.78**) and the indolic 1,2-diammonium salt (**5.79**) in the synthesis of brominated sponge alkaloids (Scheme 5.7). The β-amino indolic N-hydroxylamine (**5.80**) was reduced to **5.79**, in three steps. The first step was the cleavage of the N-O bond with the aid of titanium trichloride in dilute acid, to afford the diprotected diamine (**5.81**). Selective removal of the benzyl group in **5.81**, with Pearlman's catalyst [$Pd(OH)_2$] afforded the monoprotected diamine (**5.82**). Denis and co-workers also reported that **5.80** may be directly converted to **5.79** via catalytic hydrogenation with $Pd(OH)_2$ in a solution of MeOH-AcOH (96:4) by simply extending the reaction time. The final step involved acidic removal the carbamate protecting group to yield the 1,2 diamine salt **5.79**.

A series of S-methylthioimidate salts were synthesized concurrently with **5.79** with the intention of coupling them with **5.79**. Two 3-indole-α-oxoacetyl chlorides (**5.50** and **5.11**) were prepared from the corresponding indole (**5.83**) and 6-bromoindole (**5.84**) respectively with oxalyl chloride in ether. Compounds **5.50** and **5.11** were treated with tributyl tin hydride, and elemental sulfur in a mixture of piperidine and pyridine to afford 3-indolyl-α-ketothioamides (**5.85** and **5.86**). Finally, **5.85** and **5.86** were converted to S-methylthioimidate salts **5.77** and **5.78** by refluxing in excess methyl iodide.[418]

The S-methylthioimidate salts (**5.77** and **5.78**) were coupled with the 1,2 diamine salt (**5.79**) in MeOH and triethylamine, to afford spongotine A (**5.5**) and spongotine C (**5.87**) respectively. The oxidation of the imidazoline ring in **5.5** and **5.90**, in the presence of 2-iodoxybenzoic acid (IBX), yielded bromodeoxytopsentin (**5.8**) and isobromotopsentin (**5.20**) respectively. While this synthesis is lengthy it is highly selective and provides a useful route to many of the topsentin and spongotine classes of compounds and their respective analogues. The overall yields of **5.8** and **5.20** were *ca.* 17%.

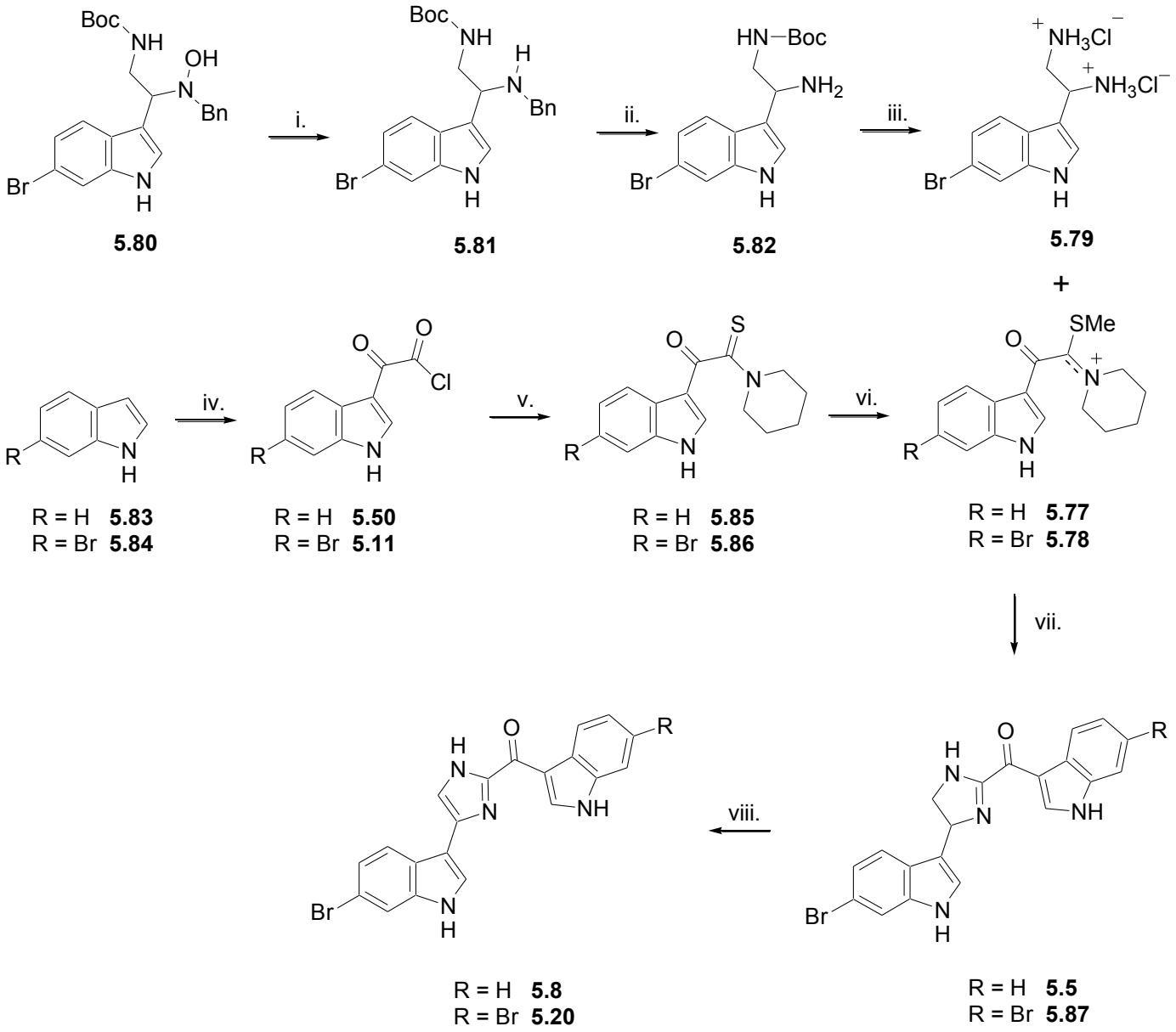

Scheme 5.7: Denis and co-workers' synthesis of the natural products **5.5**, **5.8**, **5.20** and **5.87**.[418] *Reagents and conditions:* i) $TiCl_3$, HCl *aq.*, MeOH-H_2O, RT, 15 min, 89%; ii) H_2, $Pd(OH)_2$, MeOH-AcOH, RT, 16 hrs, 93%; iii) HCl, MeOH, RT, 1 hr, 100%; iv) $(COCl)_2$, Et_2O, 0 °C, 4 hrs, 82-92%; v) *n*-Bu_3SnH, AcOEt, 0 °C, 30 min, RT, 16 hrs, S_8, piperidine, pyridine, 80 °C, 5 hrs, 31%; vi) MeI, refluxing, 5 hrs, 100%; vii) Et_3N, MeOH, RT, 48 hrs, 65-74%; viii) IBX, DMSO, RT, 15 hrs

5.4. A new approach to the synthesis of deoxytopsentin (5.33), isobromotopsentin (5.20) and 5-bromoindole imidazole (5.34)

As reviewed in the previous section, several members of the topsentin class of marine secondary metabolites have been successfully synthesized in relatively low yields five times in the past. Our proposed synthesis (Scheme 5.8) uses microwave assisted irradiation (MWI) for the high yielding preparation of the N-Boc protected indole glyoxal (**5.88**) from the N-Boc protected indole methyl ketone (**5.89**). Conversion of **5.88** into an imine intermediate in the presence of ammonium acetate would facilitate the formation of the imidazole ring (**5.90**). We also envisaged that thermal cleavage of the N-Boc carbamate bond under argon and in the absence of solvent with MWI would provide the target compounds in high yield.[419,420]

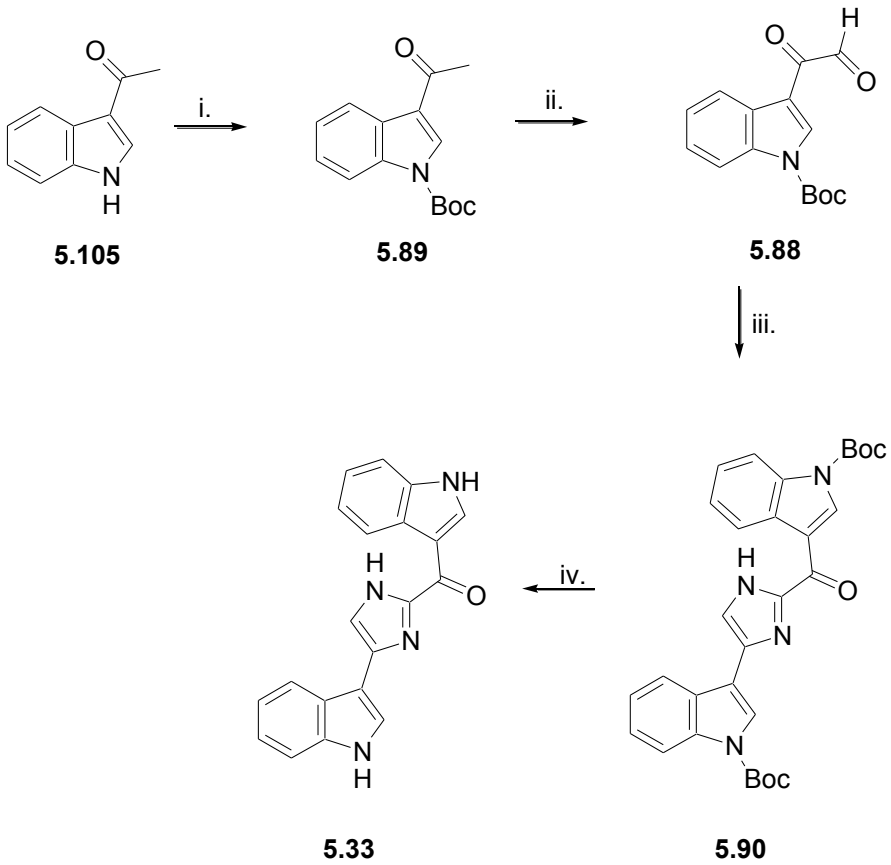

Scheme 5.8: Proposed route of synthesis of the marine metabolite **5.33**. *Reagents and conditions:* i) Boc_2O, MeCN, DMAP, 30 min; ii) SeO_2, H_2O, 1,4-dioxane, MWI; iii) NH_4OAc, EtOH, RT; 6 hrs; iv) MWI, 185 °C, Ar

5.4.1. Microwave assisted synthesis of aryl glyoxals

Glyoxals are well-established precursor for the synthesis of imidazole rings.[421-423] In 1932, Riley and co-workers,[424] first used selenium dioxide as an oxidising agent for the preparation of glyoxals from methyl ketones. This classical method for the preparation of phenyl glyoxal and substituted aryl glyoxals, via selenium dioxide oxidation under reflux (several hours to two days) in a variety of solvents *e.g.* acetone, ethanol, acetic acid or aqueous 1,4-dioxane has changed little in nearly 80 years and is still the method of choice to prepare these compounds. Successful closed-vessel microwave-accelerated selenium dioxide oxidations to afford 1,2-dicarbonyl compounds, e.g. 1,2-naphthoquinones,[425] 3-camphorquinone[426] and 6-formylpterin[427] have recently appeared in the chemistry literature.

Microwave assisted organic (MAO) synthesis has been in use since the mid-1980s,[428,429] and has become increasingly popular over the last two decades due to its ability to shorten reaction times and increase the range of possible reaction conditions.[430] Prior to MAO synthesis, the general heat transfer media for organic synthetic reactions have been oil/water/sand baths or heating mantles which are often slow and may lead to heating fluctuations which can result in the decomposition of organic compounds. With the microwave heating of organic reactions, radiation is directly and evenly applied to the reaction vessel causing rapid and uniform heating throughout the vessel and its contents,[430] thus minimizing decomposition and the formation of by-products. The use of MWI in the preparation of aryl glyoxals has appeared twice in the chemical literature, once non-reproducibly using a commercial household microwave oven,[431] and secondly in an inaccessible Russian journal.[432]

5.4.1.1. Optimization of the microwave assisted synthesis of phenyl glyoxal (5.27)

The chosen method to monitor the percentage conversion of acetophenone (**5.91**) to **5.27** was gas chromatography (GC). Since both **5.91** and phenyl glyoxal monohydrate (**5.92**) are commercially available it was decided to standardize the GC separation conditions using these two compounds. A number of GC stationary phases were tried, finally a J & W Scientific DB 225 capillary column (ID 250 µm, length 30 m), produced the most acceptable separation. The toxicity of selenium compounds is well documented.[433,434] In order to minimize exposure to SeO_2, the minimum quantities necessary to oxidize **5.92** to **5.27** were determined (Table 5.3). Quantative oxidation of **5.91** was achieved with 2.7 equivalents of SeO_2 and this equivalency of selenium dioxide was used

for all subsequent microwave assisted oxidations. Interestingly, 2.7 equivalents of SeO_2 is often used in the standard reflux preparation of aryl glyoxals.[435]

Table 5.3: Optimization of the number of selenium dioxide equivalents for the conversion of **5.91** into **5.27**[a]

SeO_2 (equiv)	% Conversion into 5.27[b]
1.0	75
1.5	87
2.0	92
2.5	99
2.7	100

[a] The reactions were conducted under the same microwave conditions, i.e. with a hold time of 15 min at a set temperature of 100 °C. Hold time is the time the microwave remains at the set temperature. In all cases the set temperature was reached within 1 min and the reaction was forced-air cooled to 50 °C over a period of 5 min and then allowed to cool to room temperature (*ca*. 20 min).
[b] The % conversion was calculated from quantitative GC analysis.

Having established the optimal equivalency of selenium dioxide for the microwave assisted synthesis of **5.27** at 100 °C we turned our attention to establishing the minimum temperature which could be used for this reaction in aqueous 1,4-dioxane (the most common solvent used for selenium dioxide oxidations of methyl ketones). While, MWI allows solvents to be heated approximately 15 °C above their boiling points,[430] Table 5.4 reveals that a temperature of 100 °C (1,4-dioxane b.p. 101 °C)[436] proved most suitable for quantative oxidation of **5.91** to **5.27**.

Table 5.4: Optimization of the reaction temperature for the conversion of **5.91** to **5.27**[a]

Temperature [°C]	% Conversion into 5.27[b]
70	30
80	49
90	88
100	100

[a] The reactions were conducted under the same microwave conditions, with a hold time of 15 min and 2.7 equivalents of SeO_2.
[b] The % conversion was calculated from quantitative GC analysis.

These optimized microwave reaction conditions were subsequently applied to the selenium dioxide oxidation of **5.91** and three *para*-substituted aryl methyl ketones **5.93-5.95**. The progress of each

reaction was monitored at hold times of 3, 6, 9, 12, 15, 18 and 21 minutes by GC-analysis (Figure 5.5). Each reaction was performed in triplicate to confirm the reproducibility of the microwave method. Interestingly, the quantitative oxidation of an activated aryl methyl ketone, e.g. **5.93** was achieved in <3 minutes, while quantitative oxidation of a deactivated aryl methyl ketone, e.g. **5.94** took six times longer under the same microwave conditions. This suggests that the activating or deactivating characteristics of the *para* substituent makes the acetyl group more or less susceptible to oxidation respectively.

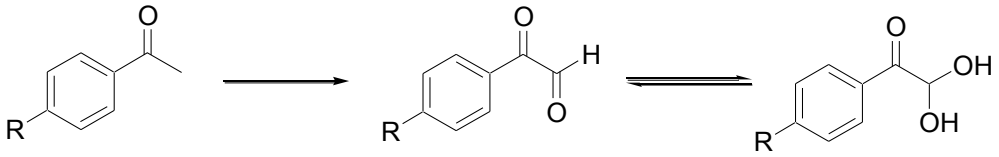

5.91 R =H
5.93 R =OMe
5.94 R =NO_2
5.95 R =Cl
5.96 R =Br
5.97 R =F

5.27 R =H
5.28 R =OMe
5.29 R =NO_2
5.30 R =Cl
5.31 R =Br
5.32 R =F

5.92 R = H
5.98 R = OMe
5.99 R = NO_2
5.100 R = Cl
5.101 R = Br
5.102 R = F

Scheme 5.9: The MAO synthesis of aryl glyoxals from methyl ketones. *Reagents and conditions:* SeO_2, H_2O, 1,4-dioxane, MWI, 25 min, 100 ˚C, 100%

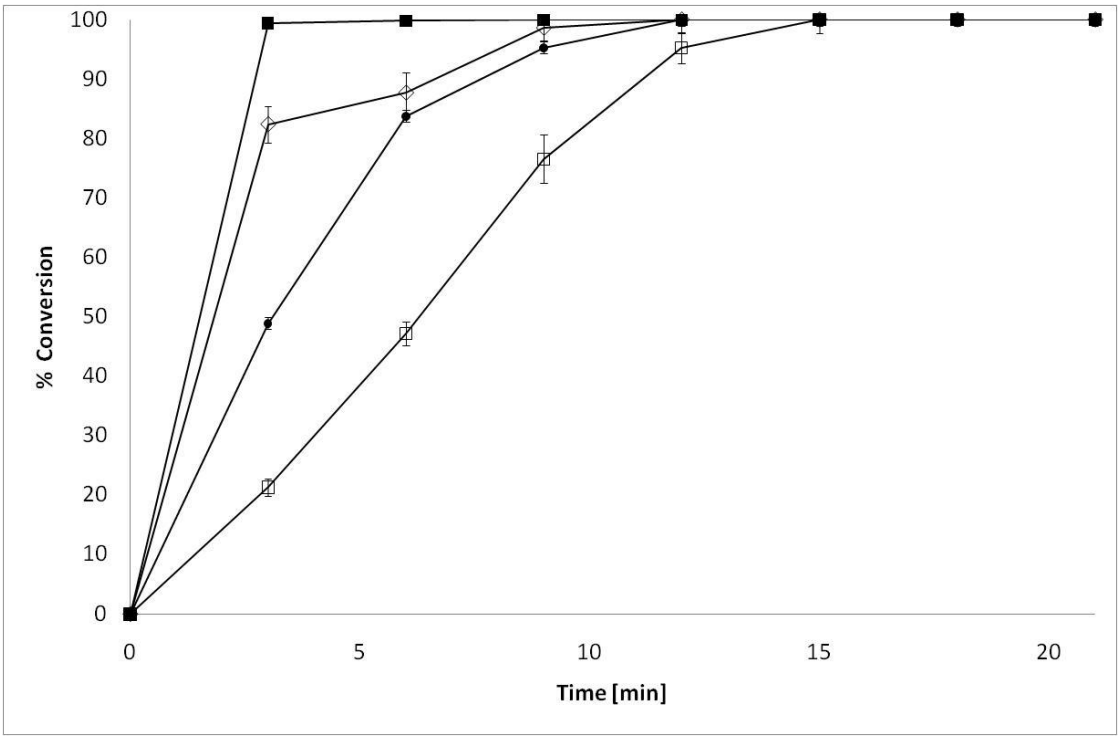

Figure 5.5: Conversion of compounds **5.91** (empty diamonds ◊); **5.93** (filled squares ■); **5.94** (empty squares □) and **5.95** (filled circles ●) to the corresponding aryl glyoxals **5.27**, **5.28**, **5.29** and **5.30** respectively.

5.4.1.2. Standardization of the GC method for quantification of glyoxal formation

The chromatographs below show the retention times of the starting material **5.91** and **5.27** (17.2 and 18.2 min respectively, Figure 5.6). As expected the ratio of **5.91 : 5.27** changes with an increase in reaction time *i.e.* the peak corresponding to **5.91** decreasing while the peak corresponding to **5.27** increases.

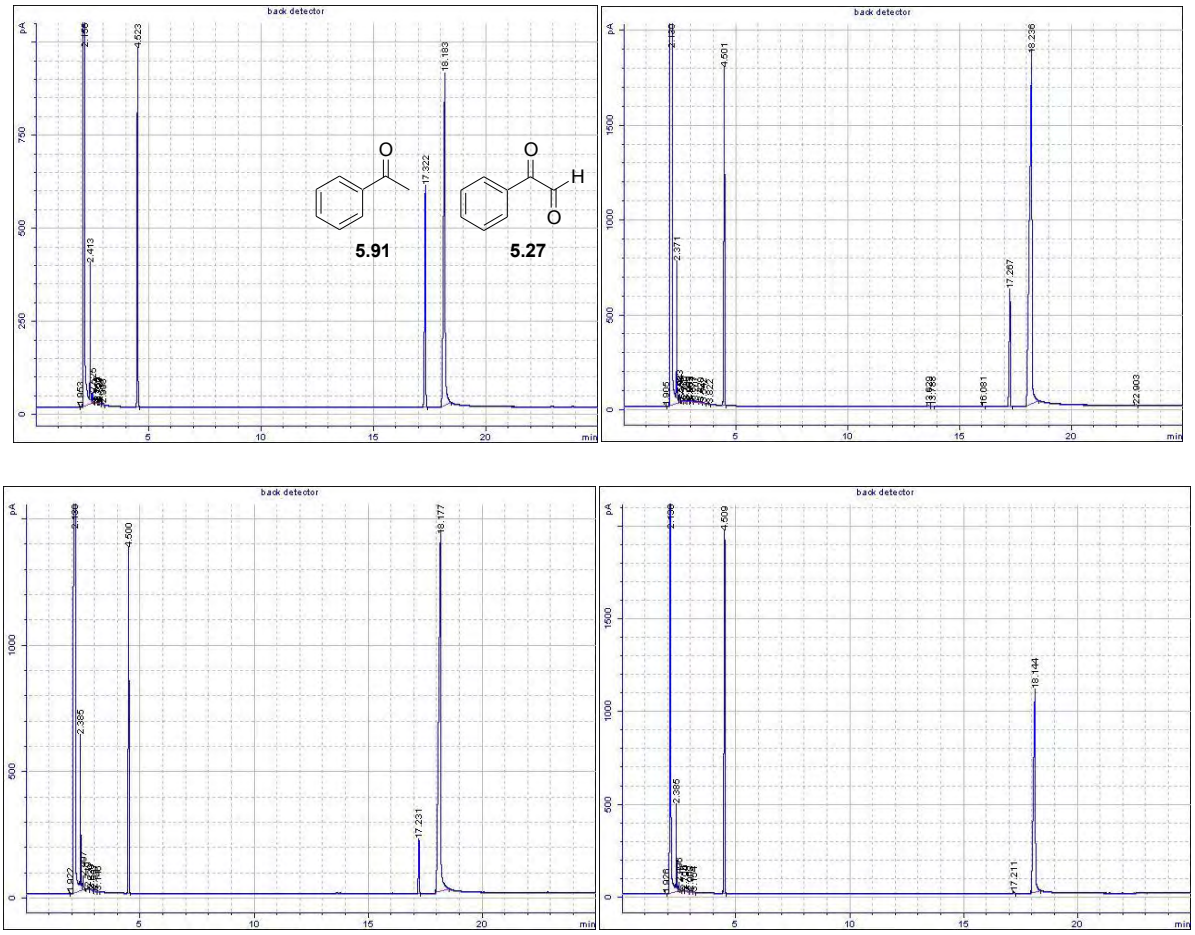

Figure 5.6: GC chromatograph of MW reaction involving acetophenone (**5.91**) at 3 min (*top left*), 6 min (*top right*), 9 min (*bottom left*) and 18 min (*bottom right*). The peak at 17.2 minutes corresponds to acetophenone while the peak at 18.2 minutes corresponds to phenyl glyoxal (**5.27**).

The detector used to produce the chromatographs shown in Figure 5.6 was a Flame Ionisation Detector (FID), which detects oxidised carbon ions.[437] The functionality of organic species, particularly carbonyls and alcohols, may result in a reduction of the FID generated peak intensity.[438] Since we were using this method to detect the formation of carbonyl containing compounds, the GC-analysis technique needed to be standardized and Equation 5.1 was derived in an attempt to standardize the GC data.

$$\text{Mole Fraction B} = \frac{\frac{b'}{f_b}}{1+\frac{b'}{f_b}} \qquad \textit{Equation 5.1}$$

Where $\mathbf{a} = \int$ acetophenone peak and $\mathbf{b} = \int$ phenyl glyoxal peak and $a' = \frac{a}{a} = 1$ and $b' = \frac{b}{a}$

When an equal concentration of acetophenone (**5.91**) and phenyl glyoxal monohydrate (**5.92**) is injected into the gas chromatograph, f_b may be calculated by $f_b = \frac{b}{a}$. Several GC chromatographs at various concentrations of **5.91** and **5.92** were recorded and the integrals of their respective peaks calculated, subsequently resulting in a calculated (Equation 5.1) average discrepancy of -7.5% in the intensity of the glyoxal peak, confirming what was reported in the literature.[438] Note the discrepancy is not consistent and increases at lower concentrations of glyoxal. The % conversion data reported in Figure 5.5 and elsewhere were corrected accordingly upwards to account for this error in the detector.

5.4.1.3. The glyoxal/glyoxal monohydrate equilibrium

Originally we attempted to isolate the glyoxal using Mikol *et al.*'s[439] vacuum distillation method. Glyoxal **5.27** distilled at 63-65 ^{o}C under 20 mmHg of pressure as a pure yellow oil. However, on contact with atmospheric moisture, white crystals of the glyoxal monohydrate **5.92** were immediately formed. The water sensitivity of glyoxals is clear from closer inspection of their structure. Additional polarization of the electrophillic aldehyde by the adjacent C-1' ketone functionality would result in a relatively more polarized C-2', susceptible to nucleophillic attack by water (Scheme 5.10). Monohydrates are more stable than their corresponding glyoxals and we therefore decided to convert all the glyoxals (**5.27**-**5.32**) to the more stable monohydrate form through refluxing in water (2 hrs) and recrystallizing the glyoxal monohydrates (**5.92** and **5.98**-**5.102**) from the aqueous solution.

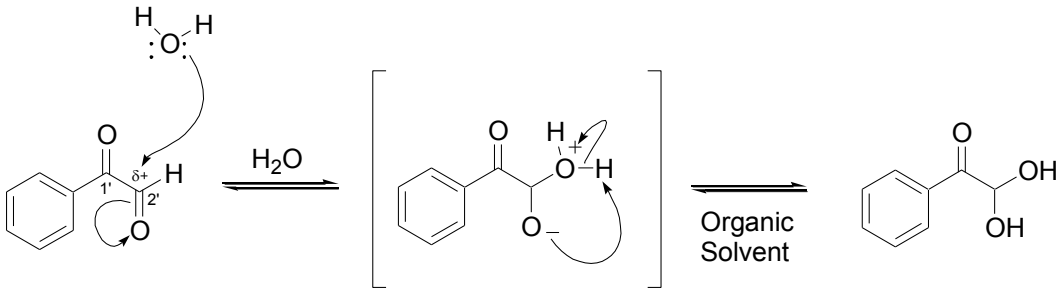

5.27 **5.92**

Scheme 5.10: Equilibrium of the nucleophillic attack of water in glyoxals

Interestingly, from our inspection of the chemistry literature most authors do not differentiate between the monohydrate or glyoxal forms, rather assuming that the monohydrate will partially revert back to the glyoxal in anhydrous non-polar conditions to form an equilibrium mixture (Scheme 5.10). For the synthesis of the imidazole the glyoxal is essential and so the equilibrium between **5.27** and **5.100** in solution was investigated using ^{1}H NMR spectroscopy. A comparative analysis in three different solvents ($CDCl_3$, DMSO-D_6 and CD_3OD) determined that the equilibrium occurred in $CDCl_3$ and DMSO-D_6. An unexpected hemiacetal formed in CD_3OD and this will be discussed later.

To the best of our knowledge, details of the kinetics of the interconversion of **5.92** and **5.27** in solution have not been reported before. The kinetics of the equilibrium between **5.92** and **5.27** in a $CDCl_3$ solution of **5.92** was explored in a ^{1}H NMR stack-plot which illustrated clearly the decay of the oxymethine proton resonance (δ_H 5.69) and the appearance and increase in intensity of the aldehyde proton signal (δ_H 9.71) with time (Figure 5.7).

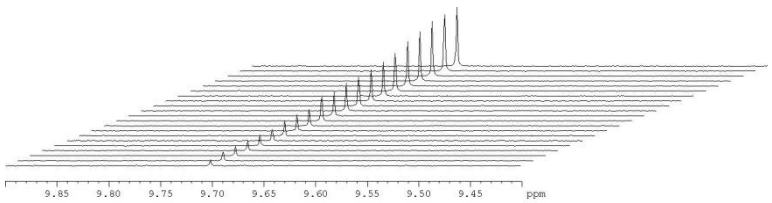

Figure 5.7: A stack plot of the downfield region (δ_H 9.40-9.90) of the ^{1}H NMR spectra ($CDCl_3$, 600 MHz) of **5.92** over time. Z-axis 10 s apart.

The conversion of **5.92** into **5.27** (Figure 5.7) in chloroform follows first-order kinetics with a rate constant of 2.0191 x 10^{-5} s^{-1} (± 0.0073 x 10^{-5} s^{-1}) and an R^2 value of 0.999 for a linear plot of ln[A] vs. time. Figure 5.8 further suggests that equilibrium concentrations of **5.92** and **5.27** are rapidly reached in the chloroform solution.

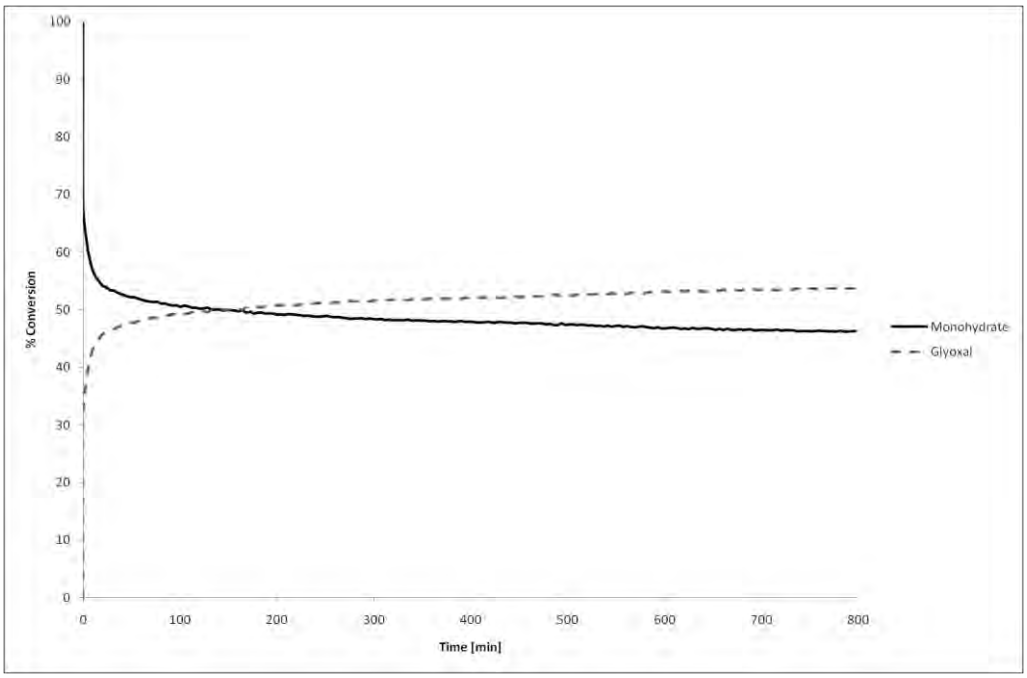

Figure 5.8: Kinetic data for the conversion of **5.92** (solid line) into **5.91** (broken line) in $CDCl_3$ at 22 ˚C.

Interestingly, the ^{1}H NMR spectra of phenylglyoxal in deuterated methanol, showed the absence of the aldehyde resonance. However, there was the appearance of a new proton signal at δ_H 5.69 ppm. This new signal, representing the oxymethine proton of a putative hemiacetal, suggests, that the hemiacetal (**5.103**) is formed in a methanol solution, by nucleophillic attack by methanol on the glyoxal aldehyde carbonyl. The presence of the hemiacetal was confirmed by HREI-TOF mass analysis (calculated for $C_9H_{10}O_3$ 166.0624. Found 166.0614, Δamu 0.001.)

Since there was no detection of an aldehyde signal, it was initially assumed there may have been deuterium exchange between the CD_3OD and the aldehyde proton. However, when calculating the kinetics of the formation of hemiacetal from the monohydrate, the sum of the concentration of these two species equal that of the total concentration (Figure 5.10). The sum of the concentrations of **5.92** and **5.104** was monitored with the addition of 1,3,5-trimethoxybenzene (10.7 mM) (TMB), as an internal NMR calibrant to calculate the relative concentrations and to ensure no deviations in the peak intensities. This showed that the aldehyde was not present or deuterated, but rather only exists as an intermediate, undetectable by NMR under the current conditions (Scheme 5.11).

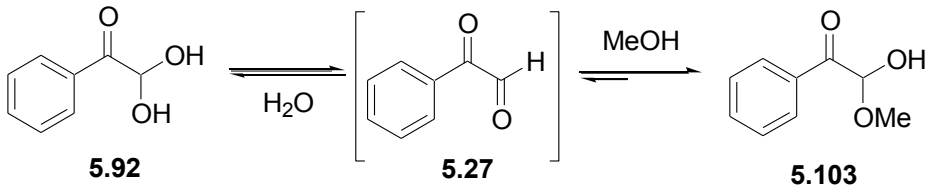

Scheme 5.11: The equilibrium in which the hemiacetal (**5.103**) forms via a glyoxal intermediate in a methanol solution.

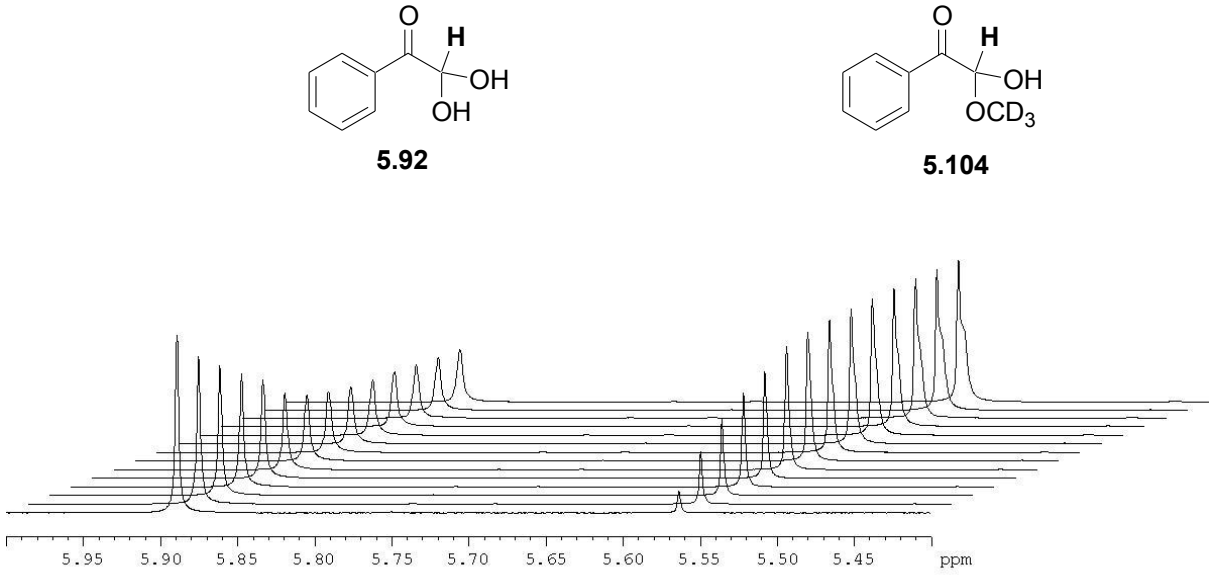

Figure 5.9: A stack plot of the region δ_H 5.40-6.00 of the ^{1}H NMR spectra (CD_3OD, 600 MHz) obtained for **5.92** over time. Z-axis 10 min apart.

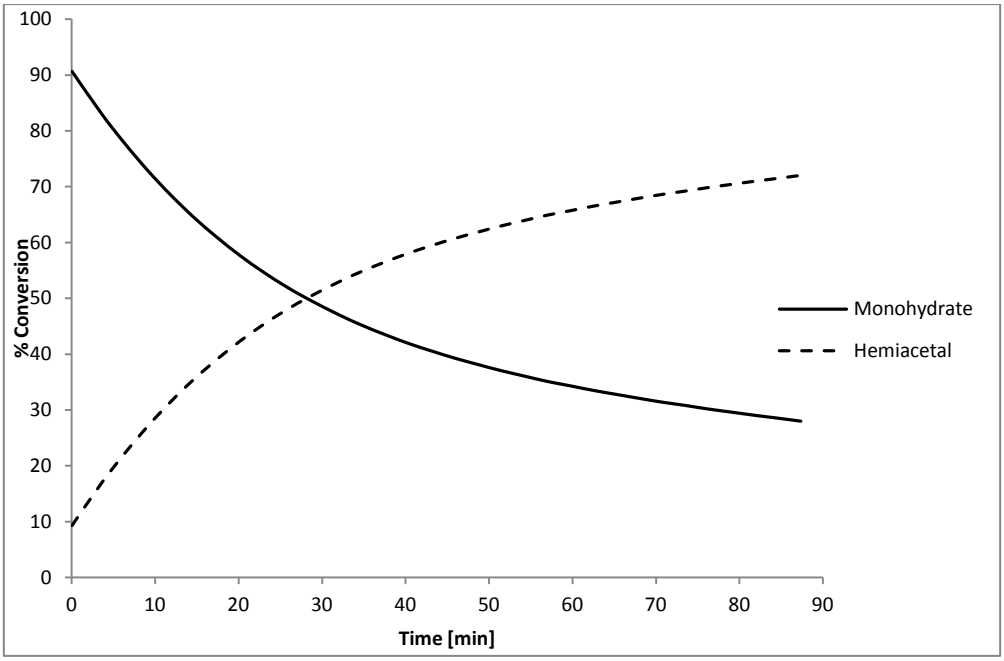

Figure 5.10: Kinetic data for the conversion of **5.92** (solid line) into **5.104** (dotted line) in CD_3OD at 22 ˚C.

Interestingly, the ^1H NMR signal of the oxymethine proton (H-2', δ_H 5.69) of **5.92** appears as a triplet with a COSY correlation to a broad singlet (O<u>H</u>, δ_H 4.16) in a $CDCl_3$ solution (Figure 5.11A). Opportunities for hydrogen bonding between the hydroxyl moieties of the germinal diol and the ketone functionality probably impede proton exchange in this compound. As expected, on the addition of D_2O to the $CDCl_3$ solution of **5.92**, the triplet collapses to a singlet and the broad singlet (δ_H 4.16) disappears (Figure 5.11B).

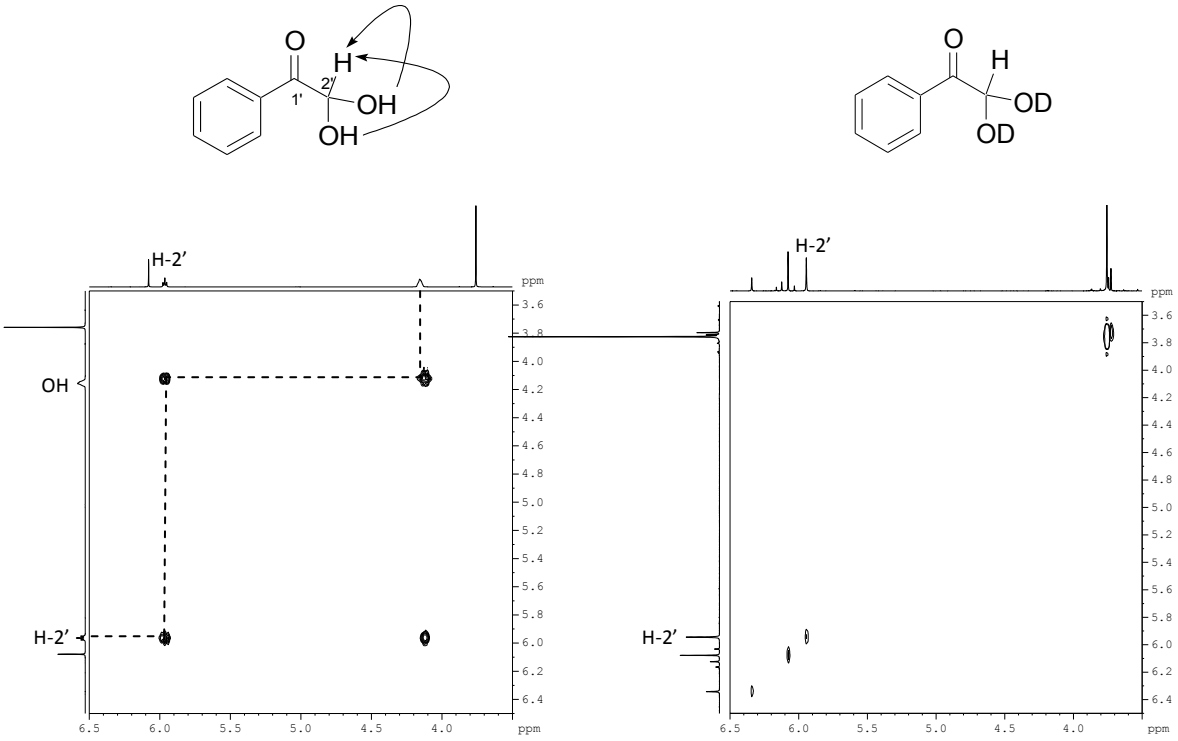

Figure 5.11: The COSY spectra (F1 and F2 = δ_H 3.55-6.50) of **5.92**. A: $CDCl_3$, 600 MHz (*Left*) B: $CDCl_3$ + D_2O (20 µL), 600MHz (*Right*). The key correlation resulting in the splitting patterns are shown in the accompanying figures.

A chloroform solution containing an equilibrium mixture of glyoxal and monohydrate yielded only a single peak when injected onto the DB-225 GC column. A similar result was obtained when the equilibrium mixture was injected onto a DB-1 column. Several repeated injections on both columns with different temperature gradients and carrier gas flow rates failed to separate the two expected peaks. We therefore proposed that the solution equilibrium between glyoxal and monohydrate could possibly be shifted completely in favour of the glyoxal by dehydration of the monohydrate during volatilization in the GC inlet (240 °C). Although the molecular ions for either **5.92** or **5.27** were absent from GC-HREIMS analysis of the single peak resulting from injection of **5.92** onto the GC column, thermogravimetric mass analysis (TGA) of crystalline **5.92** provided evidence for the facile loss of water. The mass spectrometer attached to the TGA was selectively focussed to record the change in intensity of the *m/z* = 18 ion peak with increasing temperature. Therefore, an increase in the intensity of this peak suggested the loss of a water molecule during thermal decomposition. Figure 5.12 indicates a 11.8% reduction in mass, while concurrently the *m/z* peak intensity increases at this temperature range (*ca.* 90 °C), equivalent to the loss of a small molecule with *m/z* 18.

At higher temperature a sudden loss in mass was observed corresponding to the volatilisation of the glyoxal. A total loss of mass after 135 °C, indicated that no residue was formed from thermal decomposition.

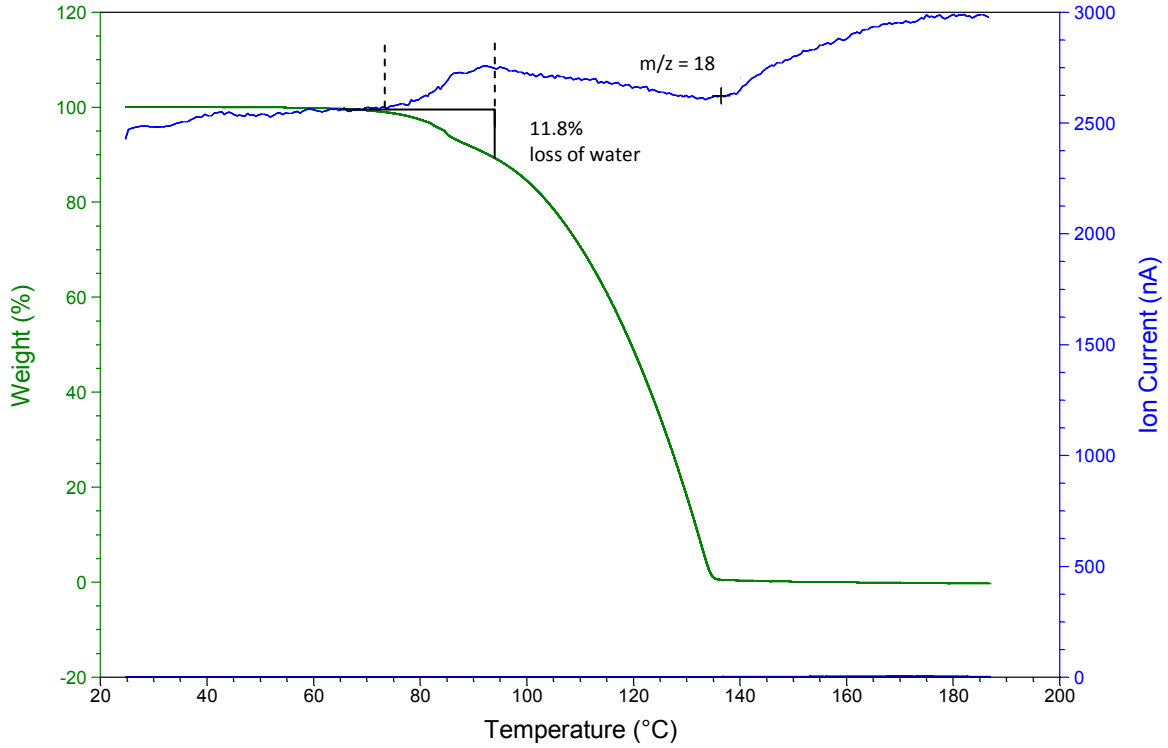

Figure 5.12: The TGA-MS spectra of **5.92**. Green line indicates the % mass loss with increase in temperature. The blue line represents the change in intensity of the *m/z* = 18 peak with an increase in temperature.

The difficulties associated with attempting to isolate the glyoxal **5.27** from the equilibrium mixture with the **5.92** required us to perturb the equilibrium in favour of the monohydrate by refluxing the glyoxal equilibrium mixtures from the selenium dioxide oxidation of **5.91** and **5.93-5.97** in water and crystallizing out the monohydrates (**5.92** and **5.98-5.102**) directly from the aqueous solution. The IR, ^{1}H, ^{13}C NMR data and melting points of **5.92** and **5.98-5.102** were consistent with published values.[421,440]

Closed-vessel microwave irradiation greatly accelerates the selenium dioxide mediated oxidation of aryl methyl ketones (**5.91** and **5.93-5.97**) to the corresponding aryl glyoxal monohydrates (**5.92** and **5.98-5.102**) in yields comparable with those obtained by traditional reflux methods (Table 5.5) of the reaction mixtures for extended periods on a heated oil bath.

Table 5.5: Comparative table of two heating methods for the formation of aryl glyoxal monohydrates **5.92** and **5.98-5.102**.

Compound	Isolated Yield Classical Heating[a] [%]	Isolated Yield MWI[b] [%]
5.92	82	84
5.98	82	84
5.99	62	62
5.100	82	81
5.101	86	89
5.102	86	87

[a] Refluxed for 12hrs.
[b] MWI for 3-20 minutes.

5.4.2. Indole glyoxal synthesis

Our approach to the synthesis of the natural product **5.33** required the initial preparation of a suitable glyoxal precursor. Our obvious starting material for a microwave assisted selenium dioxide was 3-acetylindole (**5.105**, Scheme 5.8). However, on inspection of the ^{1}H and ^{13}C NMR spectra of the oxidised product, there was no evidence of the aldehyde resonance although the methyl signal (δ_H 2.55) had completely disappeared in the ^{1}H NMR spectrum while a new quaternary carbon had appeared in the ^{13}C NMR spectrum (δ_C 166.0). The HMBC correlations from H-2 (δ_H 8.52) to C-3, C-3a, C-4, C-7a and C-1' (Figure 5.13) confirmed that the indole ring and the ketone functionality were still intact while the chemical shift of the quaternary carbon (δ_C 166.0) was suggestive of a carboxylic acid carbonyl moiety. The HREIMS fragmentation pattern (Figure 5.14) was consistent with the EIMS data reported by Bergmann *et al.,*[441] for indole-3-glyoxylic acid (**5.106**) (HREI-TOF: calculated for $C_{10}H_7O_3N$ 189.04259. Found 189.04205, Δamu 0.0005.) Faced with an over oxidation of 3-acetylindole to **5.106** we reflected on our previous preparation of **5.27-5.32** which had shown that the activity of the aromatic ring has a significant effect on the rate of microwave assisted selenium dioxide oxidation reactions. We therefore decided to reduce the influence of the indole nitrogen atom on the activity of the indole ring through conversion of **5.105** to an N-Boc carbamate ester (**5.89**, Scheme 5.12).

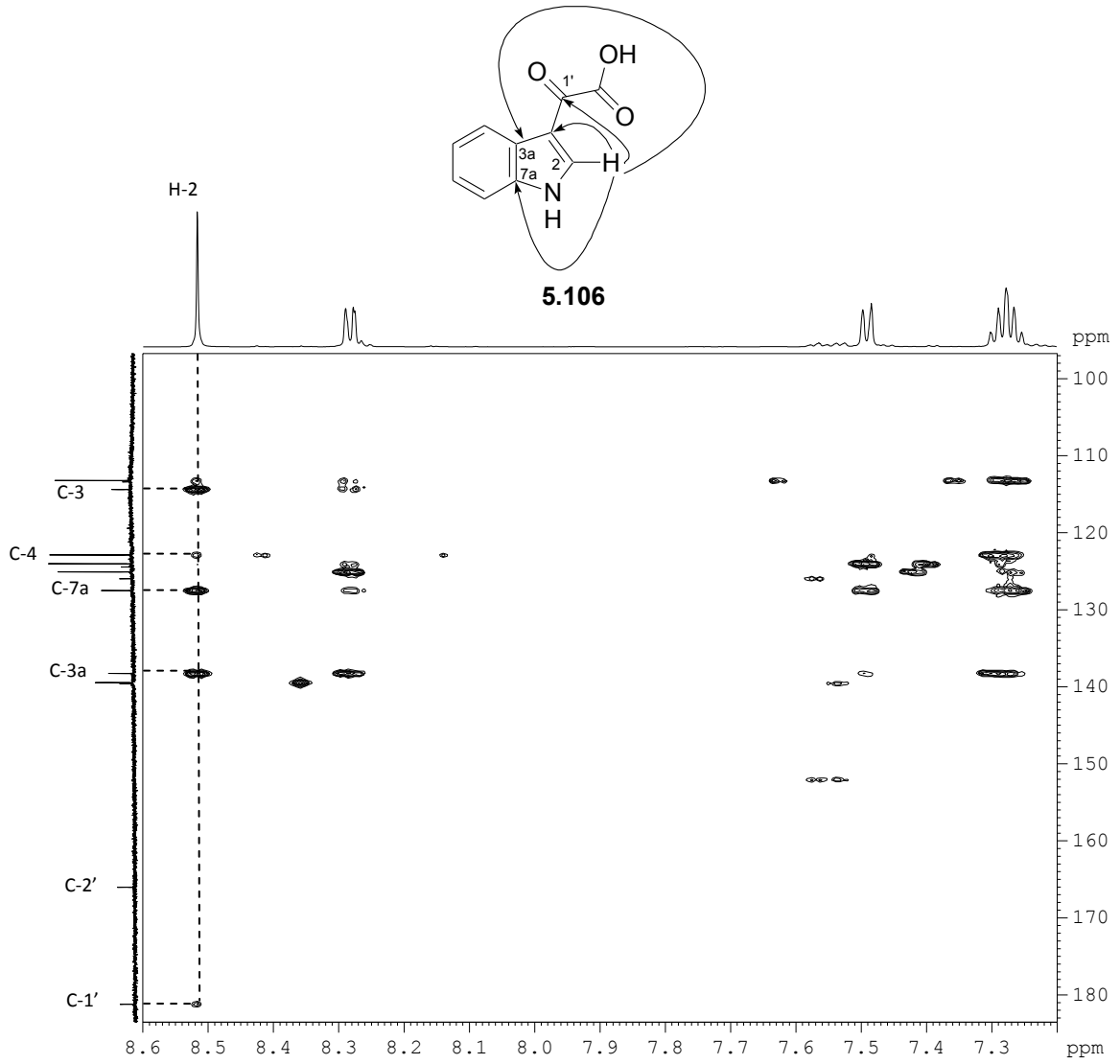

Figure 5.13: A region of the HMBC spectrum (CD_3OD, 600 MHz, delay for evolution of long range coupling [d6] = 60 msec; F1 = δ_C = 97 – 183; F2 = δ_H 7.20 – 8.60) obtained for **5.106**. Multiple bond correlations from H-2 illustrated in accompanying figure.

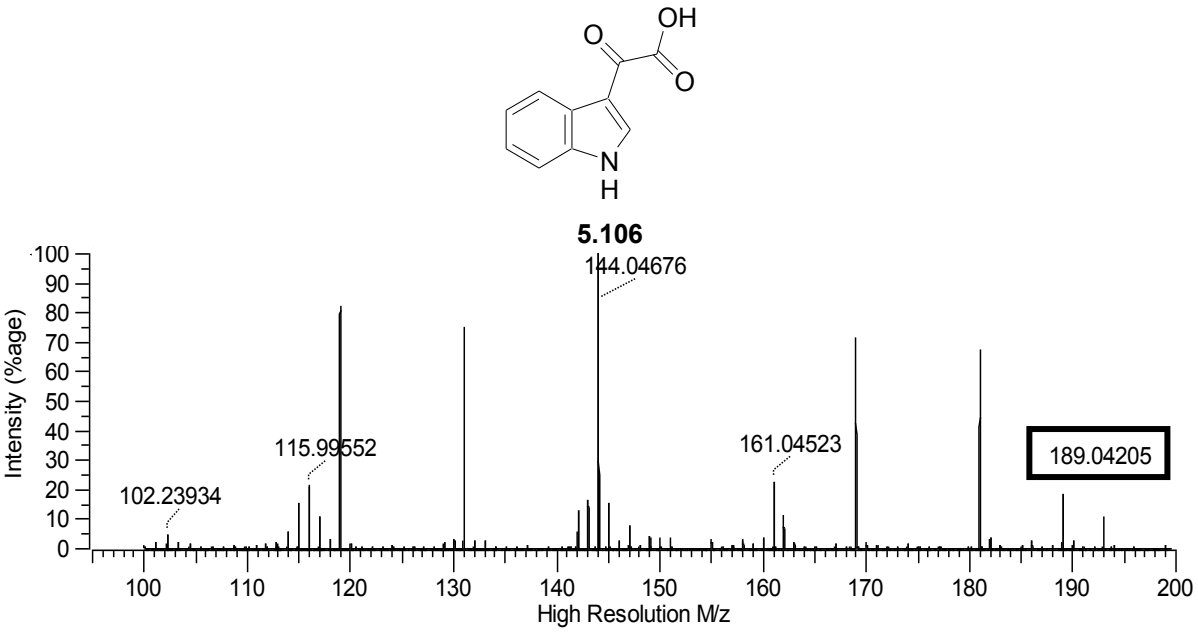

Figure 5.14: The EI fragmentation pattern of **5.106**. The *m/z* range = 95-200.

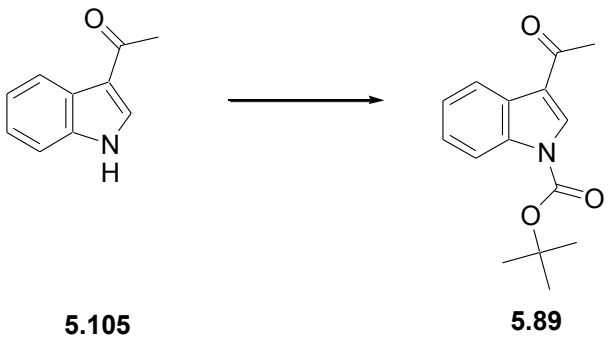

Scheme 5.12: The N-Boc protection of **5.105**. *Reagents and conditions*: Boc_2O, DMAP, MeCN, 0 ^oC, 2hrs, 100%

Initial evidence for the successful preparation of **5.89** was provided from the ^1H NMR spectrum of this compound in which a nine proton singlet (δ_H 1.67, *t*-butyl) was clearly evident. The compound was isolated from the reaction mixture as white needles (mp 140-142 ^oC lit.[442] 143-144 ^oC) in quantitative yield.

Microwave assisted selenium dioxide oxidation of **5.89** proceeded smoothly to give an equilibrium mixture of the indole glyoxal (**5.88**) and the monohydrate (**5.107**) (Scheme 5.13). The ^1H NMR spectrum of the oxidation reaction mixture of **5.89** showed two new singlets (δ_H 9.53 and 5.79) corresponding to the aldehyde proton of the glyoxal and the oxymethine proton of the monohydrate respectively. C_{18} reversed phase HPLC analysis of the crude mixture gave three peaks. One peak (t_R = 5.8 min) corresponded to unreacted **5.89**, while the remaining two peaks (t_R = 2.6 min with a

shoulder at t_R = 3.2 min) were inseparable and their relative intensities changed with each injection onto the column, thus suggesting an equilibrium mixture of **5.88** and **5.107**. Refluxing the mixture in water and subsequent cooling did not result in the crystallization of **5.107** as we observed previously. The solubility of **5.88** in dichloromethane enabled the initial separation of the organic products from the excess water soluble SeO_2 through liquid-liquid partitioning. Removal of the DCM under reduced pressure followed by semi preparative reversed phase HPLC (C_{18}, 3:2 MeCN:H_2O) gave an inseparable mixture of **5.88** and **5.107**. The HSQC and HMBC spectrum of the mixture of **5.88** and **5.107** showed sufficient signal dispersion to individually assign the NMR chemical shift data of both compounds.

5.4.3. The formation of the imidazole ring from aryl glyoxal precursors

Khalili *et al.*[399] described the formation of imidazoles via dehydrative self-condensation of two aryl glyoxals in the presence of ammonium acetate (Scheme 5.13), in which the aldehyde functionality of **5.27** is converted into a primary aldimine (**5.108**). Nucleophillic attack of **5.108** at the ketone carbonyl of another imine followed by intramolecular cyclization of the resulting adduct (**5.109**) affords the keto imidazole **5.110**.

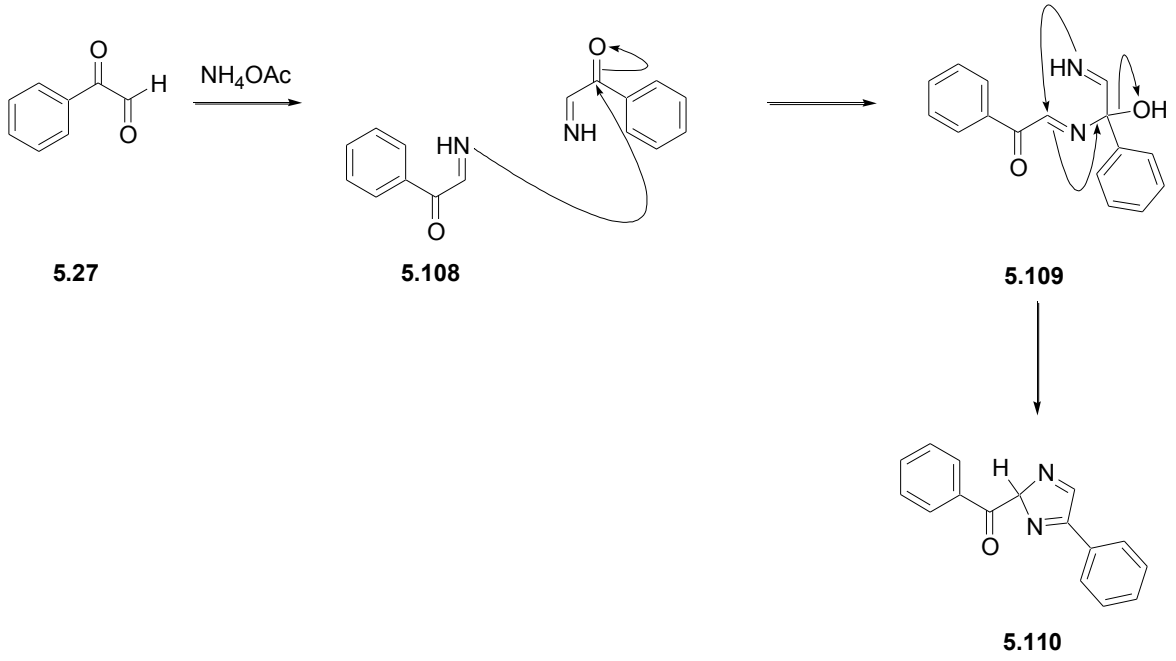

5.27 **5.108** **5.109** **5.110**

Scheme 5.13: The proposed mechanism for the formation of an imidazole ring via the *in situ* dehydrative self-condensation of phenyl glyoxal (**5.27**) in the presence of NH_4OAc. Adapted from Khalili *et al.*[399]

Khalili *et al.*[399] have proposed that the methine ring proton in **5.110** may rearrange to form two possible tautomers (**5.21a** and **5.21b** Scheme 5.14). Khalili *et al.*[399] have shown that the yields of each of these two tautomers is solvent-dependent with ethanol affording the highest overall yield of imidazoles with the greatest tautomeric regioselectivity for compounds **5.22**, **5.24** and **5.26** (Table 5.6).

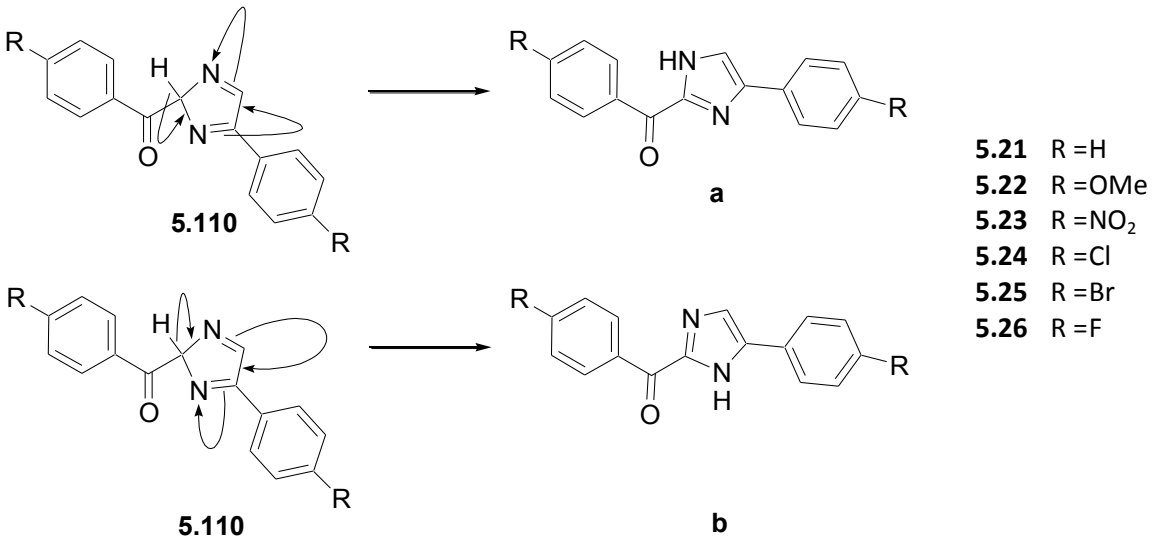

Scheme 5.14: The 1,5 –proton shift resulting in the formation of the two imidazole tautomers **a** and **b**. Adapted from Khalili and co-workers.[399]

Table 5.6: The isolated yields and tautomeric ratios (**a**/**b**) of compounds **5.22**, **5.24** and **5.26** synthesised in a variety solvents. Reproduced from Khalili.[399]

Solvent	Yield (%) for 5.22, 5.24 and 5.26	a/b ratio for 5.22, 5.24 and 5.26
H_2O	71, 69, 59,	4.80, 3.70, 5.90
EtOH	83, 71, 87	4.30, 3.90, 6.00
EtOAc	80, 56, 68	4.16, 1.10, 1.85
MeCN	62, 48, 63	2.87, 1.00, 6.25
$CHCl_3$	83, 65, 77	2.93, 1.13, 2.00
DMSO	84, 67, 65	2.92, 1.94, 6.60

In our synthesis of imidazoles **5.21-5.26** using Khalili *et al.*'s[399] method we obtained a similar mixture of tautomers **a** and **b** in an ethanol solution. We subsequently used ^{1}H NMR spectroscopy to determine the ratio of tautomers (Table 5.7) through integration of the ^{1}H NMR signals *e.g.* Figure 5.15. Interestingly, Khalili *et al.*[399] never assigned the downfield proton resonances in the ^{1}H NMR

spectrum, of the two isomeric 2-aryloylimidazoles to the protons on either N-1 or N-3, but rather arbitrarily chose isomer **a** as the upfield resonance and isomer **b** as the downfield resonace. We used molecular modelling to determine the optimized structure of each of the tautomers (**5.21a** and **b-5.26a** and **b**) in an attempt to identify the theoretically more likely major isomer. Both tautomers **5.21-5.26** were optimized using the B3LYP density function theory at 6-13G basis set. Using the minimized energies, the Boltzmann distribution was calculated from Equation 5.2:

$$\frac{N_A}{N_B} = e^{\frac{-\Delta\epsilon}{k_B T}} \qquad \textit{Equation 5. 2}$$

From the Boltzmann distributions of the two possible tautomers a putative theoretical tautomeric ratio could be calculated (Table 5.7).

Table 5.7: A comparison of the experimentally determined ratios of the two tautomers a and b, the calculated tautomeric ratios using Gaussian03 and the literature cited values.

Compound	Experimental [%][a]		Theoretical [%][b]		Khalili *et al.*[399] [%]	
	a	**b**	**a**	**b**	**a**	**b**
5.21	100	0	78	22	78[c]	22[c]
5.22	75	25	84	16	81	19
5.23	100	0	98	2	ND	ND
5.24	87	13	93	7	80	20
5.25	100	0	94	6	84[c]	16[c]
5.26	85	15	90	10	86	14

[a] Determined via integration of the NH signals δ_H 13.0-14.0 ppm in the ^{1}H NMR spectra

[b] Determined using Gaussian03[443] density function at 6-13G basis set and relative energies used to calculate Boltzmann distribution

[c] Khalili's reported ratios of **a** and **b** synthesized in a aqueous solution.

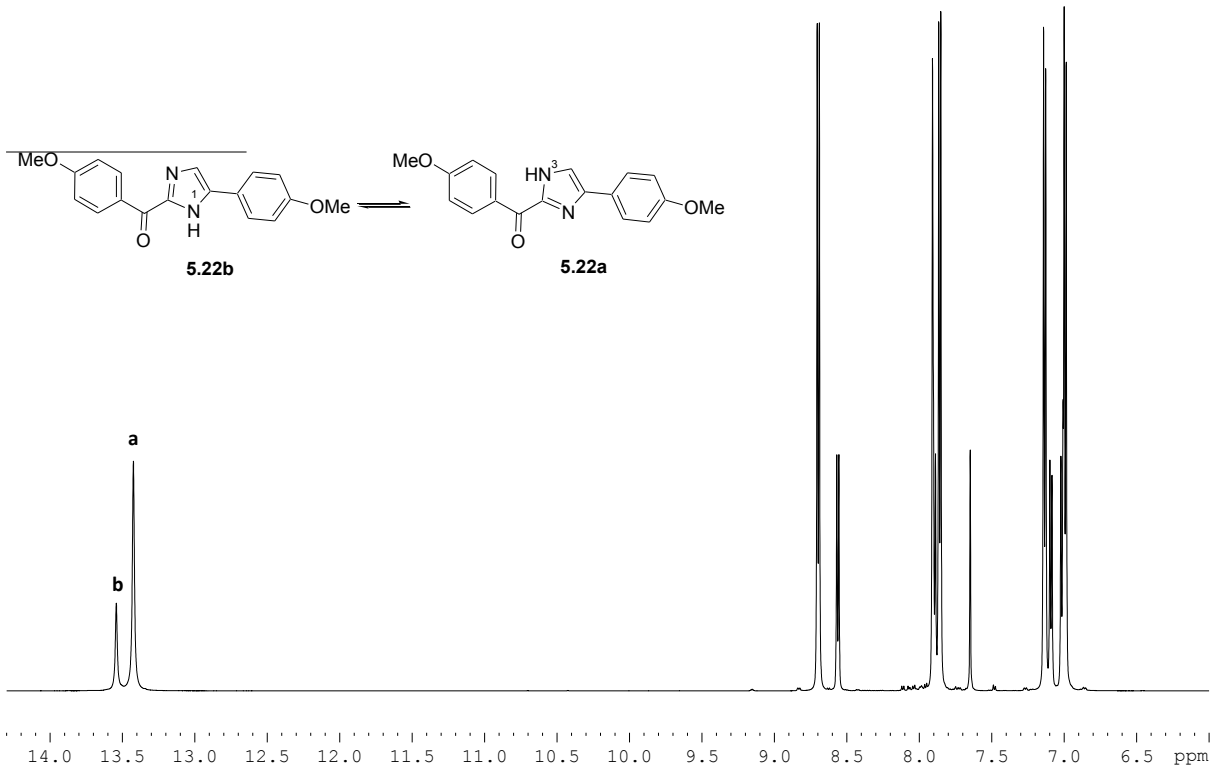

Figure 5.15: The representative downfield region (δ_H 6.0-14.3) of the ^{1}H NMR spectrum (DMSO-D_6, 600 MHz) obtained for the tautomeric mixture of **5.22** (shown inset).

Figure 5.16: The representative DFT optimized structures of **5.24a** (*left*) and **5.24b** (*right*). Visualized in DS Visualizer.[21]

From Table 5.7 we can see that tautomer **a** with the protonated N-3 atom in **5.21-5.26**, is more energetically favoured. This may be due to possible steric strain between the imidazole ring and the phenyl ring when N-1 is protonated leading to contortion of the molecule (Figure 5.16).

The seemingly random assignment of the chemical shifts of the tautomeric protons by Khalili *et al.* concerned us and we set about using 2D ^{15}N NMR spectroscopy to conclusively resolve these assignments. In the ^{15}N HMBC spectrum of **5.22** (Figure 5.17A) the methine proton on the imidazole ring will only correlate to a ^{15}N atom no more than two bonds away and provided a means of

determining the chemical shift of the N adjacent to the C-4 methine proton. A subsequent ^{15}N HSQC spectrum of the mixture of **5.22a** and **5.22b** (Figure 5.17B) will show which nitrogen of the imidazole ring is attached to the proton of the major tautomer. The spectra below shows the methine proton on C-4 in the HMBC is correlating to the same nitrogen of the major tautomer, *i.e.* N-3 (δ_N 230). It can therefore be determined that the major tautomer is **5.22a**, with the protonated nitrogen adjacent to the methine proton. This validates to the modelling data and fortuitously concurs with Khaili *et al.*'s[399] earlier random assignment. Therefore, in conclusion ^{15}N NMR spectroscopy provided a method for establishing which nitrogen atom hosted the proton of the major imidazole tautomer and conclusively resolved the structures of the major and minor tautomers.

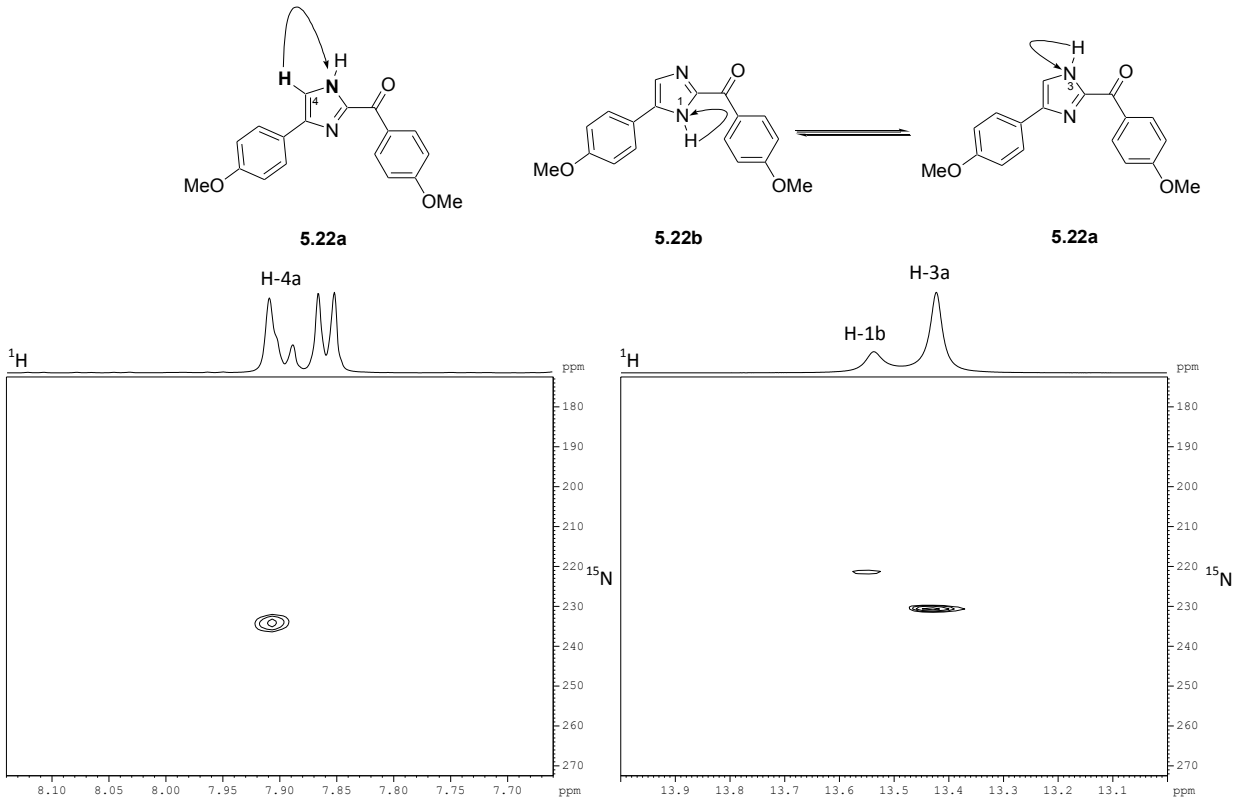

Figure 5.17: A: The ^{15}N HMBC spectrum (DMSO-D_6, 600 MHz, delay for evolution of long range coupling [d6] = 60 msec; F1 = δ_N = 170 – 273; F2 = δ_H 7.60 – 8.20) obtained for compound **5.22** (*left*).
B: The ^{15}N HSQC spectrum (DMSO-D_6, 600 MHz; F1 = δ_N = 170 – 273); F2 = δ_H 13.00 – 14.00) obtained for compound **5.22** (*right*). Key correlations illustrated in accompanying figure.

While the chemical resonances of the tautomeric mixtures of **5.21-5.26** are relatively simply to assign we expected far less spectral resolution for the more complicated bisindole compounds (**5.20**, **5.33** and **5.34**) and felt the use of the EXSY NMR experiment would be an effective tool for full individual assignment of the chemical shifts of the inseparable mixture of tautomers and EXSY data was subsequently acquired for **5.21-5.26**. **Ex**change **S**pectroscop**y** (EXSY)[444] arises from the non-coherent magnetization transfer between sites with different resonance frequencies.[445] These

magnetic transfers may occur either by exchange of nuclei in non equivalent environments (*e.g.* H-3''a to H-3''b in **5.22**, Figure 5.18) or via the exchange of atoms within a molecule (*e.g.* the 1,3 proton shift on the imidazole ring in **5.22**, Figure 5.18).[446] These exchanges are perceived as cross-peaks in the EXSY spectrum and the exchange process may be clarified by inspection.[447] EXSY NMR spectroscopy has a number of applications in organic chemistry including but not limited to proton exchanges,[448-451] chemical equilibria,[452] rotamers[453] and ring flips.[454] The EXSY NMR experiment has the same pulse sequence as a phase sensitive NOESY experiment, however if the cross-signals are in the same phase as the diagonal this indicates the exchange of protons, rather than cross relaxation detected by the NOESY experiment.[445]

By evaluating the representative EXSY spectra below of compound **5.22** (Figure 5.18), the 1,3 hydrogen shift in the imidazole ring resulting in the two tautomers was clearly shown with a cross-peaks between H-1 and H-3. The remaining cross-peaks allowed us to assign the chemical shifts of known protons of the major tautomer (determined by standard HSQC and HMBC experiments) to protons in the same relative position of the corresponding tautomer which were not apparent in the 2D NMR experiments. The assignment of the individual chemical shifts of the major and minor products of the tautomeric mixture of **5.21-5.26** using EXSY to the best of our knowledge is a first (See Chapter 6). However, the ultimate visual representation of tautomers is X-ray analysis.

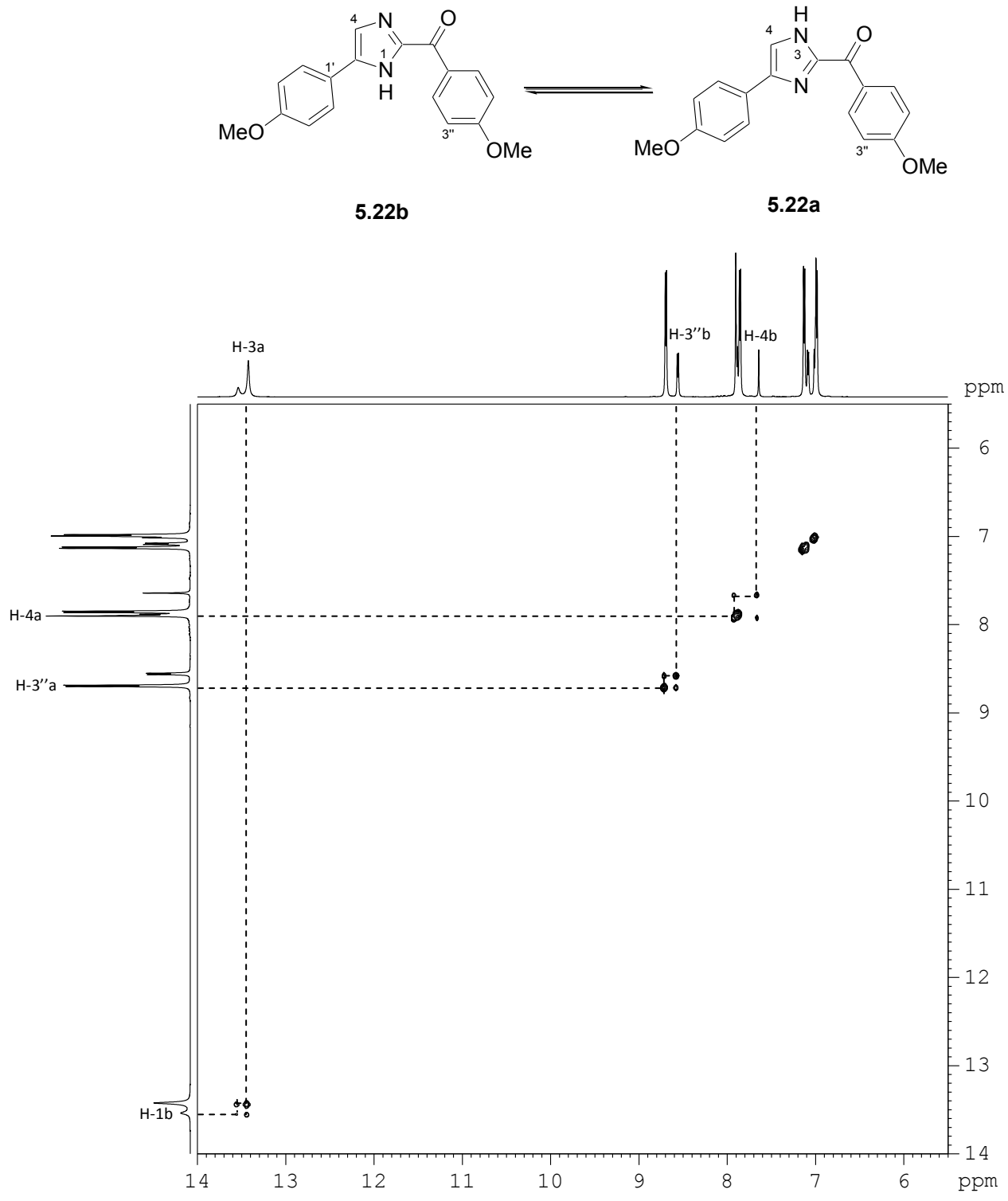

Figure 5.18: The representative downfield region (F1 and F2 = δ_H 5.5 – 14.0) of the EXSY NMR spectrum (DMSO-D_6, 600 MHz) obtained for **5.22**. The accompanying figure shows the exchange of protons in the tautomeric equilibrium.

There are several examples of crystal structures of tautomeric imidazoles in literature, Kubicki[455] showed that the crystals of some imidazole rings contain both tautomers in their unit cell, and he

later described how imidazoles have the ability to form crystal lattices as a result of imidazole-phenyl-imidazole bonds through π-stacking.[456] Mahboobi's *et al.*'s[457] crystal structure of the natural product **5.111** (Figure 5.19, CSD 215662), clearly shows the presence of one tautomer in the solid state. The N-3 atom is required as a hydrogen acceptor from a *para* substituted hydroxyl group on another unit cell, while N-1 acts as a hydrogen donor to the carbonyl of a surrounding molecule. The structure is also supported by phenyl-imidazole ring π-stacking.[457] Interestingly, our Boltzmann distribution calculations of **5.111**, revealed that protonation of the N-3 atom in the imidazole ring should be more energetically favoured. Therefore the crystal lattice of **5.111** apparently locks tautomers of this molecule into the energetically more demanding tautomer, but yet a sterically favoured conformation for crystal formation. Inspired by Mahboobi *et al.*'s ability to isolate a single tautomer of an imidazole through crystallization, we attempted to crystallize **5.21-5.26**.

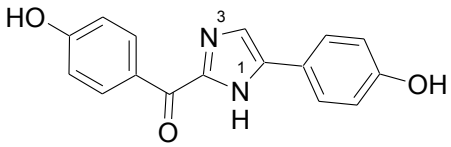

5.111

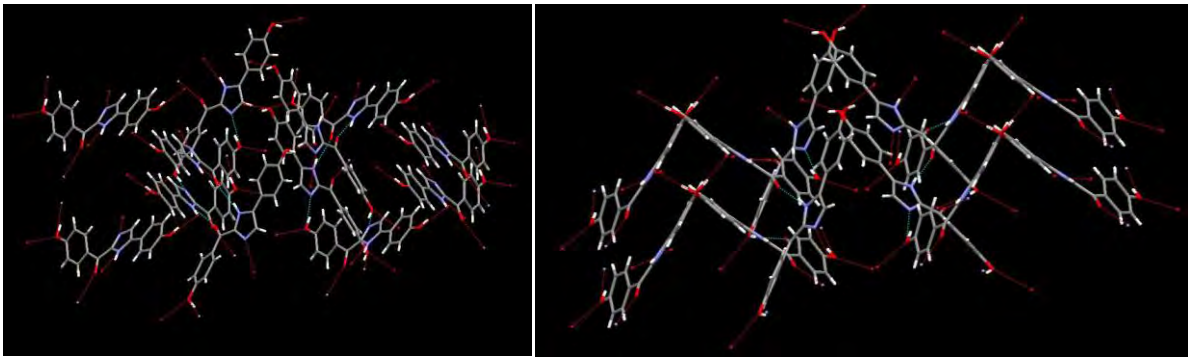

Figure 5.19: Mahboobi *et al.*'s[457] crystal lattice of **5.111**. Visualized in Mercury 2.4,[304] the unit cell view along the c-axis (*left)* and b-axis (*right*). Red dotted lines represent hydrogen bonding.

Unfortunately, Mahboobi *et al.* do not describe their method for the crystallization of **5.111**. We attempted to crystallize **5.21-5.26** using classical methods at varying temperatures and solvent systems, only to obtain microcrystals from an unusual combination of DMSO and methanol. We attempted to enlarge the crystals of **5.21-5.26** to obtain crystals suitable for X-ray analysis and hence we reverted to slow diffusion crystallization methodology. A solution of DMSO was saturated with the amorphous powder of the biphenyl imidazoles (**5.21-5.26**), which was subsequently surrounded with methanol and sealed for several weeks allowing the two solvents to slowly mix through

evaporation (Figure 5.20). Small needles of **5.21**, **5.22** and **5.24-5.26** and a brown solid (**5.23)** were obtained using this method.

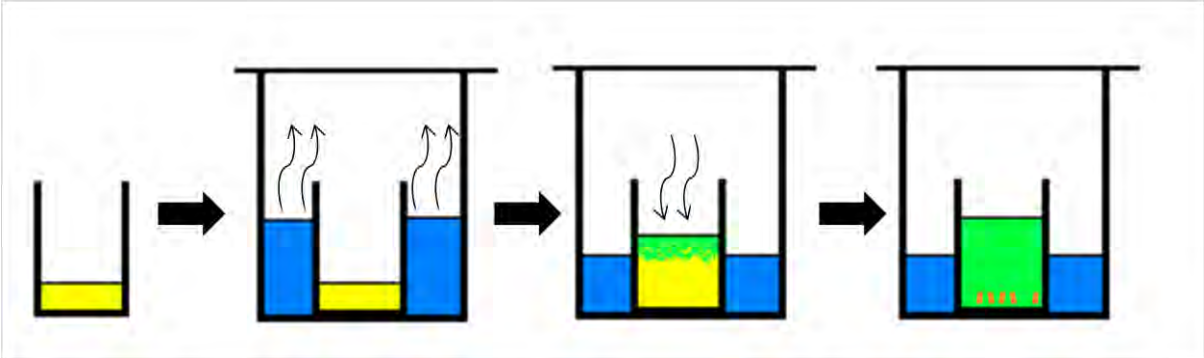

Figure 5.20: The diffusion method of crystal growth. Yellow represents a solution of biphenyl imidazole (**5.21-5.26**) in DMSO and blue represents methanol.

Unfortunately, the crystals of **5.21**, **5.22** and **5.24-5.26** were deemed too thin (average thickness was 17 µm, Figure 5.21) for X-ray diffraction and attempts to increase the thickness of the crystals through prolonged crystallization proved fruitless.

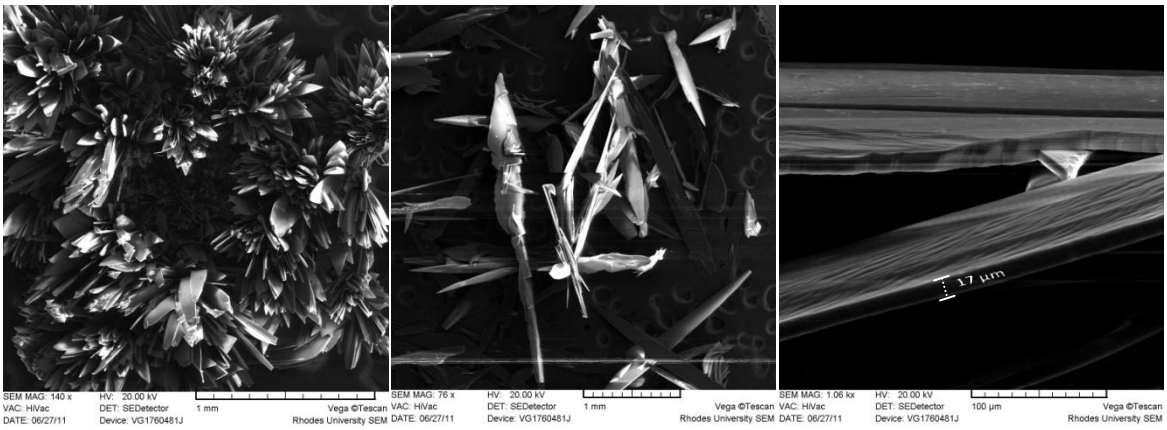

Figure 5.21: Representative SEM micrographs of compounds **5.25** at various magnifications. Images taken using a Tescan Vega scanning electron microscope at 20 kV and a working distance of 20 mm. Scale given at the bottom of the micrograph. Average thickness of crystals calculated to be 17 µm.

5.4.3.1. Improved synthesis of the ascidian natural product 5.140

In 1999, Salva and co-workers[458] reported the isolation of 2-(*p*-hydroxybenzoyl)-5-(*p*-hydroxyphenyl)

imidazole (**5.111**) from the red ascidian *Botryllus leachi* (Figure 5.22) collected off the coast of Tarifa Island, Spain. Later Mahboobi *et al.*[457] managed to synthesize and crystallize **5.111** (Scheme 5.15).

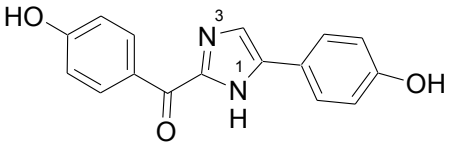

5.111

Figure 5.22: The underwater photograph of the red ascidian *Botryllus leachi (Left)*[459] and isolated metabolite 2-(*p*-hydroxybenzoyl)-5-(*p*-hydroxyphenyl) imidazole (**5.111**, *Right*).[458]

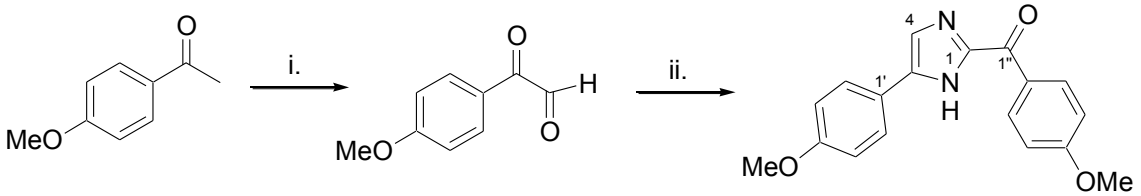

5.93 **5.28** **5.22**

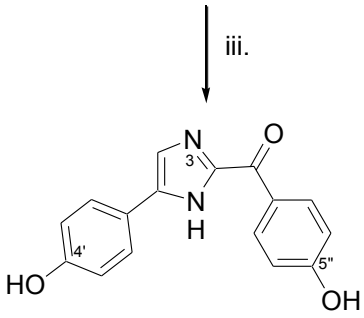

5.111

Scheme 5.15: Mahboobi *et al.*'s synthesis of the natural products **5.111**.[457] *Reagents and conditions:* i) SeO_2, MeOH, 60 °C, 5hrs, 67%; ii) NH_4OAc, AcOH; iii) HBr (48%), refluxed, 12 hrs; Pd/C (10%), H_2, RT, 12 hr, 75%

The most convenient way to synthesize **5.111** would be via a 4-hydroxyphenyl glyoxal monohydrate precursor. Unfortunately, we were unable to obtain the corresponding glyoxal monohydrate using our SeO_2 microwave method possibly due to the activation of the aryl ring. Therefore, we pursued a similar synthetic route to Mahboobi *et al.*, involving the demethylation of **5.22** as a final step.

However, our synthesis of **5.28** was completed in < 3min in quantitative yield and **5.22** was formed by stirring **5.28** in NH_4OAc for 45 min, while Mahboobi *et al.* synthesized **5.22** in 5 hrs under reflux, followed by two distillation purification steps resulting in a 67% yield. Several different methodologies for the deprotection of the methoxy functionalities on benzene rings have been described in literature. However, these demethylating procedures often require reagents such as hydrogen bromide[460] and more recently trifluoride-methyl sulphide,[461] boron tribromide[462] or iodotrimethylsilane.[463] Demethylation using these procedures afford good yields but require harsh conditions. Recently Zou *et al.*[464] have demonstrated the use of iodocyclohexane as a demethylating agent under relatively mild conditions and we found this method suitable for demethylation of **5.22** (Scheme 5.16).

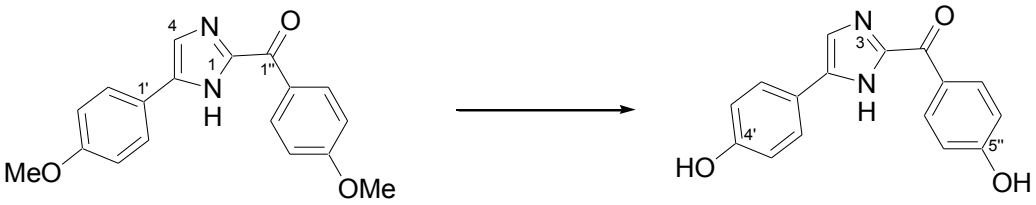

5.22 **5.111**

Scheme 5.16: The demethylation of **5.22**. *Reagents and conditions*: Iodocyclohexane, DMF, 12 hrs, refluxing under Ar, 93%

Iodocyclohexane is thermally unstable, decomposing into hydrogen iodide which effectively cleaves alkyl ethers into alcohols and alkyl iodides. The acid-catalyzed iodide ion cleavage of ethers proceeds regioselectively via an oxonium ion intermediate (**5.112**) (Scheme 5.17) with the iodide anion attacking the less sterically hindered methyl group of **5.112** to form methyl iodide and **5.111**.

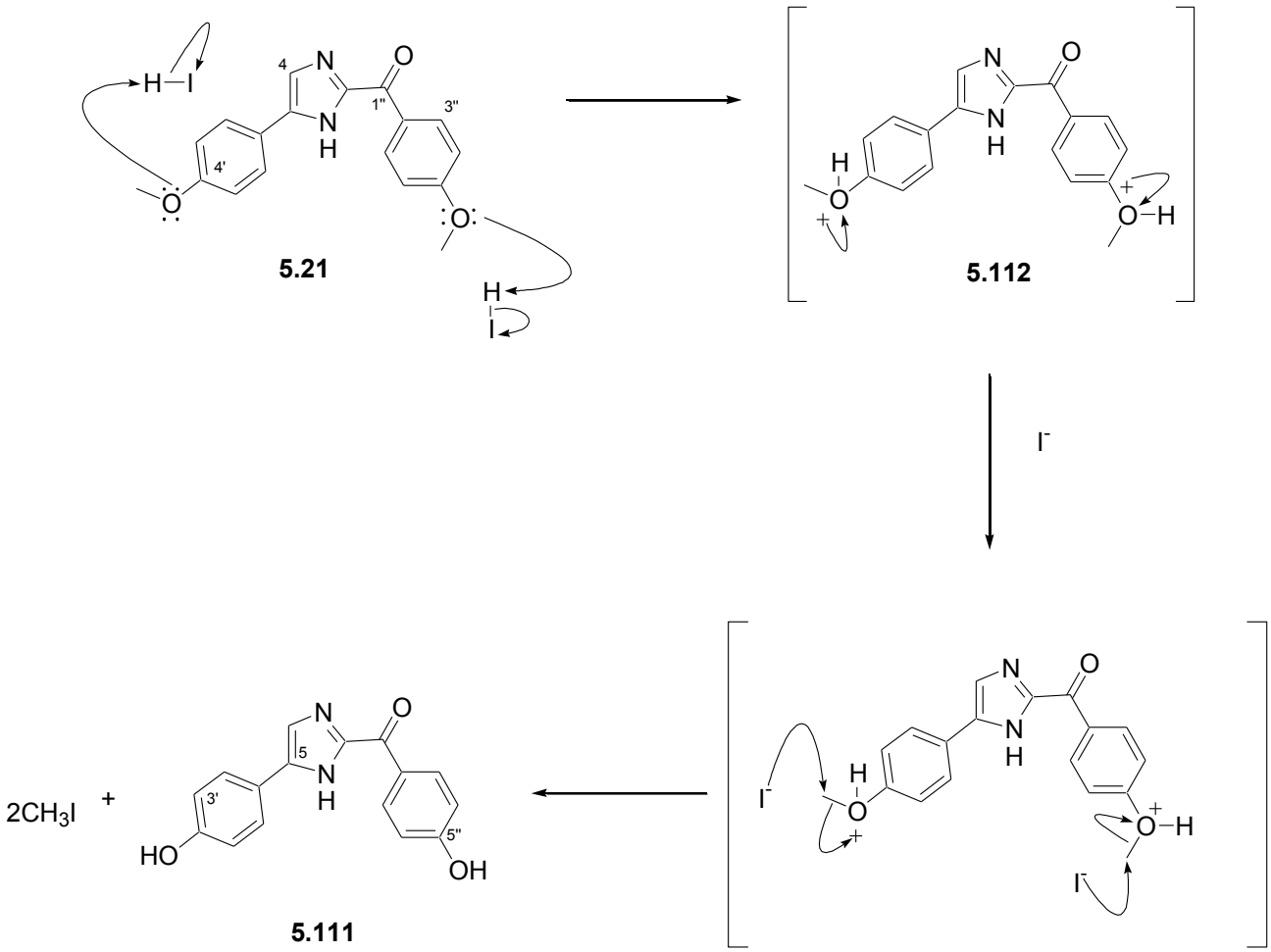

Scheme 5.17: The proposed mechanism for the demethylation of **5.21** in the presence of HI.

Initially, the iodocyclohexane demethylation reaction was refluxed under inert conditions for three hours, resulting in a mixture of unreacted starting material, two different monomethylated products and fully deprotected biphenyl imidazoles, indicated by the appearance of 8 singlets of various intensities in the downfield region, corresponding to 4 pairs of tautomers, in the ^{1}H NMR spectrum. Increasing the reaction time to 12 hrs afforded the natural product **5.111** in 93% yield, in a tautomeric a:b ratio of 75%:25%, (Boltzmann distribution calculated as a:b 74%:26%). Deprotection of the methyl ether, using Zou *et al.*'s method resulted in the easy removal of the volatile side products, *e.g.* methyl iodide, under reduced pressure. The success of the reaction was gauged by the absence of the methoxy signals (δ_H 3.79 and 3.88) in the ^{1}H NMR spectrum of **5.111**, and the appearance of a broad signal (δ_H 3.52) corresponding to the hydroxyl protons. The ^{13}C NMR data revealed a change in chemical shifts of the *para* substituted carbons, C-4' and C-5'' from δ_C 55.7 and 55.9 in the ^{13}C NMR spectrum of **5.22** to δ_C 158.7 and 163.9 in the ^{13}C NMR spectrum of **5.111** respectively. A full comparison of δ_H and δ_C of our synthetic **5.111**, Salva *et al.*'s isolated natural

product and Mahboobi *et al.*'s synthetic product can be found in Table 5.8. The ^{13}C chemical shifts for C-2 and C-5 for both our and Mahboobi's synthetic **5.111** appear to differ significantly to those values reported by Salva for the natural product. The values assigned to our synthetic **5.111** correspond to the major tautomer only, with a protonated N-3 imidazole ring (**5.111a**). The HMBC spectrum of our tautomeric mixture of **5.111**, did however show a correlation from a minor singlet δ_H 7.45 to δ_C 158.3 (H-4b to C-2b) and a minor doublet δ_H 6.80 to δ_C 156.1 (H-3''b to C-5b). We therefore concluded that the natural product Salva isolated was the tautomer **5.111b**.

Table 5.8: Comparative table of the ^{13}C and ^{1}H NMR shifts of **5.140**, the natural product and a previously synthesized product.

	5.111[a]		**Natural Product**[b, 458]		**Mahboobi's Synthetic Product**[c, 457]	
	^{13}C [ppm]	^{1}H [ppm]	^{13}C [ppm]	^{1}H [ppm]	^{13}C [ppm]	^{1}H [ppm]
1						
2	144.2		158.3		145.1	
3						
4	123.1	7.50 (s)	122.9	7.59 (s)	122.7	7.77 (s)
5	142.7		155.9		140.9	
1'	124.2		119.5		120.5	
2'	128.0	7.65 (d)	128.1	7.71 (d)	128.6	7.67 (d)
3'	116.7	6.85 (d)	117.1	6.89 (d)	116.4	6.97 (d)
4'	158.7		160.8		159.4	
1''	181.8		178.2		180.8	
2''	129.1		126.8		128.4	
3''	134.5	8.39 (d)	134.8	8.38 (d)	134.6	8.13 (d)
4''	116.7	6.90 (d)	117.2	6.84 (d)	116.2	6.90 (d)
5''	163.9		167.7		164.5	

[a] ^{1}H NMR (600 MHz) and ^{13}C NMR (150 MHz) in CD_3OD
[b] ^{1}H NMR (400 MHz) and ^{13}C NMR (100 MHz) in CD_3OD
[c] ^{1}H NMR (250 MHz) and ^{13}C NMR (62.5 MHz) in CD_3OD

5.4.4. The formation of the imidazole ring from indole glyoxal precursors

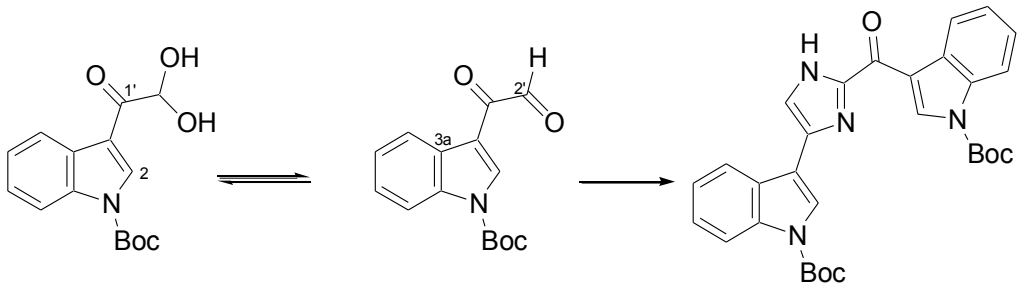

5.107 **5.88** **5.90**

Scheme 5.18: Formation of the imidazole ring from **5.88**. *Reagents and conditions:* NH_4OAc, EtOH, RT, 6 hrs, 100%

The addition of NH_4OAc to an ethanol solution of an equilibrium mixture of **5.88** and **5.107** resulted in the solution eventually turning a deep yellow colour. A yellow solid residue was obtained following removal of the solvent under reduced pressure. The yellow solid was washed with water to remove unreacted ammonium acetate and filtered. The methyl ketone **5.89** does not interfere with the formation of the imidazole and therefore the previously discussed HPLC purification of the glyoxal, to remove unreacted **5.92** may be omitted thus improving the efficiency of the reaction. The mixture of **5.89** and **5.90** was easily separated on a bench top silica column (5:1 hexane and EtOAc) with a 96% recovery of **5.90**.

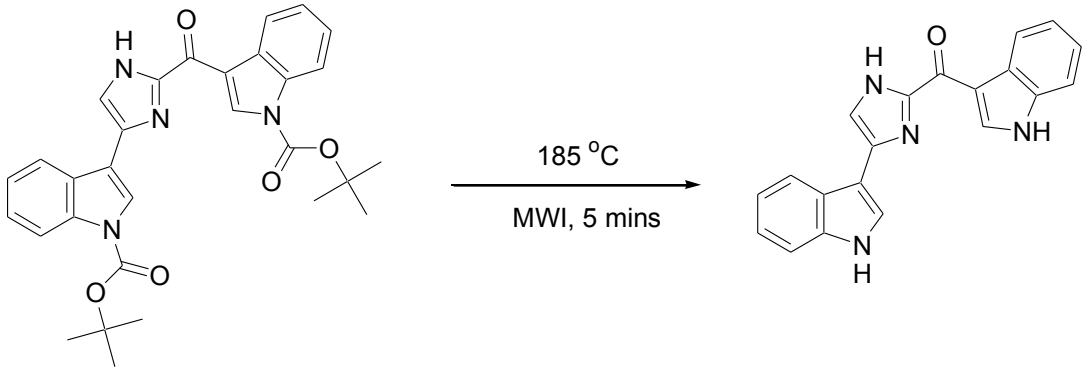

5.90 **5.33**

Scheme 5.19: The thermal deprotection of the indole rings of **5.90**. *Reagents and conditions:* MWI, 185 ˚C, 5 min, 100%

The final step in our synthesis of **5.33** required the quantitative removal of the N-Boc protecting group. The thermal lability of the carbamate has been demonstrated before where Rawal and Cava[419] reported the cleavage of N-C bond in the carbamate functionality in a number of heterocyclic compounds including one containg an indole ring *e.g.* **5.113** (Scheme 5.20), while more recently

Knölker and co-workers thermally deprotected a series of N-boc protected carbazoles *e.g.* **5.114** (Scheme 5.20).[420]

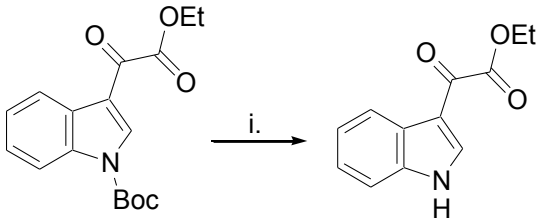

5.113

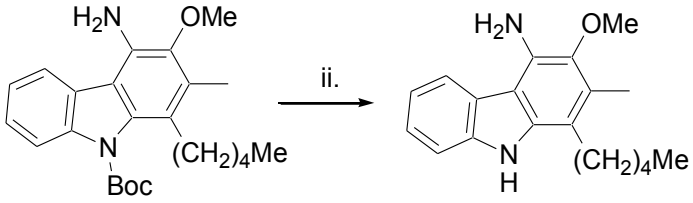

5.114

Scheme 5.20: Rawal and Cava's[419] thermal removal of carbamate ester. *Reagents and conditions:* i) Δ, 184.5 ˚C, Ar, 30 min, 99%
Knölker and co-workers'[420] thermal removal of carbamate ester. *Reagents and conditions:* ii) Δ, 180 ˚C, Ar, 45 min, 100%

We correctly envisaged that heating **5.90** under an argon atmosphere for 5 minutes in a microwave reactor would prove to be a more efficient method for quantative N-Boc deprotection. This deprotection of **5.90** is the first recorded use of microwave irradiation to effect this transformation. It was clear that the removal of the carbamate was successful as four new peaks (δ_H 12.2-11.2) appeared in ^{1}H NMR spectrum (Figure 5.23), corresponding to the pair of secondary amines of either tautomer. From the ^{1}H NMR spectrum it was clear we had prepared a mixture of tautomers almost in equal concentrations (a:b 54%:46%). Two-dimensional ^{15}N NMR was used to determine the major tautomer, as described previously. The methine proton H-4 correlates to the adjacent nitrogen (N-3, δ_N 217) in the ^{15}N HMBC (Figure 5.24, *Left*), while the ^{15}N HSQC reveals that the nitrogen at δ_N 217 correlates to the N-H of the major tautomer (δ_H 13.37; Figure 5.24, *Right*), thus confirming the major tautomer was protonated at N-3 on the imidazole ring *i.e.* **5.33a**.

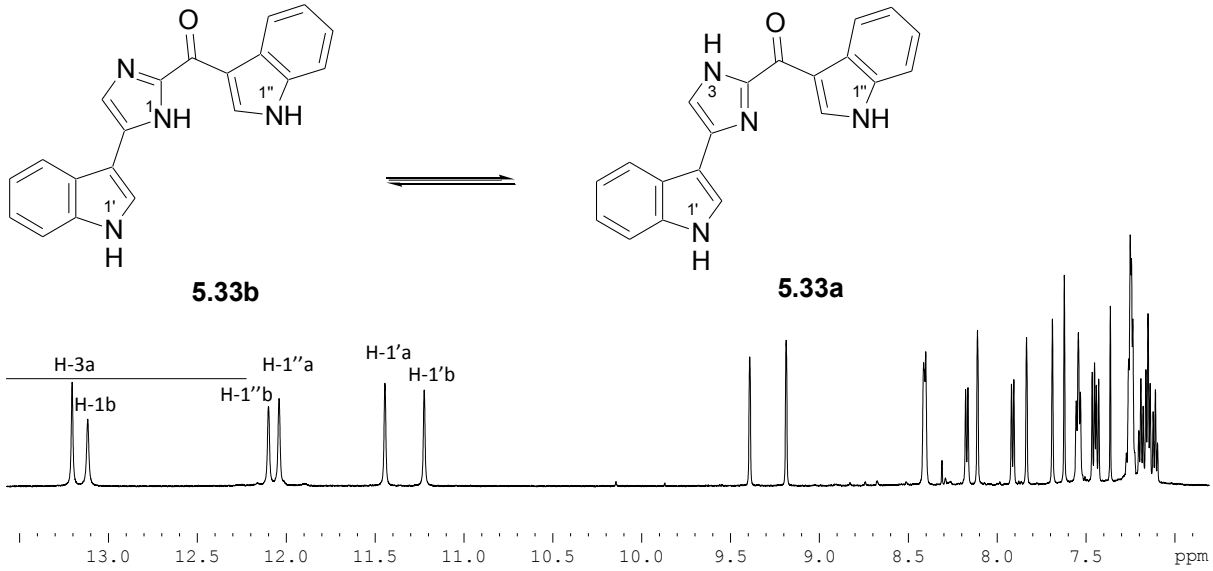

Figure 5. 23: The downfield region (δ_H 6.8-13.6) of the ^{1}H NMR spectrum (DMSO-D_6, 600 MHz) obtained for the tautomeric mixture of **5.33** (shown inset).

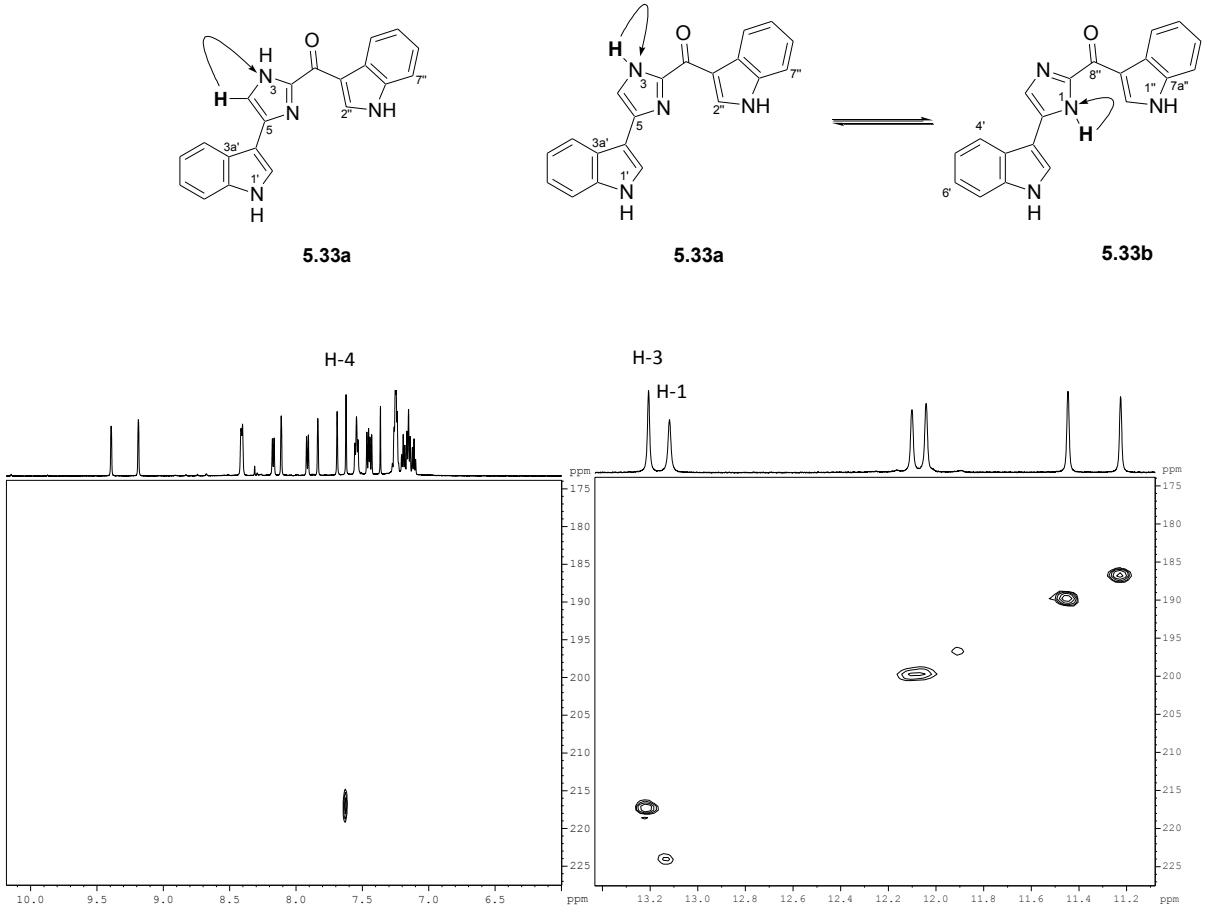

Figure 5.24: A: The ^{15}N HMBC spectrum (DMSO-D_6, 600 MHz, delay for evolution of long range coupling [d6] = 60 msec; F1 = δ_N = 174 – 227); F2 = δ_H 6.0 – 10.1) obtained for compound **5.33** (*left*). B: The ^{15}N HSQC spectrum (DMSO-D_6, 600 MHz; F1 = δ_N = 174 – 227); F2 = δ_H 11.1 – 13.4) obtained for compound **5.33** (*right*).

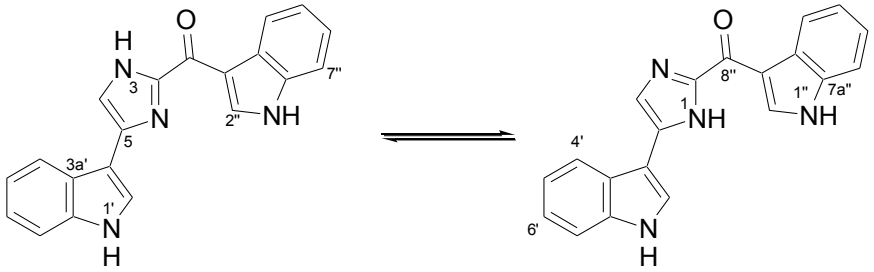

5.33a **5.33b**

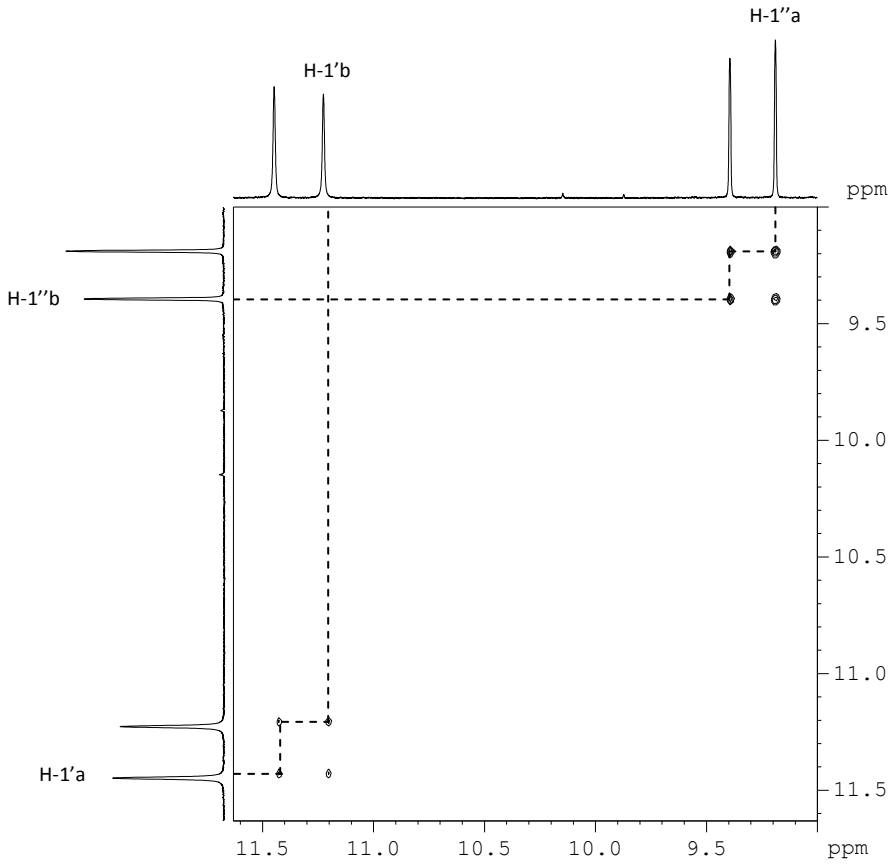

Figure 5.25: A selected portion of the downfield region (F1 and F2 = δ_H 9.0 – 11.6) of the EXSY NMR spectrum (DMSO-D_6, 600 MHz) obtained for **5.33**.

The chemical shifts assigned from the ^{1}H and ^{13}C NMR data of **5.33a** and **5.33b** are compared with Rinehart and co-workers[405] natural product in addition to Achab *et al.*'s[413] synthetic **5.33** in Table **5.9**. Both Rinehart and Achab recorded their NMR data in 1% TFA solution in DMSO-D_6 ostensibly to reduce tautomerization about the imidazole ring. We were able to use the EXSY NMR experiment (Figure 5.25) to assign ^{1}H and ^{13}C chemical shifts for both tautomers (**5.33a** and **5.33b**) for the first time, where no HSQC and or HMBC correlations were detected.

Table 5.9: Comparative table of **5.33a**, **5.33b**, Rinehart and co-workers marine natural product isolate and Achab *et al.*'s synthetic product. Values quoted in ppm and splitting patterns indicated in parentheses.

	5.33a[a]		**5.33b**[a]		**Natural Product**[b, 405]		**Synthetic Product**[c, 413]	
	^{13}C [ppm]	^{1}H [ppm]	^{13}C [ppm]	^{1}H [ppm]	^{13}C [ppm]	^{1}H [ppm]	^{13}C [ppm]	^{1}H [ppm]
1				13.12 (s)				
2	145.2		145.2		143.9		143.5	
3		13.37 (s)						
4	125.8	7.63 (s)	114.9	7.69 (s)	119.3 (d)	7.85 (s)	118.8	7.92 (s)
5	130.4		138.5		133.3		133.1	
1'		11.45 (s)		11.23 (s)		11.53 (d)		11.56 (s)
2'	124.0	8.11 (s)	122.8	7.83 (s)	124.2 (d)	8.07 (dd)	123.6	8.08 (d)
3'	104.7		110.8		105.9		105.5	
3a'	124.5		124.9		124.6		124.6	
4'	121.3	8.17 (d)	119.5	7.91 (d)	119.8 (d)	8.05 (dd)	119.6	8.04 (d)
5'	121.6	7.15 (t)	119.8	7.13 (t)	119.9 (d)	7.18 (m)	120.2	7.23 (t)
6'	122.7	7.15 (t)	121.9	7.19 (t)	121.9	7.18 (m)		7.18 (t)
7'	112.1	7.46 (s)	112.0	7.44 (d)	112.1 (d)	7.50 (dd)	112.2	7.52 (d)
7a'	136.5		136.2		136.5		136.7	
1''		12.04 (s)		12.15 (s)		12.33 (d)		12.38 (s)
2''	136.6	9.19 (s)	137.0	9.40 (s)	137.5	9.15 (d)	137.8	9.05 (d)
3''	113.7		113.9		113.8		113.7	
3a''	126.8		126.8		126.6		126.6	
4''	121.6	8.41 (d)	121.6	8.41 (d)	121.6 (d)	8.41 (dd)	121.6	8.37 (dd)
5''	121.8	7.25 (m)	121.8	7.25 (m)	122.3 (d)	7.29 (m)	122.5	7.32 (m)
6''	122.8	7.25 (m)	122.8	7.25 (m)	123.3 (d)	7.29 (m)	122.1	7.32 (m)
7''	112.3	7.54 (d)	112.3	7.54 (d)	112.6 (d)	7.59 (dd)	112.7	7.60 (m)
7a''	136.2		136.2		136.5		136.7	
8''	176.1		176.0		174.9		174.4	

[a] ^{1}H NMR (600 MHz) and ^{13}C NMR (150 MHz) in DMSO-D_6
[b] ^{1}H NMR (200 MHz) and ^{13}C NMR (125 MHz) in DMSO-D_6 + 1% TFA
[c] ^{1}H NMR (300 MHz) and ^{13}C NMR (125 MHz) in DMSO-D_6 + 1% TFA

The use of microwave technology resulted in the rapid production of **5.33** with a total yield of 86%. Compared to the other methods this is by far the quickest and the highest yielding. We extended this method in the attempted synthesis of isobromotopsentin (**5.20**) and its synthetic isomer bis-5-bromoindole imidazole (**5.34**).

5.4.5. Attempted synthesis of 5.20 and 5.34

With the success of the synthesis of **5.88** we proceeded to attempt to synthesize the 5- and 6-bromo substituted indole glyoxal precursors (**5.115** and **5.116**) required for the synthesis of **5.20** and **5.34** respectively (Scheme 5.21).

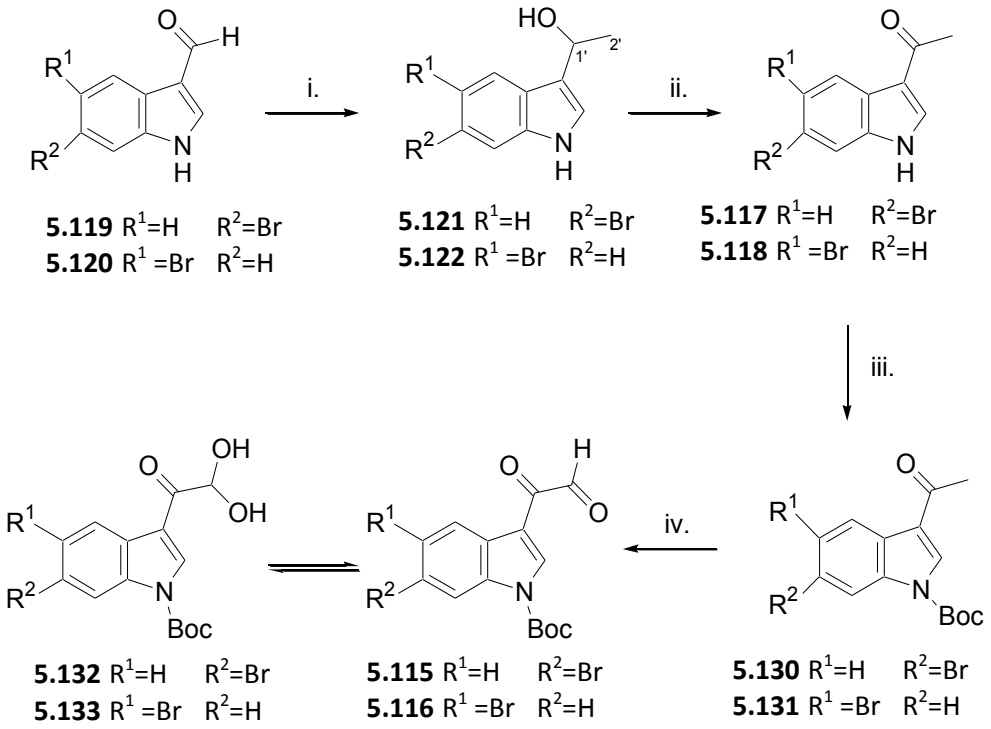

Scheme 5.21: The synthetic pathway for the synthesis of **5.115** and **5.116**. *Reagents and conditions:* i) MeMgBr, $CeCl_3$, THF, 0 ˚C, 6 hrs, 100% ii) MnO_2, DCM, RT, 48 hrs, 100% iii) Boc_2O, DMAP, MeCN, 0 °C, 2hrs, 100% iv) SeO_2, H_2O, 1,4-dioxane, MWI, 30 min, 100 ˚C, 83 -85%

Although, the brominated 3-acetylindoles **5.117** and **5.118** are not commercially available we anticipated that they could be synthesized from their respective indole-3-carboxaldehydes **5.119** and **5.120**. The bromo indole-3-carboxaldehydes (**5.119** and **5.120**) were accordingly methylated to give the racemic secondary alcohols **5.121** and **5.122**, by the anhydrous addition of methylmagnesium bromide. The ^{1}H NMR spectra showed that the synthesis of the secondary alcohol had been achieved in quantative yield, by the disappearance of the aldehyde peak (δ_H 10.04 and δ_H 10.03) and the appearance of a quartet (δ_H 5.13, δ_H 5.19) and a large doublet (δ_H 1.60, δ_H 1.65) corresponding to the oxymethine proton and methyl protons respectively in **5.121** and **5.122** (Figure 5.27). The COSY NMR spectra of **5.121** and **5.122** both showed a correlation between H-1' (δ_H 5.13, δ_H 5.19) and H-2' (δ_H 1.60, δ_H 1.65) further indicating the successful methylation of **5.119** and **5.120**. Surprisingly, the

secondary alcohols **5.121** and **5.122** rapidly degraded under ambient conditions, thus requiring oxidation soon after preparation.

Two oxidation methods were attempted for the preparation of **5.117** and **5.118**; the first involving tetrapropylammonium perruthenate (TPAP, Scheme 5.22) and the second manganese dioxide (MnO_2, Scheme 5.24).

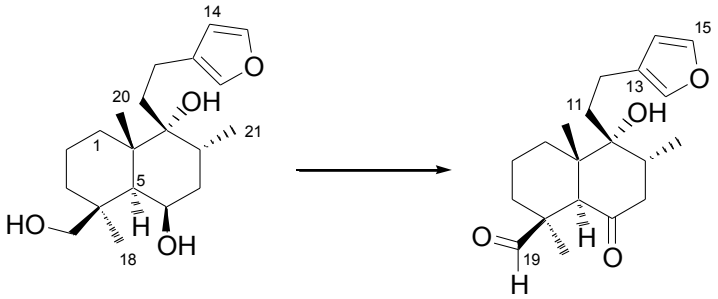

5.123 **5.129**

Scheme 5.22: The oxidation of marrubenol (**5.123**) catalyzed by TPAP. *Reagents and conditions:* TPAP, NMO, DCM, 4Å molecular sieves, RT, 3hrs 98%

Tetrapropylammonium perruthenate (TPAP) oxidation was first tested on a trial compound *viz* the natural product marrubenol (**5.123**). The TPAP salt consists of a tetrapropylammonium cation (**5.124**) and a ruthenium tetroxide anion (**5.125**) which acts a powerful oxidiser. The catalytic cycle of the ruthenium tetroxide anion is illustrated in Scheme 5.23.. The ruthenium forms an ether (**5.126**) with an alcohol (**5.127**) with subsequent dehydrative removal of both the alcohol moiety and the oxymethine proton. Anhydrous conditions are necessary for this reaction and the reaction is conducted over 4Å molecular sieves. The ruthenium anion is then replenished through the addition of *N*-methylmorpholine-*N*-oxide (NMO, **5.128**), resulting in the ruthenium tetroxide anion (**5.125**), continuing the catalytic cycle.

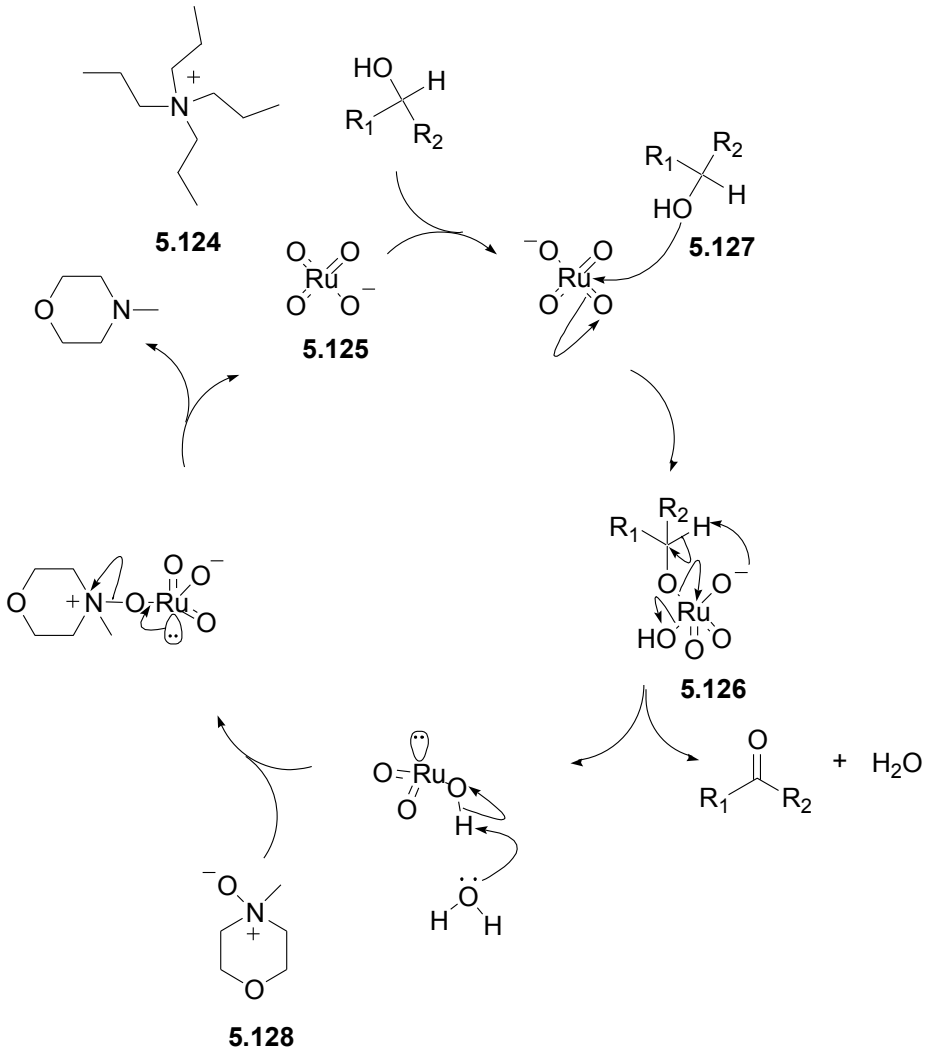

Scheme 5.23: The catalytic cycle of the ruthenium tetroxide anion (**5.125**) in the TPAP reagent with the additive NMO (**5.128**).[465]

The C-19 primary and C-6 secondary alcohols of **5.123** were successfully converted to the aldehyde and ketone respectively in a 98% yield, which can be clearly seen by the disappearance of the resonance (δ_C 65 and 69) in the ^{13}C NMR spectrum of **5.119** and the appearance of two deshielded signals (δ_C 211 and 209) in the ^{13}C NMR spectrum of **5.129** (Figure 5.26).

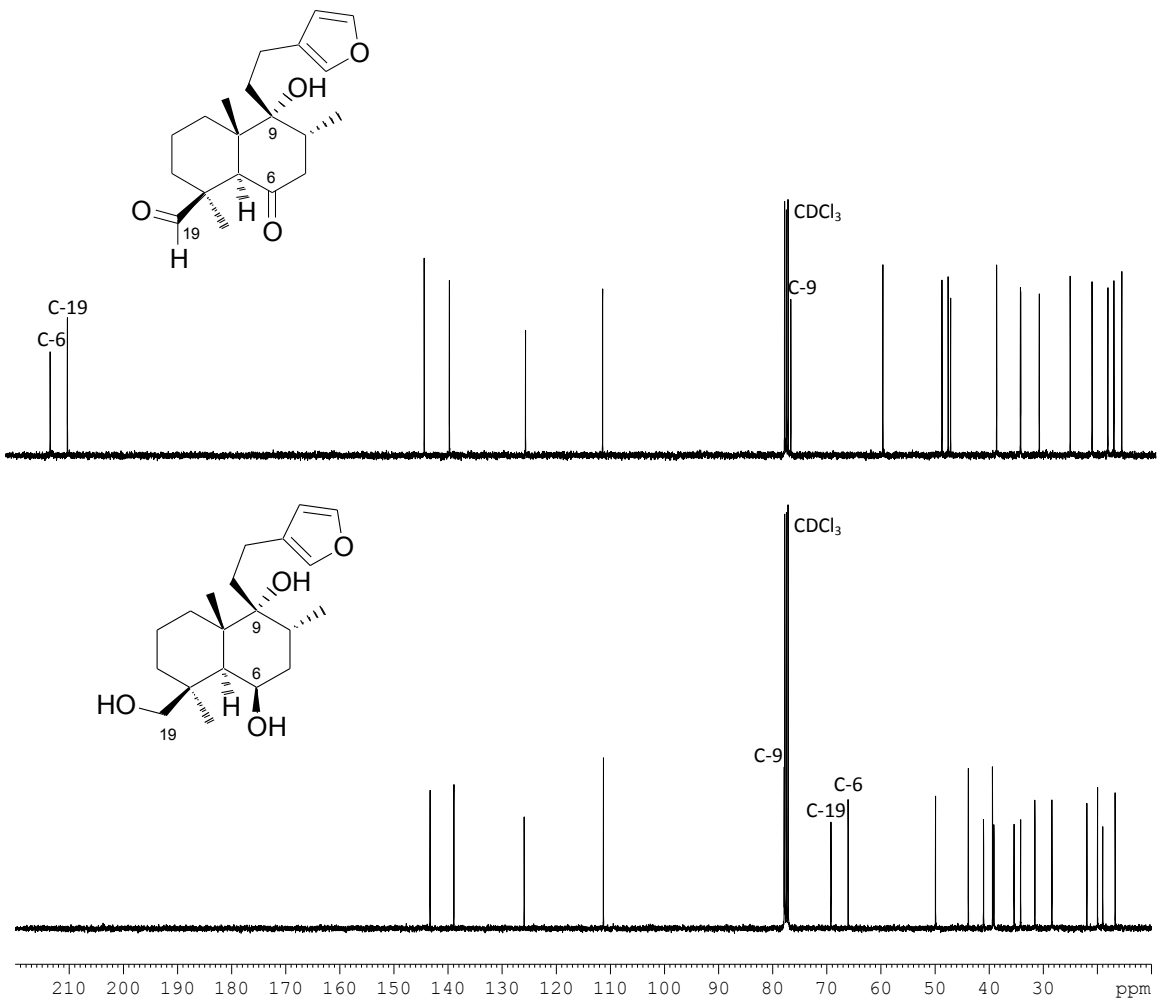

Figure 5.26: The ^{13}C NMR spectra ($CDCl_3$, 150 MHz) of marrubenol (*bottom)* and **5.129** (*above*), the product after oxidation with TPAP. The carbons of interest are labelled in accompanying figures.

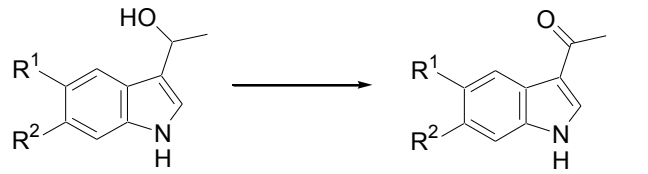

5.121 R^1=H R_2=Br
5.122 R^1=Br R_2=H

5.117 R^1=H R_2=Br
5.118 R^1=Br R_2=H

Scheme 5.24: The oxidation of **5.121** and **5.122** with manganese dioxide. *Reagents and conditions:* MnO_2, DCM, RT, 48 hrs, 100%

While we established through the oxidation of a trial compound that TPAP would be a suitable oxidizing agent for the oxidation of **5.121** and **5.122**, one major drawback of TPAP is its exorbitant cost and we decided to explore the use of the cheaper alternative, MnO_2 for the oxidation

(Scheme 5.24). MnO_2 is an effective oxidizing agent under mild conditions and has been widely used in our laboratory for oxidising benzylic alcohols. A comparison of the ^{1}H NMR of **5.121** and **5.117** shows the methyl doublet (δ_H 1.60) becomes a singlet with the successful removal of the oxymethine proton (δ_H 5.13) during oxidation (Figure 5.27).

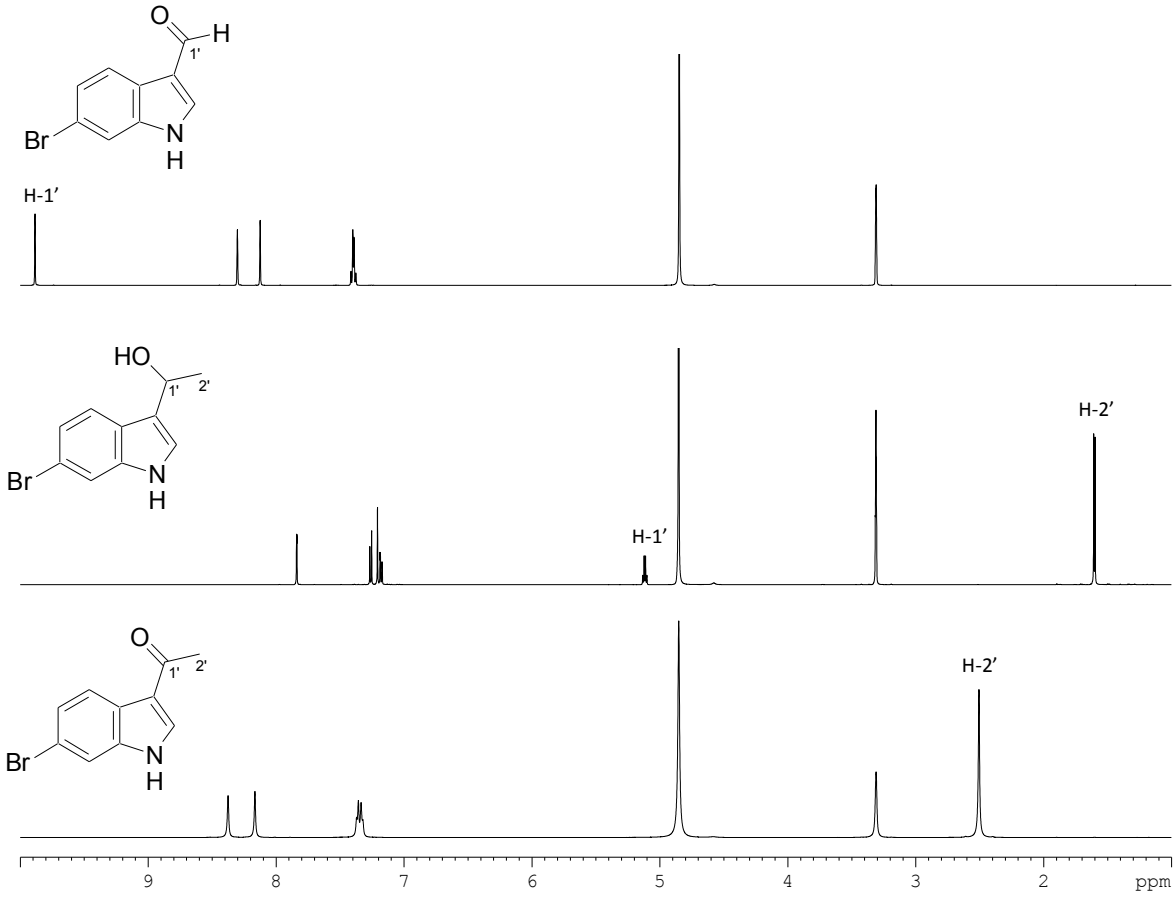

Figure 5.27: The ^{1}H NMR spectra (CD_3OD, 600MHz) of **5.119** (*top)*, **5.121** (*middle*) and **5.117** (*bottom*), the product after oxidation with MnO_2. The protons of interest labelled in accompanying figures.

The N-Boc protection of **5.117** and **5.118** afforded **5.130** and **5.131** respectively in quantitative yield. Interestingly, during the preparation of the equilibrium mixtures of glyoxals (**5.115** and **5.116**) and glyoxal monohydrate (**5.132** and **5.133**), we did encounter a minor problem in that partial deprotection of these compounds occurred resulting in complex mixtures of N-Boc protected and deprotected glyoxals (Scheme 5.25). The reason for the formation of the carbamate was to ensure the methyl ketone was not over oxidised to the glyoxylic acid by SeO_2. However, the emergence of four new singlets in the downfield region (δ_H 9.5-13.0) of the ^{1}H NMR spectrum of the reaction mixture of the SeO_2 oxidation of **5.130** and **5.131**, indicated the formation of two glyoxals, corresponding to the N-Boc protected as well as the deprotected glyoxal *e.g.* **5.115** and **5.134**. The

remaining two signals in the downfield region were broad corresponding to the protonated N-1 of the indole ring in the deprotected glyoxal (**5.134**) and deprotected glyoxal monohydrate (**5.135**). The successful oxidation to the glyoxal suggests that the thermal mediated removal of the carbamate ester occurs post oxidation. The mixture of glyoxals (**5.115**, **5.132**, **5.134** and **5.135**) was taken forward in the synthesis of **5.20** and **5.34**.

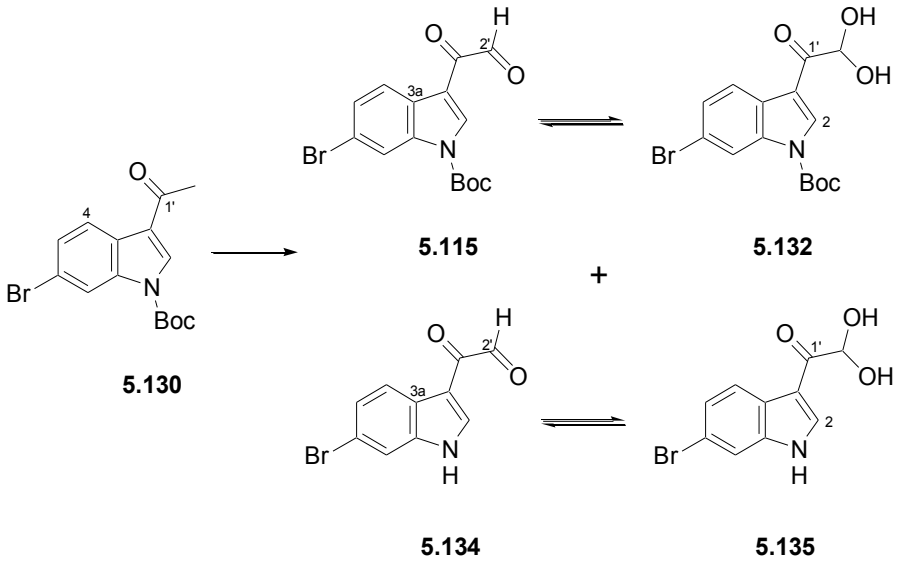

Scheme 5.25: The microwave assisted selenium oxidation of **5.130**. *Reagents and conditions:* SeO_2, H_2O, 1,4-dioxane, MWI, 30 min, 100 ˚C, 83-85%

The dehydrative condensation of the 5- or 6- brominated glyoxal mixture afforded an inseparable mixture of mono and deprotected topsentin products (Scheme 5.26). This was confirmed by HRMS revealing peaks at *m/z* = 482.9461 and 582.9989 corresponding to the $[M+H]^+$ pseudo molecular ions of compound **5.20** and **5.136** or **5.137**. Interestingly, for both the 5- and 6- brominated imidazoles, no diprotected species were detected. It was at this point that I was required to finish my laboratory research and further examination of this synthetic approach to **5.20**, **5.138-5.140** continues in our laboratory.

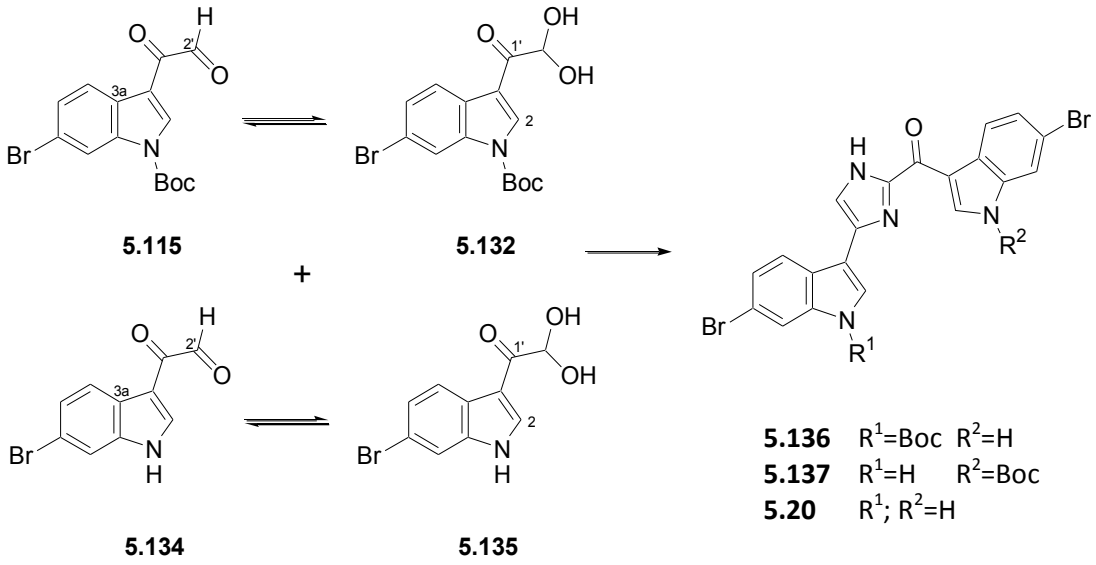

Scheme 5.26: Formation of the imidazole rings from a mixture of glyoxals (**5.115** and **5.134**). *Reagents and conditions:* NH_4OAc, EtOH, RT, 6 hrs

5.5. Conclusion

In this Chapter we have reviewed past syntheses of the topsentin class of marine bisindoles. Our microwave based synthetic approach provides a simple, quick and high yielding route to the synthesis of the sponge metabolite deoxytopsentin (**5.33**) and the ascidian metabolite **5.111**. With the use of MAO synthesis we have optimized the classic SeO_2 oxidation reaction in aryl methyl ketones as well as providing an efficient and rapid method for the removal of the Boc protecting group. We have also managed to assign the NMR data for major and minor tautomers of the imidazole containing compounds, which many authors have failed to report in the past.

Further work will be to continue the SAR study of halogenated bisindole compounds with the synthesis of **5.138-5.140**. The bisindole alkaloids **5.20**, **5.33**, **5.34** and **5.138**-**5.140** will hopefully be sent to UBC where they will be tested for their ability to selectively inhibit MRSA PK.

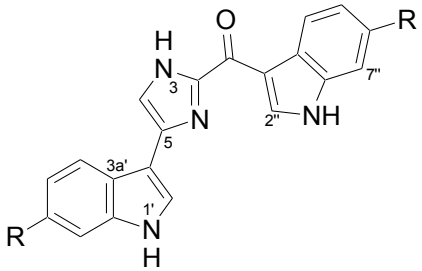

R =Cl **5.138**
R =F **5.139**
R =I **5.140**

CHAPTER 6: EXPERIMENTAL

6.1. General Procedures

6.1.1. Analytical

(i) Melting points were determined using a Reichert hot stage microscope and are uncorrected.

(ii) Optical rotations were measured using a Perkin-Elmer 141 polarimeter calibrated at the sodium D line (598 nm).

(iii) Infrared spectra were recorded on a Perkin Elmer Spectum 2000 FT-IR and DIGILAB Excalibur HE Series FTS 3100 FT-IR spectrometer.

(iv) NMR spectra were acquired on Bruker 400 MHz Avance and 600 MHz Avance II spectrometers using standard pulse sequences. Chemical shifts are reported in ppm, referenced to residual solvent resonances ($CDCl_3$ δ_H 7.25, δ_C 77.0; DMSO-D_6 δ_H 2.50, δ_C 39.50; CD_3OD δ_H 3.31, δ_C 49.00 ppm), and coupling constants are reported in Hz.

(v) The UV/vis absorbances were measured on a Varian Carrey 1E with sample solutions contained in a quartz cuvette.

(vi) HREIMS and HRFABMS data were acquired at the University of Stellenbosch and North West University respectively. MALDI-TOF mass data was acquired with a Bruker AutoFLEX III Smartbeam TOF/TOF Mass spectrometer. The instrument was operated in positive ion mode using an *m/z* range of 400 – 3000. The voltage of the ion sources were set at 19 and 16.7 kV for ion sources 1 and 2 respectively, while the lens was set at 8.50 kV. The voltages for reflectors 1 and 2 were set at 21 and 9.7 kV respectively. The spectra were acquired using α-cyano-4-hydroxycinnamic acid as the MALDI matrix, using a 354 nm Nd:YAG laser.

(vii) Full intensity data for crystals was collected on a Nonius Kappa CCD diffractometer with the crystals cooled in a steady nitrogen stream at -100 ^{o}C. The crystal structures were solved by Professor Caira at the University of Cape Town using direct methods and were fully refined by the least-squares technique. All H atoms attached to C were located and inserted in idealized positions. All hydroxyl H atoms were located and inserted with idealized O-H bonding distances at their optimised positions consistent with the observed hydrogen bonding patterns.

(viii) X-ray powder diffraction patterns were recorded on a Bruker D8, Discover equipped with a proportional counter, using Cu-Kα radiation (λ = 1.5405 Å, nickel filter). Data were collected in the range from 2θ = 5° to 30°, scanning at 1° min^{-1} with a filter time-constant of 2.5 s per step and a slit width of 6.0 mm. Samples were placed on a silicon wafer slide.

(ix) TGA analysis was done on a TA Q600 heating the sample from room temperature to 200 °C at 5 °C min^{-1} under N_2 gas. The simultaneous MS analysis of the decomposition gases was done using a Pfeifer Thermostar®.

(x) The compounds were prepared for SEM by coating them in gold using a Balzers' Spluttering device. The compounds were viewed using a Tescan Vega scanning electron microscope at 20 kV and a working distance of 20mm.

6.1.2. Chromatography

(i) Reactions were monitored by thin layer chromatography (DC-Plastikfolien Kieselgel 60 F_{254} plates) and visualized under UV light (254 nm) and developed by spraying with either 10% conc. H_2SO_4 in methanol or iodine adsorbed on silica gel. Reversed phase thin layer chromatography was performed on DC-Ferigplatten RP18 F_{245} plates. Plates were viewed under UV light (254 nm).

(ii) Kieselgel 60 (230-400 mesh) was used for initial flash chromatographic separations.

(iii) Semi-preparative NP-HPLC was performed using a Whatman's Magnum 9 Partisil 10 column (10 mm i.d., length 50 cm); RP-HPLC was performed using an Onyx Monolithic C18 column (10 mm i.d., length 10 cm), with a Waters 410 Differential Refractometer detector or a Waters 2414 Refractive Index Detector and an eluent flow rate of 4 $mL.min^{-1}$ using a Spectra-Physics Spectra-Series P100 or a Waters 1500-Series isocratic pump.

(iv) Glyoxal and methylketones were separated by an Agilent 6820 GC system using a J & W Scientific DB 225 column with an internal diameter of 250 µm and a length of 30 m. The oven was preheated to 50 ^oC and then heated at a rate of 5 $^oC.min^{-1}$ to a final temperature of

220 ^{o}C. The carrier gas was helium administered at a flow rate of 1 ml.min^{-1}. The compounds eluted were detected using FID.

6.1.3. Synthesis

(i) Reactions where exclusion of water was necessary were performed using glassware dried in a 150 °C oven overnight or dried at 600 °C with a heatgun and flushed with dry argon to remove air and moisture. All reactions were performed under an atmosphere of dry Ar.

(ii) Dry solvents were prepared by standard procedures outlined by Perrin and Amerego.[466] Immediately prior to their use THF was distilled from sodium metal/ benzophenone ketyl while Et_2O, CH_2Cl_2 and MeCN were distilled from calcium hydride and all solvents were stored over 4 Å molecular sieves under anhydrous argon. General laboratory solvents were distilled before use. All reactions were magnetically stirred. All reagents were commercially available.

(iii) Microwave reactions were carried out in a CEM Discover single-mode microwave apparatus, producing controlled irradiation at 2450 MHz, using standard 10 mL silicon-septum sealed glass pressure vials. The reactions were optimized using the temperature-time mode of operation and the temperature was monitored using an IR sensor directed at the outside wall of the reaction vial. Once the reaction was complete the reaction vessel was cooled to 50 ^{o}C by means of propelled airflow.

6.1.4. Molecular Modelling

(i) Where a X-ray crystal structure was unavailable, Accelrys Visualizer[21] was used to construct the 3-D models of compounds and exported in .mol2 format. A spin restricted DFT structural optimization, using the Gaussian03[443] suite of algorithms was performed on each structure. The parameters for the DFT runs were the 6-31G(d) basis set while the electronic correlation energy was determined using the B3LYP functional. The calculations were run on a multi-processor Linux cluster with multi-threading capabilities. Docking studies will be discussed in detail in Section 6.3.3.

6.2. Chapter 3 experimental details

6.2.1. Preparation of 3.189, 3.190, 3.194 and 3.188

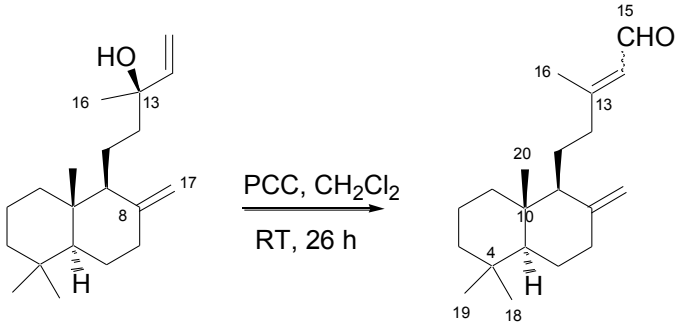

3.187 **3.189** (*E*)
3.190 (*Z*)

(+)-Manool (**3.187**, 4.455 g, 15.36 mmol) was dissolved in CH_2Cl_2 (200 mL), pyridinium chlorochromate (PCC) (10.964 g, 50.76 mmol, 3.3 equiv.) was added to solution and stirred (26 h) at ambient temperature. Diethyl ether (200 mL) was added, resulting in the formation of an orange precipitate. The solution was filtered through a Celite 545 plug and the filtrate concentrated under reduced pressure, to yield a dark brown oil. The oil was purified by silica flash chromatography (5 % EtOAc, 95 % hexane) to afford and inseparable mixture of (E)-labda-8(17)dien-15-al (**3.189**) and (Z)-labda-8(17)dien-15-al (**3.190**) in a 2:1 ratio (3.897 g, 88% yield) as a yellow oil. ^{1}H and ^{13}C NMR data consistent with literature values;[467] HRFABMS: calcd for $C_{20}H_{33}O_1$ 289.2531. Found 289.2531, Δamu 0.0000.[248]

6.2.2. Intramolecular aldol condensation of 3.189 and 3.190

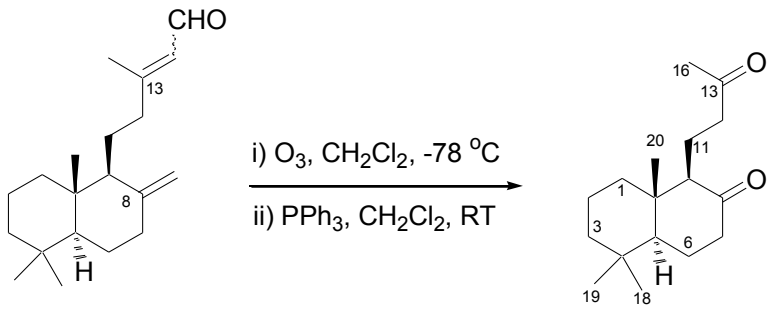

3.189 (*E*)
3.190 (Z)

3.194

The isomeric mixture of **3.189** and **3.190** (500 mg, 1.75 mmol) was dissolved in CH_2Cl_2 (25 mL) and cooled in a dry ice and acetone slurry to -78 °C. A steady stream of ozone was bubbled through the

solution (20 min) until the solution turned a pale blue colour. Nitrogen was bubbled through the solution to ensure the removal of excess O_3. Triphenylphosphine (3.3 g, 10.5 mmol, 6 equiv.) was added to the solution where it was allowed to stir for 4 hours at room temperature. Hydrogen peroxide (10 mL, 30%) was added to the cooled solution (0 ^{o}C) and stirring was continued (0.5 h). The organic solution was washed with water (3 × 5 mL) and the organic extracts dried with $MgSO_4$ and concentrated. The organic fractions were further purified via silica flash chromatography (50% EtOAc, 50% hexane) to afford **3.194** (352 mg, 76 %).

6.2.3. Cyclization of 3.194 to afford 3.188

15,16,17-Trisnorlabdane-8,13-dione (**3.194**)[467-469]**:** yellow oil; $[\alpha]_D^{20}$ -28 (c 1.3, $CHCl_3$, lit -11, c 1.05)[468]; IR (film) ν_{max} 2940, 1709, 1698, 1355, 1164 cm^{-1}; ^1H NMR (400 MHz, $CDCl_3$) δ 2.56 (ddd, *J* = 17.4, 8.3, 5.3, H-12a, 1H), 2.38 (ddd, *J*= 13.3, 4.8, 2.0, H-7b, 1H), 2.24 (m, H-7a, 1H), 2.17 (m, H-12a, 1H), 2.07 (s, H-16, 3H), 2.04 (m, H-9, 1H), 2.01 (m, H-6b, 1H), 1.79 (m, H-1b, 1H), 1.76 (ddd, *J* = 10.7, 5.3, 2.9, H-11b, 1H), 1.61 (m, H-6a, 1H), 1.59 (m, H-11a, 1H), 1.51 (m, H_2-2, 2H), 1.46 (dd, *J* = 12.9, 2.8, H-5, 1H), 1.42 (m, H-3b, 1H), 1.21 (m, H-1a and H-3a, 2H), 0.93 (s, H_3-18, 3H), 0.82 (s, H_3-19, 3H), 0.70 (s, H_3-20, 3H); ^{13}C NMR ($CDCl_3$, 100 MHz) δ 212.3 (q, C-8), 209.2 (q, C-13), 63.1 (CH, C-9), 54.1 (CH, C-5), 42.8 (CH_2, C-12), 42.7 (q, C-10), 42.6 (CH_2, C-7), 41.8 (CH_2, C-3), 39.1 (CH_2, C-1), 33.7 (q, C-4), 33.5 (CH_3, C-18), 29.9 (CH_3, C-16), 23.9 (CH_2, C-6), 21.7 (CH_3, C-19), 19.0 (CH_2, C-2), 16.1 (CH_2, C-11), 14.5 (CH_3, C-20); HRFABMS: calcd for $C_{17}H_{28}O_2$ 265.2168. Found 265.2168, Δamu 0.0000.

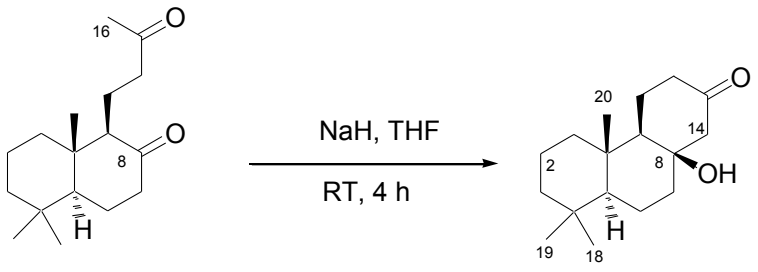

3.194 **3.188**

The diketone (**3.194**) (1.12 g, 4.2 mmol) was dissolved in dry THF (5 mL), NaH (0.49 g, 12.7 mmol, 3 equiv.) added and the solution stirred under argon (4 h). The reaction mixture was quenched with sat. aq. NH_4Cl and extracted with Et_2O (3 x 10 mL). The diethyl ether extracts were combined, washed with water (2 x 5 mL), sat. brine (1 x 5 mL) and dried over anhydrous $MgSO_4$. The diethyl

ether was removed *in vacuo* and the resultant yellow oil crystallized from 20% CH_2Cl_2 80% hexane to yield white needles of **3.188** (893 mg, 80%):

8β-Hydroxy-13-podocarpanone (**3.188**): white needles; mp 201-203 °C, lit. 204-205 °C[470]; $[\alpha]_D^{23}$ +9.8 (*c* 0.4, $CHCl_3$, lit. +11.6, *c* 2.2, $CHCl_3$)[471]; IR (film) ν_{max} 3434 (br.), 3019, 2926, 1215, 756, 668 cm^{-1}; ^1H NMR (600 MHz, $CDCl_3$) δ 2.42 (m, H-12a, 1H), 2.35 (d, *J* = 14.4, H-14β, 1H), 2.26 (m, H-12b, 1H), 2.23 (d, *J* = 14.4, H-14α, 1H), 1.92, (m, H_2-11, 2H), 1.76 (m, H-1a, 1H), 1.71 (m, H-7β, 1H), 1.60 (m, H-2a, 1H), 1.56 (m, H_2-6, and H-7α, 3H), 1.41 (m, H-2b and H-3β, 2H), 1.40 (m, H-9, 1H), 1.16 (td, *J* = 13.2, 4.4, H-3α, 1H), 0.98 (s, H_3-17, 3H), 0.94 (m, H-1a and H-5, 2H), 0.88 (s, H_3-15, 3H), 0.85 (s, H_3-16, 3H); ^{13}C NMR (150 MHz, $CDCl_3$) δ = 210.7 (q, C-13) 75.5 (q, C-8), 57.3 (CH_2, C-14), 56.1 (CH, C-5), 55.3 (CH, C-9), 42.2 (CH_2, C-7), 42.0 (CH_2, C-3), 41.5 (CH_2, C-12), 39.8 (CH_2, C-1), 37.5 (q, C-10), 33.6 (CH_3, C-15), 33.3 (q, C-4), 21.8 (CH_3, C-16), 21.4 (CH_2, C-11) , 18.4 (CH_2, C-2), 17.9 (CH_2, C-6), 15.3 (CH_3, C-17) ; EIMS *m/z* (rel. int.) 264 [M^+] (32), 250 (19), 249 (100), 179 (27), 123 (25) ; HREIMS (70 eV): calcd for $C_{17}H_{28}O_2$ 264.2089. Found 264.2083, Δamu 0.0006.

6.2.4. Grignard alkylation of 3.188

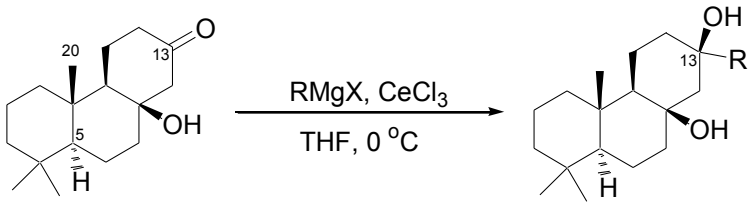

3.188

3.203 R = Me

3.204 R =

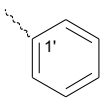

3.205 R =

3.206 R =

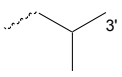

3.207 R = H

3.209 R =

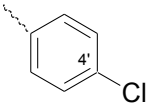

3.210 R =

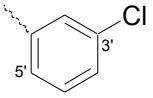

3.211 R =

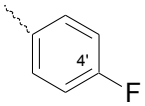

3.212 R =

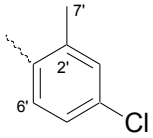

The following method is representative for the preparation of compounds **3.203-3.207** and **3.209-3.212**. A suspension of anhydrous $CeCl_3$ (137 mg, 0.57 mmol, 1.5 equiv.) in dry THF (5 mL) was stirred under argon at ambient temperature (2 h), subsequently cooled to 0 ^oC and an aliquot (1.89 mL, 0.57 mmol, 1.5 equiv.) of a THF solution of methylmagnesium bromide (3.0 M) added. The suspension was stirred (0 ^oC, 1.5 h) and a solution of **3.188** (100 mg, 0.38 mmol) in dry THF (2 mL) added. Stirring was continued (0 ^oC, 1 h) and the reaction mixture gradually allowed to reach room temperature (8 h) before quenching with sat. aqueous NH_4Cl (5 mL) and extracted with Et_2O (3 x 5 mL). The combined diethyl ether fractions were washed with water (2 x 5 mL) and sat. brine (1 x 5 mL). The organic portion was dried over anhyd. $MgSO_4$, filtered and concentrated under reduced pressure to yield a yellow oil. Further purification of the yellow oil via normal phase semi-preparative HPLC (20% EtOAc, 80% hexane) afforded a white solid which was recrystallized from MeOH to give white prisms of **3.203** (73 mg, 57%):

8β, 13β-Dihydroxy-13α-methylpodocarpane (**3.203**): white prisms from MeOH; mp 157-159 ^oC; $[\alpha]_D^{23}$ −3.2 (*c* 0.5, CH_2Cl_2); IR (film) ν_{max} 3311 (br.), 2945, 1462, 1216, 1135, 780 cm^{-1}; ^1H NMR (600 MHz, $CDCl_3$) δ 1.77 (ddd, *J* = 13.3, 7.2, 3.1, H-12a, 1H), 1.73 (dt, *J* = 13.3, 3.3 Hz, H-7β, 1H), 1.71 (m, H-11a and H-1a, 2H), 1.62 (td, *J* = 14.0, 2.8, H-14β, 1H), 1.61 (m, H-2a, 1H), 1.51 (m, H_2-6, 2H), 1.49 (m, H-11b, 1H), 1.39 (m, H-3β, 1H), 1.37 (m, H-2b, 1H), 1.33 (td, *J* = 14.2, 4.4, H-12b, 1H), 1.30 (m, H-7α, 1H), 1.28 (m, H-14α, 1H), 1.15 (s, H_3-1', 3H), 1.13 (td, *J* = 12.9, 4,3, H-3α, 1H), 1.00 (s, H_3-17, 3H), 0.85 (s, H_3-15, 3H), 0.84 (s, H_3-16, 3H), 0.83 (m, H-5 and H-9, 2H), 0.80 (m, H-1b, 1H); ^{13}C NMR (150 MHz, $CDCl_3$) δ 73.2 (q, C-8), 71.0 (q, C-13), 56.4 (CH, C-5), 56.2 (CH, C-9), 51.1 (CH_2, C-14), 42.1 (CH_2, C-7), 42.0 (CH_2, C-3), 39.8 (CH_2, C-12), 39.5 (CH_2, C-1), 37.2 (q, C-10), 33.6 (CH_3, C-15), 33.3 (q, C-4), 30.9 (CH_3, C-1'), 21.7 (CH_3, C-16), 18.4 (CH_2, C-2), 17.7 (CH_2, C-6), 16.7 (CH_2, C-11), 15.4 (CH_3, C-17); EIMS *m/z* (rel. int.) 280 [M^+] (13), 262 (82), 244 (38), 179 (75), 126 (54); HREIMS (70 eV): calcd for $C_{18}H_{32}O_2$ 280.2402. Found 280.2392 Δamu = 0.0010.

To the suspension of anhydrous $CeCl_3$ an aliquot (5.67 mL, 0.57 mmol, 1.5 equiv.) of a THF solution of phenylmagnesium bromide (1.0M) was added. A yellow oil obtained from the procedure *vide supra* was purified via normal phase semi-preparative HPLC (25% EtOAc, 75% hexane) to afford a white solid which was recrystallized from MeOH to give white orthorhombic crystals of **3.204** (38 mg, 34%).

8β, 13β-Dihydroxy-13α-phenylpodocarpane (**3.204**): white orthorhombic crystals from MeOH, mp 161-164 °C; $[\alpha]_D^{23}$ −14.4 (*c* 0.6, CH_2Cl_2); IR (film) ν_{max} 3317 (br.), 2401, 1661, 1216, 757, 668 cm^{-1}; ^1H NMR (600 MHz, $CDCl_3$) δ 7.46 (d, *J* = 7.8, H-2' and H-6', 2H), 7.33 (t, *J* = 7.4, H-3' and H-5', 2H), 7.23 (t, *J* = 7.3, H-4', 1H), 1.95 (m, H-12a, 1H), 1.86 (m, H-12b, 1H) 1.81 (dd, *J* = 14.3, 2.7, H-14β, 1H), 1.76 (m, H-1a, 1H), 1.74 (m, H-7β, 1H), 1.68 (d, *J* = 14.2, H-14α, 1H), 1.65 (m, H-11b, 1H), 1.64 (m, H-2a, 1H), 1.55 (m, H_2-6, 2H), 1.43 (m, H-2b, 1H), 1.41 (m, H-3β, 1H), 1.36 (td, *J* = 13.3, 4.6 Hz, H-7α, 1H), 1.16 (td, *J* = 13.6, 3.9, H-3α, 1H), 1.06 (s, H_3-17, 3H), 1.04 (m, H-9, 1H) 0.90 (dd, *J* = 11.3, 3.4, H-5, 1H), 0.88 (m, H-1b, 1H), 0.88 (s, H_3-15, 3H), 0.86 (s, H_3-16, 3H); ^{13}C NMR (150 MHz, $CDCl_3$) δ 148.3 (q, C-1'), 128.2 (2 x CH, C-3' and C-5'), 126.7 (CH, C-4'), 124.4 (2 x CH, C-2' and C-6'), 74.5 (q, C-13), 73.5 (q, C-8), 56.4 (CH, C-5), 56.2 (CH, C-9), 51.4 (CH_2, C-14), 42.2 (CH_2, C-3) 42.1 (CH_2, C-7), 39.8 (CH_2, C-12), 39.5 (CH_2, C-1), 37.3 (q, C-10), 33.6 (CH_3, C-15), 33.3 (q, C-4), 21.7 (CH_3, C-16), 18.4 (CH_2, C-2), 17.7 (CH_2, C-6), 16.9 (CH_2, C-11), 15.5 (CH_3, C-17); EIMS *m/z* (rel. int.) 324 [M^+] (50), 306 (24), 179, (22), 175 (100), 105 (83); HREIMS (70 eV): calcd for $C_{23}H_{34}O_2$ 324.2559. Found 324.2579 Δamu 0.002.

To the suspension of anhydrous $CeCl_3$ an aliquot (2.84 mL, 0.57 mmol, 1.5 equiv.) of a THF solution of isopropylmagnesium chloride (2.0M) was added. A yellow oil obtained from the procedure *vide supra* was purified via normal phase semi-preparative HPLC (33% EtOAc, 67% hexane) to afford **3.205** as white needles from MeOH (23 mg, 20%).

8β, 13β-Dihydroxy-13α-iso-propylpodocarpane (**3.205**): white needles from MeOH, mp 132-136 °C; $[\alpha]_D^{23}$ −16.1 (*c* 0.4, CH_2Cl_2); IR (film) ν_{max} 3303 (br.), 2946, 1702, 1451, 1190, 757 cm^{-1}; ^1H NMR (600 MHz, $CDCl_3$) δ 1.76 (m, H-7β, 1H), 1.72 (m, H-12a, 1H), 1.71 (m, H-1a and H-11a, 2H), 1.62 (m, H-2a, 1H), 1.56 (dd, *J* = 14.1, 3.0, H-14β, 1H), 1.52 (m, H_2-6, H-11b and H-1', 4H), 1.39 (m, H-2b and H-3β, 2H), 1.33 (m, H-12b, 1H), 1.30 (td, *J* = 13.3, 5.1, H-7α, 1H), 1.25 (d, *J* = 14.1, H-14α, 1H), 1.13 (td, *J* = 14.0, 3.8, H-3α, 1H), 1.00 (s, H_3-17, 3H), 0.88 (d, *J* = 7.0, H_3-2' and H_3-3', 6H), 0.87 (s, H_3-15, 3H), 0.84 (m, H-9, 1H), 0.84 (s, H_3-16, 3H), 0.82 (m, H-1b, 1H), 0.81 (m, H-5, 1H); ^{13}C NMR (150 MHz, $CDCl_3$) δ 75.2 (q, C-13), 73.2 (q, C-8), 56.7 (CH, C-5), 56.6 (CH, C-9), 46.5 (CH_2, C-14), 42.6 (CH_2, C-3) 42.3 (CH_2, C-7), 39.7 (CH_2, C-1), 37.4 (q, C-10), 38.6 (CH, C-1'), 35.0 (CH_2, C-12), 33.7 (CH_3, C-15), 33.4 (q, C-4), 21.8 (CH_3, C-16), 18.4 (CH_2, C-2), 17.9 (CH_2, C-6), 16.9 (CH_3, C-3'), 16.8 (CH_3, C-2'), 16.5 (CH_2, C-11), 15.6 (CH_3, C-17); EIMS *m/z* (rel. int.) 308 [M^+] (28), 265 (50), 248, (35), 247 (100), 141 (30); HREIMS (70 eV): calcd for $C_{20}H_{36}O_2$ 308.2715. Found 308.2717 Δamu 0.0002.

To the suspension of anhydrous $CeCl_3$ an aliquot (2.84 mL, 0.57 mmol, 1.5 equiv.) of a THF solution of isobutylmagnesium bromide (2.0M) was added. A yellow oil obtained from the procedure *vide supra* was purified via normal phase semi-preparative HPLC (17% EtOAc, 83% hexane) to yield **3.206** as white needles from MeOH (31 mg, 27%).

8β, 13β-Dihydroxy-13α-iso-butylpodocarpane (**3.206**): white needles from MeOH, mp 138-140 ^{o}C; $[\alpha]_D^{33}$ −12.1 (*c* 0.4, CH_2Cl_2); IR (film) ν_{max} 3473 (br.), 1640, 1215, 1034, 750, 667 cm^{-1}; ^{1}H NMR (600 MHz, $CDCl_3$) δ 1.83 (non, *J* = 6.5, H-2', 1H), 1.79 (m, H-12a, 1H), 1.74 (m, H-7β, 1H), 1.71 (m, H-1a and H-11a, 2H), 1.66 (dd, *J* = 14.0, 2.8, H-14β, 1H), 1.61 (m, H-2a, 1H), 1.51 (m, H_2-6, 2H), 1.50 (m, H-11b, 1H), 1.39 (m, H-2b and H-3β, 2H), 1.31 (m, H-12b, 1H), 1.30 (m, H-7α and H-1', 2H), 1.24 (d, *J* = 14.0, H-14α, 1H), 1.13 (td, *J* = 13.8, 4.0, H-3α, 1H), 1.01 (s, H_3-17, 3H), 0.94 (t, *J* = 6.2, H_3-3' and H_3-4', 6H), 0.86 (s, H_3-15, 3H), 0.85 (m, H-5 and H-9, 2H), 0.84 (s, H_3-16, 3H), 0.81 (m, H-1b, 1H); ^{13}C NMR (150 MHz, $CDCl_3$) δ 73.8 (q, C-13), 73.2 (q, C-8), 56.7 (CH, C-9), 56.6 (CH, C-5), 52.9 (CH_2, C-1'), 50.0 (CH_2, C-14), 42.5 (CH_2, C-7), 42.3 (CH_2, C-3), 39.7 (CH_2, C-1), 38.9 (CH_2, C-12), 37.4 (q, C-10), 33.7 (CH_3, C-15), 33.5 (q, C-4), 25.2 (CH_3, C-3'), 25.1 (CH_3, C-4'), 23.5 (CH, C-2'), 21.8 (CH_3, C-16), 18.6 (CH_2, C-2), 17.9 (CH_2, C-6), 16.5 (CH_2, C-11), 15.6 (CH_3, C-17); EIMS *m/z* (rel. int.) 322 [M^+] (8), 304 (42), 289, (47), 286 (100), 271 (50); HREIMS (70 eV): calcd for $C_{21}H_{38}O_2$ 322.2872. Found 322.2865 Δamu 0.0007

Purification of the product mixture afforded from the preparation of **3.206** via normal phase semi-preparative HPLC (33% EtOAc, 67% hexane), also yielded **3.207** as white monoclinic crystals from MeOH (18 mg, 19%):

8β, 13β-Dihydroxypodocarpane (**3.207**): white monoclinic crystals from MeOH, mp 157-160 ^{o}C; $[\alpha]_D^{33}$ −16.9 (*c* 0.5, CH_2Cl_2); IR (film) ν_{max} 3430 (br.), 3020, 1637, 1214, 754, 670 cm^{-1}; ^{1}H NMR (600 MHz, $CDCl_3$) δ 4.07 (br. s, H-13, 1H), 3.09 (br. s, O<u>H</u>), 2.70 (br. s, O<u>H</u>), 1.94 (quin, *J* = 13.1, 2.6 Hz, H-12β, 1H), 1.81 (dt, *J* = 14.3, 2.6, H-14β, 1H), 1.76 (m, H-11a, 1H), 1.74 (m, H-7β, 1H), 1.71 (m, H-1a, 1H), 1.62 (t, *J* = 3.45, H-2a, 1H), 1.49 (m, H-6a, 1H), 1.48 (m, H-11b, 1H), 1.46 (m, H-12α, 1H), 1.39 (m, H-14α, 1H), 1.38 (m, H-2b and H-3β, 2H), 1.33 (m, H-6b, 1H), 1.31 (m, H-7α, 1H), 1,13 (td, *J* = 13.5, 4.1, H-3α, 1H), 1.00 (s, H_3-17, 3H), 0.94 (dd, *J* = 12.6, 2.8, H-9, 1H), 0.87 (s, H_3-15, 3H), 0.83 (m, H-5, 1H), 0.83 (s, H_3-16, 3H), 0.82 (td, *J* = 13.1, 3.6, H-1b, 1H), 0.81 (m, H-5, 1H); ^{13}C NMR (150 MHz, $CDCl_3$) δ 73.4 (q, C-8), 67.7 (CH, C-13), 56.3 (CH, C-5), 56.5 (CH, C-9), 45.5 (CH_2, C-14), 42.2 (CH_2, C-3) 42.1 (CH_2, C-7), 39.4 (CH_2, C-1), 37.3 (q, C-10), 33.9 (CH_2, C-12), 33.5 (CH_3, C-15), 33.3 (q, C-4), 21.7 (CH_3, C-

16), 18.4 (CH_2, C-2), 17.6 (CH_2, C-6), 15.4 (CH_3, C-17), 14.9 (CH_2, C-11); EIMS *m/z* (rel. int.) 266 [M^+] (49), 251 (41), 233, (75), 180 (17), 179 (100); HREIMS (70 eV): calcd for $C_{20}H_{36}O_2$ 266.2246. Found 266.2239 Δamu 0.0007.

To the suspension of anhydrous $CeCl_3$ an aliquot (5.67 mL, 0.57 mmol, 1.5 equiv.) of a THF solution of 4-chlorophenylmagnesium bromide (1.0 M) was added. A yellow oil obtained from the procedure *vide supra* was purified via normal phase semi-preparative HPLC (20% EtOAc, 80% hexane) to afford a white solid which was recrystallized from MeOH to give white orthorhombic crystals of **3.209** (91 mg, 64%).

8β, 13β-Dihydroxy-13α-4´-chlorophenylpodocarpane (**3.209**)**:** white needles from MeOH (64% yield), mp 182-184 ^{o}C; $[\alpha]_D^{23}$ −94.7 (*c* 1.1, $CHCl_3$); IR (film) ν_{max} 3272 (br.), 2945, 1441, 1093, 812, 758 cm^{-1}; ^{1}H NMR (600 MHz, $CDCl_3$) δ 7.40 (d, *J* = 8.6 Hz, H-2' and H-6', 2H), 7.28 (d, *J* = 8.5, H-3' and H-5', 2H), 1.90 (m, H-12a, 1H), 1.89 (m, 11a, 1H), 1.83 (m, H-12b, 1H) 1.76 (m, H-14β, 1H), 1.75 (m, H-1a, 1H), 1.74 (m, H-7β, 1H), 1.66 (m, H-14α, 1H), 1.65 (m, H-11b, 1H), 1.63 (m, H-2a, 1H), 1.55 (m, H_2-6, 2H), 1.42 (m, H-7α, 1H), 1.41 (m, H-2b and H-3β, 2H), 1.14 (td, *J* = 13.6, 4.5, H-3α, 1H), 1.04 (s, H_3-17, 3H), 1.04 (m, H-9, 1H) 0.89 (m, H-5, 1H), 0.87 (m, H-1b, 1H), 0.87 (s, H_3-15, 3H), 0.85 (s, H_3-16, 3H); ^{13}C NMR (150 MHz, $CDCl_3$) δ 147.1 (C, C-1'), 132.6 (C, C-4'), 128.4 (2 x CH, C-3' and C-5'), 126.3 (2 x CH, C-2' and C-6'), 74.2 (C, C-13), 74.1 (C, C-8), 56.6 (CH, C-5), 56.3 (CH, C-9), 51.7 (CH_2, C-14), 42.4 (CH_2, C-3) 42.2 (CH_2, C-7), 40.1 (CH_2, C-12), 39.6 (CH_2, C-1), 37.5 (C, C-10), 33.7 (CH_3, C-15), 33.5 (C, C-4), 21.9 (CH_3, C-16), 18.6 (CH_2, C-2), 17.8 (CH_2, C-6), 17.0 (CH_2, C-11), 15.7 (CH_3, C-17); EIMS *m/z* (rel. int.) 376 [M^+] (14), 358 (32), 340, (51), 211 (40), 209 (100); HREIMS (70 eV): calcd for $C_{23}H_{33}O_2Cl$ 376.2169. Found 376.2158 Δamu 0.0011.

To the suspension of anhydrous $CeCl_3$ an aliquot (11.4 mL, 0.57 mmol, 1.5 equiv.) of a THF solution of 3-chlorophenylmagnesium bromide (0.5 M) was added. A yellow oil obtained from the procedure *vide supra* was purified via normal phase semi-preparative HPLC (20% EtOAc, 80% hexane) to afford a white solid which was recrystallized from MeOH to give white orthorhombic crystals of **3.209** (77 mg, 54%).

8β, 13β-Dihydroxy-13α-3´-chlorophenylpodocarpane (**3.210**): white needles from MeOH (54% yield), mp 199-201 °C; $[\alpha]_D^{23}$ −6.3 (*c* 0.6, $CHCl_3$); IR (film) ν_{max} 3267 (br.), 2919, 1435, 1204, 772, 692 cm^{-1}; ^1H NMR (600 MHz, $CDCl_3$) δ 7.48 (t, *J* = 1.9, H-2', 1H), 7.34 (dt, *J* = 7.9, 1.1, H-4', 1H), 7.24 (t, *J* = 7.9, H-5', 1H), 7.19 (ddd, *J* = 8.0, 1.9, 1.0, H-6', 1H) 1.91 (m, H-12a, 1H), 1.89 (m, H-11a, 1H) 1.81 (m, H-12b, 1H), 1.77 (m, H-14a, 1H), 1.76 (m, H-1a, 1H), 1.74 (m, H-7a, 1H), 1.66 (m, H-14b, H-11b, 2H), 1.64 (s, H-2a, 1H), 1.54 (m, H_2-6, H-7b 3H), 1.44 (m, H-2b, 1H), 1.41 (m, H-3β, 1H), 1.16 (td, *J* = 14.4, 4.5, H-3α, 1H), 1.04 (s, H_3-17, 3H), 1.04 (m, H-9, 1H) 0.90 (m, H-5, 1H), 0.87 (m, H-1b, 1H), 0.87 (s, H_3-15, 3H), 0.85 (s, H_3-16, 3H); ^{13}C NMR (150 MHz, $CDCl_3$) δ 150.5 (C, C-1'), 134.1 (C, C-3'), 129.4 (CH, 5'), 126.7 (CH, 6'), 125.1 (CH, 2'), 122.7 (CH, 4'), 74.0 (C, C-13), 73.9 (C, C-8), 56.3 (CH, C-5), 56.1 (CH, C-9), 51.4 (CH_2, C-14), 42.1 (CH_2, C-3) 42.0 (CH_2, C-7), 39.8 (CH_2, C-12), 39.4 (CH_2, C-1), 37.2 (C, C-10), 33.5 (CH_3, C-15), 33.3 (C, C-4), 21.6 (CH_3, C-16), 18.3 (CH_2, C-2), 17.5 (CH_2, C-6), 16.8 (CH_2, C-11), 15.5 (CH_3, C-17); EIMS *m/z* (rel. int.) 376 [M^+] (9), 340 (100), 209, (79), 204 (68), 137 (60); HREIMS (70 eV): calcd for $C_{23}H_{33}O_2Cl$ 376.2169. Found 376.2148 Δamu 0.0011.

To the suspension of anhydrous $CeCl_3$ an aliquot (2.85 mL, 0.57 mmol, 1.5 equiv.) of a THF solution of 4-fluorophenylmagnesium bromide (2.0 M) was added. A yellow oil obtained from the procedure *vide supra* was purified via normal phase semi-preparative HPLC (20% EtOAc, 80% hexane) to afford a white solid which was recrystallized from MeOH to give white orthorhombic crystals of **3.209** (71 mg, 52%).

8β, 13β-Dihydroxy-13α-4´-fluorophenylpodocarpane (**3.211**): white needles from MeOH, (52 % yield) mp 176-178 °C; $[\alpha]_D^{23}$ −105.6 (*c* 0.9, $CHCl_3$); IR (film) ν_{max} 3267 (br.), 2946, 1509, 1220, 824, 757 cm^{-1}; ^1H NMR (600 MHz, $CDCl_3$) δ 7.43 (dd, $^3J_{H,H}$ = 9.2, $^4J_{F,H}$ = 5.5, H-2' and H-6', 2H), 7.00 (dd, $^3J_{H,H}$ = 9.2, $^3J_{F,H}$ = 8.8, H-3' and H-5', 2H), 1.94 (m, H-12a, 1H), 1.90 (m, H-11a), 1.84 (m, H-12b, 1H) 1.81 (m, H-14β, 1H), 1.77 (m, H-1a, 1H), 1.76 (m, H-7β(beta), 1H), 1.66 (m, 11b, 1H), 1.65 (m, H-14α, 1H), 1.64 (m, H-2a, 1H), 1.55 (m, H_2-6, H-3α, 3H), 1.43 (m, H-2b, 1H), 1.41 (m, H-7α, 1H), 1.16 (td, *J* = 13.6, 4.4 Hz, H-3β, 1H), 1.05 (s, H_3-17, 3H), 1.05 (m, H-9, 1H) 0.91 (m, H-5, 1H), 0.88 (m, H-1b, 1H), 0.88 (s, H_3-15, 3H), 0.85 (s, H_3-16, 3H); ^{13}C NMR (150 MHz, $CDCl_3$) δ 161.6 (C, d, $^1J_{F,C}$ = 245.4, C-4'), 144.2 (C, d, $^4J_{F,C}$ = 3.3, C-1'), 126.2 (CH, d, $^3J_{F,C}$ = 7.6, C-2', C-6'), 114.1 (CH, d, $^2J_{F,C}$ = 20.8, C-3', C-5), 74.0 (C, C-13), 73.8 (C, C-8), 56.4 (CH, C-5), 56.7 (CH, C-9), 51.7 (CH_2, C-14), 42.3 (CH_2, C-3) 42.1 (CH_2, C-7), 40.0 (CH_2, C-12), 39.5 (CH_2, C-1), 37.3 (C, C-10), 33.5 (CH_3, C-15), 33.3 (C, C-4), 21.7 (CH_3, C-16), 18.4 (CH_2, C-2), 17.6 (CH_2, C-6), 16.9 (CH_2, C-11), 15.5 (CH_3, C-17); EIMS *m/z* (rel. int.) 360 [M^+] (17), 342 (26), 324,

(26), 193 (100), 123 (48); HREIMS (70 eV): calcd for $C_{23}H_{33}O_2F$ 360.2462. Found 360.2465 Δamu 0.0003.

To the suspension of anhydrous $CeCl_3$ an aliquot (11.4 mL, 0.57 mmol, 1.5 equiv.) of a THF solution of 4-chloro-2-methylphenylmagnesium bromide (0.5 M) was added. A yellow oil obtained from the procedure *vide supra* was purified via normal phase semi-preparative HPLC (17% EtOAc, 83% hexane) to afford a white solid which was recrystallized from MeOH to give white orthorhombic crystals of **3.209** (53 mg, 36%).

8β, 13β-Dihydroxy-13α-4´-chloro-2'-methylphenylpodocarpane (**3.212**): white needles from MeOH, (36% yield) mp 207-209 °C; $[\alpha]_D^{23}$ −23.6 (*c* 0.4, $CHCl_3$); IR (film) ν_{max} 3260 (br.), 2924, 1481, 1201, 862, 759 cm^{-1}; ^1H NMR (600 MHz, $CDCl_3$) δ 7.29 (d, *J* = 8.3, H-6', 1H), 7.12 (d, *J* = 2.2, H-3', 1H), 7.08 (dd, *J* = 8.5, 2.2, H-5', 1H), 2.57 (s, H-7', 3H), 2.08 (dt, *J* = 9.6, 3.1, H-12a, 1H), 2.02 (dd, *J* = 14.2, 4.0, H-14β, 1H) 1.90 (m, H-11a and H-12b, 2H), 1.76 (m, H-1a and H-7a, 2H), 1.66 (m, H-11b and H-14α, 2H) 1.65 (m, H-2a, 1H), 1.55 (m, H-6, 2H), 1.44 (t, *J* = 3.3, H-2b, 1H), 1.40 (m, H-3α, 1H), 1.15 (td, *J* = 13.5, 4.6, H-3β, 1H), 1.05 (s, H_3-17, 3H), 1.00 (m, H-9, 1H) 0.89 (m, H-5, 1H), 0.87 (s, H_3-15, 3H), 0.86 (m, H-1b, 1H), 0.85 (s, H_3-16, 3H); ^{13}C NMR (150 MHz, $CDCl_3$) δ 143.4 (C, C-1'), 138.6 (C, C-2'), 132.5 (CH, C-3'), 132.4 (C, C-4'), 126.5 (CH, C-6'), 125.4 (CH, C-5'), 75.4 (C, C-13), 73.9 (C, C-8), 56.4 (CH, C-5), 56.3 (CH, C-9), 49.0 (CH_2, C-14), 42.3 (CH_2, C-7), 42.1 (CH_2, C-3), 39.5 (CH_2, C-1), 38.5 (CH_2, C-12), 37.3 (C, C-10), 33.5 (CH_3, C-15), 33.3 (C, C-4), 22.2 (CH_3, C-7'), 21.7 (CH_3, C-16), 18.4 (CH_2, C-2), 17.6 (CH_2, C-6), 16.8 (CH_2, C-11), 15.5 (CH_3, C-17); EIMS *m/z* (rel. int.) 390 [M^+] (16), 354 (52), 223, (100), 179 (32), 153 (46); HREIMS (70 eV): calcd for $C_{24}H_{35}O_2Cl$ 390.2326. Found 390.2336 Δamu 0.001.

6.2.5. LAH reduction of 3.188

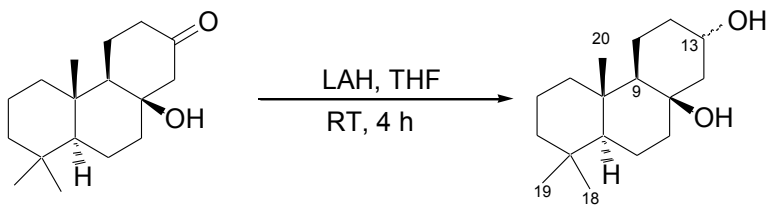

3.188

3.207 (*R*)
3.208 (S)

$LiAlH_4$ (45.7mg, 1.21 mmol, 3 equiv.) was taken up in anhydrous THF (10 mL). The ketol **3.188** (106 mg, 0.40 mmol) was added to the solution and allowed to stir under argon (4 h) at ambient temperatures. The reaction was quenched with a sat. NH_4Cl solution, which formed a precipitate on addition. The solution was filtered through a Celite 545 plug and the filtrate was washed with water (2 × 5 mL) and sat. Brine (1 x 5 mL). The organic portion was dried using anhydrous $MgSO_4$ and concentrate *in vacuo* to afford white crystals (101 mg, 91%). The product of this reaction afforded a pair of isomers in a ratio of 2:1 of **3.207** and **3.208**, with compound **3.207** being the major product.

6.2.6. Synthesis of 1-methyl-2,3,4-tetrahydro-naphthalen-1-ol (3.213)

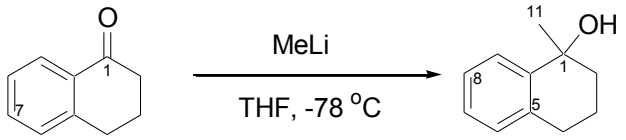

3.214 **3.213**

α-Tetralone (**3.214**, 500mg, 0.455 mL, 3.4 mmol) was dissolved in anhydrous THF (25 mL) with stirring under an argon atmosphere. The solution was cooled to -78 °C and MeLi (7 mL, 11.2 mmol, 1.6 M in THF, 3.3 equiv) added. The reaction was allowed to warm to room temperature, while stirring (12 h) and quenched with a sat. $NHCO_3$ solution (25 mL). The organic fraction was extracted with diethyl ether (2 x 25 mL). The combined organic fraction were washed with water (2 x 25 mL) and sat. brine (1 x 25 mL) and dried over $MgSO_4$. The organic fraction was concentrated under reduced pressure to yield a brown oil, which was crystallized from hot hexane to yield **3.213** as off-white needles (420 mg, 2.59 mmol, 76 % yield)

1-Methyl-2,3,4-tetrahydro-naphthalen-1-ol (**3.213**): off white needles; mp 78-79 °C; IR (solid) ν_{max} 3441 (br.), 2928, 2352, 1688, 1453 cm^{-1}; ^1H NMR ($CDCl_3$, 600 MHz) δ 7.58 (d, *J* = 7.6, H-9, 1H), 7.20 (br s, H-7 and H-8, 2H), 7.06 (d, *J* = 7.2, H-6, 1H), 2.79 (t, *J* = 5.4, H_2-4, 2H), 1.95 (t, *J* = 7.00, H_2-2, 2H), 1.60 (br s, H_2-3, 2H), 1.56 (s, H_3-11, 3H); ^{13}C ($CDCl_3$, 150 MHz) δ 142.9 (q, C-10), 136.2 (q, C-5), 128.8 (CH, C-9), 127.1 (CH, C-8), 126.3 (CH, C-7), 126.3 (CH, C-6), 70.6 (q, C-1), 39.8 (CH_2, C-2), 30.7 (CH_3, C-11), 29.9 (CH_2, C-4), 20.4 (CH_2, C-3); HREIMS (70 eV): calcd for $C_{11}H_{14}O$ 162.1045. Found 162.1048 Δamu 0.0003.

6.2.7. Synthesis of 1-isocyano-1-methyl-2,3,4-tetrahydro-naphthalene (3.215)

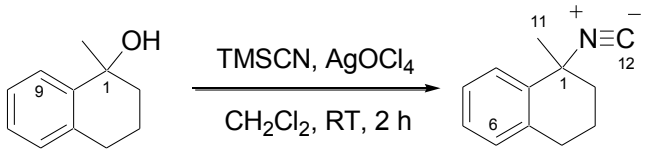

3.213 **3.215**

The tertiary alcohol **3.213** (128 mg, 0.79 mmol) was dissolved in dry DCM (1 mL) under argon. TMSCN (210 μL, 1.58 mmol, 2.0 equiv) was injected into the reaction vessel. Solid silver perchlorate (164 mg, 0.79 mmol, 1 equiv.) was added and allowed to stir at ambient temperatures (2 h). The reaction was quenched with sat. $NaHCO_3$ solution (1 mL), allowed to stir and vent for 10 minutes to remove any unreacted TMSCN. The insoluble AgOH, AgCl and $AgOCl_4$ was removed by filtering the solution through a Celite 545 plug. The Celite 545 plug was washed with ethyl acetate (100 mL) and dried with $MgSO_4$. The organic fraction was concentrated *in vacuo*. and purified on a short silica column (2:1 hexane:ethyl acetate). The isonitrile was finally purified with HPLC (12.5% EtOAc, 87.5% hexane) to yield **3.215** as a brown oil (91.8 mg, 0.190 mmol, 68 %)

1-Isocyano-1-methyl-2,3,4-tetrahydro-naphthalene (**3.215**): brown oil; IR (film) ν_{max} 2937, 2362, 2190, 1589, 1015 cm^{-1}; ^1H NMR ($CDCl_3$, 600 MHz) δ 7.47 (d, *J* = 7.6, H-9, 1H), 7.22 (br. s, H-7 and H-8, 2H), 7.09 (d, *J* = 7.2, H-6, 1H), 2.82 (t, *J* = 6.0, H_2-4, 2H), 1.90 (t, *J* = 6.9, H_2-2, 2H), 1.72 (s, H_3-11, 3H), 1.57 (br s, H_2-3, 2H); ^{13}C ($CDCl_3$, 150 MHz) δ 167.9 (q, t, $^1J_{N,C}$ = 4.4 Hz, C-12), 135.8 (q, C-10), 135.7 (q, C-5), 129.7 (CH, C-9), 127.8 (CH, C-8), 127.7 (CH, C-7), 126.7 (CH, C-6), 68.0 (q, C-1), 38.7 (CH_2, C-2), 29.2 (CH_3, C-11), 28.8 (CH_2, C-4), 19.2 (CH_2, C-3); HREIMS (70 eV): calcd for $C_{12}H_{13}N$ 171.1044. Found 171.1048 Δamu 0.0004.

6.2.8. Attempted conversion of the tertiary alcohol of 3.188 to an isonitrile functionality

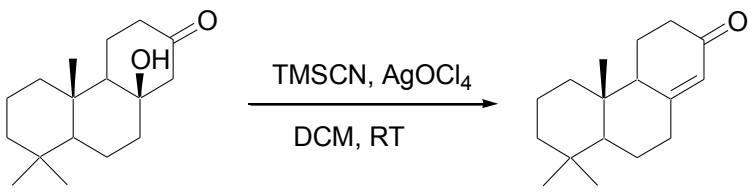

3.188 **3.217**

The tertiary alcohol **3.188** (100 mg, 0.38 mmol) was dissolved in dry DCM (1 mL) under argon. TMSCN (97 µL, 0.76 mmol, 2.0 equiv) was injected into the reaction vessel. Solid silver perchlorate (78 mg, 0.3.8 mmol, 1 equiv.) was added and allowed to stir at ambient temperatures (2 h). The reaction was quenched with sat. $NaHCO_3$ solution (1 mL), allowed to stir and vent for 10 minutes to remove any unreacted TMSCN. The insoluble AgOH, AgCl and $AgOCl_4$ was removed by filtering the solution through a Celite 545 plug. The Celite 545 plug was washed with ethyl acetate (100 mL) and dried with $MgSO_4$. The organic fraction was concentrated *in vacuo*. and purified on a short silica column (3:1 hexane:ethyl acetate). The isonitrile was finally purified with HPLC (20% EtOAc, 80% hexane) to yield **3.217** as a white crystal (67.4 mg, 0.27 mmol, 72 %). The spectroscopic and physical data of **3.217** was consistent with that published in literature.[472,473]

6.2.9. Parasite cultivation

The screening of the synthetic compounds was carried out by Dr. R. van Zyl at the University of Witwatersrand. The chloroquine-resistant Gambian FCR-3 strain was cultured *in vitro* according to the method described by Jensen and Trager.[474] For experimental purposes the cultures were synchronized with 5 % D-sorbitol when the parasites were in the ring.[475] Human ethics clearance for use of human blood was obtained from the University of the Witwatersrand Human Ethics Committee (M090532) and the University of the Witwatersrand Biosafely Committee approved the use of *Plasmodium falciparum* for *in vitro* experimental purposes (number: IOC090503).

6.2.10. Antiplasmodial screening

The antimalarial activity of the various compounds was determined using the tritiated hypoxanthine incorporation assay.[217] The parasite suspension, consisting of predominately the ring stage, was adjusted to a 0.5 % parasitemia and 1 % hematocrit and exposed to the various concentrations of compounds for a single cycle of parasite growth. All assays were carried out using untreated parasites and uninfected red blood cells as controls. Labelled ^{3}H-hypoxanthine (0.5 µCi/ well) was

added after 24 h and the cells harvested after a further 24 h incubation period. The concentration that inhibited 50 % of parasite growth (IC_{50} value) was determined from the log sigmoid dose response curve generated by the Enzfitter® software. Chloroquine, quinine, primaquine, pyrimethamine and cycloproguanil were used as the reference antimalarial agents. All compounds were tested in at least three independent experiments and statistical analysis using the student t-test performed, where a p value of less than 0.05 was regarded as significant.

6.2.11. Haemolytic screening

Freshly obtained human whole blood was washed three times by centrifugation (1500 rpm for 5 min) in isotonic phosphate buffer saline (pH 7.2) and the buffy coat and plasma discarded. The pellet was resuspended in RPMI-1640 culture media, HEPES and glucose supplemented with 10% human plasma and $NaHCO_3$ (pH7.4) to a final hematocrit of 1% (v/v). The compounds (50 and 100µM) were incubated with the erythrocytes for 48 h at 37 °C. Thereafter, the suspension was centrifuged at 1500 rpm for 5 min at room temperature and the absorbance of the supernatant read at 412 nm. The observed haemolysis was expressed as a percentage of the positive control, 0.2 % (v/v) Triton X-100.[476]

6.3. Chapter 4 experimental details

6.3.1. Pyridine hemichrome inhibition of β-haematin assay (Phi-β Assay)

A fresh haematin stock solution (1.680 mM) was prepared by dissolving porcine haemin in a solution of sodium hydroxide (0.1 M). The stock solution (20.2 µL) was pipetted into an 2.0 mL Eppendorf tube and incubated in a water bath (3-5 min at 60 °C). Stock solutions of **3.203-3.207**, **3.209-3.212** and **3.215** in methanol (168.0 mM, 10 equiv. relative to haematin) were prepared. Aliquots of these stock solutions (2.02 µL) were added to the respective Eppendorf tubes after neutralization of the haematin stock solution with HCl (2.02 µL, 1.0 M). Accuracy was important and thus all aliquots were added with Eppendorf Auto-pipettes (0.50-10.00 µL and 10.0-100.0 µL volume ranges). It is important to note that on addition of the test solutions to the neutralized haematin stock solution, no precipitation was observed. An aliquot of the control solution, chloroquine diphosphate (2.02 µL , 50.3 mM, 3.0 equiv. in 1.0 M HCl), was added to the basic haematin solution. In order to maintain

consistency methanol was added (2.02 μL) to the Eppendorf tubes containing the control and chloroquine solutions. After incubation, an aliquot of the acetate buffer (11.74 μL, the method used for preparation of the buffer is given below) was added to each Eppendorf tube and the reaction was incubated at 60 ^{o}C for 60 min. The reaction was quenched at room temperature with the addition of 5% (v/v) pyridine (900 μL, 200 mM Hepes, pH 8.2) solution followed by the addition of 5% (v/v) pyridine (1100 μL, 20 mM Hepes. pH 7.5). The Eppendorf tubes were sonicated in order to ensure complete dissolution of haematin and β-haematin, any precipitate was allowed to settle at ambient temperature for at least 15 minutes.[313] The supernatant was decanted off and transferred to a quartz cuvette in order to measure its UV/vis absorbance (350-700 nm).

6.3.1.1. Preparation of the 12.9 M acetate buffer

The preparation of the 12.9 M acetate buffer solution was prepared as follows: sodium acetate trihydrate (126.3 g) was dissolved in glacial acetic acid (94.56 mL). The solution was warmed slowly to 60 ^{o}C to ensure complete dissolution of NaOAc. This solution is required to have a pH of 5.00, which is essential for the success of the assay. The buffer solution temperature was retained (60 ^{o}C) in order to circumvent the NaOAc crystallizing out as the buffer solution, as the solution is supersaturated at ambient temperatures.[301]

6.3.2. EBHIA assay

Haematin was formed by dissolving haemin (15 mg) in NaOH (3.0 mL of 0.1 M NaOH). This solution was heated to 60 ^{o}C by emerging the reaction vessel in a preheated water-bath where the haematin solution was constantly stirred (stirrer bar 2mm in diameter and 5mm in length). The base was neutralised by the addition of 1.0M HCl (0.3 mL). The acetate buffer (1.74 mL, 12.9 M, pH 5.00, see above for preparation) was introduced into the system allow the reaction to proceed. In order to gauge to progression of the reaction after 0, 10, 30 or 60 minutes the reaction was stopped by cooling the reaction on ice for 5 minutes. The solution was filtered on an 8 μm cellulose acetate/nitrate Millipore® filter type SC, where it was thoroughly washed with water to remove any residual sodium acetate. The solid was lyophilized for 24 hours.

The effects of the inhibitors were study by conducting the reaction, with the addition of 10 equivalents, relative to haem, of compounds **3.203-3.207**, **3.209-3.212** and **3.215** and 3 equivalents

of chloroquine diphosphate, **2.4**, **2.9**, **2.15**, **2.19**, **2.34** and **2.35**. The chloroquine was added with the 1.0M HCl while the other test solutions (**2.4**, **2.9**, **2.15**, **2.19**, **2.34**, **2.35**, **3.203-3.207**, **3.209-3.212** and **3.215**) were added in a methanol solution (0.3 mL) after neutralization of the haematin solution with 1.0M HCl (0.3 mL). Neutralization of the basic solution occurred within 10 min of the addition of the haemin and allowed to incubate for 3-5 min followed by the addition of the test compounds and finally the pre-incubated buffer solution (as above). An equivalent of methanol was added to the control sample as well as the chloroquine solution in order to maintain consistency throughout the experiment.[314] The samples were incubated for 60 min where the reaction was stopped by cooling the reaction vessel on ice for 5min. The solution was filtered on an 8 µm cellulose acetate/nitrate Millipore® filter type SC, where the precipitate was thoroughly washed with water. The solid was lyopholized (24 h). While all these experiments are reproducible, the successful formation of haematin is dependent upon stirring rate, total volume, vessel dimensions, acetate concentration, pH and temperature. [301] All experimental conditions were accordingly rigorously adhered to.

6.3.3. Docking studies

(i) The receptor model for the free haem (FP) was obtained from the Cambridge Structural Database (CSD code 162267)[303] and the haem dimer group model (HD) was obtained from the Protein Database (PDB code 2q9f)[477] respectively. The FP model underwent energy optimizations using unrestricted DFT calculations in the singlet and triplet electronic states; whilst the quintet electronic state model was optimized using the LANL2DZ[346] pseudopotential to describe the iron atom and then the UB3LYP / 6-31G(d) method for all other atoms. A single-point spin unrestricted energy calculation was performed on the HD crystal structure in the singlet electronic state.

(ii) The ligand models of structures **2.4**, **2.9**, **2.15**, **2.19**, **2.34**, **2.35**, **3.203-3.207**, **3.209-3.212**, **3.215** and **4.1** were constructed and underwent DFT structural optimization. The minimized structures were imported into AutoDockTools, AutoDock atom types were assigned, Gasteiger[347] charges were added and non-polar hydrogens were merged. Bond torsions were assigned and aromatic elements identified. The assigned Gasteiger charges were substituted with MK[350] atomic charges from the DFT optimization output logs. For all atoms other than polar hydrogens and their attached heavy atom, MK[350] charges were computed with attached hydrogens' charges merged into the heavy atom. For polar hydrogens, unmerged charges were used for both the hydrogen and the heavy atom.

(iii) The minimized haem models from Section 4.4 and 4.5 were imported into AutoDockTools, AutoDock atom types were assigned, Gasteiger charges were added and non-polar hydrogens were merged. All rotational elements on the heam targets, i.e. vinyl and carboxylic acid groups, were treated as the flexible residues. The Gasteiger charges were substituted for MK atomic charges as previously mentioned.

(iv) Grid maps for each of the ligands were generated across the active sites, with surrounding residues, using a grid box of 50^3 points (0.325 Å point spacing) referenced to the iron atom. The dockings were executed according to a Lamarckian genetic algorithm to create populations containing 150 individuals and allowing for a maximum of 2.5 x 10^6 energy evaluations for each of 10 unique docks per ligand. The results were clustered and the lowest energy conformer from each cluster printed as part of the docking log file along with its associated energies. These conformers were extracted from the log file using custom scripting and visualized.

6.4. Chapter 5 experimental details

6.4.1. Preparation of aryl glyoxal monohydrates (5.92-5.102)

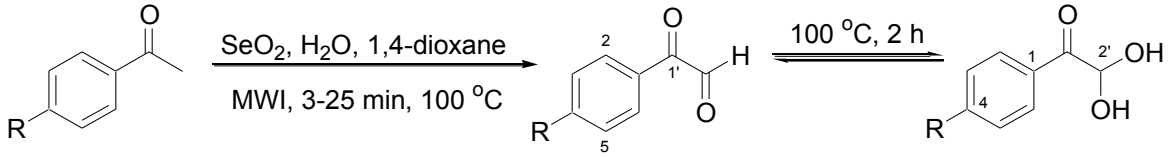

5.91	R = H	**5.27**	R = H	**5.92**	R = H
5.93	R = OMe	**5.28**	R = OMe	**5.98**	R = OMe
5.94	R = NO_2	**5.29**	R = NO_2	**5.99**	R = NO_2
5.95	R = Cl	**5.30**	R = Cl	**5.100**	R = Cl
5.96	R = Br	**5.31**	R = Br	**5.101**	R = Br
5.97	R = F	**5.32**	R = F	**5.102**	R = F

SeO_2 (360 mg, 0.3 mmol, 2.7 equiv.) was suspended in a mixture of 1,4-dioxane (1 mL) and H_2O (20 µL) and the methyl ketone, **5.91** and **5.93-5.97** (1.2 mmol) was added just before microwave irradiation [ramp time (1 min) to a maximum power of 250 W, hold time (3-18 min) at a set temperature of 100 °C]. Following microwave irradiation the reaction solution was rapidly cooled to 50 °C (5 min) by means of propelled airflow and finally allowed to cool to room temperature (*ca.* 20 min). The solution was filtered through Celite 545, in order to remove Se, and washed with MeOH (10 mL). The combined organic filtrate was concentrated under reduced pressure and the organic residue subsequently stirred in boiling H_2O (6 mL) for 2 h and filtered hot to remove any

insoluble precipitate. The aqueous filtrate was cooled on ice to afford crystals of the glyoxal monohydrate product which were collected under vacuum filtration, washed with cold H_2O and dried in a vacuum desiccator to yield the monohydrates **5.92** and **5.98-5.102**.

Phenyl glyoxal monohydrate (**5.92**) white needles from H_2O, (84 % yield) mp 78-80 ^oC, lit. 76-78 ^oC[478]; IR (solid) ν_{max} 3392 (br), 1695, 1595, 1219, 1107, 708 cm^{-1}; ^1H NMR (600 MHz, DMSO- D_6) δ 8.06 (d, *J* = 8.8, H-2 and H-6, 2H), 7.63 (t, *J* = 7.2, H-4, 1H), 7.51 (dd, *J* = 7.89, 7.82, H-3 and H-5, 2H), 5.69 (t, *J* = 7.3, H-2', 1H) ^{13}C NMR (150 MHz, DMSO-D_6) δ 196.3 (q, C-1'), 133.7 (q, C-1), 133.4 (2 x CH, C-3 and C-5), 129.4 (2 x CH, C-2 and C-6), 128.5 (CH, C-4), 89.2 (CH, C-2'); EIMS *m/z* (rel. int.) 106 (9), 105, (100), 78 (5), 77 (77), 51 (27)

4-Methoxyphenyl glyoxal monohydrate (**5.98**) white needles from H_2O, (84 % yield) mp 92-94 ^oC, lit. 93-95 ^oC[421]; IR (solid) ν_{max} 3375 (br.), 1694, 1586, 1219, 1024, 671 cm^{-1}; ^1H NMR (600 MHz, DMSO-D_6) δ 8.05 (d, *J* = 9.0, H-2 and H-6, 2H), 7.02 (d, *J* = 9.0, H-3 and H-5, 2H), 5.96 (t, *J* = 7.1 H-4, 1H), 3.84 (s, H_3-7, 3H); ^{13}C NMR (150 MHz, DMSO-D_6) δ 192.0 (q, C-1'), 163.7 (q, C-4), 131.9 (2 x CH, C-2 and C-6), 126.1 (q, C-1), 113.8 (2 x CH, C-3 and -5), 90.5 (CH, C-2'), 55.5 (CH_3, C-7); EIMS *m/z* (rel. int.) 136 (10), 135 (100), 92 (14), 77 (24), 64 (7)

4-Nitrophenyl glyoxal monohydrate (**5.99**) brown flakes from H_2O, (62 % yield) mp 70-72 ^oC, lit. 67-72 ^oC[421]; IR (solid) ν_{max} 3345 (br.), 1691, 1533, 1346, 1012, 725 cm^{-1}; ^1H NMR (600 MHz, DMSO- D_6) δ 8.35 (d, *J* = 8.8, H-2 and H-6, 2H), 8.29 (d, *J* = 8.8, H-3 and H-5, 2H), 5.91 (s, H-2', 2H); ^{13}C NMR (150 MHz, DMSO-D_6) δ 195.5 (q, C-1'), 149.9 (q, C-4), 138.8 (q, C-1), 130.8 (2 x CH, C-2 and C-6), 123.5 (2 x CH, C-3 and C-5), 89.8 (CH, C-2'); EIMS *m/z* (rel. int.) 181 (26), 150 (100), 135 (7), 104 (24), 76 (12)

4-Chlorophenyl glyoxal monohydrate (**5.100**) white needles from H_2O, (81 % yield) mp 40-41 ^oC, lit. 40-41 ^oC[479]; IR (solid) ν_{max} 3375 (br.), 1694, 1586, 1219, 1012, 810 cm^{-1}; ^1H NMR (600 MHz, DMSO-D_6) δ 8.07 (d, *J* = 8.6, H-2 and H-6, 2H), 7.58 (d, *J* = 8.3, H-3 and H-5, 2H), 5.63 (s, H-2', 1H); ^{13}C NMR (150 MHz, DMSO-D_6) δ 195.3 (q, C-1'), 138.2 (q, C-1), 132.3 (2 x CH, C-3 and C-5), 131.4 (2 x CH, C-2 and C-6), 128.7 (q, C-4), 89.7 (CH, C-2'); EIMS *m/z* (rel. int.) 170 (2), 141 (31), 139 (100), 111 (47), 75 (21)

4-Bromophenyl glyoxal monohydrate (**5.101**) white needles from H_2O, (89 % yield) mp 52-54 ^oC, lit. 51-53 ^oC[479]; IR (solid) ν_{max} 3374 (br.), 1694, 1583, 1219, 1025, 735 cm^{-1}; ^1H NMR (600 MHz, DMSO-D_6) δ 7.99 (d, *J*= 8.8, H-2 and H-6, 2H), 7.73 (d, *J* = 8.6, H-3 and H-5, 2H), 5.62 (t, *J* = 6.99, H-2', 1H); ^{13}C NMR (150 MHz, DMSO-D_6) δ 195.5 (q, C-1'), 132.7 (q, C-1), 131.6 (2 x CH, C-3 and C-5), 131.4 (2 x CH, C-2 and C-6), 127.5 (q, C-4), 89.6 (CH, C-2'); EIMS *m/z* (rel. int.) 213 (5), 186 (10), 183 (100), 155 (45), 76 (17);

4-Fluorophenyl glyoxal monohydrate (**5.102**) white needles from H_2O, (87% yield) mp 82-84 ^oC, lit. 80-82.4 ^oC[480]; IR (solid) ν_{max} 3349 (br.), 1700, 1231, 1062, 804, 686 cm^{-1}; ^1H NMR (600 MHz, DMSO-D_6) δ 8.16 (td, *J* = 6.0, $^4J_{F,H}$ = 3.3, H-2 and H-6, 2H), 7.35 (t, *J* = 8.8, $^3J_{F,H}$ = 9.7, H-3 and H-5, 2H), 5.63 (t, *J* = 6.38, H-2', 1H); ^{13}C NMR (150 MHz, DMSO-D_6) δ 195.0 (q, C-1'), 165.0 (q, $^1J_{F,C}$ = 251.4, C-4), 132.4 (2 x CH, $^3J_{F,C}$ = 9.7, C-2 and C-6), 130.2 (q, $^4J_{F,C}$ = 2.2, C-1), 116.2 (2 x CH, $^2J_{F,C}$ = 21.6, C-3 and C-5), 89.5 (CH, C-2'); EIMS *m/z* (rel. int.) 124 (7), 123 (100), 96 (5), 95 (57), 75 (14)

6.4.2. Synthesis of indole glyoxals

6.4.2.1. Preparation of 3-indolylglyoxylic acid (5.106)

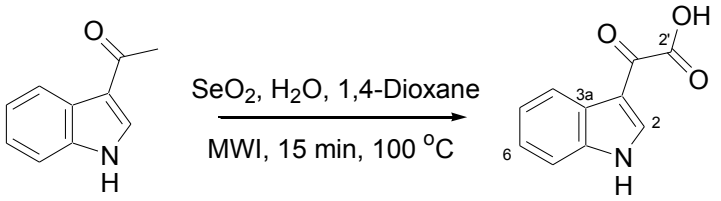

5.105 **5.106**

SeO_2 (171 mg, 1.54 mmol, 2.7 equiv) was suspended in a mixture of 1,4-dioxane (1 mL) and H_2O (20 µL) and 3-acetylindole (**5.105**, 90 mg, 0.57 mmol) was added just before microwave irradiation [ramp time (1 min) to a maximum power of 250 W, hold time (15 min) at a set temperature of 100 °C]. Following microwave irradiation the reaction solution was rapidly cooled to 50 ^oC (5 min) by means of propelled airflow and finally allowed to cool to room temperature (*ca.* 20 min). The solution was filtered through Celite 545 , in order to remove Se, and washed with CH_2Cl_2 (10 mL). The combined organic filtrate was washed with water (2 x 10 mL) and sat. brine (1 x 10mL), and the organic fraction was dried over anhydrous $MgSO_4$, filtered and concentrated under reduced pressure to afford a brick red solid (**5.106**).

3-Indolylglyoxylic acid (**5.106**) brick red solid (100% yield); IR (solid) ν_{max} 3209 (br.), 1701, 1599, 1231, 1063, 804 cm^{-1}; ^1H NMR (600 MHz, CD_3OD) δ 8.52 (s, H-2, 1H), 8.28 (d, *J* = 7.51, H-4, 1H), 7.49 (d, *J* = 7.89, H-7, 1H), 7,28 (m, H-5 and H-6, 2H); ^{13}C NMR (150 MHz, CD_3OD) δ 181.2 (q, C-1'), 166.0 (q, C-2'), 139.5 (CH, C-2), 138.3 (q, C-3a), 127.5 (q, C-7a), 125.1 (CH, C-5), 124.0 (CH, C-6), 122.9 (CH, C-4), 114.4 (q, C-3), 113.2 (CH, C-7); EIMS *m/z* (rel. int.) 189 $[M+H]^+$ (18), 161 (22), 144 (100), 115 (26), 102 (5); HREIMS (70 eV): calcd for $C_{10}H_7NO_3$ 189.0426. Found 189.0421, Δamu 0.0005

6.4.2.2. N-Boc protection of 3-acetylindol (5.105)

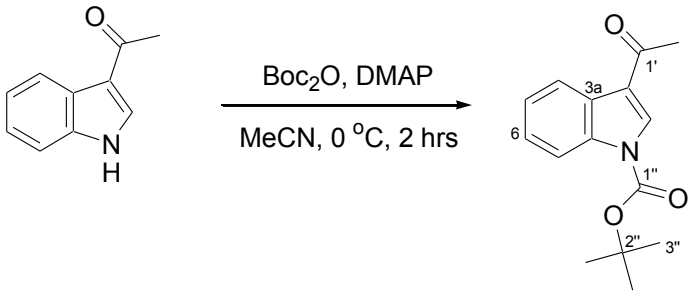

5.105 **5.89**

3-Acetylindole (**5.105**, 2.5 g, 15.7 mmol) was dissolved in dry MeCN (37.5 mL) and cooled on ice. Di-*tert*-butyl dicarbonate (5.14g, 23.6 mmol, 1.5 equiv.) was added followed by 4-dimethylaminopyridine (191.9 mg, 1.57 mmol, 0.1 equiv.) and allowed to stir under argon for two hours. The solvent and excess reagents were removed under reduced pressure to yield spectropically pure white solid of 3-acetylindole-1-carbamate (**5.89**).

3-Acetylindole-1-carbamate (**5.89**), white needles from hexane (100 % yield), mp 140-142 ^{o}C, lit. 143-144 ^{o}C[442]; IR (solid) ν_{max} 3274, 1635, 1596, 1509, 1287, 847 cm^{-1}; ^{1}H NMR (600 MHz, DMSO-D_6) δ 8.53 (s, H-2, 1H), 8.24 (d, *J* = 8.0, H-4, 1H), 8.09 (d, *J* =8.1, H-7, 1H), 7.41 (dd, *J* = 8.7, 7.8, H-6, 1H), 7.35 (dd, *J* = 8.7, 7.6, H-5, 1H), 2.55 (s, H_3-2', 3H), 1.67 (s, H_3-3'', 9H); ^{13}C NMR (150 MHz, DMSO-D_6) δ 193.8 (q, C-1'), 149.1 (q, C-1''), 135.5 (CH, C-2), 132.3 (q, C-3a), 127.3 (q, C-7a), 125.4 (CH, C-6), 124.3 (CH, C-5), 122.6 (CH, C-4), 120.6 (q, C-3), 114.9 (CH, C-7), 85.3 (q, C-2''), 28.1 (CH_3, C-3''), 27.7 (CH_3, C-2'); HREIMS (70 eV): calcd for $C_{15}H_{18}NO_3$ 260.1287. Found 260.1302, Δmmu 0.0015.

6.4.2.3. Selenium dioxide oxidation of 3-acetylindole-1-carbamate (5.89)

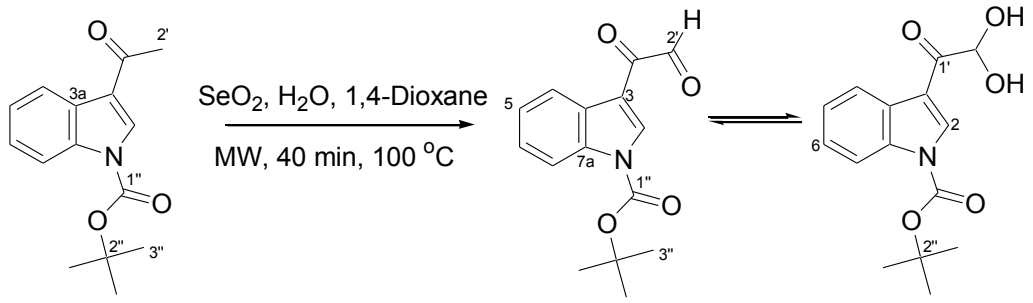

5.89 **5.88** **5.107**

SeO_2 (171 mg, 1.54 mmol, 2.7 equiv) was suspended in a mixture of 1,4-dioxane (1 mL) and H_2O (20 µL) and the indole methyl ketone, **5.89** (148 mg, 0.57 mmol) was added just before microwave irradiation [ramp time (1 min) to a maximum power of 250 W, hold time (40 min) at a set temperature of 100 °C]. Following microwave irradiation the reaction solution was rapidly cooled to 50 °C (5 min) by means of propelled airflow and finally allowed to cool to room temperature (*ca.* 20 min). The solution was filtered through Celite 545 , in order to remove Se, and washed with CH_2Cl_2 (10 mL). The combined organic filtrate was washed with water (2 x 10 mL) and sat. brine (1 x 10mL), and the organic fraction was dried over anhydrous $MgSO_4$, filtered and concentrated under reduced pressure to afford a yellow oil containing an inseparable equilibrium mixture of **5.88** and **5.107** respectively.

3-Acetylindole-1-carbamate glyoxal (**5.88**), yellow oil (86 % yield, C18 60% MeCN 40 % H_2O; 62 % of the equilibrium mixture), IR (film) ν_{max} 3405, 1741, 1665, 1450, 1236, 745 cm^{-1}; ^1H NMR (600 MHz, $CDCl_3$) δ 9.53 (s, H-2', 1H), 8.89 (s, H-2, 1H), 8.39 (d, *J* = 7.6, H-4, 1H), 8.18 (d, *J* = 7.7, H-7, 1H), 7.43 (m, H-6, 1H), 7.40 (m, H-5, 1H), 1.71 (s, H_3-3'', 9H); ^{13}C NMR (150 MHz, $CDCl_3$) δ 190.1 (CH, C-2'), 182.6 (q, C-1'), 148.6 (q, C-1''), 136.8 (CH, C-2), 135.2 (q, C-3a), 127.5 (q, C-7a), 125.8 (CH, C-6), 124.7 (CH, C-5), 122.4 (CH, C-4), 115.1 (CH, C-7), 114.0 (q, C-3), 86.0 (q, C-2''), 28.0 (CH_3, C-3''); HREIMS: calcd for $C_{15}H_{16}NO_4$ 274.1079. Found 274.1061, Δmmu 0.0018.

3-Acetylindole-1-carbamate glyoxal monohydrate (**5.107**), yellow oil (38 % of the equilibrium mixture); ^1H NMR (600 MHz, $CDCl_3$) δ 8.83 (s, H-2, 1H), 8.29 (d, *J* = 7.6, H-4, 1H), 8.14 (d, *J* = 8.2, H-7, 1H), 7.36 (m, H-6, 1H), 7.34 (m, H-5, 1H), 5.79 (s, H-2', 1H), 1.73 (s, H_3-3'', 9H); ^{13}C NMR (150 MHz, $CDCl_3$) δ 188.5 (q, C-1'), 148.6 (q, C-1''), 136.8 (CH, C-2), 135.4 (q, C-3a), 127.3 (q, C-7a), 126.1 (CH, C-

6), 124.9 (CH, C-5), 122.2 (CH, C-4), 115.2 (CH, C-7), 115.0 (q, C-3), 87.9 (CH, C-2'), 85.7 (q, C-2''), 28.0 (CH_3, C-3'')

6.4.3. Synthesis of bis phenylimidazoles (5.21-5.26)

5.92 R = H
5.98 R = OMe
5.99 R = NO_2
5.100 R = Cl
5.101 R = Br
5.102 R = F

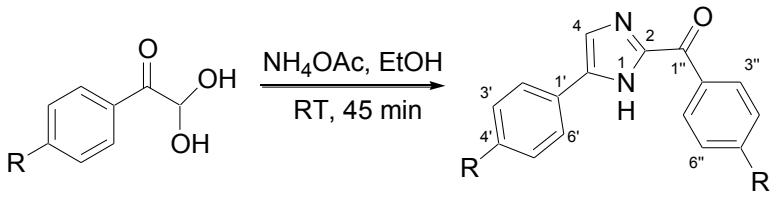

5.21 R = H
5.22 R = OMe
5.23 R = NO_2
5.24 R = Cl
5.25 R = Br
5.26 R = F

NH_4OAc (13.39 mmol, 5 equiv.) was added to an ethanol solution of **5.92**, **5.98-5.102** (2.67 mmol in 17.5 mL). The mixture was stirred at ambient temperature for 45 min until a precipitate formed. The solvent was removed *in vacuo* and the remaining precipate washed with water (20 mL) and filtered to afford tautomeric mixtures of **5.21-5.26**.

2-Benzoyl-5-phenyl-3H-imidazole (**5.21a**): yellow needles from 5% DMSO / 95 % MeOH (100 % yield) mp 203-205 ^{o}C; IR (solid) ν_{max} 3267, 1701, 1456, 1271, 866, 687 cm^{-1}; ^{1}H NMR (600 MHz, DMSO-D_6) δ 13.66 (s, NH-3, 1H), 8.04 (s, H-4, 1H), 7.93 (d, *J* = 7.4, H-2' and H-6', 2H), 7.69 (t, *J* = 7.3, H-5'', 1H), 7.60 (t, *J* = 7.6, H-3'' and H-7'', 2H), 7.56, (m, H-4'' and H-6'', 2H), 7.43 (dd, *J* = 8.3, 7.6, H-3' and H-5', 2H), 7.30 (t, *J* = 7.15, H-4', 1H); ^{13}C NMR (150 MHz, DMSO-D_6) δ 180.8 (q, C-1''), 144.7 (q, C-2), 142.9 (q, C-5), 136.0 (q, C-2''), 133.6 (q, C-1'), 133.0 (CH, C-5''), 130.6 (2 x CH, C-4'' and C-6''), 128.9 (2 x CH, C-3' and C-5'), 128.3 (2 x CH, C-3'' and C-7''), 127.1 (CH, C-4'), 124.9 (2 x CH, C-2' and C-6'), 118.6 (CH, C-4); HRESIMS (70 eV): calcd for $C_{16}H_{12}N_2O$ 249.1028 Found 249.1036, Δamu 0.0008.

2-(p-Methoxybenzoyl)-5-(p-methoxyphenyl)-3H-imidazole (**5.22a**): yellow needles from 5% DMSO / 95 % MeOH (99 % yield, 74% of tautomeric mixture) mp 219-221 ^{o}C; IR (solid) ν_{max} 3264, 1596, 1244, 1025, 829, 773, 655 cm^{-1}; ^{1}H NMR (600 MHz, DMSO-D_6) δ 13.42 (s, NH-3, 1H), 8.69 (d, *J* = 8.8 , H-3'' and H-7'', 2H), 7.91 (s, H-4, 1H), 7.85 (d, *J* = 8.6, H-2' and H-6', 2H), 7.13 (d, *J* = 8.7, H-4'' and H-6'', 2H), 6.99 (d, *J* = 8.5, H-3' and H-5', 2H), 3.88 (s, H_3-6'', 3H), 3.79 (s, H_3-5', 3H); ^{13}C NMR (150 MHz, DMSO-D_6) δ 178.9 (q, C-1''), 163.2 (q, C-5''), 158.5 (q, C-4') 144.7 (q, C-2), 142.6 (q, C-5), 133.1 (2 x CH, C-3'' and C-7''), 128.6 (q, C-2''), 126.4 (q, C-1'), 126.1 (2 x CH, C-2' and C-6'), 117.0 (CH, C-4),

114.0 (2 x CH, C-3' and C-5'), 113.7 (2 x CH, C-4'' and C-6''), 55.5 (CH_3, C-8''), 55.1 (CH_3, C-7'); HRESIMS: calcd for $C_{18}H_{17}N_2O_3$ 309.1239. Found 309.1257, Δamu 0.0018.

2-(p-Methoxybenzoyl)-5-(p-methoxyphenyl)-1H-imidazole (**5.22b**): yellow needles from 5% DMSO / 95 % MeOH (99 % yield, 26% of tautomeric mixture); ^{1}H NMR (600 MHz, DMSO-D_6) δ 13.54 (s, NH-1, 1H), 8.56 (d, *J* = 8.6 , H-3'' and H-7'', 2H), 7.89 (d, *J* = 8.6, H-2' and H-6', 2H), 7.64 (s, H-4, 1H), 7.09 (d, *J* = 8.6, H-4'' and H-6'', 2H), 7.01 (d, *J* = 8.5, H-3' and H-5', 2H), 3.86 (s, H_3-8'', 3H), 3.80 (s, H_3-7', 3H); ^{13}C NMR (150 MHz, DMSO-D_6) δ 179.0 (q, C-1''), 163.0 (q, C-5''), 159.3 (q, C-4') 145.6 (q, C-2), 135.4 (q, C-5), 132.9 (2 x CH, C-3'' and C-7''), 128.9 (q, C-2''), 127.6 (q, C-4), 127.1 (2 x CH, C-2' and C-6'), 121.3 (CH, C-1'), 114.3 (2 x CH, C-3' and C-5'), 113.5 (2 x CH, C-4'' and C-6''), 55.5 (CH_3, C-8''), 55.2 (CH_3, C-7')

2-(p-Nitrobenzoyl)-5-(p-nitrophenyl)-3H-imidazole (**5.23a**): (90 % yield); IR (solid) ν_{max} 3274, 1635, 1596, 1331, 1289, 848 cm^{-1}; ^{1}H NMR (600 MHz, DMSO-D_6) δ 13.94 (s, NH-3, 1H), 8.66 (d, *J* = 8.4, H-3'' and H-7'', 2H), 8.35 (d, H-4'' and H-6'', 2H), 8.28 (s, H-4, 1H), 8.21 (d, *J* = 8.6, H-3' and H-5', 2H), 8.11 (d, *J* = 8.6, H-2' and H-6', 2H); ^{13}C NMR (150 MHz, DMSO-D_6) δ 179.5 (q, C-1''), 149.7 (q, C-5''), 146.1 (q, C-4') 144.9 (q, C-2), 141.2 (q, C-5), 141.0 (q, C-2''), 140.7 (q, C-1'), 131.9 (2 x CH, C-3'' and C-7''), 125.6 (2 x CH, C-2' and C-6'), 124.1 (2 x CH, C-3' and C-5'), 123.3 (2 x CH, C-4'' and C-6''), 122.1 (CH, C-4); HRESIMS: calcd for $C_{17}H_{28}O_2$ 264.2089. Found 264.2083, Δamu 0.0006.

2-(p-Chlorobenzoyl)-5-(p-chlorophenyl)-3H-imidazole (**5.24a**): yellow needles from 5% DMSO / 95 % MeOH (100 % yield, 87% of tautomeric mixture) mp 2.47-249 ^{o}C; IR (solid) ν_{max} 3269, 1612, 1444, 1291, 833, 769; ^{1}H NMR (600 MHz, DMSO-D_6) δ 13.72, (s, NH-3, 1H), 8.50 (d, *J* = 8.4 , H-3'' and H-7'', 2H), 8.14 (s, H-4, 1H), 7.87 (d, *J* = 8.2, H-2' and H-6', 2H), 7.80 (d, *J* = 8.4, H-4'' and H-6'', 2H), 7.60 (d, *J* = 8.3, H-3' and H-5', 2H); ^{13}C NMR (150 MHz, DMSO-D_6) δ 179.6 (q, C-1''), 144.5 (q, C-2), 141.8 (q, C-5), 134.8 (q, C-5''), 132.8 (q, C-4'), 132.6 (2 x CH, C-3'' and C-7''), 131.5 (2 x CH, C-3' and C-5'), 131.4 (CH, C-4'' and C-6''), 127.4 (q, C-2''), 126.8 (2 x CH, C-2' and C-6'), 120.1 (q, C-1'), 119.4 (CH, C-4); HREIMS: calcd for $C_{16}H_{11}N_2OCl_2$ 317.0248. Found 317.0233, Δamu 0.0015.

2-(p-Chlorobenzoyl)-5-(p-chlorophenyl)-1H-imidazole (**5.24b**): yellow needles from 5% DMSO / 95 % MeOH (100 % yield, 13% of tautomeric mixture); ^{1}H NMR (600 MHz, DMSO-D_6) δ 13.89 (s, NH-1, 1H), 8.60 (d, *J* = 8.5 , H-3'' and H-7'', 2H), 8.14 (s, H-4, 2H), 7.95 (d, *J* = 8.3, H-2' and H-6', 2H), 7.67 (d, *J* = 8.4, H-4'' and H-6'', 2H), 7.49 (d, *J* = 8.2, H-3' and -5', 2H); ^{13}C NMR (150 MHz, DMSO-D_6) δ 179.4 (q, C-1''), 144.5 (q, C-2), 141.8 (q, C-5), 138.2 (q, C-5''),134.5 (q, C-2''), 132.6 (2 x CH, C-3'' and C-7''), 132.5 (CH, C-4'), 131.6 (q, C-1'), 128.6 (2 x CH, C-3' and C-5'), 128.5 (CH, C-4'' and C-6''), 126.5 (2 x CH, C-2' and C-6'), 119.3 (CH, C-4)

2-(p-Bromobenzoyl)-4-(p-bromophenyl)-3H-imidazole (**5.25a**): yellow needles from 5% DMSO / 95 % MeOH (63 % yield) mp 202-204 ^{o}C; IR (solid) ν_{max} 3264, 1610, 1289, 901, 829, 766 cm^{-1}; ^{1}H NMR (600 MHz, DMSO-D_6) δ 13.72, (s, NH-3, 1H), 8.50 (d, *J* = 8.5 , H-3'' and H-7'', 2H), 8.15 (s, H-4, 1H), 7.88 (d, *J* = 8.5, H-2' and H-6', 2H), 7.81 (d, *J* = 8.5, H-4'' and H-6'', 2H), 7.61 (d, *J* = 8.7, H-3' and H-5', 2H); ^{13}C NMR (150 MHz, DMSO-D_6) δ 179.9 (q, C-1''), 144.5 (q, C-2), 141.8 (q, C-5), 134.8 (q, C-5''), 132.8 (q, C-1'), 132.6 (2 x CH, C-3'' and C-7''), 131.6 (2 x CH, C-3' and C-5'), 131.6 (2 x CH, C-4'' and C-6''), 127.5 (q, C-2''), 126.9 (2 x CH, C-2' and C-6'), 120.1 (q, C-4'), 119.4 (CH, C-4); HRESIMS: calcd for $C_{16}H_{11}N_2OBr_2$ 404.9238. Found 404.9252, Δmmu 0.0014.

2-(p-Fluorobenzoyl)-5-(p-fluorophenyl)-3H-imidazole (**5.26a**): yellow needles from 5% DMSO / 95 % MeOH (63 % yield, 85% of tautomeric mixture) mp 240-242 ^{o}C; IR (film) ν_{max} 3273, 1596, 1509, 1289, 846, 697 cm^{-1}; ^{1}H NMR (600 MHz, DMSO-D_6) δ 13.64 (s, NH-3, 1H), 8.71 (t, *J* = 8.8, $^{4}J_{F,H}$ = 6.9, H-3'' and H-7'', 2H), 8.06 (s, H-4, 1H), 7.96 (t, *J* = 8.6, $^{4}J_{F,H}$ = 9.9, H-2' and H-6', 2H), 7.41 (d, *J* = 4.8, $^{3}J_{F,H}$ = 9.8, H-4'' and H-6'', 2H), 7.24 (d, *J* = 5.0, $^{3}J_{F,H}$ = 9.7, H-3' and H-5', 2H); ^{13}C NMR (150 MHz, DMSO-D_6) δ 179.0 (q, C-1''), 165.0 (q, $^{1}J_{F,C}$ = 253.1, C-5''), 161.5 (q, $^{1}J_{F,C}$ = 243.1, C-4'), 144.5 (q, C-5), 142.0 (q, C-2), 133.7 (2 x CH, $^{3}J_{F,C}$ = 9.7, C-3'' and C-7''), 132.5 (CH, $^{4}J_{F,C}$ = 2.1, C-2''), 130.2 (CH, $^{4}J_{F,C}$ = 2.1, C-1'), 128.5 (CH, $^{3}J_{F,C}$ = 8.6, C-4'' and C-6''), 126.8 (2 x CH, $^{3}J_{F,C}$ = 8.7, C-2' and C-6'), 118.5 (CH, C-4), 114.8 (CH, $^{2}J_{F,C}$ = 21.7, C-4'' and C-6'') 114.7 (CH, $^{2}J_{F,C}$ = 22.0, C-3' and C-5'); HREIMS: calcd for $C_{16}H_{11}N_2OF_2$ 285.0839. Found 285.0855, Δamu 0.0016.

2-(p-Fluorobenzoyl)-5-(p-fluorophenyl)-1H-imidazole (**5.26b**): yellow needles from 5% DMSO / 95 % MeOH (63 % yield, 15% of tautomeric mixture); ^{1}H NMR (600 MHz, DMSO-D_6) δ 13.81 (s, NH-1, 1H), 8.57 (m, H-3'' and H-7'', 2H), 8.06 (s, H-4, 1H), 7.89 (m, H-2' and H-6', 2H), 7.41 (m, H-4'' and H-6'', 2H), 7.24 (m, H-3' and H-5', 2H); ^{13}C NMR (150 MHz, DMSO-D_6) δ 179.4 (q, C-1''), 165.0 (q, $^{1}J_{F,C}$ = 249.6, C-5''), 161.5 (q, $^{1}J_{F,C}$ = 247.3, C-4'), 146.0 (q, C-5), 142.2 (q, C-2), 133.7 (2 x CH, $^{3}J_{F,C}$ = 9.8, C-3'' and C-7''), 132.4 (CH, $^{4}J_{F,C}$ = 2.0, C-2''), 130.2 (CH, $^{4}J_{F,C}$ = 2.0, C-1'), 128.1 (2 x CH, $^{3}J_{F,C}$ = 8.7, C-2' and C-6'), 128.0 (CH, $^{3}J_{F,C}$ = 8.5, C-4'' and C-6''), 117.9 (CH, C-4), 114.6 (CH, $^{2}J_{F,C}$ = 21.3, C-4'') 114.5 (CH, $^{2}J_{F,C}$ = 22.1, C-3' and C-5')

6.4.3.1. Synthesis of the ascidian natural product 2-(p-hydroxybenzoyl)-5-(p-hydroxyphenyl)-3H-imidazole (5.111)

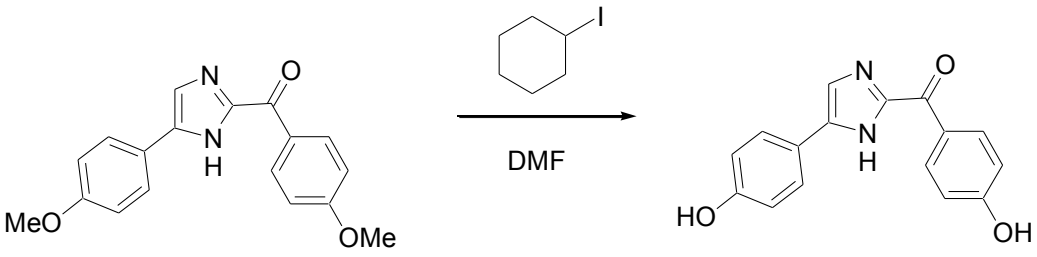

5.22 **5.111**

A solution of **5.22** (100 mg, 0.325 mmol) and iodocyclohexane (3.25 mmol, 10 equiv.) in DMF (1 mL) was refluxed under argon for 12 h. The reaction was quenched with H_2O and the organic fraction taken up in EtOAc. The organic layer was washed with sat. $NaHSO_3$ solution (2x 5 mL) and sat. brine (1 x 5mL) and dried with anhydrous $MgSO_4$. The solvent was removed under reduced pressure to yield a yellow solid **5.111** in 93% yield.

2-(p-Hydroxybenzoyl)-5-(p-hydroxyphenyl)-3H-imidazole (**5.111a**): yellow needles from 5% DMSO / 95 % MeOH (93 % yield, 74% of tautomeric mixture) mp 293-295 ^{o}C, lit. 295-297^{o}C[457]; IR (film) ν_{max} 3370, 3254 (br.), 1620, 1290, 871, 711 cm^{-1}; ^{1}H NMR (600 MHz, DMSO-D_6) δ 13.42 (s, NH-3, 1H), 8.69 (d, *J* = 8.8 , H-3'' and H-7'', 2H), 7.91 (s, H-4, 1H), 7.85 (d, *J* = 8.6, H-2' and H-6', 2H), 7.13 (d, *J* = 8.7, H-4'' and H-6'', 2H), 6.99 (d, *J* = 8.5, H-3' and H-5', 2H); ^{13}C NMR (150 MHz, DMSO-D_6) δ 178.9 (q, C-1''), 163.2 (q, C-5''), 158.5 (q, C-4') 144.7 (q, C-2), 142.6 (q, C-5), 133.1 (2 x CH, C-3'' and C-7''), 128.6 (q, C-2''), 126.4 (q, C-1'), 126.1 (2 x CH, C-2' and C-6'), 117.0 (CH, C-4), 114.0 (2 x CH, C-3' and C-5'), 113.7 (CH, C-4'' and C-6''), 55.5 (CH_3, C-6''), 55.1 (CH_3, C-5'); HRESIMS: calcd for $C_{16}H_{13}N_2O_3$ 281.0926. Found 281.0925, Δamu 0.0001.

6.4.4. Synthesis of the sponge natural product deoxytopsentin (5.33)

6.4.4.1. Synthesis of N-Boc protected deoxytopsentin (5.90)

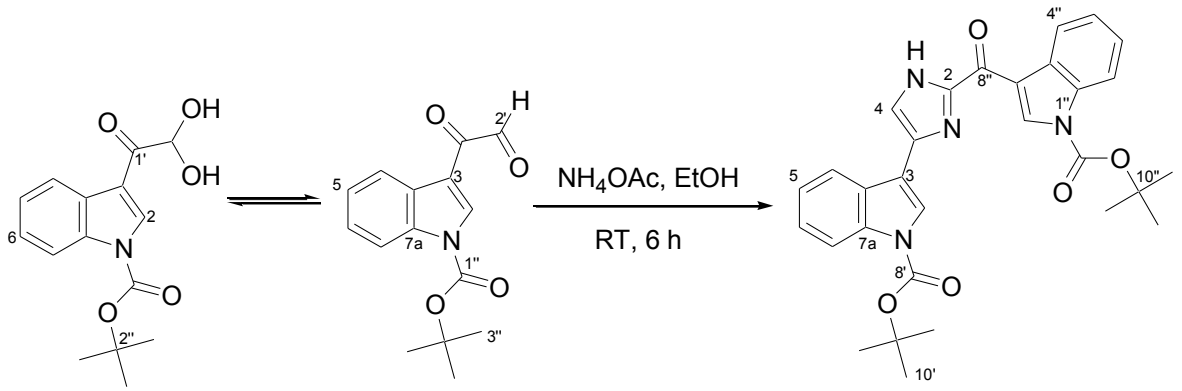

5.107 **5.88** **5.90**

The equilibrium mixture of glyoxal (**5.88**) and glyoxal monohydrate (**5.107**) (85 mg, 0.311 mmol) were dissolved in EtOH (2 mL) and ammonium acetate (120 mg, 1.56 mmol, 5 equiv.) added. The solution was stirred at room temperature until a yellow precipitate formed (6 h). The solvent was removed under reduced pressure resulting in a yellow solid. This yellow solid was washed with water and filtered under vacuum. The protected imidazole was purified through a silica flash column (80% EtOAc : 20% hexane) to afford **5.90** (78.6 mg, 96%).

(Indol-3-yl)[5-(indol-3-yl)-3H-imidazol-2-yl]-bis(1,1-dimethylethyl) ester (**5.90**) IR (solid) ν_{max} 2980, 1741, 1667, 1370, 1150, 749 cm^{-1}; ^{1}H NMR (600 MHz, $CDCl_3$) δ 13.68 (s, NH-3, 1H), 9.78 (s, H-2'', 1H), 8.45 (d, *J* = 7.1, H-7', 1H), 8.27 (m, H-4'', H-7'', 2H), 8.16 (d, *J* = 7.7, H-4', 1H), 8.02 (s, H-2', 1H), 7.61 (s, H-4, 1H), 7.42 (m, H-5'' and H-6'', 2H), 7.37 (m, H-5' and H-6', 2H), 1.72 (s, H_3-10', 9H), 1.71, (s, H_3-11'', 9H); ^{13}C NMR (150 MHz, $CDCl_3$) δ 177.0 (q, C-8''), 149.1 (q, C-9''), 148.6 (q, C-8'), 145.2 (q, C-2), 137.7 (CH, C-2''), 135.6 (q, C-7a'), 135.3 (q, C-7a''), 137.9 (q, C-5), 127.9 (q, C-3a''), 125.5 (CH, C-6), 124.6 (q, C-3a'), 124.6 (CH, C-5''), 124.4 (CH, C-6'), 122.7 (CH, C-5'), 122.5 (CH, C-2'), 122.4 (CH, C-7'), 120.7 (CH, C-4'), 120.4 (CH, C-7''), 116.8 (q, C-3''), 115.8 (CH, C-4), 115.1 (CH, C-4''), 114.7 (q, C-3'), 85.5 (q, C-10''), 85.1 (q, C-9'), 28.2 (CH_3, C-11''), 28.1 (CH_3, C-10'); HREIMS: calcd for $C_{30}H_{31}N_4O_5$ 527.2294. Found 527.2304, Δamu 0.0010.

6.4.4.2. Deprotection of 5.90

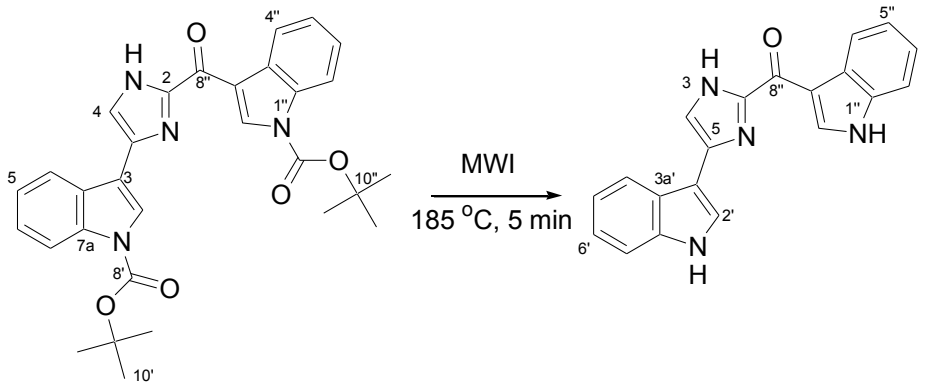

5.90 **5.33**

The carbamate protection groups were removed through thermal decomposition. The dried oil (338.6 mg) was placed in a sealed microwave vessel under argon and heated to 185 °C for 5 min. The mixture was then dissolved in methanol and filtered through Celite 545. The methanol was removed by evaporation to afford tautomeric mixture (54%:46%) of deoxytopsentin (**5.33**) as a yellow solid (209 mg) in quantative yield.

3-H-Deoxytopsentin (**5.33a**), yellow oil (100 % yield, 54 % of tautomeric mixture), IR (solid) ν_{max} 2160, 1589, 1414, 1103, 852, 735 cm^{-1}; ^{1}H NMR (600 MHz, DMSO- D_6) δ 13.37 (s, NH-3, 1H), 12.04 (s, NH-1'', 1H), 11.45 (s, NH-1', 1H), 9.19 (s, H-2'', 1H), 8.41 (d, *J* = 7.4, H-4'', 1H), 8.17 (d, *J* = 7.9, H-4', 1H), 8.11 (s, H-2', 1H), 7.63 (s, H-4, 1H), 7.54 (t, *J* = 7.1, 8.3, H-7'', 1H), 7.46 (d, *J* = 7.5, H-7', 1H), 7.25 (m, H-5'', H-6'', 1H), 7.15 (t, *J* = 7.5, 8.0, H-5', H-6', 2H); ^{13}C NMR (150 MHz, DMSO-D_6) δ 176.1 (q, C-8''), 145.2 (q, C-2), 136.6 (CH, C-2''), 136.5 (q, C-7a'), 136.2 (q, C-7a''), 130.4 (q, C-5), 126.8 (q, C-3a''), 125.8 (CH, C-4), 124.5 (q, C-3a'), 124.0 (CH, C-2'), 122.8 (CH, C-6''), 122.7 (CH, C-6'), 121.8 (CH, C-5''), 121.6 (2xCH, C-5', C-4''), 121.3 (CH, C-4'), 113.7 (q, C-3''), 112.3 (CH, C-7''), 112.1 (CH, C-7'), 104.7 (q, C-3'); ^{15}N NMR (60 MHz, DMSO-D_6) δ 215.7 (NH, N-3), 194.0 (NH, N-1''), 188.1 (NH, N-1'); HREIMS: calcd for $C_{20}H_{15}N_4O$ 327.1246. Found 327.1244, Δamu 0.0002.

1-H-Deoxytopsentin (**5.33b**), yellow oil (100 % yield, 46 % of tautomeric mixture); ^{1}H NMR (600 MHz, DMSO-D_6) δ 13.12 (s, NH-1, 1H), 12.15 (s, NH-1'', 1H), 11.23 (s, NH-1', 1H), 9.40 (s, H-2'', 1H), 8.41 (d, *J* = 7.4, H-4'', 1H), 7.91 (d, *J* = 8.1, H-4', 1H), 7.83 (1H, s, H-2'), 7.69 (s, H-4, 1H), 7.54 (t, *J* = 7.1, 8.3, H-7'', 1H), 7.44 (d, *J* = 7.9, H-7', 1H), 7.25 (m, H-5'', H-6'', 2H), 7.19 (t, *J* = 7.8, 8.2, H-6', 1H), 7.13 (t, *J* = 7.5, 8.3, H-5', 1H); ^{13}C NMR (150 MHz, DMSO-D_6) δ 176.0 (q, C-8''), 145.2 (q, C-2), 138.5 (q, C-5), 137.0 (CH, C-2''), 136.2 (2xq, C-7a', C-7a''), 126.8 (q, C-3a''), 124.9 (q, C-3a'), 122.8 (2xCH, C-2', C-6''), 121.9 (CH, C-6'), 121.8 (CH, C-5''), 121.6 (CH, C-4''), 119.8 (CH, C-5'),119.5 (CH, C-4'), 114.9 (CH, C-

4'), 113.9 (q, C-3''), 112.3 (CH, C-7''), 112.0 (CH, C-7'), 110.8 (q, C-3'); ^{15}N NMR (60 MHz, DMSO-D_6) δ 222.4 (NH, N-1), 198.0 (NH, N-1''), 185.1 (NH, N-1'); HREIMS: calcd for $C_{20}H_{15}N_4O$ 327.1246. Found 327.1244, Δamu 0.0002.

6.4.5. Attempted synthesis of isobromotopsentin and 5.34

6.4.5.1. Grignard synthesis of 3-(1-hydroxyethyl)-6-bromo-indole (5.121) and 3-(1-hydroxyethyl)-5-bromo-indole (5.122)

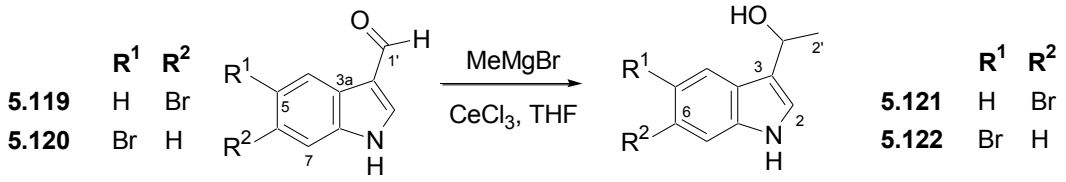

The following method is representative for the preparation of compounds **5.121** and **5.122**. A suspension of anhydrous $CeCl_3$ (426 mg, 3.35 mmol, 1.5 equiv.) in dry THF (7 mL) was stirred under argon at ambient temperature (2 h), cooled to 0 °C and an aliquot (2.23 mL, 6.69 mmol, 3.0 equiv.) of a THF solution of methylmagnesium bromide (3.0 M) added. The suspension was stirred (0 °C, 1.5 h) and a solution of **5.119** (500 mg, 2.23 mmol) in dry THF (6 mL) added. Stirring was continued (0 °C, 1 h) and the reaction mixture gradually allowed to reach room temperature (4 h) before quenching with sat. aqueous NH_4Cl (5 mL) and extracted with Et_2O (3 x 5 mL). The combined ether fractions were washed with water (2 x 5 mL), sat. brine (1 x 5 mL), dried over anhyd. $MgSO_4$, filtered and concentrated under reduced pressure to yield a yellow oil. Recrystallization from MeOH afforded white prisms of **5.121** (533 mg, 100%):

3-(1-Hydroxyethyl)-6-bromo-indole (**5.121**) white needles from DCM, (100% yield) mp 120-122 °C; IR (solid) ν_{max} 3114, 2603, 1431, 1171, 875, 789 cm^{-1}; ^{1}H NMR (600 MHz, CD_3OD) δ 7.59 (d, *J* = 8.4, H-5, 1H), 7.51 (s, H-7, 1H), 7.17 (s, H-2, 1H), 7.12 (d, *J* = 8.4, H-4, 1H), 5.13 (q, *J* = 6.7, H-1', 1H), 1.60 (d, *J* = 6.7, H_3-2', 3H); ^{13}C NMR (150 MHz, CD_3OD) δ 139.2 (q, C-7a), 126.2 (q, C-3a), 123.1 (CH, C-2), 122.8 (CH, C-4), 121.8 (CH, C-5), 121.5 (q, C-3), 115.8 (q, C-6), 115.1 (CH, C-7), 64.6 (CH, C-1'), 24.2 (CH_3, C-2'); EIMS *m/z* (rel. int.) 222 [M+] (100), 194 (12), 143 (23), 111 (12), 88 (11); HREIMS: calcd for $C_{10}H_9ONBr$ 221.9918. Found 221.9910, Δamu 0.0008.

3-(1-Hydroxyethyl)-5-bromo-indole (**5.122**) white needles from DCM, (100% yield) mp 119-120 ^{o}C; IR (solid) ν_{max} 3223, 2585, 2162, 1371, 994, 759 cm^{-1}; ^{1}H NMR (600 MHz, $CDCl_3$) δ 8.02 (s, NH-1, 1H), 7.91 (s, H-4, 1H), 7.28 (d, *J* = 8.9, H-6, 1H), 7.23 (d, *J* = 8.6, H-7, 1H), 7.15 (s, H-2, 1H), 5.19 (q, *J* = 6.5, H-1', 1H), 1.65 (d, *J* = 6.5, H_3-2', 3H); ^{13}C NMR (150 MHz, $CDCl_3$) δ 135.2 (q, C-7a), 127.5 (q, C-3a), 125.2 (CH, C-6), 122.4 (CH, C-4), 121.8 (CH, C-2), 121.0 (q, C-3), 113.0 (q, C-5), 112.6 (CH, C-7), 64.0 (CH, C-1'), 23.8 (CH_3, C-2'); EIMS *m/z* (rel. int.) [M+] 222 (100), 142 (22), 115 (160), 89 (6), 71 (10); HREIMS: calcd for $C_{10}H_9ONBr$ 221.9918. Found 221.9910, Δamu 0.0008.

6.4.5.2. Trial tetrapropylammonium perruthenate oxidation of the natural product marrubiin (5.123)

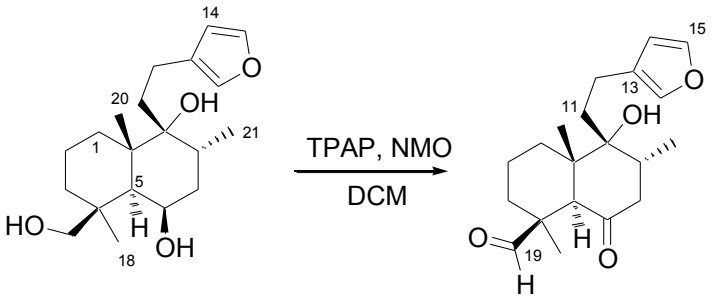

5.123 **5.129**

Tetrapropylammonium perruthenate (0.031 mmol, 0.1 equiv.) was added to a solution of **5.123** (101 mg, 0.313 mmol), N-methylmorpholine N-oxide (95 mg, 0.814 mmol, 2.6 equiv.) and powdered molecular sieves (4 Å, 30 mg) in anhydrous CH_2Cl_2 (5 mL). The reaction was allowed to stir for 3 h under an argon atmosphere at room temperature. The molecular sieves were removed by filtering the solution through Celite 545 plug and washed with DCM. The solvent was removed under reduced pressure and redissolved in EtOAc. The solution was filtered through a silica plug using EtOAc as a mobile phase. The isolated oil was further purified by HPLC (25% EtOAc, 75% Hexane) to afford **5.129** in 98% yield.

Marrubenone (**5.129**), white needles needles from hexane, (98 % yield) mp 110-112 ^{o}C, lit. 110-111 ^{o}C[481]; ^{1}H NMR (400 MHz, $CDCl_3$) δ 10.34 (s, H-19, 1H), 7.37 (s, H-15, 1H), 7.26 (s, H-16, 1H), 6.29 (s, H-14, 1H), 3.26 (s, H-5, 1H), 2.57, (m, H-7a, 1H), 2.55 (m, H_2-12, 2H), 2.28 (septet, *J* = 6.6, H-8, 1H), 2.17 (dd, *J* = 12.8, 4.5, H-7b, 1H), 2.11 (dt, *J* = 13.4, 3.8, H-1a, 1H), 1.96 (m, H-11a, 1H), 1.85 (m, H-11b, 1H), 1.72 (q, *J* = 7.8, H-3a, 1H), 1.57 (m, H-3b, 1H), 1.54 (m, H_2-2, 2H), 1.15 (s, H_3-18, 3H), 1.07 (d, *J* = 6.6, H_3-21, 3H), 0.92 (m, H-1b, 1H), 0.84 (s, H_3-20, 3H); ^{13}C NMR (100 MHz, $CDCl_3$) δ 211.9, (q, C-6),

208.7 (CH, C-19), 143.6 (CH, C-15), 139.0 (CH, C-16), 125.1 (q, C-13), 111.0 (CH, C-14), 76.7 (q, C-9), 59.9 (CH, C-5), 49.1 (q, C-10), 48.0 (q, C-4), 47.5 (CH_2, C-7), 39.1 (CH, C-8), 34.8 (CH_2 x 2, C-11, C-1), 31.4, (CH_2, C-3), 25.7 (CH_3, C-18), 18.8 (CH_2, C-2), 17.7 (CH_3, C-20), 16.3 (CH_3, C-21)

6.4.5.3. Manganese dioxide oxidation of 5.121 and 5.122

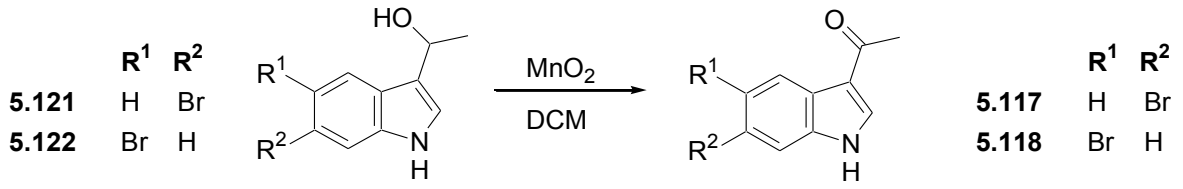

	R^1	R^2
5.121	H	Br
5.122	Br	H

	R^1	R^2
5.117	H	Br
5.118	Br	H

This method is representative for the synthesis of **5.117** and **5.118**. The alcohol (**5.121**, 322 mg, 1.33 mmol) was dissolved in anhydrous CH_2Cl_2 (50 mL), MnO_2 (3.5 g, 40.5 mmol, 30 equiv.) was added and the mixture was stirred under argon at ambient temperatures for 24 h. The insoluble MnO_2 was removed *viz.* filtration through Celite 545 and washed with EtOAc (200 mL). The solvent was removed under reduced pressure to afford the respective pure brominated 3-acetylindole, which required no further purification.

3-Acetyl-6-bromo-indole (**5.121**), red needles from chloroform (98 % yield), mp 162-164 ^{o}C; IR (solid) ν_{max} 2272, 1621, 1516, 1415, 840, 715 cm^{-1}; ^{1}H NMR (600 MHz, CD_3OD) δ 8.15 (s, H-2, 1H), 8.12 (d, *J* = 8.5, H-4, 1H), 7.61 (s, H-7, 1H), 7.31 (d, *J* = 8.5, H-5, 1H), 2.51 (s, H_3-2', 3H); ^{13}C NMR (150 MHz, CD_3OD) δ 194.9 (q, C-1'), 137.8 (q, C-7a), 134.6 (CH, C-2), 124.8 (CH, C-5), 124.3 (q, C-3a), 122.8 (CH, C-4), 117.1 (q, C-3), 116.1 (q, C-6), 114.4 (CH, C-7), 25.7 (CH_3, C-2'); EIMS *m/z* (rel. int.) 236 [M^+] (45), 224 (91), 222, (100), 194 (16), 115 (18); HREIMS: calcd for $C_{10}H_8NOBr$ 236.9789. Found 236.9808, Δamu 0.0019.

3-Acetyl-5-bromo-indole (**5.122**), purple needles from chloroform (98 % yield), mp 164-165 ^{o}C; IR (solid) ν_{max} 2272, 1621, 1516, 1415, 938, 712 cm^{-1}; ^{1}H NMR (600 MHz, CD_3OD) δ, 8.17 (s, H-2, 1H), 8.13 (d, *J* = 8.4, H-7, 1H) 7.35 (m, H-4, 1H), 7.33 (m, H-6, 1H), 2.51 (s, H_3-2', 3H); ^{13}C NMR (150 MHz, CD_3OD) δ 196.3 (q, C-1'), 137.1 (q, C-7a), 136.5 (CH, C-2), 128.5 (q, C-3a), 127.1 (CH, C-6), 125.4 (CH, C-7), 118.0 (q, C-3), 116.6 (q, C-5), 114.5 (CH, C-4), 27.1 (CH_3, C-2'); EIMS *m/z* (rel. int.) 236 [M^+] (47),

224 (93), 222, (100), 194 (12), 143 (21); HREIMS: calcd for $C_{10}H_8NOBr$ 236.9789. Found 236.9808, Δamu 0.0019.

6.4.5.4. N-Boc protection of 5.117 and 5.118

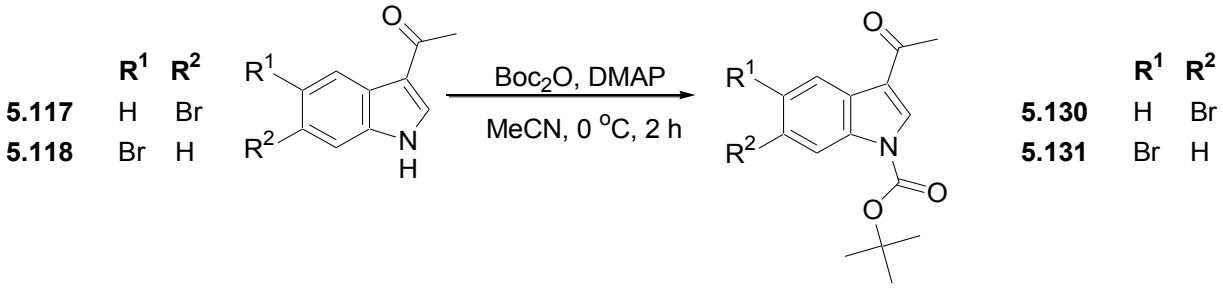

Brominated 3-acetylindoles (**5.117** or **5.118**, 200 mg, 0.84 mmol) was dissolved in dry MeCN (2.5 mL) and cooled on ice. Di-*tert*-butyl dicarbonate (275 g, 1.26 mmol, 1.5 equiv.) was added followed by 4-dimethylaminopyridine (10.3 mg, 84 µmol, 0.1 equiv.) and each solution allowed to stir under argon for two hours. The solvent and excess reagents were removed under reduced pressure to yield spectropically pure white solids of **5.130** and **5.131**.

3-Acetyl-6-bromo-indole-1-carbamate (**5.130**), white needles from hexane (100 % yield), mp 196-198 °C; IR (solid) ν_{max} 1729, 1665, 1362, 1151, 844 cm^{-1}, 763; ^{1}H NMR (600 MHz, CD_3OD) δ 8.31 (s, H-7, 1H), 8.22 (d, *J* = 8.3, H-4, 1H), 8.16 (s, , H-2, 1H), 7.46 (d, *J* = 8.3, H-5, 1H), 2.55 (s, H_3-2', 3H), 1.70 (s, H_3-3'', 9H); ^{13}C NMR (150 MHz, CD_3OD) δ 193.6 (q, C-1'), 148.7 (q, C-1''), 136.6 (q, C-7a), 132.5 (CH, C-2), 127.7 (CH, C-5), 126.2 (q, C-3a), 123.9 (CH, C-4), 120.3 (q, C-3), 119.5 (q, C-6), 118.5 (CH, C-7), 86.1 (q, C-2''), 28.1 (CH_3, C-3''), 27.7 (CH_3, C-2')

3-Acetyl-5-bromo-indole-1-carbamate (**5.131**), white needles from hexane (100 % yield), mp 195-197 °C; IR (solid) ν_{max} 3274, 1635, 1596, 1509, 1287, 847 cm^{-1}; ^{1}H NMR (600 MHz, $CDCl_3$) δ 8.46 (s, H-4, 1H), 8.12 (s, H-2, 1H), 7.79 (d, *J* =8.8, H-7, 1H), 7.40 (d, *J* = 8.7, 7.8, H-6, 1H), 2.48 (s, H_3-2', 3H), 1.64 (s, H_3-3'', 9H); ^{13}C NMR (150 MHz, $CDCl_3$) δ 1 93.4 (q, C-1'), 148.7 (q, C-1''), 134.3 (q, C-7a), 132.9 (CH, C-2), 128.9 (q, C-3a), 128.5 (CH, C-6), 125.4 (CH, C-4), 119.8 (q, C-3), 118.1 (q, C-5), 116.3 (CH, C-7), 85.9 (q, C-2''), 28.1 (CH_3, C-3''), 27.6 (CH_3, C-2')

6.4.5.5. Attempted synthesis of the brominated indole glyoxals

This method is representative for the conversion of **5.130** and **5.131** to their respective glyoxals. SeO_2 (281 mg, 2.53 mmol, 2.7 equiv) was suspended in a mixture of 1,4-dioxane (1 mL) and H_2O (20 µL) and the indole methyl ketone, **5.130** (200 mg, 0.94 mmol) was added just before microwave irradiation [ramp time (1 min) to a maximum power of 250 W, hold time (40 min) at a set temperature of 100 °C]. Following microwave irradiation the reaction solution was rapidly cooled to 50 °C (5 min) by means of propelled airflow and finally allowed to cool to room temperature (*ca.* 20 min). The solution was filtered through Celite 545 , in order to remove Se, and washed with CH_2Cl_2 (10 mL). The combined organic filtrate was washed with water (2 x 10 mL) and sat. brine (1 x 10mL), and the organic fraction was dried over anhydrous $MgSO_4$, filtered and concentrated under reduced pressure to afford a yellow oil containing an inseparable mixture of N-Boc protected glyoxal (**5.115**) and monohydrate (**5.132**) as well as the deprotected glyoxal (**5.134**) and monohydrate (**5.135**).

6.4.5.6. Attempted synthesis of N-Boc protected isobromotopsentin (5.20)

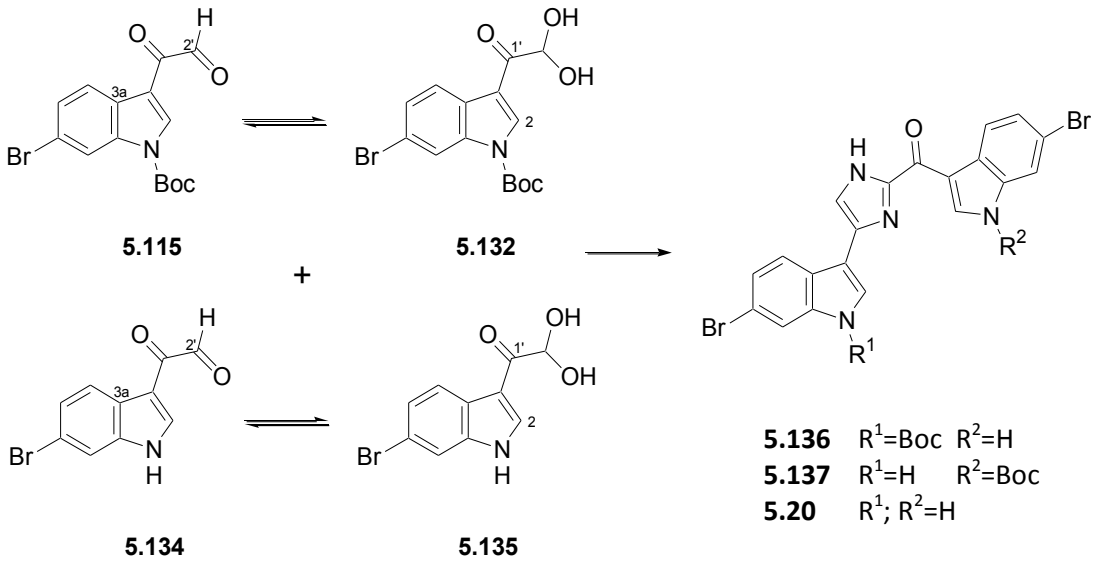

The mixture of glyoxals (**5.115** and **5.134**) and glyoxal monohydrate (**5.132** and **5.135**) (50 mg, *ca.* 0.136 mmol) were dissolved in EtOH (2 mL) and ammonium acetate (52 mg, 0.68 mmol, 5 equiv.) added. The solution was stirred at room temperature until a yellow precipitate formed (6 h). The

solvent was removed under reduced pressure resulting in a yellow solid. This yellow solid was washed with water and filtered under vacuum, resulting in an inseparable mixture of **5.136**, **5.137** and **5.20**.

(Indol-3-yl)[5-(indol-3-yl)-3H-imidazol-2-yl]-1-methylethyl ester (**5.136** and **5.137**)*;* HREIMS: calcd for $C_{25}H_{21}N_4O_3Br_2$ 582.9980. Found 582.9989, Δamu 0.0009.

Isobromotopsentin (**5.20**); HREIMS: calcd for $C_{20}H_{13}N_4OBr_2$ 482.9456. Found 482.9461, Δamu 0.0005.

REFERENCES

1. Newman, D. J. and Cragg, G. M. *J. Nat. Prod.* **2007**, *70*, 461-477
2. Cragg, G. M.; Grothaus, P. G. and Newman, D. J. *Chem. Rev.* **2009**, *109*, 3012-3043
3. Brusca, R. C. and Brusca, G. J. *Invertebrates*, Sinauer Associates, Sunderland, MA., 1990; 4-5
4. Erwin, P. M.; Lopez-Legentil, S. and Schuhmann, P. W. *Ecol. Econ.* **2010**, *70*, 445-451
5. Mayer, A. M. S.; Glaser, K. B.; Cuevas, C.; Jacobs, R. S.; Kem, W.; Little, R. D.; McIntosh, J. M.; Newman, D. J.; Potts, B. C. and Shuster, D. E. *Trends Pharmacol. Sci.* **2010**, *31*, 255-265
6. Lipsky, M. S. and Sharp, L. K. *J. Am. Board Fam. Med.* **2001**, *14*, 362-367
7. Bergmann, W. and Feeney, R. J. *J. Org. Chem.* **1951**, *16*, 981-987
8. Absalon, M. J. and Smith, F. O. *Expert Opin. Pharmaco.* **2009**, *10*, 57-79
9. Thomas, X. *Expert Opin. Pharmaco.* **2009**, *10*, 221-237
10. Whitley, R. *Curr. Opin. Infect. Dis.* **2004**, *17*, 243-246
11. Miljanich, G. P. *Curr. Opin. Med. Chem.* **2004**, *11*, 3029-3040
12. McGivern, J. G. *Drug. Discov. Today* **2006**, *11*, 245-253
13. McIntosh, J. M.; Corpuz, G. O.; Layer, R. T.; Garrett, J. E.; Wagstaff, J. D.; Bulaj, G.; Vyazovkina, A.; Yoshikami, D.; Cruz, L. J. and Olivera, B. M. *J. Biol. Chem.* **2000**, *275*, 32391-32397
14. Rinehart, K. L.; Holt, T. G.; Fregeau, N. L.; Stroh, J. G.; Keifer, P. A.; Sun, F.; Li, L. H. and Martin, D. G. *J. Org. Chem.* **1990**, *55*, 4512-4515
15. Wright, A. E.; Forleo, D. A.; Gunawardana, G. P.; Gunasekera, S. P.; Koehn, F. E. and Mcconnell, O. J. *J. Org. Chem.* **1990**, *55*, 4508-4512
16. Zewail-Foote, M. and Hurley, L. H. *J. Am. Chem. Soc.* **2001**, *123*, 6485-6495
17. Takebayashi, Y.; Pourquier, P.; Zimonjic, D. B.; Nakayama, K.; Emmert, S.; Ueda, T.; Urasaki, Y.; Kanzaki, A.; Akiyama, S.; Popescu, N.; Kraemer, K. H. and Pommier, Y. *Nat. Med.* **2001**, *7*, 961-966
18. Jackson, K. L.; Henderson, J. A. and Phillips, A. J. *Chem. Rev.* **2009**, *109*, 3044-3079
19. Jefferson, E. *FDA approves new treatment option for late-stage breast cancer (Press Release)* FDA: Silver Spring, MD;
20. Kuznetsov, G.; Towle, M. J.; Cheng, H. S.; Kawamura, T.; TenDyke, K.; Liu, D.; Kishi, Y.; Yu, M. J. and Littlefield, B. A. *Cancer Res.* **2004**, *64*, 5760-5766
21. *Discovery Studio Visualizer, Release 2.0*, version Accelrys Software Inc.: 2007
22. Bai, R.; Friedman, S. J.; Pettit, G. R. and Hamel, E. *Biochem. Pharmacol.* **1992**, *43*, 2637-2645
23. Steube, K. G.; Grunicke, D.; Pietsch, T.; Gignac, S. M.; Pettit, G. R. and Drexler, H. G. *Leukemia* **1992**, *6*, 1048-1053
24. Lippert, J. W. *Bioorg. Med. Chem.* **2007**, *15*, 605-615
25. U.S. National Institutes of Health. www.clinicaltrials.gov (accessed Nov. 2011)
26. Fenical, W.; Jensen, P. R. and Cheng, X. C., *Halimide, a cytotoxic marine natural product, and derivatives thereof*, WO/1999/48889, The Regents of the University of California, Oakland, CA, May 30 2000
27. Nicholson, B.; Lloyd, G. K.; Miller, B. R.; Palladino, M. A.; Kiso, Y.; Hayashi, Y. and Neuteboom, S. T. C. *Anti-Cancer Drugs* **2006**, *17*, 25-31
28. King, H. *J. Chem. Soc.* **1939**, 1364-1366

29. Kem, W. R.; Mahnir, V. M.; Prokai, L.; Papke, R. L.; Cao, X. F.; LeFrancois, S.; Wildeboer, K.; Prokai-Tatrai, K.; Porter-Papke, J. and Soti, F. *Mol. Pharmacol.* **2004**, *65*, 56-67
30. Olincy, A.; Harris, J. G.; Johnson, L. L.; Pender, V.; Kongs, S.; Allensworth, D.; Ellis, J.; Zerbe, G. O.; Leonard, S.; Stevens, K. E.; Stevens, J. O.; Martin, L.; Adler, L. E.; Soti, F.; Kem, W. R. and Freedman, R. *Arch. Gen. Psychiat.* **2006**, *63*, 630-638
31. Scott, J. D. and Williams, R. M. *Chem. Rev.* **2002**, *102*, 1669-1730
32. Mitsiades, C. S.; Ocio, E. M.; Pandiella, A.; Maiso, P.; Gajate, C.; Garayoa, M.; Vilanova, D.; Montero, J. C.; Mitsiades, N.; McMullan, C. J.; Munshi, N. C.; Hideshima, T.; Chauhan, D.; Aviles, P.; Otero, G.; Faircloth, G.; Mateos, M. V.; Richardson, P. G.; Mollinedo, F.; San Miguel, J. F. and Anderson, K. C. *Cancer Res.* **2008**, *68*, 5216-5225
33. Look, S. A.; Fenical, W.; Matsumoto, G. K. and Clardy, J. *J. Org. Chem.* **1986**, *51*, 5140-5145
34. Roussis, V.; Wu, Z. D.; Fenical, W.; Strobel, S. A.; Vanduyne, G. D. and Clardy, J. *J. Org. Chem.* **1990**, *55*, 4916-4922
35. Abatis, D.; Vagias, C.; Galanakis, D.; Norris, J. N.; Moreau, D.; Roussakis, C. and Roussis, V. *Tetrahedron Lett.* **2005**, *46*, 8525-8529
36. Montesinos, M. C.; Gadangi, P.; Longaker, M.; Sung, J.; Levine, J.; Nilsen, D.; Reibman, J.; Li, M.; Jiang, C. K.; Hirschhorn, R.; Recht, P. A.; Ostad, E.; Levin, R. I. and Cronstein, B. N. *J. Exp. Med.* **1997**, *186*, 1615-1620
37. Feling, R. H.; Buchanan, G. O.; Mincer, T. J.; Kauffman, C. A.; Jensen, P. R. and Fenical, W. *Angew. Chem. Int. Edit.* **2003**, *42*, 355-357
38. Fenical, W.; Jensen, P. R.; Palladino, M. A.; Lam, K. S.; Lloyd, G. K. and Potts, B. C. *Bioorgan. Med. Chem.* **2009**, *17*, 2175-2180
39. Talpir, R.; Benayahu, Y.; Kashman, Y.; Pannell, L. and Schleyer, M. *Tetrahedron Lett.* **1994**, *35*, 4453-4456
40. Kuznetsov, G.; TenDyke, K.; Towle, M. J.; Cheng, H. S.; Liu, J. K.; Marsh, J. P.; Schiller, S. E. R.; Spyvee, M. R.; Yang, H.; Seletsky, B. M.; Shaffer, C. J.; Marceau, V.; Yao, Y.; Suh, E. M.; Campagna, S.; Fang, F. G.; Kowalczyk, J. J. and Littlefield, B. A. *Mol. Cancer Ther.* **2009**, *8*, 2852-2860
41. *Convention on Biological Diversity* **1992**, *Rio Janeiro*,
42. Andersen, R. J. and Williams, D. E. *Chemistry in the Marine Enviroment*, 1st Ed. ed.; Royal Society of Chemistry, Cambridge, 2000; 55-79
43. Querellou, J., Børresen, T., Boyen, C., Dobson, A., Höfle, M., Ianora, A., Jaspars, M., Kijjoa, A., Olafsen, J., Rigos, G., and Wijffels, R. *Marine Biotechnology: A New Vision and Strategy for Europe,* **2009**, 15 37-59
44. Li, J. W. H. and Vederas, J. C. *Science* **2009**, *325*, 161-165
45. Proksch, P.; Edrada-Ebel, R. A. and Ebel, R. *Mar. Drugs* **2003**, *1*, 5-17
46. NCI National Cancer Institute. www.cancer.gov (accessed Aug. 2011)
47. Munro, M. H. G.; Blunt, J. W.; Dumdei, E. J.; Hickford, S. J. H.; Lill, R. E.; Li, S. X.; Battershill, C. N. and Duckworth, A. R. *J. Biotechnol.* **1999**, *70*, 15-25
48. Ikeda, Y.; Idemoto, H.; Hirayama, F.; Yamamoto, K.; Iwao, K.; Asao, T. and Munakata, T. *J. Antibiot.* **1983**, *36*, 1279-1283

49. Cuevas, C. and Francesch, A. *Nat. Prod. Rep.* **2009**, *26*, 322-337
50. Butler, M. S. *J. Nat. Prod.* **2004**, *67*, 2141-2153
51. World Health Organization *Factsheet No. 290 (World Health Organization, Geneva, 2011)*
52. Sachs, J. and Malaney, P. *Nature* **2002**, *415*, 680-685
53. Breman, J. G. *Am. J. Trop. Med. Hyg.* **2001**, *64*, 1-11
54. Winstanley, P. *Lancet* **2001**, *1*, 242-250
55. Baton, L. A. and Ranford-Cartwright, L. C. *Trends Parasitol.* **2005**, *21*, 573-580
56. Drakeley, C.; Sutherland, C.; Bouserna, J. T.; Sauerwein, R. W. and Targett, G. A. T. *Trends Parasitol.* **2006**, *22*, 424-430
57. Ghosh, A.; Edwards, M. J. and Jacobs-Lorena, M. *Parasitol. Today* **2000**, *16*, 196-201
58. Sinden, R. E. *Parasitology* **1983**, *86*, 7-28
59. Janse, C. J.; Vanderklooster, P. F. J.; Vanderkaay, H. J.; Vanderploeg, M. and Overdulve, J. P. *T. Roy. Soc. Trop. Med. Hy.* **1986**, *80*, 154-157
60. Moreira, C. K.; Marrelli, M. T. and Jacobs-Lorena, M. *Int. Parasitol.* **2004**, *34*, 1431-1440
61. Langer, R. C. and Vinetz, J. M. *Trends Parasitol.* **2001**, *17*, 269-272
62. Shahabuddin, M. and Pimenta, P. F. P. *Proc. Natl. Acad. Sci. U. S. A.* **1998**, *95*, 3385-3389
63. King, C. A. *Parasitol. Today* **1988**, *4*, 315-319
64. Sidjanski, S. and Vanderberg, J. P. *Am. J. Trop. Med. Hyg.* **1997**, *57*, 426-429
65. Frevert, U. *Trends Parasitol.* **2004**, *20*, 417-424
66. Pradel, G. and Frevert, U. *Hepatology* **2001**, *33*, 1154-1165
67. Meis, J. F. G. M.; Verhave, J. P.; Brouwer, A. and Meuwissen, J. H. E. T. *Z. Parasitenkol.* **1985**, *71*, 473-483
68. Mota, M. M.; Pradel, G.; Vanderberg, J. P.; Hafalla, J. C. R.; Frevert, U.; Nussenzweig, R. S.; Nussenzweig, V. and Rodriguez, A. *Science* **2001**, *291*, 141-144
69. Kaiser, K.; Camargo, N. and Kappe, S. H. I. *J. Exp. Med.* **2003**, *197*, 1045-1050
70. Shortt, H. E. and Garnham, P. C. C. *Nature* **1948**, *161*, 126
71. Meis, J. F. G. M.; Verhave, J. P.; Jap, P. H. K. and Meuwissen, J. H. E. T. *Cell Tissue Research* **1985**, *241*, 353-360
72. Meis, J. F. G. M.; Verhave, J. P.; Jap, P. H. K. and Meuwissen, J. H. E. T. *J. Protozool.* **1985**, *32*, 694-699
73. Pinder, J. C.; Fowler, R. E.; Bannister, L. H.; Dluzewski, A. R. and Mitchell, G. H. *Parasitol. Today* **2000**, *16*, 240-245
74. Mills, J. P.; Diez-Silva, M.; Quinn, D. J.; Dao, M.; Lang, M. J.; Tan, K. S. W.; Lim, C. T.; Milon, G.; David, P. H.; Mercereau-Puijalon, O.; Bonnefoy, S. and Suresh, S. *Proc. Natl. Acad. Sci. U. S. A.* **2007**, *104*, 9213-9217
75. Miller, L. H.; Baruch, D. I.; Marsh, K. and Doumbo, O. K. *Nature* **2002**, *415*, 673-679
76. Cowman, A. F. and Crabb, B. S. *Cell* **2006**, *124*, 755-766
77. Suresh, S.; Spatz, J.; Mills, J. P.; Micoulet, A.; Dao, M.; Lim, C. T.; Beil, M. and Seufferlein, T. *Acta Biomater.* **2005**, *1*, 15-30
78. Glenister, F. K.; Coppel, R. L.; Cowman, A. F.; Mohandas, N. and Cooke, B. M. *Blood* **2002**, *99*, 1060-1063

79. Nash, G. B.; Obrien, E.; Gordonsmith, E. C. and Dormandy, J. A. *Blood* **1989**, *74*, 855-861
80. Dondorp, A. M.; Pongponratn, E. and White, N. J. *Acta Trop.* **2004**, *89*, 309-317
81. Langreth, S. G. and Peterson, E. *Infect. Immun.* **1985**, *47*, 760-766
82. Khan, S. M. and Waters, A. P. *Trends Parasitol.* **2004**, *20*, 575-580
83. Rathore, D.; Jani, D.; Nagarkatti, R. and Kumar, S. *Drug. Discov. Today* **2006**, *3*, 153-157
84. Krugliak, M.; Zhang, J. M. and Ginsburg, H. *Mol. Biochem. Parasitol.* **2002**, *119*, 249-256
85. Fenton, H. J. H. *J. Chem. Soc.* **1894**, *65*, 899-911
86. Haber, F. and Weiss, J. *Naturwissenschaften* **1932**, *20*, 948-950
87. Sullivan, D. J. *Int. Parasitol.* **2002**, *32*, 1645-1653
88. Loria, P.; Miller, S.; Foley, M. and Tilley, L. *Biochem. J.* **1999**, *339*, 363-370
89. Fairfield, A. S.; Abosch, A.; Ranz, A.; Eaton, J. W. and Meshnick, S. R. *Mol. Biochem. Parasitol.* **1988**, *30*, 77-82
90. Gamain, B.; Langsley, G.; Fourmaux, M. N.; Touzel, J. P.; Camus, D.; Dive, D. and Slomianny, C. *Mol. Biochem. Parasitol.* **1996**, *78*, 237-248
91. Hunt, N. H. and Stocker, R. *Blood Cells* **1990**, *16*, 499-526
92. Egan, T. J. *Mol. Biochem. Parasitol.* **2008**, *157*, 127-136
93. Schacter, B. A. *Semin. Hematol.* **1988**, *25*, 349-369
94. Dorn, A.; Vippagunta, S. R.; Matile, H.; Jaquet, C.; Vennerstrom, J. L. and Ridley, R. G. *Biochem. Pharmacol.* **1998**, *55*, 727-736
95. Ribeiro, M. C. D.; Augusto, O. and Ferreira, A. M. D. *J. Inorg. Biochem.* **1997**, *65*, 15-23
96. Bohle, D. S.; Dinnebier, R. E.; Madsen, S. K. and Stephens, P. W. *J. Biol. Chem.* **1997**, *272*, 713-716
97. Oliveira, M. F.; Timm, B. L.; Machado, E. A.; Miranda, K.; Attias, M.; Silva, J. R.; Dansa-Petretski, M.; de Oliveira, M. A.; de Souza, W.; Pinhal, N. M.; Sousa, J. J. F.; Vugman, N. V. and Oliveira, P. L. *FEBS Lett.* **2002**, *512*, 139-144
98. Foote, S. J. and Cowman, A. F. *Acta Trop.* **1994**, *56*, 157-171
99. Hall, K. A.; Newton, P. N.; Green, M. D.; De Veij, M.; Vandenabeele, P.; Pizzanelli, D.; Mayxay, M.; Dondorp, A. and Fernandez, F. M. *Am. J. Trop. Med. Hyg.* **2006**, *75*, 804-811
100. Baird, J. K. *Am. J. Trop. Med. Hyg.* **2007**, *76*, 201-202
101. Ratsimbasoa, A.; Randriamanantena, A.; Raherinjafy, R.; Rasoarilalao, N. and Menard, D. *Am. J. Trop. Med. Hyg.* **2007**, *76*, 481-485
102. Rakotonirina, H.; Barnadas, C.; Raherijafy, R.; Andrianantenaina, H.; Ratsimbasoa, A.; Randrianasolo, L.; Jahevitra, M.; Andriantsoanirina, V. and Menard, D. *Am. J. Trop. Med. Hyg.* **2008**, *78*, 217-221
103. Wongsrichanalai, C. and Meshnick, S. R. *Emerg. Infect. Disease* **2008**, *14*, 716-719
104. Craft, J. C. *Curr. Opin. Microbiol.* **2008**, *11*, 428-433
105. Macreadie, I.; Ginsburg, H.; Sirawaraporn, W. and Tilley, L. *Parasitol. Today* **2000**, *16*, 438-444
106. Loeb, R. F. and Clarke, W. M. *J. Am. Med. Assoc.* **1946**, *130*, 1069-1070
107. Schlitzer, M. *Arch. Pharm.* **2008**, *341*, 149-163
108. Taylor, W. R. J. and White, N. J. *Drug Safety* **2004**, *27*, 25-61

109. Tingle, M. D.; Jewell, H.; Maggs, J. L.; Oneill, P. M. and Park, B. K. *Biochem. Pharmacol.* **1995**, *50*, 2119-2119
110. Naisbitt, D. J.; Ruscoe, J. E.; Williams, D.; Oneill, P. M.; Pirmohamed, M. and Park, B. K. *J. Pharmacol. Exp. Ther.* **1997**, *280*, 884-893
111. Olliaro, P.; Nevill, C.; Lebras, J.; Ringwald, P.; Mussano, P.; Garner, P. and Brasseur, P. *Lancet* **1996**, *348*, 1196-1201
112. Hoppe, H. C.; van Schalkwyk, D. A.; Wiehart, U. I. M.; Meredith, S. A.; Egan, J. and Weber, B. W. *Antimicrob. Agents Chemother.* **2004**, *48*, 2370-2378
113. Famin, O. and Ginsburg, H. *Biochem. Pharmacol.* **2002**, *63*, 393-398
114. Foley, M. and Tilley, L. *Int. Parasitol.* **1997**, *27*, 231-240
115. Ridley, R. G. *Nature* **2002**, *415*, 686-693
116. Pasvol, G. and Phil, D. *Infect. Dis. Clin. N. Am.* **2005**, *19*, 211-240
117. Cowman, A. F. and Foote, S. J. *Int. Parasitol.* **1990**, *20*, 503-513
118. Price, E. J.; Bevan, J. S. and Rees, A. *Br. J. Clin. Pract.* **1992**, *46*, 138-139
119. Gottschall, J. L.; Elliot, W.; Lianos, E.; McFarland, J. G.; Wolfmeyer, K. and Aster, R. H. *Blood* **1991**, *77*, 306-310
120. Glynne, P.; Salama, A.; Chaudhry, A.; Swirsky, D. and Lightstone, L. *Am. J. Kidney Dis.* **1999**, *33*, 133-137
121. Ezzet, F.; van Vugt, M.; Nosten, F.; Looareesuwan, S. and White, N. J. *Antimicrob. Agents Chemother.* **2000**, *44*, 697-704
122. Winstanley, P. A. *Parasitol. Today* **2000**, *16*, 146-153
123. Kokwaro, G.; Mwai, L. and Nzila, A. *Expert Opin. Pharmaco.* **2007**, *8*, 75-94
124. Chotivanich, K.; Sattabongkot, J.; Udomsangpetch, R.; Looareesuwan, S.; Day, N. P. J.; Coleman, R. E. and White, N. J. *Antimicrob. Agents Chemother.* **2006**, *50*, 1927-1930
125. White, N. J. *Antimicrob. Agents Chemother.* **1997**, *41*, 1413-1422
126. Woodrow, C. J.; Haynes, R. K. and Krishna, S. *Postgrad. Med.* **2005**, *81*, 71-78
127. Kannan, R.; Kumar, K.; Sahal, D.; Kukreti, S. and Chauhan, V. S. *Biochem. J.* **2005**, *385*, 409-418
128. Eckstein-Ludwig, U.; Webb, R. J.; van Goethem, I. D. A.; East, J. M.; Lee, A. G.; Kimura, M.; O'Neill, P. M.; Bray, P. G.; Ward, S. A. and Krishna, S. *Nature* **2003**, *424*, 957-961
129. Fidock, D. A.; Eastman, R. T.; Ward, S. A. and Meshnick, S. R. *Trends Parasitol.* **2008**, *24*, 537-544
130. Dahl, E. L.; Shock, J. L.; Shenai, B. R.; Gut, J.; Derisi, J. L. and Rosenthal, P. J. *Antimicrob. Agents Chemother.* **2006**, *50*, 3124-3131
131. Ramya, T. N. C.; Mishra, S.; Karmodiya, K.; Surolia, N. and Surolia, A. *Antimicrob. Agents Chemother.* **2007**, *51*, 307-316
132. Ashley, E. A. and White, N. J. *Curr. Opin. Infect. Dis.* **2005**, *18*, 531-536
133. Lell, B. and Kremsner, P. G. *Antimicrob. Agents Chemother.* **2002**, *46*, 2315-2320
134. Goodman, C. D.; Su, V. and McFadden, G. I. *Mol. Biochem. Parasitol.* **2007**, *152*, 181-191
135. Harinasuta, T.; Migasen, S. and Boonag, D. *UNESCO First Regional Symposium on Scientific Knowledge of Tropical Parasites* **1962**, *University of Singapore, Singapore*, 148-153

136. Wernsdorfer, W. H. and Payne, D. *Pharmacol. Ther.* **1991**, *50*, 95-121
137. Wongsrichanalai, C.; Pickard, A. L.; Wernsdorfer, W. H. and Meshnick, S. R. *Lancet Infectious Diseases* **2002**, *2*, 209-218
138. Verdier, F.; Lebras, J.; Clavier, F.; Hatin, I. and Blayo, M. C. *Antimicrob. Agents Chemother.* **1985**, *27*, 561-564
139. Yayon, A.; Cabantchik, Z. I. and Ginsburg, H. *Proc. Natl. Acad. Sci. U. S. A.* **1985**, *82*, 2784-2788
140. Geary, T. G.; Divo, A. D.; Jensen, J. B.; Zangwill, M. and Ginsburg, H. *Biochem. Pharmacol.* **1990**, *40*, 685-691
141. Krogstad, D. J.; Gluzman, I. Y.; Kyle, D. E.; Oduola, A. M. J.; Martin, S. K.; Milhous, W. K. and Schlesinger, P. H. *Science* **1987**, *238*, 1283-1285
142. Djimde, A.; Doumbo, O. K.; Cortese, J. F.; Kayentao, K.; Doumbo, S.; Diourte, Y.; Dicko, A.; Su, X. Z.; Nomura, T.; Fidock, D. A.; Wellems, T. E.; Plowe, C. V. and Coulibaly, D. *N. Engl. J. Med.* **2001**, *344*, 257-263
143. Foote, S. J.; Thompson, J. K.; Cowman, A. F. and Kemp, D. J. *Cell* **1989**, *57*, 921-930
144. Babiker, H. A.; Pringle, S. J.; Abdel-Muhsin, A.; Mackinnon, M.; Hunt, P. and Walliker, D. *J. Infect. Dis.* **2001**, *183*, 1535-1538
145. Mayor, A. G.; Gomez-Olive, X.; Aponte, J. J.; Casimiro, S.; Mabunda, S.; Dgedge, M.; Barreto, A. and Alonso, P. L. *J. Infect. Dis.* **2001**, *183*, 1413-1416
146. Basco, L. K. and Ringwald, P. *J. Infect. Dis.* **2001**, *183*, 1828-1831
147. Chen, N.; Russell, B.; Staley, J.; Kotecka, B.; Nasveld, P. and Cheng, Q. *J. Infect. Dis.* **2001**, *183*, 1543-1545
148. Pillai, D. R.; Labbe, A. C.; Vanisaveth, V.; Hongvangthong, B.; Pomphida, S.; Inkathone, S.; Zhong, K. and Kain, K. C. *J. Infect. Dis.* **2001**, *183*, 789-795
149. Vieira, P. P.; Alecrim, M. D.; da Silva, L. H. P.; Gonzalez-Jimenez, I. and Zalis, M. G. *J. Infect. Dis.* **2001**, *183*, 1832-1833
150. vonSeidlein, L.; Duraisingh, M. T.; Drakeley, C. J.; Bailey, R.; Greenwood, B. M. and Pinder, M. *T. Roy. Soc. Trop. Med. Hy.* **1997**, *91*, 450-453
151. Flueck, T. P.; Jelinek, T.; Kilian, A. H. D.; Adagu, I. S.; Kabagambe, G.; Sonnenburg, F. and Warhurst, D. C. *Trop. Med. Int. Health* **2000**, *5*, 174-178
152. Price, R. N.; Cassar, C.; Brockman, A.; Duraisingh, M.; van Vugt, M.; White, N. J.; Nosten, F. and Krishna, S. *Antimicrob. Agents Chemother.* **1999**, *43*, 2943-2949
153. Povoa, M. M.; Adagu, I. S.; Oliveira, S. G.; Machado, R. L. D.; Miles, M. A. and Warhurst, D. C. *Exp. Parasitol.* **1998**, *88*, 64-68
154. Zalis, M. G.; Pang, L.; Silveira, M. S.; Milhous, W. K. and Wirth, D. F. *Am. J. Trop. Med. Hyg.* **1998**, *58*, 630-637
155. Nagesha, H. S.; Din, S.; Casey, G. J.; Susanti, A. I.; Fryauff, D. J.; Reeder, J. C. and Cowman, A. F. *T. Roy. Soc. Trop. Med. Hy.* **2001**, *95*, 43-49
156. Olliaro, P. *Pharmacol. Ther.* **2001**, *89*, 207-219
157. Nocht, B. and Werner, H. *Dtsch Med Wochenschr* **1910**, *36*, 1557-1560

158. Adams, A. R. D. and Seaton, D. R. *T. Roy. Soc. Trop. Med. Hy.* **1949**, *42*, 314-316
159. Walker, A. J. and Lopez-Antunano, F. J. *T. Roy. Soc. Trop. Med. Hy.* **1968**, 654-667
160. Harinasuta, T.; Viravan, C. and Reid, H. A. *Lancet* **1967**, *1*, 1117-1119
161. Nosten, F.; Terkuile, F.; Chongsuphajaisiddhi, T.; Luxemburger, C.; Webster, H. K.; Edstein, M.; Phaipun, L.; Thew, K. L. and White, N. J. *Lancet* **1991**, *337*, 1140-1143
162. Jelinek, T.; Grobusch, M. P. and Loscher, T. *Eur. J. Clin. Microbiol.* **2001**, *20*, 284-286
163. Yang, H.; Lui, D.; Fan, B.; Yang, P.; Li, X.; Li, C.; Dong, Y. and Yang, C. *T. Roy. Soc. Trop. Med. Hy.* **2003**, *97*, 226-228
164. Looareesuwan, S.; Kyle, D. E.; Viravan, C.; Vanijanonta, S.; Wilairatana, P. and Wernsdorfer, W. H. *Am. J. Trop. Med. Hyg.* **1996**, *54*, 205-209
165. Baird, J. K. *N. Engl. J. Med.* **2005**, *352*, 1565-1577
166. Wolfe, E. B.; Parise, M. E.; Haddix, A. C.; Nahlen, B. L.; Ayisi, J. G.; Misore, A. and Steketee, R. W. *Am. J. Trop. Med. Hyg.* **2001**, *64*, 178-186
167. Looareesuwan, S.; Chulay, J. D.; Canfield, C. J. and Hutchinson, D. B. A. *Am. J. Trop. Med. Hyg.* **1999**, *60*, 533-541
168. Hudson, A. T. *Parasitol. Today* **1993**, *9*, 66-68
169. Vaidya, A. B.; Lashgari, M. S.; Pologe, L. G. and Morrisey, J. *Mol. Biochem. Parasitol.* **1993**, *58*, 33-42
170. Krungkrai, J. *BBA - Gen. Subjects* **1995**, *1243*, 351-360
171. Painter, H. J.; Morrisey, J. M.; Mather, M. W. and Vaidya, A. B. *Nature* **2007**, *446*, 88-91
172. Rosenthal, P. J. *J. Exp. Biol.* **2003**, *206*, 3735-3744
173. Kaschula, C. H.; Egan, T. J.; Hunter, R.; Basilico, N.; Parapini, S.; Taramelli, D.; Pasini, E. and Monti, D. *J. Med. Chem.* **2002**, *45*, 3531-3539
174. Walsh, D. S.; Looareesuwan, S.; Wilairatana, P.; Heppner, D. G.; Tang, D. B.; Brewer, T. G.; Chokejindachai, W.; Viriyavejakul, P.; Kyle, D. E.; Milhous, W. K.; Schuster, B. G.; Horton, J.; Braitman, D. J. and Brueckner, R. P. *J. Infect. Dis.* **1999**, *180*, 1282-1287
175. Bitonti, A. J.; Sjoerdsma, A.; Mccann, P. P.; Kyle, D. E.; Oduola, A. M. J.; Rossan, R. N.; Milhous, W. K. and Davidson, D. E. *Science* **1988**, *242*, 1301-1303
176. Martin, S. K.; Oduola, A. M. J. and Milhous, W. K. *Science* **1987**, *235*, 899-901
177. Sowunmi, A.; Oduola, A. M. J.; Ogundahunsi, O. A. T. and Salako, L. A. *Trop. Med. Int. Health* **1998**, *3*, 177-183
178. Alibert, S.; Santelli-Rouvier, C.; Pradines, B.; Houdoin, C.; Parzy, D.; Karolak-Wojciechowska, J. and Barbe, J. *J. Med. Chem.* **2002**, *45*, 3195-3209
179. Batra, S.; Srivastava, P.; Roy, K.; Pandey, V. C. and Bhaduri, A. P. *J. Med. Chem.* **2000**, *43*, 3428-3433
180. Alonso, P. L.; Sacarlal, J.; Aponte, J. J.; Leach, A.; Macete, E.; Milman, J.; Mandomando, I.; Spiessens, B.; Guinovart, C.; Espasa, M.; Bassat, Q.; Aide, P.; Ofori-Anyinam, O.; Navia, M. M.; Corachan, S.; Ceuppens, M.; Dubois, M. C.; Demoitie, M. A.; Dubovsky, F.; Menendez, C.; Tornieporth, N.; Ballou, W. R.; Thompson, R. and Cohen, J. *Lancet* **2004**, *364*, 1411-1420

181. Aponte, J. J.; Aide, P.; Renom, M.; Mandomando, I.; Bassat, Q.; Sacarlal, J.; Manaca, M. N.; Lafuente, S.; Barbosa, A.; Leach, A.; Lievens, M.; Vekemans, J.; Sigaugue, B.; Dubois, M. C.; Demoitie, M. A.; Sillman, M.; Savarese, B.; Mcneil, J. G.; Macete, E.; Ballou, W. R.; Cohen, J. and Alonso, P. L. *Lancet* **2007**, *370*, 1543-1551

182. Bejon, P.; Lusingu, J.; Olotu, A.; Leach, A.; Lievens, M.; Vekemans, J.; Mshamu, S.; Lang, T.; Gould, J.; Dubois, M.; Demoitie, M.; Stallaert, J. F.; Vansadia, P.; Carter, T.; Njuguna, P.; Awuondo, K. O.; Malabeja, A.; Abdul, O.; Gesase, S.; Mturi, N.; Drakeley, C. J.; Savarese, B.; Villafana, T.; Ballou, W. R.; Cohen, J.; Riley, E. M.; Lemnge, M. M.; Marsh, K. and von Seidlein, L. *N. Engl. J. Med.* **2008**, *359*, 2521-2532

183. Abdulla, S.; Oberholzer, R.; Juma, O.; Kubhoja, S.; Machera, F.; Membi, C.; Omari, S.; Urassa, A.; Mshinda, H.; Jumanne, A.; Salim, N.; Shomari, M.; Aebi, T.; Schellenberg, D. M.; Carter, T.; Villafana, T.; Demoitie, M. A.; Dubois, M. C.; Leach, A.; Lievens, M.; Vekemans, J.; Cohen, J.; Ballou, W. R. and Tanner, M. *N. Engl. J. Med.* **2008**, *359*, 2533-2544

184. Olotu, A.; Lusingu, J.; Leach, A.; Lievens, M.; Vekemans, J.; Msham, S.; Lang, T.; Gould, J.; Dubois, M. C.; Jongert, E.; Vansadia, P.; Carter, T.; Njuguna, P.; Awuondo, K. O.; Malabeja, A.; Abdul, O.; Gesase, S.; Mturi, N.; Drakeley, C. J.; Savarese, B.; Villafana, T.; Lapierre, D.; Ballou, W. R.; Cohen, J.; Lemnge, M. M.; Peshu, N.; Marsh, K.; Riley, E. M.; von Seidlein, L. and Bejon, P. *Lancet Infectious Diseases* **2011**, *11*, 102-109

185. Asante, K. P.; Abdulla, S.; Agnandji, S.; Lyimo, J.; Vekemans, J.; Soulanoudjingar, S.; Owusu, R.; Shomari, M.; Leach, A.; Jongert, E.; Salim, N.; Fernandes, J. F.; Dosoo, D.; Chikawe, M.; Issifou, S.; Osei-Kwakye, K.; Lievens, M.; Paricek, M.; Moller, T.; Apanga, S.; Mwangoka, G.; Dubois, M. C.; Madi, T.; Kwara, E.; Minja, R.; Hounkpatin, A. B.; Boahen, O.; Kayan, K.; Adjei, G.; Chandramohan, D.; Carter, T.; Vansadia, P.; Sillman, M.; Savarese, B.; Loucq, C.; Lapierre, D.; Greenwood, B.; Cohen, J.; Kremsner, P.; Owusu-Agyei, S.; Tanner, M. and Lell, B. *Lancet Infectious Diseases* **2011**, *11*, 741-749

186. Fact Sheet: RTS,S Malaria Vaccine Candidate. www.gsk.com (accessed Oct. 2011)

187. Agnandji, S.; Lell, B.; Soulanoudjingar, S.; Fernandes, J. F.; Abossolo, B. P.; Conzelman, C.; Methogo, B. G.; Doucka, Y.; Flaman, A.; Mordmüller, B.; Issifou, S.; Kremsner, P.; Sacarlal, J.; Aide, P.; Lanaspa, M.; Aponte, J. J.; Nhamuave, A.; Quelhas, D.; Bassat, Q.; Mandjate, S.; Macete, E.; Alonso, P. L.; Abdulla, S.; Salim, N.; Juma, O.; Shomari, M.; Shubis, K.; Machera, F.; Hamad, A. S.; Minja, R.; Mtoro, A.; Tabatabai, M.; Aide, P.; Urassa, A.; Ali, A. M.; Mwangoka, G.; Tanner, M.; Tinto, H.; D'Alessandro, U.; Sorgho, H.; Valea, I.; Tahita, M. C.; Kaboré, W.; Ouédraogo, S.; Sandrine, Y.; Guiguemdé, R. T.; Ouédraogo, J. B.; Hamel, M. J.; Kariuki, S.; Odero, C.; Oneko, M.; Otieno, K.; Awino, N.; Omoto, J.; Williams, J.; Muturi-Kioi, V.; Laserson, K. F.; Slutsker, L.; Otieno, W.; Otieno, L.; Nekoye, O.; Gondi, S.; Otieno, A.; Ogutu, B.; Wasuna, R.; Owira, V.; Jones, D.; Onyango, A. A.; Njugina, P.; Chilengi, R.; Akoo, P.; Kerubo, C.; Gitaka, J.; Maingi, C.; Lang, T.; Olotu, A.; Tsofa, B.; Bejon, P.; Peshu, N.; Marsh, K.; Owusu-Agyei, S.; Asante, K. P.; Osei-Kwakye, K.; Boahen, O.; Ayamba, S.; Kayan, K.; Owusu-Ofori, R.; Dosoo, D.; Asante, I.; Adjei, G.; Adjei, G.; Chandramohan, D.; Greenwood, B.; Lusingu, J.; Gesase, S.; Malabeja, A.; Abdul, O.; Kilavo, H.; Mahende, C.; Liheluka, E.; Lemnge, M. M.; Theander, T.; Drakeley, C.; Ansong, D.; Agbenyega, T.; Adjei, S.; Boateng, H. O.; Rettig, T.; iBawa, J.; Sylverken, J.; Sambian, D.; Agyekum, A.; Owusu, L.; Martinson, F.;

Hoffman, I.; Mvalo, T.; Kamthunzi, P.; Nkomo, R.; Msika, A.; Jumbe, A.; Chome, N.; Nyakuipa, D.; Chintedza, J.; Ballou, W. R.; Bruls, M.; Cohen, J.; Guerra, Y.; Jongert, E.; Lapierre, D.; Leach, A.; Lievens, M.; Ofori-Anyinam, O.; Vekemans, J.; Carter, T.; Leboulleux, D.; Loucq, C.; Radford, A.; Savarese, B.; Schellenberg, D. M.; Sillman, M.; Vansadia, P. and RTS, S. C. T. P. *N. Engl. J. Med.* **2011**, *365*, 1863-1875

188. *First results from ongoing Phase III trial show malaria vaccine candidates, RTS,S* reduces the risk of malaria by half in African children aged 5 to 17 months (Press Release)* GlaxoSmithKline plc.: Brentford, Middlesex;
189. Arno, M.; Betancur-Galvis, L.; Gonzalez, M. A.; Sierra, J. and Zaragoza, R. J. *Bioorg. Med. Chem.* **2003**, *11*, 3171-3177
190. Cafieri, F.; Fattorusso, E.; Magno, S.; Santacroce, C. and Sica, D. *Tetrahedron* **1973**, *29*, 4259-4262
191. Fattorusso, E.; Magno, S.; Mayol, L.; Santacroce, C. and Sica, D. *Tetrahedron* **1975**, *31*, 269-270
192. Diblasio, B.; Fattorusso, E.; Magno, S.; Mayol, L.; Pedone, C.; Santacroce, C. and Sica, D. *Tetrahedron* **1976**, *32*, 473-478
193. Collins, P. *Coral Research Foundation*, Palau, **2011**
194. Angerhofer, C. K.; Pezzuto, J. M.; Konig, G. M.; Wright, A. D. and Sticher, O. *J. Nat. Prod.* **1992**, *55*, 1787-1789
195. Konig, G. M.; Wright, A. D. and Angerhofer, C. K. *J. Org. Chem.* **1996**, *61*, 3259-3267
196. Wright, A. D.; Wang, H. Q.; Gurrath, M.; Konig, G. M.; Kocak, G.; Neumann, G.; Loria, P.; Foley, M. and Tilley, L. *J. Med. Chem.* **2001**, *44*, 873-885
197. Wattanapiromsakul, C.; Chanthathamrongsiri, N.; Bussarawit, S.; Yuenyongsawad, S.; Plubrukarn, A. and Suwanborirux, K. *Can. J. Chem.* **2009**, *87*, 612-618
198. Aviles, E. and Rodriguez, A. D. *Org. Lett.* **2010**, *12*, 5290-5293
199. Miyaoka, H.; Shimomura, M.; Kimura, H.; Yamada, Y.; Kim, H. S. and Wataya, Y. *Tetrahedron* **1998**, *54*, 13467-13474
200. Burreson, B. J.; Christophersen, C. and Scheuer, P. J. *Tetrahedron* **1975**, *31*, 2015-2018
201. Gulavita, N. K.; Desilva, E. D.; Hagadone, M. R.; Karuso, P.; Scheuer, P. J.; Vanduyne, G. D. and Clardy, J. *J. Org. Chem.* **1986**, *51*, 5136-5139
202. Sun, J. Z.; Chen, K. S.; Liu, H. L.; van Soest, R. and Guo, Y. W. *Helv. Chim. Acta* **2010**, *93*, 517-521
203. Adendorff, M. R. *Marine Anti-Malarial Isonitriles: A Synthetic and Computational Approach,* Masters Thesis, Rhodes University, 2010
204. Wright, A. D.; McCluskey, A.; Robertson, M. J.; MacGregor, K. A.; Gordon, C. P. and Guenther, J. *Org. Biomol. Chem.* **2011**, *9*, 400-407
205. Linn, T. Z.; Awale, S.; Tezuka, Y.; Banskota, A. H.; Kalauni, S. K.; Attamimi, F.; Ueda, J.; Asih, P. B. S.; Syafruddin, D.; Tanaka, K. and Kadota, S. *J. Nat. Prod.* **2005**, *68*, 706-710
206. Kalauni, S. K.; Awale, S.; Tezuka, Y.; Banskota, A. H.; Linn, T. Z.; Asih, P. B. S.; Syafruddin, D. and Kadota, S. *Biol. Pharm. Bull* **2006**, *29*, 1050-1052
207. Sathe, M. and Kaushik, M. P. *Bioorg. Med. Chem. Lett.* **2010**, *20*, 1312-1314

208. da Silva, A. A.; Resende, D. O.; Fukui, M. J.; Santos, F. F.; Pauletti, P. M.; Cunha, W. R.; Silva, M. L. A.; Gregorio, L. E.; Bastos, J. K. and Nanayakkara, N. P. D. *Fitoterapia* **2009**, *80*, 478-482
209. Uys, A. C. U.; Malan, S. F.; van Dyk, S. and van Zyl, R. L. *Bioorgan. Med. Chem. Lett.* **2002**, *12*, 2167-2169
210. Loyola, L. A.; Borquez, J.; Morales, G.; San Martin, A.; Darias, J.; Flores, N. and Gimenez, A. *Phytochemistry* **2004**, *65*, 1931-1935
211. Adelekan, A. M.; Prozesky, E. A.; Hussein, A. A.; Urena, L. D.; van Rooyen, P. H.; Liles, D. C.; Meyer, J. J. M. and Rodriguez, B. *J. Nat. Prod.* **2008**, *71*, 1919-1922
212. Sutthivaiyakit, S.; Mongkolvisut, W.; Prabpai, S. and Kongsaeree, P. *J. Nat. Prod.* **2009**, *72*, 2024-2027
213. Jullian, V.; Bonduelle, C.; Valentin, A.; Acebey, L.; Duigou, A. G.; Prevost, M. F. and Sauvain, M. *Bioorgan. Med. Chem. Lett.* **2005**, *15*, 5065-5070
214. Clarkson, C.; Campbell, W. E. and Smith, P. *Planta Medica* **2003**, *69*, 720-724
215. Chukwujekwu, J. C.; Smith, P.; Coombes, P. H.; Mulholland, D. A. and van Staden, J. *J. Ethnopharmacol.* **2005**, *102*, 295-297
216. Lekphrom, R.; Kanokmedhakul, S. and Kanokmedhakul, K. *Planta Med.* **2010**, *76*, 726-728
217. van Zyl, R. L.; Khan, F.; Edwards, T. J. and Drewes, S. E. *S. Afr. J. Sci.* **2008**, *104*, 62-64
218. Thongnest, S.; Mahidol, C.; Sutthivaiyakit, S. and Ruchirawat, S. *J. Nat. Prod.* **2005**, *68*, 1632-1636
219. Wangchuk, P.; Bremner, J. B.; Samten; Skelton, B. W.; White, A. H.; Rattanajak, R. and Kamchonwongpaisan, S. *J. Ethnopharmacol.* **2010**, *130*, 559-562
220. Riel, M. A.; Kyle, D. E. and Milhous, W. K. *J. Nat. Prod.* **2002**, *65*, 614-615
221. Abad, A.; Arno, M.; Marin, M. L. and Zaragoza, R. J. *J. Chem. Soc. , Perkin Trans. 1* **1993**, 1861-1867
222. Appenzeller, J.; Mihci, G.; Martin, M. T.; Gallard, J. F.; Menou, J. L.; Boury-Esnalllt, N.; Hooper, J.; Petek, S.; Chevalley, S.; Valentin, A.; Zaparucha, A.; Al Mourabit, A. and Debitus, C. *J. Nat. Prod.* **2008**, *71*, 1451-1454
223. Marcos, I. S.; Garcia, N.; Sexmero, A. J.; Basabe, P.; Diez, D. and Urones, J. G. *Tetrahedron* **2005**, *61*, 11672-11678
224. Piers, E. and Roberge, J. Y. *Tetrahedron Lett.* **1992**, *33*, 6923-6926
225. Ospina, C. A.; Rodriguez, A. D.; Ortega-Barria, E. and Capson, T. L. *J. Nat. Prod.* **2003**, *66*, 357-363
226. Marrero, J.; Rodriguez, A. D.; Baran, P.; Raptis, R. G.; Sanchez, J. A.; Ortega-Barria, E. and Capson, T. L. *Org. Lett.* **2004**, *6*, 1661-1664
227. Ospina, C. A.; Rodriguez, A. D.; Sanchez, J. A.; Ortega-Barria, E.; Capson, T. L. and Mayer, A. M. S. *J. Nat. Prod.* **2005**, *68*, 1519-1526
228. Rodriguez, I. I.; Rodriguez, A. D. and Zhao, H. *J. Org. Chem.* **2009**, *74*, 7581-7584
229. Rodriguez, A. D. and Ramirez, C. *Org. Lett.* **2000**, *2*, 507-510
230. Wei, X. M.; Rodriguez, A. D.; Baran, P. and Raptis, R. G. *J. Nat. Prod.* **2010**, *73*, 925-934
231. Rodriguez, A. D.; Gonzalez, E. and Ramirez, C. *Tetrahedron* **1998**, *54*, 11683-11729
232. Lane, A. L.; Stout, E. P.; Lin, A. S.; Prudhomme, J.; Le Roch, K.; Fairchild, C. R.; Franzblau, S. G.; Hay, M. E.; Aalbersberg, W. and Kubanek, J. *J. Org. Chem.* **2009**, *74*, 2736-2742

233. Stout, E. P.; Prudhomme, J.; Le Roch, K.; Fairchild, C. R.; Franzblau, S. G.; Aalbersberg, W.; Hay, M. E. and Kubanek, J. *Bioorg. Med. Chem. (Lett.)* **2010**, *20*, 5662-5665
234. Discher, D. E. and Carl, P. *Cell. Mol. Biol. Lett.* **2001**, *6*, 593-606
235. Ziegler, H. L.; Franzyk, H.; Sairafianpour, M.; Tabatabai, M.; Tehrani, M. D.; Bagherzadeh, K.; Hagerstrand, H.; Staerk, D. and Jaroszewski, J. W. *Bioorgan. Med. Chem.* **2004**, *12*, 119-127
236. Asili, J.; Lambert, M.; Ziegler, H. L.; Staerk, D.; Sairafianpour, M.; Witt, M.; Asghari, G.; Ibrahimi, I. S. and Jaroszewski, J. W. *J. Nat. Prod.* **2004**, *67*, 631-637
237. Sheetz, M. P. and Singer, S. J. *J. Cell Biol.* **1976**, *70*, 247-251
238. Sheetz, M. P. and Singer, S. J. *J. Proc. Natl. Acad. Sci. U. S. A.* **1974**, *71*, 4457-4461
239. Desai, S. A.; Bezrukov, S. M. and Zimmerberg, J. *Nature* **2000**, *406*, 1001-1005
240. Ziegler, H. L.; Staerk, D.; Christensen, J.; Hviid, L.; Hagerstrand, H. and Jaroszewski, J. W. *Antimicrob. Agents Chemother.* **2002**, *46*, 1441-1446
241. Ziegler, H. L.; Staerk, D.; Christensen, J.; Olsen, C. E.; Sittie, A. A. and Jaroszewski, J. W. *J. Nat. Prod.* **2002**, *65*, 1764-1768
242. Ziegler, H. L.; Jensen, T. H.; Christensen, J.; Staerk, D.; Hagerstrand, H.; Sittie, A.; Olsen, C. E.; Staalso, T.; Epke, P. and Jaroszewski, J. W. *Planta Med.* **2002**, *68*, 547-549
243. Isomaa, B.; Hagerstrand, H. and Paatero, G. *Biochim. Biophys. Acta* **1987**, *899*, 93-103
244. Van Wyk, A. W. W.; Lobb, K. A.; Caira, M. R.; Hoppe, H. C. and Davies-Coleman, M. T. *J. Nat. Prod.* **2007**, *70*, 1253-1258
245. Hoshino, T.; Nakano, C.; Ootsuka, T.; Shinohara, Y. and Hara, T. *Org. Biomol. Chem.* **2011**, *9*, 2156-2165
246. Sundararaman, P. and Herz, W. *J. Org. Chem.* **1977**, *42*, 813-819
247. Ravn, M. M.; Coates, R. M.; Flory, J. E.; Peters, R. J. and Croteau, R. *Org. Lett.* **2000**, *2*, 573-576
248. van Wyk, A. W. W. *Studies in Marine Diterpene Chemistry,* PhD Thesis, Rhodes University, 2007
249. Clayden, J., Greeves, N., Warren, S., and Wothers, P. *Organic Chemistry*, 1st ed.; Oxford University Press, New York, 2001; 938-939
250. Hatano, M.; Suzuki, S. and Ishihara, K. *J. Am. Chem. Soc.* **2006**, *128*, 9998-9999
251. Imamoto, T.; Takiyama, N.; Nakamura, K.; Hatajima, T. and Kamiya, Y. *J. Am. Chem. Soc.* **1989**, *111*, 4392-4398
252. Ashby, E. C. *Pure and Applied Chemistry* **1980**, *52*, 545-569
253. Imamoto, T. *Pure and Applied Chemistry* **1990**, *62*, 747-752
254. Kagan, H. B. and Namy, J. L. *Tetrahedron* **1986**, *42*, 6573-6614
255. Matsukawa, S.; Funabashi, Y. and Imamoto, T. *Tetrahedron Lett.* **2003**, *44*, 1007-1010
256. Corey, E. J. and Ha, D. C. *Tetrahedron Lett.* **1988**, *29*, 3171-3174
257. Imamoto, T.; Takiyama, N. and Nakamura, K. *Tetrahedron Lett.* **1985**, *26*, 4763-4766
258. Maruoka, K.; Itoh, T.; Sakurai, M.; Nonoshita, K. and Yamamoto, H. *J. Am. Chem. Soc.* **1988**, *110*, 3588-3597
259. Caira, M. R. *pers. commun.* 2010
260. Simpson, J. H. *Organic Structure Determination*, 1st ed.; Elsevier, London, 2008; 113

261. Roy, S. C.; Rana, K. K.; Guin, C. and Banerjee, B. *Synlett* **2003**, 221-222
262. Hubbard, A.; Okazaki, T. and Laali, K. K. *Aust. J. Chem.* **2007**, *60*, 923-927
263. Mendonca, G. F. and de Mattos, M. C. S. *Quim. Nova* **2008**, *31*, 798-801
264. Duddeck, H. and Islam, M. R. *Tetrahedron* **1981**, *37*, 1193-1197
265. Kitano, Y.; Chiba, K. and Tada, M. *Tetrahedron Lett.* **1998**, *39*, 1911-1912
266. Kitano, Y.; Chiba, K. and Tada, M. *Synthesis-Stuttgart* **2001**, 437-443
267. Kitano, Y.; Ito, T.; Suzuki, T.; Nogata, Y.; Shinshima, K.; Yoshimura, E.; Chiba, K.; Masahiro, T. A. and Sakaguchi, I. *J. Chem. Soc. , Perkin Trans. 1* **2002**, 2251-2255
268. Socrates, G. *Infrared and Raman Characteristic Group Frequencies*, 3rd ed.; John Wiley & Sons, Chichester, 2001; 86
269. Goble, J. L. *The druggable antimalarial target 1-deoxy-D-xylulose-5-phosphate reductoisomerase:purification, kinetic characterization and inhibition studies,* PhD Thesis, Rhodes University, 2011
270. Singh, N.; Cheve, G.; Avery, M. A. and McCurdy, C. R. *Curr. Opin. Pharm. Design.* **2007**, *13*, 1161-1177
271. Gräwert, T.; Groll, M.; Rohdich, F.; Bacher, A. and Eisenreich, W. *Cell. Mol. Life. Sci.* **2011**,
272. Lois, L. M.; Campos, N.; Putra, S. R.; Danielsen, K.; Rohmer, M. and Boronat, A. *Proc. Natl. Acad. Sci. U. S. A.* **1998**, *95*, 2105-2110
273. Takahashi, S.; Kuzuyama, T.; Watanabe, H. and Seto, H. *Proc. Natl. Acad. Sci. U. S. A.* **1998**, *95*, 9879-9884
274. Rohdich, F.; Wungsintaweekul, J.; Fellermeier, M.; Sagner, S.; Herz, S.; Kis, K.; Eisenreich, W.; Bacher, A. and Zenk, M. H. *Proc. Natl. Acad. Sci. U. S. A.* **1999**, *96*, 11758-11763
275. Luttgen, H.; Rohdich, F.; Herz, S.; Wungsintaweekul, J.; Hecht, S.; Schuhr, C. A.; Fellermeier, M.; Sagner, S.; Zenk, M. H.; Bacher, A. and Eisenreich, W. *Proc. Natl. Acad. Sci. U. S. A.* **2000**, *97*, 1062-1067
276. Herz, S.; Wungsintaweekul, J.; Schuhr, C. A.; Hecht, S.; Luttgen, H.; Sagner, S.; Fellermeier, M.; Eisenreich, W.; Zenk, M. H.; Bacher, A. and Rohdich, F. *Proc. Natl. Acad. Sci. U. S. A.* **2000**, *97*, 2486-2490
277. Krasutsky, S. G. *Synthesis of substrate analogues of the methylerythritol phosphate pathway,* PhD Thesis, The University of Utah, 2011
278. Rohdich, F.; Hecht, S.; Gartner, K.; Adam, P.; Krieger, C.; Amslinger, S.; Arigoni, D.; Bacher, A. and Eisenreich, W. *Proc. Natl. Acad. Sci. U. S. A.* **2002**, *99*, 1158-1163
279. Proteau, P. J. *Bioorg. Chem.* **2004**, *32*, 483-493
280. Argyrou, A. and Blanchard, J. S. *Biochemistry* **2004**, *43*, 4375-4384
281. Umeda, T.; Tanaka, N.; Kusakabe, M.; Kitade, Y. and Nakamura, K. T. *Scientific Reports* **2011**, *9*, 1-8
282. Reuter, K.; Sanderbrand, S.; Jomaa, H.; Wiesner, J.; Steinbrecher, I.; Beck, E.; Hintz, M.; Klebe, G. and Stubbs, M. T. *J. Biol. Chem.* **2002**, *277*, 5378-5384
283. Hoeffler, J. F.; Tritsch, D.; Grosdemange-Billiard, C. and Rohmer, M. *Eur. J. Biochem* **2002**, *269*, 4446-4457
284. Arigoni, D.; Giner, J. L.; Sagner, S.; Wungsintaweekul, J.; Zenk, M. H.; Kis, K.; Bacher, A. and Eisenreich, W. *Chem. Commun.* **1999**, 1127-1128

285. Okuhara, M.; Kuroda, Y.; Goto, T.; Okamoto, M.; Terano, H.; Kohsaka, M.; Aoki, H. and Imanaka, H. *J. Antibiot.* **1980**, *33*, 24-28
286. Zeidler, J.; Schwender, J.; Muller, C.; Wiesner, J.; Weidemeyer, C.; Beck, E.; Jomaa, H. and Lichtenthaler, H. K. *Z. Naturforsch. , C: Biosci.* **1998**, *53*, 980-986
287. Jomaa, H.; Wiesner, J.; Sanderbrand, S.; Altincicek, B.; Weidemeyer, C.; Hintz, M.; Turbachova, I.; Eberl, M.; Zeidler, J.; Lichtenthaler, H. K.; Soldati, D. and Beck, E. *Science* **1999**, *285*, 1573-1576
288. Steinbacher, S.; Kaiser, J.; Eisenreich, W.; Huber, R.; Bacher, A. and Rohdich, F. *J. Biol. Chem.* **2003**, *278*, 18401-18407
289. Haemers, T.; Wiesner, J.; Van Poecke, S.; Goeman, J.; Henschker, D.; Beck, E.; Jomaa, H. and Van Calenbergh, S. *Bioorg. Med. Chem. (Lett.)* **2006**, *16*, 1888-1891
290. Devreux, V.; Wiesner, J.; Jomaa, H.; Van der Eycken, J. and Van Calenbergh, S. *Bioorgan. Med. Chem. Lett.* **2007**, *17*, 4920-4923
291. Herforth, C.; Wiesner, J.; Heidler, P.; Sanderbrand, S.; Van Calenbergh, S.; Jomaa, H. and Link, A. *Bioorg. Med. Chem.* **2004**, *12*, 755-762
292. Gelb, M. H. *Curr. Opin. Chem. Biol.* **2007**, *11*, 440-445
293. Fitch, C. D. and Kanjananggulpan, P. *J. Biol. Chem.* **1987**, *262*, 15552-15555
294. Slater, A. F. G.; Swiggard, W. J.; Orton, B. R.; Flitter, W. D.; Goldberg, D. E.; Cerami, A. and Henderson, G. B. *Proc. Natl. Acad. Sci. U. S. A.* **1991**, *88*, 325-329
295. Bohle, D. S.; Conklin, B. J.; Cox, D.; Madsen, S. K.; Paulson, S.; Stephens, P. W. and Yee, G. T. *ACS Sym. Ser.* **1994**, *572*, 497-515
296. Buller, R.; Peterson, M. L.; Almarsson, O. and Leiserowitz, L. *Cryst. Growth Des.* **2002**, *2*, 553-562
297. Huey, R.; Morris, G. M.; Olson, A. J. and Goodsell, D. S. *J. Comput. Chem.* **2007**, *28*, 1145-1152
298. Asghari-Khiavi, M.; Vongsvivut, J.; Perepichka, I.; Mechler, A.; Wood, B. R. and Bohle, D. S. *J. Inorg. Biochem.* **2011**, *(Accepted)*,
299. Sullivan, D. J.; Gluzman, I. Y.; Russell, D. G. and Goldberg, D. E. *Proc. Natl. Acad. Sci. U. S. A.* **1996**, *93*, 11865-11870
300. Sullivan, D. J.; Matile, H.; Ridley, R. G. and Goldberg, D. E. *J. Biol. Chem.* **1998**, *273*, 31103-31107
301. Egan, T. J.; Mavuso, W. W. and Ncokazi, K. K. *Biochemistry* **2001**, *40*, 204-213
302. Cornell, W. D.; Cieplak, P.; Bayly, C. I. and Kollman, P. A. *J. Am. Chem. Soc.* **1993**, *115*, 9620-9631
303. Pagola, S.; Stephens, P. W.; Bohle, D. S.; Kosar, A. D. and Madsen, S. K. *Nature* **2000**, *404*, 307-310
304. Macrae, C. F.; Bruno, I. J.; Chrisholm, J. A.; Edgington, P. R.; McCabe, P.; Pidcock, E.; Rodriguez-Monge, L.; Taylor, R.; van de Streek, J. and Woods, P. A. *J. Appl. Crystallogr.* **2008**, *41*, 466-470
305. Slater, A. F. G. and Cerami, A. *Nature* **1992**, *355*, 167-169
306. Dorn, A.; Stoffel, R.; Matile, H.; Bubendorf, A. and Ridley, R. G. *Nature* **1995**, *374*, 269-271
307. Sullivan, D. J.; Gluzman, I. Y. and Goldberg, D. E. *Science* **1996**, *271*, 219-222
308. Dorn, A.; Vippagunta, S. R.; Matile, H.; Bubendorf, A.; Vennerstrom, J. L. and Ridley, R. G. *Biochem. Pharmacol.* **1998**, *55*, 737-747

309. Kurosawa, Y.; Dorn, A.; Kitsuji-Shirane, M.; Shimada, H.; Satoh, T.; Matile, H.; Hofheinz, W.; Masciadri, R.; Kansy, M. and Ridley, R. G. *Antimicrob. Agents Chemother.* **2000**, *44*, 2638-2644
310. Basilico, N.; Pagani, E.; Monti, D.; Olliaro, P. and Taramelli, D. *J. Antimicrob. Chemoth.* **1998**, *42*, 55-60
311. Parapini, S.; Basilico, N.; Pasini, E.; Egan, T. J.; Olliaro, P.; Taramelli, D. and Monti, D. *Exp. Parasitol.* **2000**, *96*, 249-256
312. Baelmans, R.; Deharo, E.; Bourdy, G.; Munoz, V.; Quenevo, C.; Sauvain, M. and Ginsburg, H. *J. Ethnopharmacol.* **2000**, *73*, 271-275
313. Ncokazi, K. K. and Egan, T. J. *Anal. Biochem.* **2005**, *338*, 306-319
314. Egan, T. J.; Ross, D. C. and Adams, P. A. *FEBS Lett.* **1994**, *352*, 54-57
315. Sullivan, A. D.; Ittarat, I. and Meshnick, S. R. *Parasitology* **1996**, *112*, 285-294
316. Berger, B. J.; Bendrat, K. and Cerami, A. *Anal. Biochem.* **1995**, *231*, 151-156
317. Stiebler, R.; Soares, J. B. R. C.; Timm, B. L.; Silva, J. R.; Mury, F. B.; Dansa-Petretski, M. and Oliveira, M. F. *J. Bioenerg. Biomembr.* **2011**, *43*, 93-99
318. Trang, D. T. X.; Huy, N. T.; Uyen, D. T.; Sasai, M.; Shiono, T.; Harada, S. and Kamei, K. *Anal. Biochem.* **2006**, *349*, 292-296
319. Hoang, A. N.; Ncokazi, K. K.; de Villiers, K. A.; Wright, D. W. and Egan, T. J. *Dalton Trans.* **2010**, *39*, 1235-1244
320. Choi, C. Y.; Schneider, E. L.; Kim, J. M.; Gluzman, I. Y.; Goldberg, D. E.; Ellman, J. A. and Marletta, M. A. *Chem. Biol.* **2002**, *9*, 852-853
321. Jani, D.; Nagarkatti, R.; Beatty, W.; Angel, R.; Slebodnick, C.; Andersen, J.; Kumar, S. and Rathore, D. *PLoS Pathog.* **2008**, *4*,
322. Mury, F. B.; da Silva, J. R.; Ferreira, L. S.; Ferreira, B. D.; de Souza, G. A.; Souza-Neto, J. A.; Ribolla, P. E. M.; Silva, C. P.; do Nascimento, V. V.; Machado, O. L. T.; Berbert-Molina, M. A. and Dansa-Petretski, M. *PLoS One* **2009**, *4*,
323. Egan, T. J. and Ncokazi, K. K. *J. Inorg. Biochem.* **2005**, *99*, 1532-1539
324. Marques, H. M.; Munro, O. Q. and Crawcour, M. L. *Inorg. Chim. Acta* **1992**, *196*, 221-229
325. Pagola, S.; Stephens, P. W.; Bohle, D. S.; Kosar, A. D. and Madsen, S. K. *Nature* **2000**, *404*, 307-310
326. Hempelmann, E. and Marques, H. M. *J. Pharmacol. Toxicol. Methods* **1994**, *32*, 25-30
327. O'Keeffe, D. H.; Barlow, C. H.; Smythe, G. A.; Fuchsman, W. H.; Moss, T. H.; Lilienthal, H. R. and Caughey, W. S. *Bioinorg. Chem.* **1975**, *5*, 125-147
328. Slater A.F.G.; Swiggard W.J.; Orton, B. R.; Flitter, W. D.; Goldberg, D. E.; Cerami, A. and Henderson, G. B. *Proc. Natl. Acad. Sci. U. S. A.* **1990**, *88*, 325-329
329. Tripathi, A. K.; Khan, S. I.; Walker, L. A. and Tekwani, B. L. *Anal. Biochem.* **2004**, *325*, 85-91
330. Dinnebier, R. E. and Billinge, S. J. L. *Powder Diffraction Theory and Practice*, 1st ed.; The Royal Society of Chemistry, Cambridge, 2008
331. Solomonov, I.; Osipova, M.; Feldman, Y.; Baehtz, C.; Kjaer, K.; Robinson, I. K.; Webster, G. T.; McNaughton, D.; Wood, B. R.; Weissbuch, I. and Leiserowitz, L. *J. Am. Chem. Soc.* **2007**, *129*, 5779-5779
332. Egan, T. J.; Hempelmann, E. and Mavuso, W. W. *J. Inorg. Biochem.* **1999**, *73*, 101-107

333. Bohle, D. S.; Kosar, A. D. and Stephens, P. W. *Acta Crystallogr. D.* **2002**, *58*, 1752-1756
334. Noland, G. S.; Briones, N. and Sullivan, D. J. *Mol. Biochem. Parasitol.* **2003**, *130*, 91-99
335. Kuter, D.; Chibale, K. and Egan, T. J. *J. Inorg. Biochem.* **2011**, *105*, 684-692
336. Iftimie, R.; Minary, P. and Tuckerman, M. E. *Proc. Natl. Acad. Sci. U. S. A.* **2005**, *102*, 6654-6659
337. Warshel, A. and Weiss, R. M. *J. Am. Chem. Soc.* **1980**, *102*, 6218-6226
338. Hehre, W. J., Yu, J., Klunzinger, P. E., and Lou, L. *A Brief Guide to Molecular Mechanics and Quantum Chemical Calculations*, 1st ed.; Wavefunctions Inc., Irvine, 1998; 90-94
339. Lee, H. S. and Tuckerman, M. E. *J. Phys. Chem. A* **2006**, *110*, 5549-5560
340. Kohn, W. and Sham, L. J. *Phys. Rev.* **1965**, *140*, A1133-A1138
341. Perdew, J. P.; Burke, K. and Ernzerhof, M. *Phys. Rev. Lett.* **1996**, *77*, 3865-3868
342. Møller, C. and Plesset, M. S. *Phys. Rev.* **1934**, *46*, 618-622
343. Becke, A. D. *Phys. Rev. A* **1988**, *38*, 3098-3100
344. Lee, C. T.; Yang, W. T. and Parr, R. G. *Phys. Rev. B* **1988**, *37*, 785-789
345. Araujo, J. Q.; Carneiro, J. W. D.; De Araujo, M. T.; Leite, F. H. A. and Taranto, A. G. *Bioorg. Med. Chem.* **2008**, *16*, 5021-5029
346. Hay, P. J. and Wadt, W. R. *J. Chem. Phys.* **1985**, *82*, 299-310
347. Gasteiger, J. and Marsili, M. *Tetrahedron* **1980**, *36*, 3219-3228
348. Sousa, S. F.; Fernandes, P. A. and Ramos, M. J. *Proteins: Struct. Funct. Bioinf.* **2006**, *65*, 15-26
349. Mulliken, R. S. *J. Chem. Phys.* **1955**, *23*, 1841-1845
350. Singh, U. C. and Kollman, P. A. *J. Comput. Chem.* **1984**, *5*, 129-145
351. Löwdin, P. O. *Phys. Rev.* **1955**, *97*, 1474-1489
352. Gilson, M. K.; Gilson, H. S. R. and Potter, M. J. *J. Chem. Inf. Comput. Sci.* **2003**, *43*, 1982-1997
353. Bayly, C. I.; Cieplak, P.; Cornell, W. D. and Kollman, P. A. *J. Phys. Chem.* **1993**, *97*, 10269-10280
354. Reed, A. E.; Curtiss, L. A. and Weinhold, F. *Chem. Rev.* **1988**, *88*, 899-926
355. de Villiers, K. A.; Marques, H. M. and Egan, T. J. *J. Inorg. Biochem.* **2008**, *102*, 1660-1667
356. Basco, L. K.; Gillotin, C.; Gimenez, F.; Farinotti, R. and Lebras, J. *Br. J. Clin. Pharmaco.* **1992**, *33*, 517-520
357. Hare, R. *Med. His.* **1982**, *26*, 1-24
358. Georgopapadakou, N. H. *Antimicrob. Agents Chemother.* **1993**, *37*, 2045-2053
359. Kreiswirth, B.; Kornblum, J.; Arbeit, R. D.; Eisner, W.; Maslow, J. N.; Mcgeer, A.; Low, D. E. and Novick, R. P. *Science* **1993**, *259*, 227-230
360. Katayama, Y.; Ito, T. and Hiramatsu, K. *Antimicrob. Agents Chemother.* **2000**, *44*, 1549-1555
361. The Futurists: Looking Toward A.D. 2000, *Time*, 25 Feb. 1966,
362. Lyon, B. R. and Skurray, R. *Microbiol. Rev.* **1987**, *51*, 88-134
363. Cole, M.; Kenig, M. D. and Hewitt, V. A. *Antimicrob. Agents Chemother.* **1973**, *3*, 463-468
364. Stapleton, P. D. and Taylor, P. W. *Sci. Prog.* **2002**, *85*, 57-72
365. Poole, K. *Curr. Opin. Microbiol.* **2001**, *4*, 500-508
366. Bradford, P. A. *Clin. Microbiol. Rev.* **2001**, *14*, 933-951

367. Roberts, M. C.; Sutcliffe, J.; Courvalin, P.; Jensen, L. B.; Rood, J. and Seppala, H. *Antimicrob. Agents Chemother.* **1999**, *43*, 2823-2830
368. Pearson, H. *Nature* **2002**, *418*, 469-469
369. Kluytmans, J. and Struelens, M. *Br. Med. J.* **2009**, *338*, 532-537
370. Miller, L. G. and Diep, B. A. *Clin. Infect. Dis.* **2008**, *46*, 752-760
371. Patti, J. M.; Allen, B. L.; McGavin, M. J. and Hook, M. *Anu. Rev. Microbiol.* **1994**, *48*, 585-617
372. Sritharan, M. and Sritharan, V. *Indian J Med Microbiol.* **2004**, *22*, 140-142
373. Fowler, T.; Wann, E. R.; Joh, D.; Johansson, S. A.; Foster, T. J. and Hook, M. *Eur. J. Cell. Biol.* **2000**, *79*, 672-679
374. Schwarz-Linek, U.; Hook, M. and Potts, J. R. *Mol. Microbiol.* **2004**, *52*, 631-641
375. Tang, Y. W. and Stratton, C. W. *Clin. Lab. Med.* **2010**, *30*, 179-208
376. Deisenhofer, J. *Biochemistry* **1981**, *20*, 2361-2370
377. Gladstone, G. P. and Van Heyningen, W. E. *Br J. Exp. Pathol.* **1957**, *38*, 123-137
378. Gordon, R. J. and Lowy, F. D. *Clin. Infect. Dis.* **2008**, *46*, S350-S359
379. Foster, T. J. *Nat. Rev. Microbiol.* **2005**, *3*, 948-958
380. Lowy, F. D. *N. Engl. J. Med.* **1998**, *339*, 520-532
381. Morell, E. A. and Balkin, D. M. *Yale J. Biol. Med.* **2010**, *83*, 223-233
382. Todd, J.; Fishaut, M.; Kapral, F. and Welch, T. *Lancet* **1978**, *2*, 1116-1118
383. Chua, K.; Laurent, F.; Coombs, G.; Grayson, M. L. and Howden, B. P. *Clin. Infect. Dis.* **2011**, *52*, 99-114
384. Udo, E. E.; Pearman, J. W. and Grubb, W. B. *J. Hop. Infect.* **1993**, *25*, 97-108
385. Deleo, F. R.; Otto, M.; Kreiswirth, B. N. and Chambers, H. F. *Lancet* **2010**, *375*, 1557-1568
386. Chambers, H. F. and Deleo, F. R. *Nat. Rev. Microbiol.* **2009**, *7*, 629-641
387. Prevost, G.; Cribier, B.; Couppie, P.; Petiau, P.; Supersac, G.; Finckbarbancon, V.; Monteil, H. and Piemont, Y. *Infect. Immun.* **1995**, *63*, 4121-4129
388. Tenover, F. C. and Goering, R. V. *J. Antimicrob. Chemother.* **2009**, *64*, 441-446
389. Zoraghi, R.; See, R. H.; Axerio-Cilies, P.; Kumar, N. S.; Gong, H. S.; Moreau, A.; Hsing, M.; Kaur, S.; Swayze, R. D.; Worrall, L.; Amandoron, E.; Lian, T.; Jackson, L.; Jiang, J. H.; Thorson, L.; Labriere, C.; Foster, L.; Brunham, R. C.; McMaster, W. R.; Finlay, B. B.; Strynadka, N. C.; Cherkasov, A.; Young, R. N. and Reiner, N. E. *Antimicrob. Agents Chemother.* **2011**, *55*, 2042-2053
390. Cherkasov, A.; Hsing, M.; Zoraghi, R.; Foster, L. J.; See, R. H.; Stoynov, N.; Jiang, J. H.; Kaur, S.; Lian, T. A.; Jackson, L.; Gong, H. S.; Swayze, R.; Amandoron, E.; Hormozdiari, F.; Dao, P.; Sahinalp, C.; Santos-Filho, O.; Axerio-Cilies, P.; Byler, K.; McMaster, W. R.; Brunham, R. C.; Finlay, B. B. and Reiner, N. E. *J. Proteome Res.* **2011**, *10*, 1139-1150
391. Fraser, H. B.; Hirsh, A. E.; Steinmetz, L. M.; Scharfe, C. and Feldman, M. W. *Science* **2002**, *296*, 750-752
392. Valentin, G.; Chiarelli, L.; Fortin, R.; Speranza, M. L.; Galizzi, A. and Mattevi, A. *J. Biol. Chem.* **2000**, *275*, 18145-18152

393. Zoraghi, R.; Worrall, L.; See, R. H.; Strangman, W.; Popplewell, W. L.; Gong, H.; Samaai, T.; Swayze, R. D.; Kaur, S.; Vuckovic, M.; Finlay, B. B.; Brunham, R. C.; McMaster, W. R.; Davies-Coleman, M. T.; Strynadka, N. C.; Anderson, R. J. and Reiner, N. E. *J. Biol. Chem.* **2011**, *(In press)*,
394. Strangman, W.; Zoraghi, R.; See, R. H.; Gong, H.; Popplewell, W. L.; Davies-Coleman, M. T.; Reiner, N. E. and Andersen, R. J. *52nd ASP Conference* **2011**, *San Diego*,
395. Politzer, P.; Lane, P.; Concha, M. C.; Ma, Y. G. and Murray, J. S. *J. Mol. Model.* **2007**, *13*, 305-311
396. Parisini, E.; Metrangolo, P.; Pilati, T.; Resnati, G. and Terraneo, G. *Chem. Soc. Rev.* **2011**, *40*, 2267-2278
397. Auffinger, P.; Hays, F. A.; Westhof, E. and Ho, P. S. *Proc. Natl. Acad. Sci. U. S. A.* **2004**, *101*, 16789-16794
398. Metrangolo, P.; Neukirch, H.; Pilati, T. and Resnati, G. *Acc. Chem. Res.* **2005**, *38*, 386-395
399. Khalili, B.; Tondro, T. and Hashemi, M. M. *Tetrahedron* **2009**, *65*, 6882-6887
400. Yang, C. G.; Huang, H. and Jiang, B. *Curr. Opin. Org. Chem.* **2004**, *8*, 1691-1720
401. Bao, B. Q.; Sun, Q. S.; Yao, X. S.; Hong, J. K.; Lee, C. O.; Sim, C. J.; Im, K. S. and Jung, J. H. *J. Nat. Prod.* **2005**, *68*, 711-715
402. Jung, J. H.; Shinde, P. B.; Hong, J. K.; Liu, Y. H. and Sim, C. J. *Biochem. Syst. Ecol.* **2007**, *35*, 48-51
403. Bao, B.; Zhang, P.; Lee, Y.; Hong, J.; Lee, C. O. and Jung, J. H. *Mar. Drugs* **2007**, *5*, 31-39
404. Bartik, K.; Braekman, J. C.; Daloze, D.; Stoller, C.; Huysecom, J.; Vandevyver, G. and Ottinger, R. *Can. J. Chem.* **1987**, *65*, 2118-2121
405. Tsujii, S.; Rinehart, K. L.; Gunasekera, S. P.; Kashman, Y.; Cross, S. S.; Lui, M. S.; Pomponi, S. A. and Diaz, M. C. *J. Org. Chem.* **1988**, *53*, 5446-5453
406. Morris, S. A. and Andersen, R. J. *Tetrahedron* **1990**, *46*, 715-720
407. Sakemi, S. and Sun, H. H. *J. Org. Chem.* **1991**, *56*, 4304-4307
408. Murray, L. M.; Lim, T. K.; Hooper, J. N. A. and Capon, R. J. *Aust. J. Chem.* **1995**, *48*, 2053-2058
409. Shin, J.; Seo, Y.; Cho, K. W.; Rho, J. R. and Sim, C. J. *J. Nat. Prod.* **1999**, *62*, 647-649
410. Casapullo, A.; Bifulco, G.; Bruno, I. and Riccio, R. *J. Nat. Prod.* **2000**, *63*, 447-451
411. Braekman, J. C.; Daloze, D. and Stoller, C. *B. Soc. Chim. Belg.* **1987**, *96*, 809-812
412. Miyake, F. Y.; Yakushijin, K. and Horne, D. A. *Org. Lett.* **2000**, *2*, 2121-2123
413. Achab, S. *Tetrahedron Lett.* **1996**, *37*, 5503-5506
414. Mal, S. K.; Bohe, L. and Achab, S. *Tetrahedron* **2008**, *64*, 5904-5914
415. Kawasaki, I.; Katsuma, H.; Nakayama, Y.; Yamashita, M. and Ohta, S. *Heterocycles* **1998**, *48*, 1887-1901
416. Kawasaki, I.; Yamashita, M. and Ohta, S. *Chem. Pharm. Bull.* **1996**, *44*, 1831-1839
417. Guinchard, X.; Vallee, Y. and Denis, J. N. *Org. Lett.* **2007**, *9*, 3761-3764
418. Guinchard, X.; Vallee, Y. and Denis, J. N. *J. Org. Chem.* **2007**, *72*, 3972-3975
419. Rawal, V. H. and Cava, M. P. *Tetrahedron Lett.* **1985**, *26*, 6141-6142
420. Knott, K. E.; Auschill, S.; Jager, A. and Knölker, H. J. *Chem. Commun.* **2009**, 1467-1469
421. Reid, C. M.; Ebikeme, C.; Barrett, M. P.; Patzewitz, E. M.; Muller, S.; Robins, D. J. and Sutherland, A. *Bioorg. Med. Chem. (Lett.)* **2008**, *18*, 2455-2458
422. Zuliani, V.; Fantini, M.; Nigam, A.; Stables, J. P.; Patel, M. K. and Rivara, M. *Bioorg. Med. Chem.* **2010**, *18*, 7957-7965

423. Ettari, R.; Pinto, A. and Micale, N. *ARKIVOC* **2009**, 227-234
424. Riley, H. L.; Morely, J. F. and Friend, N. A. C. *J. Chem. Soc.* **1932**, 1875-1883
425. Gelman, D. M. and Perlmutter, P. *Tetrahedron Lett.* **2009**, *50*, 39-40
426. Belsey, S.; Danks, T. N. and Wagner, G. *Synth. Commun.* **2006**, *36*, 1019-1024
427. Goswami, S. and Adak, A. K. *Synth. Commun.* **2003**, *33*, 475-480
428. Gedye, R.; Smith, F.; Westaway, K.; Ali, H.; Baldisera, L.; Laberge, L. and Rousell, J. *Tetrahedron Lett.* **1986**, *27*, 279-282
429. Giguere, R. J.; Bray, T. L.; Duncan, S. M. and Majetich, G. *Tetrahedron Lett.* **1986**, *27*, 4945-4948
430. Lidstrom, P.; Tierney, J.; Wathey, B. and Westman, J. *Tetrahedron* **2001**, *57*, 9225-9283
431. Paul, S.; Gupta, M.; Gupta, R. and Loupy, A. *Synthesis* **2002**, *1*, 75-78
432. Khrustalev, D. P.; Suleimenova, A. A.; Fazylov, S. D.; Gazaliev, A. M. and Muldakhmetov, Z. M. *Izv. Nats. Akad. Nauk. Resp. Kaz, Ser. Khim.* **2007**, *3*, 22-24
433. Spallholz, J. E. *Free Radical Bio. Med.* **1994**, *17*, 45-64
434. Hogberg, J. and Alexander, J. *Handbook on the Toxicology of Metals*, 3rd ed.; Academic Press, Burlington, 2007; 783-807
435. Marchand, N. J.; Grée, D. M.; Martelli, J. T. and Grée, R. L. *J. Org. Chem.* **1996**, *61*, 5063-5072
436. Linde, D. R. *CRC Handbook of Chemistry and Physical Data*, 73rd ed.; CRC Press Inc., Boca Raton, 1993; 3-218
437. Holm, T. *J. Chromatogr. , A* **1999**, *842*, 221-227
438. Saint Laumer, J. Y.; Cicchetti, E.; Merle, P.; Egger, J. and Chaintreau, A. *Anal. Chem.* **2010**, *82*, 6457-6462
439. Mikol, G. J. and Russel, G. A. *Org. Synth.* **1968**, ***48***, 109-111
440. Joshi, K. C.; Pathak, V. N. and Goyal, M. K. *J. Heterocycl. Chem.* **1981**, *18*, 1651-1653
441. Bergmann, T.; Schories, D. and Steffan, B. *Tetrahedron* **1997**, *53*, 2055-2060
442. Danheiser, R. L.; Brisbois, R. G.; Kowalczyk, J. J. and Miller, R. F. *J. Am. Chem. Soc.* **1990**, *112*, 3093-3100
443. *Gaussian03*, version 01; Frisch, M. J.; Trucks, G. W.; Schlegel, H. B.; Scuseria, G. E.; Robb, M. A.; Cheeseman, J. R.; Montgomery Jr, J. A.; Vreven, T.; Kudin, K. N.; Burant, J. C.; Millam, J. M.; Iyengar, S. S.; Tomsai, J.; Barone, V.; Mennucci, B.; Cossi, M.; Scalmani, G.; Rega, N.; Petersson, G. A.; Nakatsuji, H.; Hada, M.; Ehara, M.; Toyota, K.; Kukuda, R.; Hasegawa, J.; Ishida, M.; Nakajima, T.; Honda, Y.; Kitao, O.; Nakai, H.; Klene, M.; Li, X.; Knox, J. E.; Hratchian, H. P.; Cross, J. B.; Bakken, V.; Adamo, C.; Jaramillo, J.; Gomperts, R.; Stratmann, R. E.; Yazyev, O.; Austin, A. J.; Cammi, R.; Pomelli, C.; Ocherski, J. W.; Ayala, P. Y.; Morokuma, K.; Voth, G. A.; Salvador, P.; Dannenberg, J. J.; Zakrzewski, V. G.; Dapprich, S.; Daniels, A. D.; Strain, M. C.; Farkas, O.; Malick, D. K.; Rabuck, A. D.; Raghavachari, K.; Foresman, J. B.; Oritz, J. V.; Cui, Q.; Baboul, A. G.; Clifford, S.; Cioslowski, J.; Stefanov, B. B.; Liu, G.; Liashenko, A.; Piskorz, P.; Komaromi, I.; Martin, R. L.; Fox, D. J.; Keith, T.; Al-Laham, M. A.; Peng, C. Y.; Nanayakkara, A.; Challacombe, M.; Gill, P. M. W.; Johnson, B.; Chen, W.; Wong, M. W.; Gonzalez, C. and Pople, J. A. Gaussian Inc.: Wallingford, CT, 2004
444. Jeener, J.; Meier, B. H.; Bachmann, P. and Ernst, R. R. *J. Chem. Phys.* **1979**, *71*, 4546-4553
445. Pons, M. and Millet, O. *Prog. Nucl. Magn. Reson. Spectrosc.* **2001**, *38*, 267-324

446. Perrin, C. L. and Dwyer, T. J. *Chem. Rev.* **1990**, *90*, 935-967
447. Braun, S., Kalinowski, H.-O., and Berger, S. *150 and More Basic NMR Experiments*, 2nd ed.; Wiley-VCH, Weinheim, 1998; 420-422
448. Perrin, C. L. and Johnston, E. R. *J. Am. Chem. Soc.* **1981**, *103*, 4697-4703
449. Perrin, C. L.; Johnston, E. R.; Lollo, C. P. and Kobrin, P. A. *J. Am. Chem. Soc.* **1981**, *103*, 4691-4696
450. Perrin, C. L. and Johnston, E. R. *Can. J. Chem.* **1981**, *59*, 2527-2535
451. Perrin, C. L. and Gipe, R. K. *J. Am. Chem. Soc.* **1984**, *106*, 4036-4038
452. Kuchel, P. W.; Bulliman, B. T.; Chapman, B. E. and Mendz, G. L. *J. Magn. Reson.* **1988**, *76*, 136-142
453. Willem, R.; Jans, A.; Hoogzand, C.; Gielen, M.; Vanbinst, G. and Pepermans, H. *J. Am. Chem. Soc.* **1985**, *107*, 28-32
454. Paquette, L. A.; Wang, T. Z.; Luo, J. M.; Cottrell, C. E.; Clough, A. E. and Anderson, L. B. *J. Am. Chem. Soc.* **1990**, *112*, 239-253
455. Kubicki, M. *Acta Crystallogr. , Sect. B: Struct. Sci.* **2004**, *60*, 191-196
456. Kubicki, M. *J. Mol. Struct.* **2004**, *698*, 67-73
457. Mahboobi, S.; Sellmer, A.; Burgemeister, T.; Lyssenko, A. and Schollmeyer, D. *Monatsh. Chem.* **2004**, *135*, 333-342
458. Duran, R.; Zubia, E.; Ortega, M. J.; Naranjo, S. and Salva, J. *Tetrahedron* **1999**, *55*, 13225-13232
459. superstock.com 1566-323263. www.superstock.com (accessed 2011)
460. Horton, W. J. and Spence, J. T. *J. Am. Chem. Soc.* **1958**, *80*, 2453-2456
461. Konieczny, M. T.; Maciejewski, G. and Konieczny, W. *Synthesis-Stuttgart* **2005**, 1575-1577
462. Ryu, I.; Matsubara, H.; Yasuda, S.; Nakamura, H. and Curran, D. P. *J. Am. Chem. Soc.* **2002**, *124*, 12946-12947
463. Younis, Y. M. H. *Int. J. Chem.* **2001**, *11*, 75-85
464. Zuo, L.; Yao, S. Y.; Wang, W. and Duan, W. H. *Tetrahedron Lett.* **2008**, *49*, 4054-4056
465. Ley, S. V.; Norman, J.; Griffith, W. P. and Marsden, S. P. *Synthesis-Stuttgart* **1994**, 639-666
466. Armarego, W. L. F. and Perrin, D. D. *Purification of Laboratory Chemicals*, 4th ed.; The Bath Press, Bath, 1998
467. Ravn, M. M.; Coates, R. M.; Flory, J. E.; Peters, R. J. and Croteau, R. *Org. Lett.* **2000**, *2*, 573-576
468. Do Khac Manh, D.; Fetizon, M. and Flament, J. P. *Tetrahedron* **1975**, *31*, 1897-1902
469. Bastard, J.; Duc, D. K.; Fetizon, M.; Francis, M. J.; Grant, P. K.; Weavers, R. T.; Kaneko, C.; Baddeley, G. V.; Bernassau, J. M.; Burfitt, I. R.; Wovkulich, P. M. and Wenkert, E. *J. Nat. Prod.* **1984**, *47*, 592-599
470. Grant, P. K. and Hodges, R. *J. Chem. Soc.* **1960**, 5274-5275
471. van Wyk, A. W. W.; Lobb, K. A.; Caira, M. R.; Hoppe, H. C. and Davies-Coleman, M. T. *J. Nat. Prod.* **2007**, *70*, 1253-1258
472. Abad, A.; Arno, M.; Domingo, L. R. and Zaragoza, R. J. *Tetrahedron* **1985**, *41*, 4937-4940
473. Villamizar, J. E.; Gamez, C.; Alcala, A.; Salazar, F.; Tropper, E.; Angarita, A. and Canudas, N. *Synth. Commun.* **2011**, *41*, 1733-1741
474. Trager, W. and Jensen, J. B. *Science* **1976**, *193*, 673-675

475. Lambros, C. and Vanderberg, J. P. *J. Parasitol.* **1979**, *65*, 418-420

476. Sharma, P. and Sharma, J. D. *J. Ethnopharmacol.* **2001**, *74*, 239-243

477. Mast, N.; Whitet, M. A.; Bjorkhem, I.; Johnson, E. F.; Stout, C. D. and Pikuleva, I. A. *Proc. Natl. Acad. Sci. U. S. A.* **2008**, *105*, 9546-9551

478. Schubert, H.; Hellwig, A. and Bleichert, J. L. *J. Praktische. Chemie.* **1964**, *24*, 125-131

479. Arnold, R. T. and Fuson, R. C. *J. Am. Chem. Soc.* **1936**, *58*, 1295-1296

480. Minor, J. T. and Vanderwerf, C. A. *J. Org. Chem.* **1952**, *17*, 1425-1430

481. Fulke, J. W. B. and McCrindle, R. *Chem. Ind.* **1965**, *15*, 647-648